

**Characterization of the  
Embryonic Kidney Development  
in *Danio rerio***

and

**Functional Analysis of Arl13b/ Scorpion  
during Embryonic Development in *Danio rerio***

Dissertation zur Erlangung des Doktorgrades  
der Mathematisch-Naturwissenschaftlichen Fakultät  
der Christian-Albrechts-Universität  
zu Kiel

Vorgelegt von  
Anna Sunjin Lee

New Haven  
2009



## TABLE of CONTENTS

TABLE of CONTENTS .....	I
Erklärung.....	VIII
List of Figures.....	IX
List of Tables.....	XII
List of Abbreviations.....	XIII
1. GENERAL INTRODUCTION .....	1
1.1. Human Ciliopathies .....	1
1.2. PKD.....	1
1.3. Second Hit Model.....	2
1.4. Polycystin-1 and Polycystin-2 .....	2
1.5. Joubert Syndrome.....	3
1.6. The Structure of Cilia .....	4
1.7. Intraflagellar Transport.....	5
1.8. Retinal cysts and Cilia.....	6
1.7. Zebrafish Kidney .....	7
GOALS of THESIS PROJECT .....	9
Project 1 .....	9
Characterization of the Wildtype Kidney Development in <i>Danio rerio</i> .....	9
Project 2.....	10
Functional analysis of Arl13b/ Scorpion during embryonic development in <i>Danio rerio</i> .	10
3. MATERIALS.....	11
3.1. Living Materials .....	11
3.1.1. <i>Danio rerio</i> .....	11
3.1.2. <i>Escherichia coli</i> .....	11
3.1.3. <i>Saccharomyces cerevisiae</i> .....	11
3.2. Chemicals and Solutions.....	12
3.2.1. Buffer and Media.....	12
3.2.2. Immunohistochemistry .....	16
3.2.3. In situ hybridization .....	17

TABLE of CONTENTS

---

3.2.4. Electron microscopy.....	19
3.3. Antibodies .....	20
3.3.1. Primary antibodies .....	20
3.3.2. Secondary antibodies.....	20
3.4. Plasmids.....	21
3.5. Morpholino oligonucleotides.....	21
3.6. DNA Buffer and Reagents.....	22
3.7. DNA and RNA Kits .....	23
3.8. RNA.....	23
3.8.1. In vitro transcription of capped mRNA .....	23
3.8.2. Purification of RNA.....	23
3.9. Protein Purification .....	24
3.9.1. DEAE Blue Gel Purification.....	24
3.9.2. Affinity purification .....	24
3.9.3. SDS PAGE.....	25
3.9.4. Coomassie Staining .....	26
3.9.5. Protein kits .....	27
3.10. Yeast-two-hybrid libraries.....	27
3.11. TUNEL Assay.....	27
3.12. Chemicals .....	28
3.13. Other consumables .....	30
3.14. Equipment.....	31
3.15. Microscopes .....	31
4. METHODS .....	33
4.1. Zebrafish maintenance.....	33
4.1.1. Zebrafish Lines.....	33
4.1.2. Anaesthetizing Zebrafish.....	33
4.1.3. Fin Clipping of Zebrafish .....	33
4.1.4. Extracting Genomic DNA from Tail Biopsy .....	34
4.2. Live embryo imaging.....	34
4.2.1. Methylcellulose.....	34
4.3. Fixation.....	34
4.3.1. Formalin .....	34

---

TABLE of CONTENTS

---

4.3.2. Dent's .....	35
4.3.3. Bouin's .....	35
4.3.4. Dehydration of embryos .....	35
4.4. Histological Analysis .....	36
4.5. Transmission electron microscopy .....	37
4.6. <i>In situ</i> hybridization .....	37
4.7. Cryostat sections.....	40
4.8. Microtome sections .....	40
4.9. Immunostaining.....	40
4.10. Microinjection .....	41
4.11. Morpholinos.....	42
4.12. <i>In vitro</i> transcription of mRNA .....	43
4.13. Recovery and Purification of RNA.....	45
4.14. Recovery and Purification of DNA.....	45
4.14.1. PCR purification Kit .....	45
4.14.2. Gel Extraction Kit .....	46
4.15. Standard PCR.....	46
4.16. Cloning .....	47
4.17. Sequencing .....	47
4.18. RT-PCR analysis.....	47
4.19. Heat shock transformation of competent cells .....	47
4.20. Glycerol stocks.....	48
4.21. Purification of Plasmid DNA .....	48
4.22. Agarose Gel Electrophoresis .....	50
4.23. Expression and Purification of GST-Fusion-proteins .....	50
4.24. Peptide Antibody .....	51
4.25. DEAE Affi-Gel Blue Gel purification .....	52
4.25.1. Preparing Blue Gel Column .....	52
4.25.2. Purifying Serum on Blue Gel.....	52
4.25.3. Ammonium Sulfate Precipitation .....	52
4.25.4. Dialysis.....	53
4.26. Bugbuster.....	53
4.27. Protein Purification on Immobilized Glutathione .....	54
4.27.1. Glutathione beads regeneration.....	54

TABLE of CONTENTS

---

4.27.2. Aqueous Coupling of Affi Gel ..... 54  
4.27.3. Purifying Serum on Affi Column ..... 55  
4.28. TUNEL Assay..... 55  
4.29. BrdU Proliferation Assay ..... 56  
4.30. SDS PAGE..... 56  
4.31. Western Blot..... 58  
4.32. Live imaging of cilia beating ..... 58  
4.33. Yeast two hybrid assay ..... 59

Project 1

CHARACTERIZATION of the EMBRYONIC KIDNEY DEVELOPMENT in *Danio rerio*

5.1. INTRODUCTION..... 63  
5.1.1. *Wilm's tumor suppressor (WT1)*..... 63  
5.1.2. *Pax2*..... 63  
5.1.3. *vHnf1*..... 64  
5.1.4. Mesenchymal-to-Epithelial Transition ..... 65  
5.1.5. Renal Epithelial Polarity ..... 66  
5.1.6. Mechanisms of Lumen Formation..... 66  
5.1.7. Planar Cell Polarity (PCP)..... 67  
5.1.8. Cilia and Wnt Signaling ..... 67  
5.1.9. Cyst and PCP..... 68  
5.2. RESULTS..... 70  
5.2.1. Variant hepatic nuclear factor1 (*vHnf1*) antibody specifically labels the intermediate mesoderm ..... 70  
5.2.2. Lumen formation starts at the 10-12 somite stage..... 74  
5.2.3. Centrosome relocalization in the intermediate mesoderm ..... 76  
5.2.4. Cilia formation in the kidney duct ..... 78  
5.2.5. The pronephric duct is narrowing and elongating during development..... 81  
5.2.6. The Zebrafish pronephros shows a low rate of proliferation throughout development..... 83  
5.2.7. The intermediate mesoderm undergoes rearrangement during kidney development..... 86  
5.2.8. Inhibition of the planar cell polarity pathway leads to duct dilation..... 86

5.2.9. Disruption of PCP does not inhibit apico-basal polarity in the pronephric duct..... 91  
 5.3. DISCUSSION..... 91

Project 2

Part I: CHARACTERIZATION of the *arl13b/scorpion*<sup>hi459</sup> MUTANT AND MORPHANT

6.1. INTRODUCTION..... 97  
 6.1.1. PKD and Joubert syndrome ..... 97  
 6.1.2. Cilia as mechanosensor ..... 99  
 6.1.3. Polarity and secretion..... 100  
 6.1.4. Zebrafish pronephros ..... 100  
 6.1.5. *scorpion*<sup>hi459</sup> mutant..... 101  
 6.2. RESULTS..... 103  
 6.2.1. Phenotype of *scorpion*<sup>hi459</sup> mutants ..... 103  
 6.2.2. Cystic dilations first appear in medial tubules in *scorpion*<sup>hi459</sup> mutants ..... 105  
 6.2.3. Proliferation in the duct is secondary to dilation..... 107  
 6.2.4. *arl13b/ scorpion* morphants phenocopy the *scorpion*<sup>hi459</sup> mutant phenotype ..... 109  
 6.2.5. The *arl13b/ scorpion* morpholino is specific ..... 111  
 6.2.6. *Arl13b/ Scorpion* is expressed in various ciliated tissues..... 111  
 6.2.7. Otic vesicles in *arl13b/ scorpion* morphants and *sco*<sup>hi459</sup> mutants ..... 113  
 6.2.8. Small eye phenotype in severe *arl13b/ sco* morphants and *sco*<sup>hi459</sup> mutants..... 114  
 6.2.9. *Arl13b/ Scorpion* is necessary for maintenance of photoreceptor OS ..... 116  
 6.2.10. *sco*<sup>hi459</sup> mutant embryos exhibit excessive apoptosis in retinal photoreceptor layer and outer segment atrophy ..... 118  
 6.2.11. Kupffer's vesicle in *scorpion*<sup>hi459</sup> mutants ..... 120  
 6.2.12. *arl13b/ scorpion* morphants display left/right axis randomization..... 122  
 6.2.13. The Kupffer's vesicle structure itself is formed in *scorpion*<sup>hi459</sup> mutant and morphants ..... 123  
 6.2.14. Cilia formation in the KV is disrupted in *arl13b/ scorpion* morphants ..... 125  
 6.2.15. *arl13b/scorpion* morphants display altered Nodal related signaling pathway ... 127  
 6.2.18. Kidney specific PCP is disrupted in *scorpion*<sup>hi459</sup> mutants ..... 133  
 6.2.19 Axonemal ultrastructure of pronephric duct cilia in *sco*<sup>hi459</sup> mutant embryos ..... 135  
 6.2.20. Cilia motility is defective in *scorpion*<sup>hi459</sup> mutants..... 137  
 6.2.21. Cilia of multiciliated cells grow long in *sco*<sup>hi459</sup> mutant embryos ..... 139

TABLE of CONTENTS

---

6.2.22. Arl13b/ Scorpion mislocalizes to apical membrane in *ift57<sup>hi3417</sup>* mutants ..... 140

6.2.23. The pronephric duct in *scorpion<sup>hi459</sup>* mutants grossly maintains apical/basolateral polarity..... 144

6.3. DISCUSSION..... 147

6.3.1. Arl13b/ Scorpion plays a global role in ciliated tissues ..... 147

6.3.2. Pathogenesis of duct dilation and cyst formation in *scorpion<sup>hi459</sup>* mutants ..... 148

6.3.3. IFT and Arl13b/ Scorpion ..... 149

6.3.4. Apico-basolateral polarity ..... 150

6.3.5. Ciliary tufts in *scorpion<sup>hi459</sup>* mutant embryos..... 151

6.3.6. Arl13b/ Sco and laterality formation ..... 153

6.3.7. *arl13b/ sco* mutant embryos and the Arl13b null mutant *hennin*..... 157

6.3.8. Arl13b/ Sco and retinal atrophy ..... 158

Project 2

Part II: FUNCTIONAL ANALYSIS of Arl13b/ Scorpion DURING EMBRYONIC DEVELOPMENT in *Danio rerio*

7.1. INTRODUCTION..... 161

7.1.1. Arl13b and Joubert syndrome ..... 161

7.1.2. *hennin* and *scorpion<sup>hi459</sup>* ..... 161

7.1.3. Intraflagellar transport ..... 161

7.1.4. Ciliary localization signal ..... 162

7.1.5. Rescue experiments ..... 163

7.1.5. Yeast two hybrid..... 164

7.2. RESULTS..... 165

7.2.1. Arl13b/ Scorpion is highly conserved among species..... 165

7.2.2. Sco-eGFP localizes to cilia in the pronephric duct..... 167

7.2.3. The small GTPase domain of Arl13b/Scorpion is necessary but not sufficient for its cilia localization ..... 169

7.2.4. The coiled coil region of Arl13b/ Scorpion is necessary for cilia localization ..... 172

7.2.5. Part of the C-terminus is required for targeting Arl13b/ Scorpion to the cilium ... 172

7.2.6. GTP binding activity is not necessary for cilia localization of Arl13b/ Scorpion .. 173

7.2.7. Cilia localization of Arl13b/Scorpion is necessary for phenotype rescue ..... 175



TABLE of CONTENTS

---

7.2.8. The coiled-coil motif and GTPase domain are necessary for the rescue capabilities of Arl13b/ Scorpion.....	176
7.2.9. Change of GTP binding activity of small GTPase domain inhibits its rescue ability .....	176
7.2.10. C-terminus of Arl13b/ Scorpion is not necessary for rescue ability.....	177
7.2.11. Identification of putative interacting partners for Arl13b/ Scorpion.....	179
7.2.12. Transformation of both, embryonic human kidney cDNA library as well as adult zebrafish library, is highly efficient .....	180
7.2.13. Putative Arl13b/ Scorpion interacting proteins isolated from the human embryonic kidney library .....	183
7.2.14. Putative interacting proteins of Arl13b/Scorpion from adult zebrafish cDNA ....	184
7.3. DISCUSSION.....	187
8. SUMMARY.....	196
9. REFERENCES.....	199
10. ACKNOWLEDGEMENTS .....	221
11. Curriculum Vitae.....	223
12. ANHANG.....	225

## ERKLÄRUNG

Hiermit erkläre ich gemäß §10 der Promotionsordnung der Mathematisch-Naturwissenschaftlichen Fakultät der Christian-Albrechts-Universität zu Kiel, dass ich die vorliegende Arbeit unter wissenschaftlicher Leitung von Prof. Dr. Zhaoxia Sun und Prof. Dr. Thomas Bosch selbstständig und ohne fremde Hilfe verfasst habe. Weiterhin habe ich keine anderen als die von mir angegebenen Quellen und Hilfsmittel benutzt und die den Werken wörtlich oder inhaltlich entnommenen Stellen als solche kenntlich gemacht. Die vorliegende Arbeit entstand unter Einhaltung der Regeln guter wissenschaftlicher Praxis. Die Arbeit wurde bisher keiner anderen Universität zur Begutachtung vorgelegt.

New Haven, den.....

.....

Anna Sunjin Lee

## List of Figures

Figure 1	Cilia play diverse roles and are localized on various tissues.....	5
Figure 2	Model describing the cilium as mechano-sensory organelle .....	7
Figure 3	Schematic development of the zebrafish kidney and expression pattern of kidney specific transcription factors.....	65
Figure 4	Cells rearrange and polarize to form pronephric duct .....	70
Figure 5	<i>vHnf1</i> expression during embryogenesis .....	71
Figure 6	Domains of <i>vHnf1</i> in zebrafish and choice of antigenic regions for antigenic peptides.....	73
Figure 7	Analysis of lumen formation during embryonic kidney development.....	75
Figure 8	Centrosome relocalization during embryonic kidney development .....	77
Figure 9	Analysis of cilia formation during embryonic kidney development .....	79
Figure 10	Maturation of the zebrafish pronephric duct .....	80
Figure 11	Cells undergo rearrangement during embryonic kidney development .....	82
Figure 12	Analysis of proliferation during kidney development .....	84
Figure 13	Cells of the intermediate mesoderm undergo realignment during embryogenesis .....	86
Figure 14	Canonical wnt signaling and PCP signaling pathway and diagram of Dsh-DEP construct.....	88
Figure 15	Disruption of PCP signaling pathway leads to duct dilatino and increase in cell number in duct circumference .....	90
Figure 16	Joubert Syndrome (JS) is diagnosed by the neurological finding of a “molar tooth sign” (MTS) on MRI. ....	98
Figure 17	<i>scorpion</i> <sup>hi459</sup> mutants develop kidney cysts .....	104
Figure 18	Temporal and spatial analysis of cyst formation in <i>scorpion</i> <sup>hi459</sup> mutants.....	106
Figure 19	Average cell number surrounding the medial tubules in <i>scorpion</i> <sup>hi459</sup> mutants is increased at 2 dpf and 4 dpf.....	108
Figure 20	The <i>arl13b</i> / <i>scorpion</i> morphant phenocopies the <i>scorpion</i> <sup>hi459</sup> mutant phenotype.....	110

LIST of FIGURES

Figure 21	Arl13b/ Scorpion is expressed on cilia in multiple ciliated tissues in zebrafish .....	112
Figure 22	Number of otoliths in otic vesicles is not significantly altered in <i>sco</i> <sup>hi459</sup> mutants and <i>arl13b/sco</i> morphants respectively .....	113
Figure 23	Severely edemic <i>scorpion</i> <sup>hi459</sup> mutant and <i>arl13b/ sco</i> morphant embryos exhibit a smaller eye size.....	115
Figure 24	Arl13b/ Sco is necessary for maintenance of photoreceptor outer segments.....	117
Figure 25	<i>scorpion</i> <sup>hi459</sup> mutant embryos show excessive apoptosis in photoreceptor layer and have degenerated photoreceptor outer segments .....	119
Figure 26	<i>scorpion</i> <sup>hi459</sup> mutants show situs solitus and exhibit maternal contribution.....	121
Figure 27	<i>arl13b/ scorpion</i> morphants display randomized heart looping. ....	122
Figure 28	Quantification of the KV size .....	124
Figure 29	Quantification of cilia length in the KV .....	125
Figure 30	Arl13b/ Scorpion is required for cilia formation in Kupffer's vesicle.....	126
Figure 31	Model of Nodal related signaling pathway in zebrafish .....	127
Figure 32	<i>arl13b/ scorpion</i> morphants display altered <i>spaw</i> expression .....	129
Figure 33	Ciliary defects in <i>scorpion</i> <sup>hi459</sup> mutants .....	130
Figure 34	<i>scorpion</i> <sup>hi459</sup> mutants maintain cilia in MCC but lose intracellular PCP .....	132
Figure 35	Organ specific planar cell polarity in the kidney duct is disrupted in <i>scorpion</i> <sup>hi459</sup> mutants .....	134
Figure 36	The axoneme of remaining cilia in <i>scorpion</i> <sup>hi459</sup> mutants have an intact (9+2) ultrastructure .....	136
Figure 37	Pronephric cilia in <i>scorpion</i> <sup>hi459</sup> mutants remain motile but show aberrant beating kinetics .....	138
Figure 38	<i>scorpion</i> <sup>hi459</sup> mutant cilia grow long but appear disorganized .....	140
Figure 39	Scorpion localization in <i>ift57</i> <sup>hi3417</sup> mutants at 4 dpf .....	142
Figure 40	In <i>ift57</i> <sup>hi3417</sup> mutants Arl13b/ Scorpion is mistargeted to apical membrane and inversely correlates with WGA expression .....	143
Figure 41	Apico-basolateral polarity in <i>scorpion</i> <sup>hi459</sup> mutants is grossly intact while basolateral membrane is not as organized .....	146

Figure 42	Arl13b/ Scorpion is conserved among different species.....	166
Figure 43	Overexpressied Scorpion-eGFP localizes to the pronephric duct cilia .....	168
Figure 44	The small GTPase domain is nessecary but not sufficient for cilia targeting of Arl13b/Scorpion .....	171
Figure 45	The enzymatic activity of the small GTPase domain does not influence cilia targeting whereas the coiled coil domain and C- terminus of Arl13b/ Scorpion are required for ciliary targeting .....	174
Figure 46	Schematic diagram explaining the principle of the yeast-two-hybrid.....	179
Figure 47	Diagram of the yeast-two-hybrid assay from testing the bait construct to analyzing the positive clones.....	182

## List of Tables

Table 1	Number of cells in the duct of wildtype and <i>scorpion</i> <sup>hi459</sup> mutant embryos at 2 dpf and 4 dpf. ....	108
Table 2	<i>arl13b/ scorpion</i> morphants can be rescued by coinjection of <i>scorpion</i> mRNA. ....	111
Table 3	Number of otoliths in otic vesicles is more variable in <i>arl13b/ scorpion</i> morphants and mutants, but not statistically significant .....	114
Table 4	Data of quantification of the small eye phenotype in severe edemic <i>arl13b/ sco</i> morphants and <i>scorpion</i> <sup>hi459</sup> mutants .....	115
Table 5	Asymmetric heart positioning in <i>arl13b/scorpion</i> morphants .....	122
Table 6	Data for analysis of the size of the Kupffer's vesicle in WT, control morphants and <i>arl13b/ scorpion</i> morphants .....	124
Table 7	Data for analysis of cilia length in the Kupffer's vesicle in WT, control morphants and <i>arl13b/sco</i> morphants. ....	125
Table 8	<i>spaw</i> expression in <i>arl13b/ scorpion</i> morphants .....	129
Table 9	Statistical analysis of data plotted in Figure 37. ....	138
Table 10	Schematic of <i>Arl13b/ Scorpion</i> deletion constructs .....	169
Table 11	Summary of rescue experiments performed on offspring of <i>scorpion</i> <sup>hi459</sup> heterozygous crosses.....	178
Table 12	List of putative protein interactors of <i>Arl13b/ Scorpion</i> using the human embryonic kidney library.....	183
Table 13	List of putative interactors of the yeast two hybrid screen using the zebrafish adult cDNA library. ....	185

## List of Abbreviations

A	Adenine
AB	Antibody
Ac-tub	Acetylated alpha-tubulin
Ade	Adenine
AMCA	Aminomethylcoumarin acetate
AP	Alkaline phosphate
aPKC	Atypical Protein kinase C
APS	Ammonium peroxydisulfate
arl13b	Danio rerio Arl13b gene
Arl13b	Murine Arl13b gene
ARL13B	Human Arl13b gene
ATP	Adenosine triphosphate
BCIP	5-bromo-4-chloro-3-indolyl phosphate
BDM	2,3-Butanedione monoxime
bp	Base pair
BrdU	5-bromo-2-deoxyuridine
BSA	Bovine serum albumin
C	Cytosine
Cdh17	Cadherin 17
cDNA	Complementary DNA
cntrl	Control
CTP	Cytosin triphosphate
Da	Dalton
DAPI	4',6-diamidino-2-phenylindol
DNA	Deoxyribonucleic acid
dNTP	Deoxynucleotidetriphosphate
DMF	Dimethylformamide
DMSO	Dimethylsulfoxid
DN	Dominant negative
dpf	Days post fertilization
DTT	Dithiothreitol
E.coli	Escherichia coli
ECL	Enhanced chemiluminescence
EDTA	Ethylenediaminetetraacetic acid
e.g.	For example
EGFP	Enhanced green fluorescent protein
ER	Endoplasmatic reticulum
FITC	Fluorescein isothiocyanat
g	Gravity (9.81m/s <sup>2</sup> )
G	Guanine
GFP	Green fluorescent protein
GST	Glutathione S transferase
GTP	Guanosin triphosphate
g-tub	Gamma-tubulin

## LIST of ABBREVIATIONS

---

H/E	Hematoxylin and eosin
HEPES	N-2-hydroxyethylpiperazin-N'-2-ethansulfonacid
His	Histidine
Hpf	Hours post fertilization
HRP	Horse reddish peroxidase
Hrs	Hours
HS	Horse serum
i.e.	That is
ISH	In situ hybridization
JS	Joubert syndrome
JSRD	Joubert syndrome and related disorders
kDa	Kilo Dalton
Kb	Kilo bases
LB	Luria Bertani medium
Leu	Leucine
LiAc	Lithium acetate
M	Molar
MESAB	3-amino-benzoic acid ethyl ester
mg	Microgram
mg	Milligram
min	Minutes
ml	Microliter
ml	Milliliter
mM	Milli molar
MO	Morpholino
MRI	Magnetic resonance imaging
mRNA	Messenger RNA
MTOC	Microtubule organizing center
MTS	Molar tooth sign
MW	Molecular weight
Na <sup>+</sup> /K <sup>+</sup> -ATPase	Sodium potassium Adenosintriphosphosphatase
NBT	Nitro blue tetrazolium
OD	Optical density
o/n	Overnight
PBS	Phosphate buffered saline
PC-2	Polycystin 2
PCR	Polymerase chain reaction
PH3	Phosphorylated histone H 3
PKD	Polycystic kidney disease
PTU	Phenylthiourea
RA	Retinoic acid
RNA	Ribonucleic acid



LIST of ABBREVIATIONS

---

rpm	Rounds per minute
RT	Room temperature
RT-PCR	Reverse transcription polymerase chain reaction
s	Seconds
S	Somite
Sc <sub>o</sub>	Arl13b/ scorpion <sup>hi459</sup> protein (Danio rerio)
sco	Arl13b/ scorpion <sup>hi459</sup> gene (Danio rerio)
SDS-PAGE	Sodium dodecyl sulfate polyacrylamide gel electrophoresis
T	Thymidine
TEMED	N,N,N',N'-tetramethyldiamin
Tris	Tris(hydroxymethyl)aminomethan
Trp	Tryptophane
TUNEL	Terminal deoxynucleotidyl transferase dUTP nick end labeling
UTP	Uracil triphosphate
UTR	Untranslated region
UV	Ultra violet
V	Voltage
vHnf1	Variant hepatic nuclear factor 1
v/v	Volume per volume
WGA	Wheat germ agglutine
w/v	Weight per volume
WT	Wildtype

# 1. GENERAL INTRODUCTION

## 1.1. Human Ciliopathies

Many human diseases and syndromes with a wide spectrum of disorders whose etiologies lie in defective cilia have been classed together under the term “ciliopathy”. Ciliopathic diseases often have overlapping clinical features such as obesity, cystic kidneys and livers, polydactyly, *situs inversus*, mental retardation and retinal dystrophy. The gene products that cause ciliopathies are localized to the cilium or basal body, the anchoring structure of the cilium and when mutated result in a structural and / or functional defect of the cilium.

Cilia can be motile or non-motile, with motile cilia being able to form coordinated beating to establish fluid flow and cell motility (sperm). Motile cilia on the apical surface of airway epithelia, kidney ducts, brain ventricles or oviducts beat in a coordinated manner to push fluid in one specific direction. Non-motile cilia, also called primary cilia, are ubiquitous on almost every cell surface and were long thought of as ‘vestigial’ organelles. Only recently have primary cilia been emerging as sensory organelles, transducing extracellular signals to the intracellular space for signaling and have been shown to be involved in wnt signaling, hedgehog signaling, PCP signaling and regulation of calcium homeostasis.

## 1.2. PKD

Polycystic kidney disease (PKD) is a group of monogenetic disorders that are characterized by renal cyst development and is the most common cause for kidney failure. PKD can be inherited in an autosomal dominant form (ADPKD) or autosomal recessive form (ARPKD). ADPKD is one of the most common monogenetic disorders in humans and is diagnosed in 400-1000 live births (Torres *et al.*, 2007). ADPKD patients are characterized by development of multiple, bilateral, focal, fluid filled cysts in the kidney which lead to a gross distortion of the normal kidney architecture and in 50% of ADPKD patients will progress to end stage renal failure (ESRF) by the age of 60, requiring dialysis or organ transplants. ADPKD patients show also extra renal defects, mostly in the liver, pancreas and cardiovascular system.

ARPKD is inherited in an autosomal recessive manner and occurs with a frequency of 1: 20 000 live births and is associated with a high infant mortality rate. ARPKD is typically diagnosed *in utero*.

ADPKD shows genetic heterogeneity with 85% of cases having mutations in PKD1, however, mutations in PKD2 have been associated with a better prognosis than mutations in PKD1 (Hateboer *et al.*, 1999). PKD1 and PKD2 encode integral membrane proteins polycystin-1 and polycystin-2 respectively and mutations in either one result in ADPKD (Torres *et al.*, 1999; Calvet and Grantham, 2001; Stayner and Zhou, 2001).

ADPKD caused by mutations in either *PKD1* or *PKD2* are indistinguishable, suggesting that these two genes function in the same pathway or complex. A large number of different mutations in both genes have been identified, but the type of mutation was not shown to strongly correlate to the phenotype (Rosetti *et al.*, 2002; Magistroni *et al.*, 2003). ARPKD is caused by mutations in a single gene called *PKHD1* (Onuchic *et al.*, 2002) and the gene product is called fibrocystin.

### **1.3. Second Hit Model**

Screening of cyst lining epithelial cells for PKD1 and PKD2 respectively identified a loss of heterozygosity along other additional somatic mutations (Pei *et al.*, 1999; Qian *et al.*, 1996). This suggested that the focal cyst formation in ADPKD patients may be due to somatic second hits. The second hit model describes that in a non cystic renal epithelium a single germline mutation in either PKD1 or PKD2 is present but is not sufficient to cause cystic phenotype. A subsequent somatic mutation (second hit) in the remaining PKD allele would result in a complete loss of the normal gene function and to the development of a cystic epithelium.

### **1.4. Polycystin-1 and Polycystin-2**

PKD1 encodes polycystin-1, an extremely large integral membrane protein with 4320 amino acids. It is predicted to have 11 transmembrane domains, a short intracellular domain and an extracellular tail with multiple domains which have been associated with protein-protein and protein-carbohydrate interaction (Hughes *et al.*, 1995). The intracellular domain contains a coiled coil domain, a G-protein-binding site and multiple predicted phosphorylation sites suggesting it might be a cell-surface receptor in cell-cell

or cell-matrix signaling. PKD2 encodes a 968 amino acid protein called polycystin-2. Polycystin-2 has 6 transmembrane domains, a calcium-binding region and homology to the transient receptor potential superfamily of calcium permeable ion channels (Mochizuki *et al.*, 1996).

Polycystin-1 localizes to adhesion junctions and focal adhesion in renal epithelial cells, suggesting a role in cell-cell adhesion and cell-matrix adhesion (Foggensteiner *et al.*, 2000; Wilson *et al.*, 1999). In addition, it is expressed on the basal body and cilia where it colocalizes with polycystin-2 (Barr *et al.*, 1999; Yoder *et al.*, 2002; Pazour *et al.*, 2002). Another subcellular localization of polycystin-2 is the endoplasmic reticulum and sarcoplasmic reticulum (Cai *et al.*, 1999; Qian *et al.*, 2003).

### 1.5. Joubert Syndrome

Joubert syndrome (JS) is an autosomal-recessive human ciliopathy disorder that mainly affects the brain stem and cerebellum and is characterized by severe psychomotor delay, oculomotor apraxia, hypotonia, ataxia and rapid breathing defects. The diagnosis is typically confirmed via magnetic resonance imaging (MRI) by the presence of a patho-neurological finding called “molar tooth sign” (MTS). MTS has cerebellar peduncles and a deepened interpeduncular fossa combined with cerebellar vermis hypoplasia (Louie and Gleeson, 2005). Approximately a quarter of JS patients also has Nephronophthisis. Nephronophthisis is a genetic disorder which results from a mutation in NPHP (nephrocystin) and consists of tubulointerstitial fibrosis and cysts at the corticomedullary junction. Another group of disorders called Joubert syndrome and related disorders (JSRD) present a MTS but additional defects that are not restricted to the nervous system, e.g. polydactyly, cystic kidneys, hepatic fibrosis and retinitis pigmentosa among others. Seven genes have been identified so far to cause JSRD when mutated: AHI1 (gene product called Jouberein), MKS6, ARL13B, NPHP1, CEP290, RPGRIP1L and CC2D2A (details in chapter 2). Several of those genes are similar to those mutated in Meckel-gruber syndrome (MKS), a disease which is characterized by renal cystic dysplasia, central nervous defects, polydactyly and hepatic fibrosis.

*Arl13b/ Sco* which has been found in the classical form of JS recently (Cantagrel *et al.*, 2008) is the gene mutated in *Arl13b/ scorpion*<sup>hi459</sup> mutants in zebrafish and the mutant that is characterized in more detail in this presented work.

I will refer to the *Ar113b/ scorpion*<sup>hi459</sup> zebrafish mutant as *scorpion (sco)* for simplicity reasons throughout my thesis.

## 1.6. The Structure of Cilia

Cilia are microtubule-based, membrane-enclosed, hair-like organelles that extend from the apical cell surface into the extracellular space. The basal body is the anchor of the cilium, nucleates the microtubule axoneme and is located beneath the plasma membrane. Cilia can be present in two different forms that can be distinguished by their ultra structure: (9+2) and (9+0) axonemes which can be visualized by electron microscopy. (9+2) describes an ultra structure of nine outer microtubule doublets that are arranged in a circle and a central pair of microtubules in the middle. Generally (9+2) cilia tend to be motile, appear clustered on the surface and beat coordinately to promote fluid flow. All microtubule doublets of (9+2) cilia consist of an “A” strand (made of 13 tubulin protofilaments) and “B” tubule (made of 10 tubulin protofilaments). Additionally, each doublet contains inner and outer dynein arms, radial spokes and nexin links. (9+2) cilia are thought to be motile and primary (9+0) cilia that lack the central pair, dynein arms and radial spokes have been thought to be immotile and present as single cilia on the cell surface. Exceptions from this rule are nodal cilia which are localized in the embryonic node. Nodal cilia are solitary organelles that possess a (9+0) microtubule architecture, but possess the ability to move to create a fluid flow in the node (Nonaka *et al.*, 1998).

Two examples of the wide range of different cilia are shown in figure 1. Cilia on respiratory epithelia are responsible for the clearance of mucus from the respiratory tract and cilia on ependymal cells move cerebrospinal fluid through the spinal cord and brain ventricles. Renal cilia in humans are immotile and have a (9+0) ultra structure and only during embryogenesis have fetal kidneys been shown to exhibit (9+2) cilia transiently, which might be motile. In zebrafish, the pronephros displays (9+2) renal cilia which have been shown to be motile and to create fluid flow towards the cloaca.

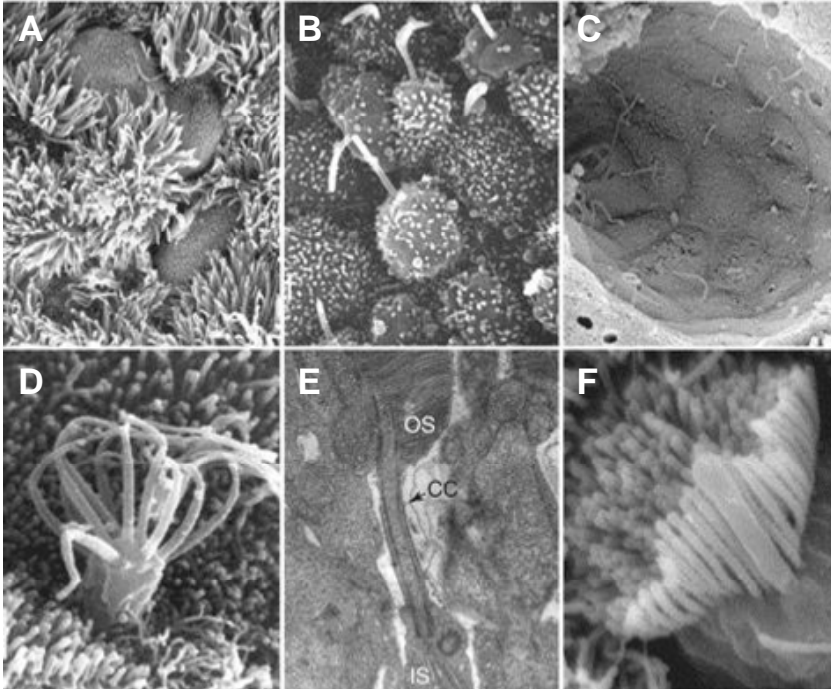


**Fig. 1: Cilia play diverse roles and are localized on various tissues.**

(A) Multiciliated cells of the respiratory tract with non-ciliated cells in between, which are mucus-secreting goblet cells. (B) Cilia of the embryonic node, which are single ciliated and responsible for directed fluid flow. (C) Cilia of the kidney duct showing cilia extending from the epithelium into the lumen of the duct. (D) Olfactory cilia. (E) Connecting cilium of a mouse rod photoreceptor cell. (F) Stereociliary bundle with kinocilium.

Picture taken from Eley *et al.*, 2005.

### 1.7. Intraflagellar Transport

The cilium is formed and maintained by addition of subunits to microtubule plus-ends in the ciliary tip which is facilitated by intraflagellar transport (IFT) and microtubule based motor proteins, such as kinesin (anterograde transport) as well as dynein (retrograde transport). The cilium does not contain any machinery for protein biosynthesis, thus relies on the constant supply of cargo (such as receptors and structural proteins) to form and maintain the cilium. IFT serves that function and shuttles between the cell body and the cilium to transport cargo to the cilium and deliver ciliary signals back to the cytoplasm. At the base of the cilium, in a region called transition zone, cargo is sorted and loaded onto motor proteins that are responsible for anterograde transport (kinesin-II). The retrograde transport is facilitated by another motor protein called dynein.

The IFT complex is a multiprotein complex (17 IFT proteins in total) that is subdivided into complexes A and B.

### **1.8. Retinal cysts and Cilia**

Cloning the mutated gene in the oakridge polycystic kidney (orpk) mouse provided the first link between cilia and cystic kidney disease. The homologue of the mutated gene in *Chlamydomonas* is called IFT88, is part of the intraflagellar transport (IFT) machinery and responsible for the formation and maintenance of the flagellum/ cilium (Pazour *et al.*, 2000; Taulman *et al.*, 2001). Orpk mice were shown to display shorter, malformed cilia as well (Pazour *et al.*, 2000, Yoder *et al.*, 2002) indicating that cilia and the regulation of the lumen diameter might be linked. Following studies indeed showed that many proteins involved in cystic diseases localize to the cilium or basal body, including polycystin-1, polycystin-2, cystin (cpk mouse), polaris, inversin as well as polycystin homologues in *C.elegans* (Barr *et al.*, 2001; Morgan *et al.*, 2002; Pazour *et al.*, 2002; Qin *et al.*, 2001; Yoder *et al.*, 2002). Another piece of evidence showing cilia as a central player for cyst formation is the finding that disruption in Kif3a, a motor subunit of kinesin-II results in a renal cystic phenotype in mice. The cystic phenotype was directly correlated to the loss of cilia; cells of the distal nephron with disrupted kif3a had no cilia and were cystic whereas adjacent cells of the proximal tubule which expressed normal kif3a, were able to form cilia and remained non cystic (Marszalek *et al.*, 1999; Lin *et al.*, 2003)

Polycystin1 and polycystin-2 act in a complex to form a channel which is thought to act as flow sensor on the cilium (Nauli *et al.*, 2003). Fig.2 describes the model of the cilium acting as a mechanosensory organell. Mechanical or flow-induced bending of the cilium induces a Ca-influx into the cell through the polycystin-2 channel complex (Praetorius *et al.*, 2001). This mechanosensory response is lost in polycystin-1 deficient cells (Nauli *et al.*, 2003), suggesting that the polycystin complex is a mechanosensitive ion channel or a true mechanosensor. Additionally, removal of cilia in vitro resulted in a failure to increase the intracellular calcium level in response to laminar flow, indicating that the cilium indeed is responsible for both sensing flow and inducing the intracellular calcium response (Praetorius *et al.*, 2003).

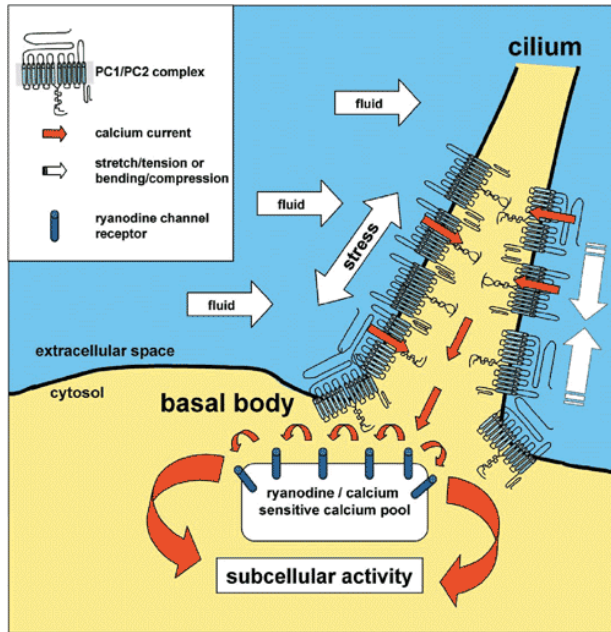


**Fig. 2: Model describing the cilium as a mechano-sensory organelle.**

Polycystin-1 and polycystin-2 form a  $\text{Ca}^{2+}$ -channel complex in the plasma membrane of the cilium. Bending or movement of the cilium during normal tubule growth triggers the channels to open and results in a  $\text{Ca}^{2+}$  influx, which is further amplified by release of intracellular  $\text{Ca}^{2+}$  stores. This can lead to inhibition of the canonical wnt signaling pathway thus anti-proliferative signals.

Picture taken from Nauli *et al.*, 2003.

## 1.7. Zebrafish Kidney

Zebrafish is an ideal model organism to study embryonic developmental questions. Embryos are transparent and develop outside of the mother animal, the fish exhibit high fecundity and can easily be manipulated via microinjections. The zebrafish pronephros represents only form of many vertebrate kidney forms that have evolved to regulate blood fluid and electrolyte homeostasis. Despite having differences in their morphology, the mammalian kidney and the zebrafish pronephros share many features at the cellular and molecular level. It is comprised of only two nephrons compared with 1 million in a mammalian kidney. Two glomeruli are fused at the midline and contain fenestrated epithelia and podocytes for ultrafiltration. Pronephric tubules emanate caudally from the glomeruli and connect to pronephric ducts that fuse at the cloaca to shunt out the filtrate.

Renal epithelial cells in zebrafish are ciliated and cilia exhibit a (9+2) microtubule architecture and are motile in contrast to mouse kidney cilia which are (9+0) and immotile. The coordinated beating of renal cilia is thought to provide a directional fluid flow towards the cloaca. The zebrafish pronephros is formed within the first 2 days of embryonic development and uses the same genes (*pax2*, *wt-1* and *vhnf1*) and same cell



types (podocytes, endothelial cells and tubular epithelial cells) to form the kidney that are used in frog, chicken or the mammalian kidney. Furthermore, genes that are mutated in human cystic kidney diseases have been identified in a large scale zebrafish mutagenesis screen and showed kidney cysts (Sun *et al.*, 2004). Interestingly most of those gene products localize to the cilium, again supporting a central role for the cilium for the maintenance of renal lumen size and epithelial integrity.

Genes that are mutated in human cystic kidney diseases, such as polycystins, have been shown to be essential for the pronephros development in zebrafish as well, showing that zebrafish is a good model organism to study kidney development and disease which might lead to further understanding nephrogenesis and the pathogenesis of renal diseases such as PKD.

## **GOALS of THESIS PROJECT**

My thesis work entails two different projects.

### **Project 1**

#### **Characterization of the Wildtype Kidney Development in *Danio rerio***

Human ADPKD is one of the most common monogenetic disorders in humans leading to kidney failure. We used zebrafish as a model organism to study PKD in the zebrafish pronephros. Zebrafish PKD mutants develop cysts during embryogenesis which are visible at 2 days post fertilization (dpf). However, not much is known about the embryonic kidney development and most studies until now were performed on the level of gene expression levels. Therefore I sought to analyze the embryonic kidney development in my first project using a custom made antibody that would allow us to visualize the developing kidney.

#### **Specific aims**

- Generate a specific marker for the intermediate mesoderm that will enable the analysis of the embryonic kidney development.
- When does the intermediate mesoderm become polarized?
- When does the intermediate mesoderm form a lumen?
- Which mechanism leads to cavitation in the zebrafish pronephros?

## Project 2

### Characterization and Functional analysis of the *scorpion*<sup>hi459</sup> Mutant

Joubert syndrome (JS) is a human disorder which mainly affects the brain; however Joubert syndrome and related disorders (JSRD) show kidney cysts and additional extrarenal malformations. Recently Arl13B was found in patients with the classical form of JS. Arl13B is an Arf-like GTPase and the causative mutation in the *scorpion*<sup>hi459</sup> (*sco*) zebrafish mutant. In this project of my thesis I sought to analyze the role of Arl13b/*scorpion* in zebrafish in detail.

There have been contradicting reports whether loss of apico-basolateral polarity leads to duct dilation and cyst formation. Furthermore, it is not clear whether hyperproliferation is a cause or consequence of duct dilation. Lastly, we conducted a functional analysis for the Scorpion protein, investigating which regions of the protein are responsible for Scorpion's exclusive expression pattern to the ciliary axoneme and testing whether it's ciliary localization is directly

#### Specific aims

- Temporal and spatial analysis of the cyst formation in *scorpion*
- Is duct dilation cause or consequence of hyperproliferation?
- Does Scorpion have functions outside the brain (JS patients show mainly brain malformations), and if so, what are the phenotypes?
- Does loss of apico-basolateral polarity lead to duct dilation and cyst formation in *scorpion*?
- Does Scorpion protein contain a cilia localization sequences?
- Is the cilia localization essential for Scorpion's functional properties?

### 3. MATERIALS

#### 3.1. *Living Materials*

##### 3.1.1. *Danio rerio*

Throughout this study *Danio rerio* in a TAB 5 and TAB 14 background were used. Embryos were obtained through natural spawning.

##### 3.1.2. *Escherichia coli*

For cloning purposes several *E.coli* bacteria were used.

<b>Competent bacteria</b>	<b>Source</b>
Top10 competent cells	Invitrogen
XL10Gold competent cells	Stratagene
Origami competent cells	Novagen

*E.coli* cells were kept at -80°C in glycerol stocks.

##### 3.1.3. *Saccharomyces cerevisiae*

For the yeast-two-hybrid system, two different yeast strains were used.

<b>Competent Yeast strain</b>	<b>Source</b>
AH109	Clontech
mAV203	Clontech

Yeast cells were kept in a glycerol stock at -80°C.

## 3.2. Chemicals and Solutions

### 3.2.1. Buffer and Media

#### 3.2.1.1. Embryo media

Reagent	Amount
NaCl	34.4 g
KCl	1.52 g
CaCl <sub>2</sub> · 2H <sub>2</sub> O	5.8 g
MgSO <sub>4</sub> · 7H <sub>2</sub> O	9.8 g
ddH <sub>2</sub> O	up to 2 L

Embryo medium was diluted with deionized water to a final concentration of 1x, dyed with Bromphenol blue (1:1000) and stored at RT.

#### 3.2.1.1. Western Blot

##### SDS loading buffer (2x)

Reagent	Amount
SDS	4 %
DTT	0.2 M
Sodium phosphate buffer, pH 7.0	10 mM
Glycerol	20 %
Bromphenol Blue	0.2 %
β-mercaptoethanol	5 %

##### Electrophoresis buffer (10x)

Reagent	Amount
Tris (Tris (Hydroxymethyl)-Aminomethan)	30.3 g
Glycin	144 g
SDS	1 g
ddH <sub>2</sub> O	Ad 1 L

Adjust pH to 8.2.

### 3. MATERIALS

---

#### Western Blot Transfer buffer (10x)

<b>Reagent</b>	<b>Amount</b>
Tris base	60.6
Glycine	288 g
ddH <sub>2</sub> O	Ad 2 L

#### Western Blot transfer buffer (1x)

<b>Reagent</b>	<b>Concentraion</b>
Tris base	25 mM
Glycine	192 mM
Methanol	20 %

For 1x transfer buffer the following reagents were pipetted:

<b>Reagent</b>	<b>Amount</b>
Transfer buffer (10x)	400 ml
ddH <sub>2</sub> O	2800 ml
Methanol	800 ml

#### Ponceau Stain Staining solution

0.5 g Ponceau S wre dissolved in 1.0 ml glacial acetic acid. Volume was adjusted to to 100 ml with MQ water. Final solution was 0.5% Ponceau/1% acetic acid.

#### TBS (Tris-buffered saline),(10x)

<b>Reagent</b>	<b>Amount</b>
Tris base	48.4 g
NaCl	160 g
ddH <sub>2</sub> O	1600 ml

Concentrated HCl was added to adjust the pH to approximately 7.8, the solution was cooled down completely. The pH was adjusted to a final of 7.5 with 6N HCl and the total volume brought to 2 L.

TBS-T (1L)

<b>Reagent</b>	<b>Amount</b>
TBS (10x)	100 ml
Tween-20	1 ml
ddH <sub>2</sub> O	900 ml

Blocking Solution

<b>Reagent</b>	<b>Amount</b>
Skin milk powder	5 g
TBST	100 ml

For 2 blots 100 ml blocking solution were prepared and stored at 4°C until ready to use.

Detection System

Enhanced Chemiluminescence (ECL) Plus Western Blotting Detection Reagents (Amersham).

**3.2.1.2. Yeast Media**YPDA:

<b>Reagent</b>	<b>Amount</b>	<b>Source</b>
Difco peptone	20 g/L	Beckton Dickenson
Yeast extract	10 g/L	Beckton Dickenson
Agar (for plates only)	20 g/L	American Bioanalytical
Adenine	0.003 %	Sigma

Autoclave and store at room temperature.

SD Minimal Base

<b>Reagent</b>	<b>Amount</b>	<b>Source</b>
SD Base	26.7 g	Clontech
DO supplement	0.6 g	Clontech

Add amino acids, autoclave and store at room temperature.

### 3. MATERIALS

---

#### TE buffer

<b>Reagent</b>	<b>Final concentration</b>
Tris	10 mM
EDTA	1 mM

The pH was adjusted to pH 7.5 with HCl.

#### Z-buffer

<b>Reagent</b>	<b>Final concentration</b>
Na <sub>2</sub> HPO <sub>4</sub>	60 mM
Na <sub>2</sub> HPO <sub>4</sub> .H <sub>2</sub> O	40 mM
KCl	10 mM
MgSO <sub>4</sub> . 7H <sub>2</sub> O	1 mM
2-Mercaptoethanol	39 mM

The Z-buffer was prepared in ddH<sub>2</sub>O and stored at RT. X-Gal was added freshly prior to conducting the assay to a final concentration of 1 mg/ ml X-Gal.

#### X-Gal Stock Solution

100 mg X-gal (5-bromo-4-chloro-3-indolyl- $\beta$ -D-galactopyranoside) were dissolved in 1 ml DMF (N,N-Dimethylformamide) resulting in a 100x stock solution The solution was stored at 4°C protected from light.

#### 50% PEG 3350

Polyethylenglycol was diluted 1:1 (v/v) with ddH<sub>2</sub>O and autoclaved briefly and stored at room temperature.

#### 40% Dextrose (w/v)

Dextrose was dissolved in ddH<sub>2</sub>O to a final concentration of 40% (w/v). autoclaved and stored at room temperature.

#### PEG/LiAc solution

PEG/ LiAc (Polyethylene glycol/ lithium acetate) solution was prepared freshly each time. The final concentration was following: 40% PEG 3350, 1x TE buffer, 1x LiAc



### 3.2.1.3. Bacteria media

#### LB (Luria Bertani) broth

<b>Reagent</b>	<b>Amount</b>
Tryptone	10 g
Yeast extract	5 g
NaCl	10 g
ddH <sub>2</sub> O	Ad 1 L

Autoclave and store at RT.

LB medium was supplemented with 50 µg/ml ampicillin or kanamycin and used for propagation of ampicillin and kanamycin resistant bacteria respectively in shake-flasks.

### 3.2.2. Immunohistochemistry

#### 3.2.2.1. Fixative solutions

##### Formalin

Diluted formalin solution in PBT (1:2.7).

##### Dent's Fixative

80% methanol

20% DMSO (dimethylsulfoxide)

##### Bouin's Fixative

70% Picric acid

25-37% Formaldehyde

5% Glacial Acetic Acid

#### 3.2.2.2. Permeabilization

##### Acetone

Pre-cooled acetone for 7 minutes at -20°C.

Proteinase K

<b>Age</b>	<b>Volume in 1ml PBT buffer</b>	<b>Incubation Length</b>
8-14 Somites	1 µl Proteinase K [10mg/ml]	2min
20-25 hpf	1µl Proteinase K [10mg/ml]	10 min
30-34 hpf	2µl Proteinase K [10mg/ml]	10 min
>48 hpf	5µl Proteinase K [10mg/ml]	10 min

**3.2.2.3. Blocking buffer**

PBT buffer with 10% horse serum, bovine serum or goat serum.

**3.2.2.4. Washing buffer**

PBT buffer

**3.2.2.5. Mounting medium**

Vecta shield hard set mounting medium

Vectorlaboratories

**3.2.3. In situ hybridization**

Anti-digoxigenin-AP, Fab fragment

Roche

NBT

1,5 % NBT (nitro blue tetrazolium) in 70 % DMF (Dimethylformamide)

Roche

BCIP

1 % BCIP (5-bromo-4-chloro-3-indolyl phosphate) In 100 % DMF (Dimethylformamide)

Roche

Blocking reagent

Roche

MABT:

MAB + 0.1% tween-20

0.1M Triethanolamine HCL, pH 8.0:

triethanolamine HCL	9.25 g
H <sub>2</sub> O	400 ml

Adjust pH to 8.0 with 10 N NaOH,  
fill with ddH<sub>2</sub>O to 500 ml

BABB:

Benzylbenzoate : benzylalcohol (2:1)

Blocking buffer:

MABT

2% Boehringer Mannheim blocking reagent

Incubate at 65 °C and cool down, store at -20°C

Add 10% serum

Hybridisation+ buffer (hyb+):

final concentration

50 % Formamide

5x SSC

50 µg/ml Heparin

1 mg/ml yeast RNA

0.1 % Tween-20

Citric acid

Hybridization- -buffer (hyb-):

Hyb+ without heparin and yeast RNA

Alkaline phosphate buffer (AP buffer):

100 mM TrisHCl pH 9.5

50 mM MgCl<sub>2</sub>

100 mM NaCl

0.2 % Tween-20

0.2 % Triton X-100

One drop of Levamisole per 5 ml AP buffer was added freshly prior to use.

### **3.2.4. Electron microscopy**

#### **3.2.4.1. Fixative solutions**

##### Fixative 1

4 % Paraformaldehyde

0.1 % Glutaraldehyde

0.1 M Hepes

##### Fixative 2

4 % Paraformaldehyde

0.1 M Hepes

#### **3.2.4.2. Staining solution**

##### Washing buffer

Phosphate buffered saline

50mM Sodium maleate buffer (pH 5.2)

##### Staining solution

2% Uranyl acetate (in maleate buffer)

##### Infiltration

Solution 1: 50 % Propylene oxide/ 50 % Epon

Solution 2: 100% Epon

### 3.3. Antibodies

#### 3.3.1. Primary antibodies

<b>Name (Host animal)</b>	<b>Dilution</b>	<b>Source</b>
Anti-Acetylated-alpha-tubulin (mouse)	1:5000	Sigma
Anti-Beta-tubulin (mouse)	1:2000	Sigma
Anti-gamma-tubulin (mouse)	1:250	Sigma
Anti-vHnf1 (rabbit)	1:250; 1:2000	Custom
Anti-phosphorylated Histone H2B (mouse)	1:1000	Upstate
Anti-scorpion (rabbit)	1:1000	Custom
Anti-BrdU (mouse)	1:100	Sigma
Anti-aPKC (rabbit)	1:200	Santa Cruz
Anti-Cdh17 (rabbit)	1:200	Custom
Anti-Cdh17 (chicken)	1:500	Custom
Anti-polycystin-2 (rabbit)	1:200	Ian Drummond
Anti-Na <sup>+</sup> /K <sup>+</sup> -ATPase (α6F) (mouse)	1:5	DHSB

#### 3.3.2. Secondary antibodies

<b>Name (Host animal)</b>	<b>Dilution</b>	<b>Source</b>
Anti-mouse-Rhodamine (goat)	1:200	Jackson immuno Lab
Anti-mouse-FITC (goat)	1:200	Jackson immuno Lab
Anti-rabbit-FITC (goat)	1:200	Jackson immuno Lab
Anti-rabbit-Rhodamine (Donkey)	1:200	Jackson immuno Lab
Anti-chicken-FITC (donkey)	1:200	Jackson immuno Lab
Anti-chicken-AMCA (donkey)	1:200	Jackson immuno Lab
DAPI	1:5000	Jackson immuno Lab
Rhodamine Phalloidin	1:800	Invitrogen
WGA-FITC	1:250	Jackson immuno Lab

### 3.4. Plasmids

Name	Insert	Vector	Source
pCS2+	-	pCS2+	Addgene
pGEX4T1	-	pGEX4T1	Clontech
pGBKT7	-	pGBKT7	Clontech
pDONR221	-	pDONR221	Nathan Lawson
pCSDest2	-	pCSDest2	Nathan Lawson
P3E-eGFPpA	-	P3E-eGFPpA	Nathan Lawson
		pEGFP	Invitrogen
pCS2-vHnf1	vHnf1	pCS2+	Zhaoxia Sun
459-eGFP	sco-eGFP	pCS2+	Zhaoxia Sun
$\Delta$ (1-25)-eGFP	sco- $\Delta$ (1-25)-eGFP	pCS2+	Sunjin Lee
$\Delta$ (20-128)-eGFP	sco $\Delta$ (20-128)-eGFP	pCS2+	Zhaoxia Sun
$\Delta$ (1-170)-eGFP	sco $\Delta$ (1-170)-eGFP	pCS2+	Sunjin Lee
GTPase-eGFP	sco $\Delta$ (195-407)-eGFP	pCS2+	Zhaoxia Sun
$\Delta$ CC-eGFP	sco $\Delta$ (195-243)-eGFP	pCSDest2	Neil Duldulao
CC-eGFP	sco-(195-243)-eGFP	pCS2+	Sunjin Lee
$\Delta$ Glu-eGFP	sco $\Delta$ (244-318)-eGFP	pCSDest2	Neil Duldulao
$\Delta$ (319-393)-eGFP	sco $\Delta$ (319-393)-eGFP	pCSDest2	Neil Duldulao
$\Delta$ (308-407)-eGFP	sco $\Delta$ 308-407)-eGFP	pCS2+	Sunjin Lee
$\Delta$ (394-407)-eGFP	sco $\Delta$ 394-407)-eGFP	pCSDest2	Neil Duldulao
T35N-eGFP	Sco(T35N)-eGFP	pCS2+	Sunjin Lee
T35K-eGFP	Sco(T35K)-eGFP	pCS2+	Zhaoxia Sun
pCS2-cmlc2	cmlc2	pCS2+	Zhaoxia Sun
pCS2-spaw	spaw	pCS2+	Zhaoxia Sun

### 3.5. Morpholino oligonucleotides

The scorpion AUG morpholino was designed to target following sequence:

5' TTTCCCCCTAAATGCTTTCACTGG 3'.

As a negative control, following control Morpholino was used:

5' CCTCTTACCTCAGTTACAATTTATA 3'

### 3.6. DNA Buffer and Reagents

#### TAE buffer (50x)

<b>Reagent</b>	<b>Amount</b>
Tris (Tris-hydroxymethyl-aminomethane)	Invitrogen
Boric acid	Stratagene
0.5 M EDTA	Novagen
ddH <sub>2</sub> O	Ad 1L

#### 0.7% Agarose gel

<b>Reagent</b>	<b>Amount</b>
Agarose	0.7 % (w/v)
TAE buffer	1x
Ethidiumbromide	0.5 µg/ml

#### Agarose Gel loading buffer (6x)

<b>Reagent</b>	<b>Concentration</b>
Glycerol	12 % (v/v)
Na <sub>2</sub> EDTA	60 mM
SDS	0.6 % (w/v)
Bromphenol blue	0.003 % (w/v)

#### DNA 1kb molecular weight ladder

1 kb ladder	Invitrogen
-------------	------------

#### PCR buffer (10x), homemade

200mM Tris, pH8.4  
500mM KCl

<u>dNTP mix</u>	Invitrogen
-----------------	------------

### **3.7. DNA and RNA Kits**

<b>Kit</b>	<b>Source</b>
QIAquick PCR purification kit	Qiagen
Quick Spin columns, G-50 Sephadex Columns for radiolabeled	Boehringer
RNA purification	Mannheim
Gel extraction Kit	Quiagen
Plasmid Maxi Kit	Quiagen
Plasmid Midi Kit	Quiagen
Plasmid Mini Kit	Quiagen
Zymoprep II Kit	Zymoresearch

### **3.8. RNA**

#### **3.8.1. In vitro transcription of capped mRNA**

Ambion mMessage mMachine Kit	Ambion
RNA polymerase buffer (10x)	NEB
RNase inhibitor	Roche
RNA CAP structure analogue 7mG(5')ppp(5')G sodium salt	NEB
Dithiothreitol (DTT)	NEB
RNA SP6 Polymerase	NEB
RNA T7 Polymerase	NEB
DNase I	Roche

#### **3.8.2. Purification of RNA**

Rneasy Mini Kit	Quiagen
-----------------	---------



### **3.9. Protein Purification**

#### **3.9.1. DEAE Blue Gel Purification**

Pre-wash buffer

0.1 M Acetic acid

1.4 M NaCl

40% Isopropanol

Adjust pH to pH3.

Running buffer

Phosphate buffered saline (PBS)

Regeneration buffer

2 M guanidine HCl in PBS

#### **3.9.2. Affinity purification**

Beads:

Glutathione-agarose

BD Biosciences

1M IPTG:

(Isopropyl- $\alpha$ -thio-Galactopyranosid)

2.5 g in 10 ml ddH<sub>2</sub>O, filtersterilized

American Biosciences

TG buffer:

0.1% Triton-X 100

1% glycerol

GST elution buffer:

50mM Tris, pH 8.0

10mM reduced glutathione

in ddH<sub>2</sub>O

Dialysis buffer:

PBS

Glutathione beads regeneration buffer 1:

0.1M Tris, pH 8.5

0.5M NaCl

0.1% SDS

Glutathione beads regeneration buffer 2:

0.1M Sodium acetate, pH 4.5

0.5M NaCl

0.1% SDS

### 3.9.3. SDS PAGE

Resolving gel 10 %

<b>Reagent</b>	<b>Volume</b>
40 % Bis/acrylamide	3.75 ml
1.5 M Tris, pH 8.8	3.75 ml
20 % SDS	75 µl
ddH <sub>2</sub> O	7.4 ml
10 % APS	50 µl
TEMED	10 µl

Stacking gel

<b>Reagent</b>	<b>Volume</b>
40 % Bis/acrylamide	490 µl
0.5 M Tris pH 6.8	1.25 ml
20 % SDS	25 µl
ddH <sub>2</sub> O	3.2 ml
10 % APS	25 µl
TEMED	5 µl

Electrophoresis buffer

<b>Reagent</b>	<b>Volume</b>
Tris	30.3 g
Glycin	144 g
SDS	1 g

### 3. MATERIALS

---

ddH<sub>2</sub>O Up to 1 l  
Adjust pH to 8.3

#### Sample buffer

<b>Reagent</b>	<b>Volume</b>
SDS	6% (w/v)
Glycerin	30% (v/v)
Tris-Buffer 1 M, pH 6,8	200 mM
Bromphenolblue	0,005% (w/v)
β-Mercaptoethanol	2-5% (v/v)

#### Protein Standards

All blue protein standard	Biorad
Dual color protein standard	Biorad

### 3.9.4. Coomassie Staining

#### SDS-fixative

<b>Reagent</b>	<b>Volume</b>
Methanol	600 ml
Acetic acid	700 ml
ddH <sub>2</sub> O	Ad 10 L

#### Coomassie Blue Staining Solution

<b>Reagent</b>	<b>Volume</b>
Methanol	410 ml
Glacial Acetic Acid	70 ml
Coomassie Blue	0,125 g
ddH <sub>2</sub> O	510 ml

**Coomassie Blue Destaining Solution**

<b>Reagent</b>	<b>Volume</b>
Methanol	410 ml
Glacial Acetic Acid	70 ml
ddH <sub>2</sub> O	510 ml

**3.9.5. Protein kits**

Protein Assay kit	Pierce
ECL Plus western Blot Detection System	GE Healthcare
DryEase mini-Gel Drying System	Invitrogen

**3.10. Yeast-two-hybrid libraries****Matchmaker cDNA libraries**

<b>Organism</b>	<b>Tissue source</b>	<b>Age</b>
Zebrafish (mixed sex)	Entire fish	1 month old
Human (mixed sex)	Kidney	Fetus, gestational week 21-30

**3.11. TUNEL Assay**

<b>Reagent</b>	<b>Volume</b>	<b>Source</b>
TUNEL enzyme	5 $\mu$ l	Roche
TUNEL label	45 $\mu$ l	Roche

**3.12. Chemicals**

<b>Chemicals</b>	<b>Source</b>
Acetic acid	T.J.Baker
Acetic anhydride	VWR
Acrylamide/Bisacrylamide	American Bioanalytical
Adenine Hemisulfate	Sigma
Agar	American Bioanalytical
Agarose	American Bioanalytical
Ammonium sulfate	T.J.Baker
Ampicillin	VWR
Ammonium persulfate	T.J.Baker
Bacto yeast extract	Beckton Dickenson
Boehringer Mannheim Blocking reagent (BMB)	Boehringer Mannheim
Bouin fixation fluid	VWR
BrdU	Sigma
Bromphenol Blue	T.J.Baker
2,3-Butanedione monoxime (BDM)	T.J.Baker
Calcium chloride dihydrate	T.J.Baker
Coomassie Blue	T.J.Baker
Dextrose	T.J.Baker
Difco yeast nitrogen base w/o amino acids	Beckton Dickinson
DO-supplement (-Ade, -His, -Leu, -Trp)	Clontech
DMF [Dimethylformamide]	T.J.Baker
DMSO [Dimethylsulfoxide]	T.J.Baker
EDTA, [Ethylenediaminetetraacetic acid], 0.5M, pH 8.0	American Bioanalytical
Ethanol	Pharmaco-Aaper
Ethidium Bromide	VWR
Formalin buffered, 10%	Harleco
Formamide	VWR
Glutathione, reduced	GE Healthcare
Glycerol, anhydrous	American Bioanalytical

### 3. MATERIALS

---

Glycine	American Bioanalytical
Hematoxylin	VWR
Hepes	American Bioanalytical
L-Histidine	Sigma
Hydrogen Peroxide	EMD
Immobilized Glutathione	Fisher
Isopropyl- $\beta$ -D1-thio-Galactopyranoside (IPTG)	American Biosciences
Kanamycin	VWR
Lavamisole Solution	Vector
L-Leucine	Sigma
Lithium Acetate	Sigma
Lithium Chloride	EMP
Magnesium Chloride	T.J.Baker
Magnesium Sulfate	T.J.Baker
$\beta$ -Mercaptoethanol	American Bioanalytical
MESAB (3-amino-benzoic acid ethyl ester)	Sigma
Methanol	T.J.Baker
Methylcellulose	Sigma
Methylene Blue	T.J.Baker
Milk, instant, non-fat dry	Carnation
Minimal SD base	Clontech
Nonident P40	Sigma
Normal Horse Serum	Vector
10x PBS	American Bioanalytical
Potassium Acetate	T.J.Baker
Potassium Chloride	T.J.Baker
Potassium Phosphate	T.J.Baker
Phenol red	Sigma
Ponceau S	Sigma
2-Propanol	T.J.Baker
Proteinase K	VWR
PTU (1-Phenyl-2-thiourea)	Sigma
SDS (Sodium dodecyl sulfate)	American bioanalytical

Sodium Acetate	J.T.Baker
Sodium Azide	VWR
Sodium Chloride	T.J.Baker
Sucrose	VWR
TBE buffer, (10X)	Ambion
TEMED	American Bioanalytical
[N,N,N',N'-Tetramethylethylenediamine]	
Triethylamine	Mallinckrodt
Triethanolamin	Sigma
Tris [Hydroxymethyl] aminomethane	American Bioanalytical
Triton-X 100	T.J.Baker
L-Tryptophane	Sigma
Tween-20	Sigma
Vectashield Hard Set mounting medium	Vector

### **3.13. Other consumables**

Cell culture tube	BD-Falcon
Centricon Plus20	Millipore
Centrifugal device	Beckman
Centrifuge tube	Beckman
Eppendorf tubes	Dot scientific
Falcon Tube	BD-Falcon
JB-4	Polysciences
Kim wipe	Kimberley Clarke
Microsep 10K omega	Pall
Nanosep 10K omega	Pall
Nitrocellulose Membrane	Bio Rad
Parafilm "M"	Pechiney Plastic Packaging Company
PCR tubes	USA scientific
Pipettes	Eppendorf
Pipette tips	USA Scientific Inc.

Sllide-A-Lyzer dialysis cassette	Thermo scientific
Weighing paper	Fischer scientific
Whatman paper 3MM	Whatman
Vacuumfilter	Millipore

### **3.14. Equipment**

70°C incubator	VWR
Borosilicate glass capillaries	World precision instruments
Centrifuges	Sorvall
Centrifuge 5810R	Precision
Cryostat	Leica
Developer cassette	Amersham
Flaming/brown micropipette puller, model P-97	Sutter instruments
Hot plate/ magnetic stirrer	VWR
Microtome	Reichert
PCR machine	Biorad
pH meter	Beckman
PV830 Pneumatic Pico Pump Injector	WPI
Scale AB 54-S	Mettler Toledo
Scale PB 3001-S	Mettler Toledo
Tabletop centrifuge	VWR
Vortex, mini	VWR
Waterbath	Precision
Western Blot transfer tank	Biorad
Yeast Culture Shaker	Sartorius
Zebrafish Incubator	VWR

### **3.15. Microscopes**

<b>Microscopes</b>	<b>Source</b>
Zeiss Axioplan2 imaging	Zeiss
Leica, KL 1500 LCD	Leica



### 3. MATERIALS

---

Nikon, Eclipse, E800

Nikon

Zeiss axiovert 200

Zeiss

Tecnai 12 Biotwin

FEI

## **4. METHODS**

### ***4.1. Zebrafish maintenance***

#### **4.1.1. Zebrafish Lines**

Wildtype TAB5 or TAB14 zebrafish were maintained and raised as described in Westerfield, 1995 (The Zebrafish Book, Eugene, OR: University of Oregon Press). Embryos were kept in embryo medium at 28.5C and staged according their somite number or hours post fertilization (hpf) described in Kimmel, *et al.*, 1995. *sco*<sup>hi459</sup> were obtained from a large insertional mutagenesis screen (Sun *et al.*, 2004).

#### **4.1.2. Anaesthetizing Zebrafish**

Adult zebrafish need to be anaesthetized before being fixed or having the tail fins clipped. MESAB (3-Amino-benzoic acid ethyl ester or Tricaine is a very common fish anesthesia. MESAB was diluted in fish system water from a 25x stock solution. Fish were put into MESAB solution for the shortest period of time possible to immobilize them and after fin clipping returned into the water. The fish recovered within couple minutes and were swimming.

#### **4.1.3. Fin Clipping of Zebrafish**

Starting at the age of 6 weeks progeny from heterozygous fish were genotyped. In order to obtain genomic DNA a tail biopsy was taken. After anaesthetizing the fish it was placed onto a piece of parafilm and a small piece of the tail fin was clipped off with a blade. The fin clip was placed into a labeled eppendorf tube containing lysis buffer and the fish put into a small beaker where it remained until the genotype was determined. To avoid cross contamination the parafilm was replaced every time and the blade cleaned carefully as well.

#### **4.1.4. Extracting Genomic DNA from Tail Biopsy**

The eppendorf tube containing 50  $\mu$ l lysis buffer, proteinase K and a piece of the tail fin was incubated rotating at 55°C for 2 hours or overnight. 1 $\mu$ l of the concentrated tail DNA was diluted into 20  $\mu$ l water. The samples were incubated at 94°C for 15 minutes to inactivate proteinase K. 1  $\mu$ l of the diluted sample was used in a standard PCR reaction. Afterwards the genotype was determined by running the PCR sample on a DNA agarose gel.

#### **4.2. Live embryo imaging**

Embryos were grown to the desired stage and manually dechorionated if necessary. Embryos older than 24 hpf were incubated in MESAB. Embryos were positioned on glass depression slides and light microscopy was performed on Leica, KI 1500 LCD microscope.

##### **4.2.1. Methylcellulose**

Methylcellulose is convenient for mounting live embryos for observation or taking images under the compound microscope due to the fish being immobilized and the compound being non toxic. A small amount of 3% methylcellulose (in fish water) was dabbed onto a depression slide and the dechorionated embryo was placed on top of it. A little bit of fish water was used to cover the embryo to prevent dehydration. After images were taken or the phenotype observed, the fish was put back into a petri dish with fish water.

#### **4.3. Fixation**

##### **4.3.1. Formalin**

Even though most antibodies perform better with Dent's fixed tissues, some antibodies, especially vHnf1, show superior performance in formalin fixed tissues. Every antibody has to be tested empirically.

The formalin fixative was freshly prepared each time. 1 part formalin solution was diluted with 1.7 parts of PBT buffer. Embryos were incubated in formalin fixative for 2 hours at room temperature followed by incubation in pre cooled acetone for 7 minutes at -20°C to permeabilize the tissue. The embryos were washed in PBT buffer three times for 5 minutes each time and dechorionated manually under the dissecting microscope using forceps.

#### **4.3.2. Dent's**

Dent's fixative is a mixture of 80% methanol and 20% Dimethyl Sulfoxide (DMSO). The fixative was stored at -20 °C. Zebrafish were anaesthetized in MESAB and fixed in pre cooled Dent's fixative overnight at -20 °C. Embryonic zebrafish do not need to be anaesthetized and were put into Dent's immediately. The next day the fixative was replaced with 100% methanol and fish were stored at -20°C until the experiment was conducted.

#### **4.3.3. Bouin's**

For histological analysis it is important to preserve as much of the morphology as possible and Bouin's fixative was used for that purpose. Embryos were fixed with Bouin's fixative at room temperature overnight. Bouin's does stain the embryos yellow. This yellow staining was removed with five washes each five minutes with PBT buffer.

#### **4.3.4. Dehydration of embryos**

Fixed embryos can be dehydrated and stored for a long time (several years) at -20C. In order to dehydrate embryos they were incubated in 50% methanol in PBT for five minutes, then in fresh methanol and stored in methanol at -20°C. To rehydrate embryos they were taken out of the freezer and rehydrated through 50% methanol in PBT for five minutes, followed by a wash in PBT for another five minutes.

## **4.4. Histological Analysis**

### **4.4.1. Embedding of Zebrafish**

#### JB-4

JB-4 Embedding Kit is a polymer embedding material that allows a high level of morphological detail. It was used to embed embryos that were sectioned for histological analysis.

#### JB-4 Infiltration Solution

JB-4 infiltration solution was prepared freshly every time it was used. 0.64 g of JB-4 Plus catalyst powder was added to 10 ml of JB-4 Plus solution A in a Falcon tube. The tube was rocked for one hour at room temperature or until the powder was completely dissolved. Fish embryos were incubated in the JB-4 infiltration solution rocking for 2 hours at RT.

#### JB-4 Embedding Solution

For each batch of embryos 1 ml fresh infiltration solution and 67  $\mu$ l JB-4 plus solution B were mixed in an eppendorf tube and kept on ice to delay polymerization. The JB-4 mold was filled with cold embedding solution. After several embryos were added, they were aligned and orientated using the tip of a needle. The polymerization process requires anaerobic conditions therefore the molds were covered with parafilm and capped tightly. The molds were left undisturbed over night at room temperature to ensure proper polymerization. The next day the embryos were removed from the mold and cut to 4  $\mu$ m sections with the microtome.

### **4.4.2. Hematoxylin and Eosin staining**

Hematoxylin and eosin staining was performed on JB4- sections of Bouin's fixed embryos.

#### **4.5. Transmission electron microscopy**

Embryos were grown to the 4 dpf and processed as follows. Embryos were fixed in Karnovsky's glutaraldehyde fixative for 1 hour at room temperature, washed in cacodylate buffer, post fixed in Palade's osmium for 1 hour at room temperature and washed again in cacodylate buffer. Embryos were stained with Kellenburger and dehydrated through a series of ethanol dilutions. Embryos were subsequently infiltrated with propylene oxide and embedded in Epon. Ultra thin sections were obtained with a Leica Ultracut UCT cryo-ultramicrotome, post stained with uranyl acetate and lead acetate, and viewed on a Tecnai 12 Biotwin electron microscope.

#### **4.6. In situ hybridization**

##### **4.6.1. Preparation of RNA Probe**

10 µg PCS2-cmlc2 and PCS2-southpaw plasmid were linearized for 2 hours at 37°C with an appropriate restriction enzyme at the 5' end.

<b>Reagent</b>	<b>Volume</b>
Plasmid DNA	10 µg
Reaction Buffer [10x]	10 µl
Restriction Enzyme	5 µl
ddH <sub>2</sub> O	Ad 100 µl

5 µl of the total reaction volume were run on a DNA agarose gel to verify complete linearization and the reaction purified using the QIAquick PCR purification kit (Quiagen).

##### **4.6.2. Synthesis of Digoxigenin-Labeled RNA Probe**

The RNA probe was synthesized in an in vitro transcription reaction and set up the following way:

<b>Reagent</b>	<b>Volume</b>
Linearized template DNA	1-2 µg
NTP mixture [10mM]	2 µl

RNA Polymerase Buffer [10x]	2 $\mu$ l
T3 or T7 Polymerase	1.5 $\mu$ l
RNase Inhibitor	0.5 $\mu$ l
ddH <sub>2</sub> O	ad 20 $\mu$ l

The eppendorf tube was incubated for 2 hours at 37 C. Afterwards 1 $\mu$ l DNaseI was added and incubated for 30 minutes. The probe was cleaned up using a Quickspin G-50 Sephadex Column (Boehringer Mannheim) or Mini Quickspin column. Afterwards a sample was run on a DNA agarose gel to check the product size and the the concentration determined by spectrophotometry. 500 $\mu$ l of hybridization buffer were added and stored at -20°C. The titer of the working solution had to be determined with each preparation.

#### 4.6.3. Used In situ probes:

cmlc2 (cardiac myosin light chain2)

spaw (southpaw)

#### 4.6.4. Tissue preparation

Zebrafish embryos were fixed overnight at 4°C in fresh diluted formalin solution (1 part formalin: 3 parts PBT). The next day the embryos were washed twice in PBT buffer, manually dechorionated and washed again in PBT three times. The tissues were dehydrated by placing them in 50% methanol (in PBT buffer) followed by 100% methanol and stored at -20C overnight. The embryos were rehydrated through 50% methanol (in PBT) followed by PBT.

Afterwards all embryos older than 24 hours were digested with Proteinase K the following way:

<b>Age</b>	<b>Volume in 1ml PBT buffer</b>	<b>Incubation Length</b>
8-14 Somites	1 $\mu$ l Proteinase K [10mg/ml]	2min
20-25 hpf	1 $\mu$ l Proteinase K [10mg/ml]	10 min
30-34 hpf	2 $\mu$ l Proteinase K [10mg/ml]	10 min
>48 hpf	5 $\mu$ l Proteinase K [10mg/ml]	10 min

Proteinase K was washed out carefully with PBT buffer and the embryos were refixed for 15 minutes in diluted formalin fixative (1 part formalin, 3 parts PBT). Afterwards the embryos were washed briefly in deionized water and incubated in 0.1M Triethanolamine hydrochloride (pH 8.0)/ 0.25% Acetic Anhydride solution for 30 minutes at RT. This was followed by three washed with PBT buffer, each 5 minutes.

#### **4.6.5. Hybridization**

The embryos were prehybridized in Hyb- buffer for 5 minutes at 70°C and transferred to hyb+ buffer for 30 minute incubation at 70°C. The probe was allowed to denature at 70°C for 5 minutes and the embryos hybridized with the probe overnight at 70°C.

#### **4.6.6. Washes and Detection of Signal**

The next day preheated 50% formamide/2x SSC/ PBT buffer was added to the embryos and incubated twice at 70°C for 30 minutes. The solution was replaced by 2x SSC/ PBT buffer and incubated for 10 minutes at 70°C followed by two additional incubation steps of 0.2x SSC/ PBT for each 30 minutes at 70°C. The tissues were then washed with MABT buffer at RT for 5 minutes twice. The embryos were blocked with MAB/BMB blocking solution for 30 minutes at RT. Then the embryos were incubated with AP-conjugated anti-digoxigenin antibody (1:3000) in blocking solution for 2 hours at RT, washed for 30 minutes in MABT/ 10% serum and washed in MABT overnight. The next morning the embryos were incubated twice (each 5 minutes) with alkaline phosphatase buffer and then stained for 30 minutes (for cmlc2) and overnight (for spaw) with NBT/BCIP (5 µl NBT [100mg/ml], 3.75 µl BCIP [50mg/ml] in 1ml AP buffer) and washed after staining had development three times with PBT buffer.

The embryos were fixed in formalin for 20 minutes to stop the reaction and cleared in glycerol. Light images were taken with the Leica, KL1500 LCD microscope.



#### **4.7. Cryostat sections**

Embryos at the desired stage were fixed in either Dent's fixative or in Formalin solution as described before. After rinsing in PBT buffer, the embryos were incubated in 10% sucrose until they sank to the bottom of the eppendorf tube and transferred into 25% sucrose solution over night at 4°C or at room temperature for one hour. The embryos were then transferred into a mold, covered with OCT mounting medium and oriented using needles. To freeze the blocks, the molds were placed into Isopentene solution, swimming in a liquid nitrogen bath. Cryostat cross sections were cut at 12-14  $\mu\text{m}$  thickness and the region of the embryo verified under the light microscope. Sections were dried at room temperature and stored at -20°C.

For immunocytochemistry on cryostat sections, sections were thawed and rehydrated at room temperature with PBT and blocked in 10% HS/ PBT for 30 min, RT. The rest of the protocol is described in detail in the following paragraph.

#### **4.8. Microtome sections**

Embryos were embedded in JB-4 resin overnight as described under 4.4.1. The specimen is visible in the JB-4 polymer block since the resin is colorless. Excess of the resin was roughly trimmed with a razor blade and further trimmed with a glass blade. The embryo sample cut with a microtome into 4  $\mu\text{m}$  thin sections. Droplets of filtered water were pipetted onto a glass slide (12 droplets per slide) and each section was transferred onto a droplet after cutting using a forceps. The surface tension of the water droplet will straighten the tissue and minimize wrinkling. After 12 sections were placed onto the glass slide, the slide was transferred onto a warm plate to facilitate quick evaporation of the water.

#### **4.9. Immunostaining**

Immunostainings were performed on formalin or Dent's fixed embryos. After fixation in formalin fixative, embryos were incubated in pre cooled acetone for 7 minutes at -20°C. Acetone was washed out carefully with PBT buffer (3 times, 5 minutes). After adding PBT embryos were blocked 30 minutes at room temperature using PBT buffer containing either 10% horse serum, normal goat serum or fetal bovine serum. The

primary antibody was incubated in blocking solution for either 2 hours at room temperature or overnight at 4°C. The primary antibody was washed out with PBT buffer (5 times, 20 minutes each) and incubated with an appropriate secondary antibody in blocking solution for 2 hours at room temperature. In order to avoid bleaching of the fluorescent secondary antibody the samples were shielded from light with aluminum foil from this step forward. Afterwards the secondary antibody was washed out carefully with PBT buffer as well (5 times, 20 minutes each).

To mount embryos, zebrafish were manually deyolked in a Petri dish with PBT buffer using two forceps. Up to 1 dpf old embryos were flat mounted onto a glass slide on their ventral side. In order to reduce unspecific background, embryos 2 dpf and older were dissected along the midline and the head removed. The remaining tissue was flatmounted on the ventral side as well. For analysis of 5 dpf old embryos, some kidney ducts were completely microdissected manually from the embryonic tissue to reduce signal of axon tracts which are abundant throughout the embryo at this stage.

Vecta shield mounting solution was used to reduce bleaching of the fluoreophores and embryos were covered with a glass cover slip. The slides were allowed to dry and harden at room temperature in the dark before analyzing them under a microscope.

## ***4.10. Microinjection***

### **4.10.1. Preparing Injection plates**

To immobilize zebrafish eggs and facilitate good orientation of the egg, it is very helpful to have a microinjection plate which holds the eggs neatly in place. 20ml of 1% agarose were poured onto a petri dish and a injection mold was carefully placed on top. The agarose was allowed to solidify and the molds removed. The finished plates were sealed with parafilm and stored at 4°C.

### **4.10.2. Pulling Micropipettes**

Having a good injection needle is the key for microinjections. Needles with a long shank tend to break more easily and can bend on, rather than penetrate, the chorion. Needles with a short shank are sturdier, but can be damaging to the embryos as they tend to thicken quite quickly. Needles somewhere in between give the best results. After the

micropipette puller was allowed to warm up, micropipettes were pulled using borosilicate glass capillaries using following settings:

Pressure=500, Heat=640, Pull=50, Velocity=100, Time=150, Loops=0. Micropipettes were pulled and stored until ready to use for microinjections.

#### **4.10.3. Injection Volume**

To ensure that the same amount of mRNA or Morpholino was injected each time, the concentration as well as the injection volume was determined and kept constant in each experiment. To measure the injection volume one droplet of mineral oil was put onto a micrometer and injected with the dyed morpholino or mRNA. Since the sample is hydrophilic and mixed with phenol red it will stay separated from the surrounding mineral oil sinking slowly to the bottom of the micrometer. The diameter of the sinking droplet was measured and kept constant for each experiment by adjusting the pressure and duration of injection.

#### **4.10.4. Injection of zebrafish embryos**

Around 50 zebrafish eggs were put into the lanes of the injection plate and covered with a little bit of embryo medium to prevent dehydration. After filling the micropipette each egg was injected through the chorion into the yolk cell. In zebrafish, egg activation and fertilization initiate cytoplasmic streaming towards the animal pole, thus allowing mRNA or morpholinos being delivered from the yolk cell into the animal cell without damaging the animal cell by injection. In case of rescue experiments morpholinos were coinjected along with mRNA into the egg yolk.

After the injections were done all eggs were put into a clean petri dish with fresh embryo medium and incubated at 28.5°C.

#### **4.11. Morpholinos**

Morpholinos are synthetic molecules of usually 25 bp in length that are structurally similar to the natural DNA. Morpholinos share standard nucleic acid bases (A, C, G, T) with DNA but use a different backbone. Instead of deoxyribose and ribose rings characteristic of DNA and RNA respectively, morpholinos use morpholine rings and are linked through phosphorodiamidate groups instead of the anionic phosphodiester linkage

found groups (Summerton and Weller, 1997). Morpholinos are highly specific and have a high affinity for mRNA. They can block translation initiation (by targeting the 5' UTR through the first 25 bases of coding sequence) and modify splicing events (by targeting splice junctions).

Morpholino antisense oligonucleotides were designed to target the translation initiation site (targeting the the 5' UTR through the first 25 bases of coding sequence) resulting in a protein knock down. For each target mRNA a start site morpholino (AUG morpholino) and a control morpholino were used. A 2 mM stock solution was prepared and stored at -20°C. The working solution concentration had to be determined empirically. The morpholino was diluted in sterile water and 0.025 % phenol red solution. Prior to injections the morpholino working solution was heated up to 65°C for 5 minutes and snap cooled on ice immediately to ensure complete denaturation. The tube was briefly spun and stored on ice after the experiment was conducted and returned to the -20°C freezer immediately afterward. 0.5 nl of either scorpion or control morpholinos were injected per embryo at a concentration of 1 mM.

#### **4.12. In vitro transcription of mRNA**

mRNAs have a characteristic 5'-cap which consists of a terminal 7-methylguanosine residue that is linked through a 5'-5'-triphosphate bond to the first transcribed nucleotide. 5'-cap structures are critical for recognition by the ribosome and protection from RNases. In vitro transcribed RNA mimics most eukaryotic mRNA found in vivo because it has a 7-methyl guanosine cap structure at the 5' end and can be used to globally overexpress a certain gene of interest in the zebrafish embryo.

To obtain large amounts of mRNA two different protocols for in vitro transcription were followed: a) Sun Lab protocol for in vitro transcription of mRNA and b) Ambion mMessage mMachine Kit.

##### **4.12.1. Linearization of Plasmid DNA**

The plasmid DNA has to be linearized downstream of the target before setting up the in vitro transcription since circular plasmid templates will lead to long, heterogenous RNA transcripts. Since all cDNAs were subcloned in a pCS2+ plasmid, NotI was used to cut 3' after the cDNA insert. The whole sample was loaded on a DNA agarose gel to verify that

it was completely linearized. The single band was cut out, gel purified and the concentration determined by spectrophotometry.

#### 4.12.2. Sun Lab Protocol for in vitro Transcription

The following components were pipetted into an eppendorf tube and incubated at 42°C for 3 hours.

<b>Reagent</b>	<b>Volume</b>
Linearized DNA	2.5 µg
RNA polymerase buffer (10x)	5 µl
RNase inhibitor	1µl
CAP analogue	12.5 µl [10mM]
ATP, GTP, UTP, CTP each	0.25 µl [100mM]
DTT	1 µl [1M]
RNA polymerase (SP6)	2µl
ddH2O	Add to final volume of 50 µl

After the first incubation step 2µl of fresh SP6 RNA polymerase were added and incubated for 2 additional hours at 42°C. Afterwards 2µl of DNaseI were added and incubated to 37°C for 30 minutes. The reaction was purified using a RNA purification column and 2µl run on a fresh DNA agarose gel.

#### 4.12.3. Ambion mMessage mMachine Kit

All reagents of the kit were thawed and kept on ice except the 10x reaction buffer which has to be stored at room temperature. To avoid coprecipitation of the reaction buffer and template DNA, the reaction was assembled at room temperature. In an eppendorf tube the following components were assembled in the order they are stated:

<b>Reagent</b>	<b>Volume</b>
ddH2O	to final volume of 20 µl
2x NTP/CAP	10 µl
reaction buffer (10x)	2 µl

linearized template DNA	1 $\mu$ g
SP6 enzyme mix.	2 $\mu$ l

The eppendorf tube was pipetting up and down gently and microfuged briefly to collect the reaction mixture at the bottom of the tube. Afterwards the tube was incubated at 37°C for 2 hours. To remove the template DNA 1  $\mu$ l TURBO DNase was added and incubated for 15 minutes at 37°C.

#### ***4.13. Recovery and Purification of RNA***

To purify probes for in situ hybridization or mRNA after in vitro transcription, Quickspin G-50 Sephadex Columns for radiolabeled RNA purification and Mini Quickspin columns were used.

The RNA purification column was mixed, the cap and bottom tip removed and inserted into an empty eppendorf tube. A gentle spin at a tabletop centrifuge (1000g, 1 min) was done to pack the column. The column was transferred into a fresh eppendorf tube. The in vitro transcribed mix was loaded onto the column and spun at 1000g for 4 minutes to elute the RNA. 2  $\mu$ l of the purified RNA were run on a freshly prepared DNA agarose gel to determine purity and approximate concentration. The accurate concentration was measured by spectrophotometry. The purified RNA sample was aliquoted and stored at -80°C.

#### ***4.14. Recovery and Purification of DNA***

##### **4.14.1. PCR purification Kit**

DNA fragments were purified from a restriction digestion using the QIAquick PCR purification kit from Quiagen. 5 volumes of PB buffer were added to the reaction mixture and mixed thoroughly. The mixture was put on a column and spun for 30 seconds, maximal speed on a table top centrifuge. The flow through was discarded and the column washed with 750  $\mu$ l PE buffer. The column was spun again for 30 seconds and the flow through discarded again. Another dry spin at maximal speed was done to dry the column. EB elution buffer was added to the middle of the column and after 1 minute eluted into a fresh eppendorf tube with a short spin at maximal speed.

#### 4.14.2. Gel Extraction Kit

The DNA band was visualized under a UV-lamp and excised using a sharp scalpel. The Gel was mixed with 3 volumes of QG buffer and heated at 50°C until the gel was dissolved. Afterwards the solution was vortexed and mixed with 1 volume of isopropanol, loaded onto Quiaquick spin column and centrifuged for 1 min, at RT. The flow through was discarded and the column washed with PE buffer twice. The flow through was discarded again and the column spun again to remove all traces of buffer. The plasmid was eluted with 40 µl EB buffer which was allowed to stand on the column for 2 minutes before spinning. The eluate was reloaded onto the column and spin again.

#### 4.15. Standard PCR

Reagent	Volume
Water	13 µl
10x PCR Buffer	2 µl
50mM MgCl <sub>2</sub>	0.8 µl
10mM dNTP	0.8 µl
10uM Primer1	0.8 µl
10uM Primer2	0.8 µl
Taq Polymerase	0.8 µl
Diluted DNA Solution	1 µl

One sample without DNA template as well as one without Primer and Template were used as negative controls.

The PCR program heat activated the polymerase by heating the samples up to 95°C for 15 minutes. Denaturation of DNA followed at 95°C for 30 seconds. The annealing phase was performed at an appropriate temperature for 30 seconds. Elongation of the PCR product was done at 72°C for 30 seconds. The cycle was repeated for 30 times and completed by a 10 minute synthesis phase. All samples were kept at 4°C until further processing.

#### **4.16. Cloning**

The *vHnf1* PCR fragments as well as the backbone vector PGEX4T1 were digested with EcoRI and XhoI, loaded on to DNA agarose gel (0.8%) and run at 100V. DNA bands were excised and purified using the gel extraction kit. The *vHnf1* PCR fragments were ligated with the digested pGEX4T1 vector (1 $\mu$ l digested vector plasmid, 7 $\mu$ l PCR amplificate, 1 $\mu$ l T4 ligation buffer, 1 $\mu$ l T4 ligase).

#### **4.17. Sequencing**

In order to verify the sequence of cloned plasmids, samples were send to the W.M. Keck facility at Yale University. In a bar code labeled sequencing tube 19.2  $\mu$ l water, 0.8  $\mu$ l primer (10  $\mu$ M) and 4  $\mu$ l DNA were mixed and send for sequencing. Sequences were blasted in pubmed and aligned using DNASTAR software.

#### **4.18. RT-PCR analysis**

RT-PCR was performed on isolated RNA at indicated developmental stages using TRIzol reagent (Invitrogen). The RNA (2-5ug) was used to produce complementary DNA (cDNA) with random hexamers (Invitrogen), oligo dT (Invitrogen), or gene specific primers in separate reactions. Scorpion expression was analyzed by RT-PCR using 50-100ng of the resulting cDNA. Actin ( $\alpha$ -cardiac actin) was amplified as control. PCR conditions were as follows: 2.5 units of platinum Taq DNA polymerase in the supplied buffer (Invitrogen), 2mM MgSO<sub>4</sub>, 0.2 mM of each deoxyribonucleotide triphosphate (dNTP), 0.2  $\mu$ M of each Primer. PCR amplification was as follows: 94° for 5 min, 94° for 30 s, 60° for 30 s, 72° for 60s, for 35 cycles, then 72° for 10 min. RT-PCR amplicons were analyzed on a 2-3 % agarose gel by ethidium bromide staining and fragments were then cloned, amplified and isolated before sequencing to confirm the presence of the transcript.

#### **4.19. Heat shock transformation of competent cells**

Homemade chemically competent E. coli cells and DH10B cells were used for plasmid expression and Origami or XL-10Gold respectively for protein expression. All cells were



stored at  $-80^{\circ}\text{C}$ , thawed quickly and stored on ice. 50  $\mu\text{l}$  of competent cells were mixed with up to 10  $\mu\text{l}$  of the DNA solution and incubated on ice for 30 minutes. The cells were heat shocked at  $42^{\circ}\text{C}$  for 90 seconds (45 seconds for origami cells) and the tubes returned on ice for another 2 minutes. 200  $\mu\text{l}$  of prewarmed LB medium was added and the reaction tube was incubated at  $37^{\circ}\text{C}$  shaking for one hour. 100  $\mu\text{l}$  were plated onto an LB agar plate with appropriate antibiotics and incubated at  $37^{\circ}\text{C}$  overnight. Afterwards the LB agar plate was screened for colonies.

#### **4.20. Glycerol stocks**

Transformed bacteria and yeast can be stored for prolonged periods in glycerol containing media at  $-80^{\circ}\text{C}$ . Bacteria were grown overnight in 3 ml LB medium containing appropriate antibiotics. Auxotroph yeast cells were grown overnight in liquid SD medium lacking one of the essential aminoacids. 0.5 ml of the o/n culture were added to 0.5 ml of 80 % sterile glycerol, vortexed and frozen and stored at  $-80^{\circ}\text{C}$ .

##### **4.20.1. Recovery from Glycerol stock**

With a sterile pipette tip a little bit of the frozen glycerol stock was scraped off and streaked onto the agar plate.

#### **4.21. Purification of Plasmid DNA**

##### **4.21.1. Plasmid Mini Purification**

After overnight incubation of the agar plates at  $37^{\circ}\text{C}$ , single colonies were picked to inoculate 3 ml of LB containing the appropriate antibiotics in conical plastic tubes. The cultures were incubated shaking at 300 rpm at  $37^{\circ}\text{C}$  overnight.

The next morning 1.5 ml of the cell suspension was centrifuged to harvest the cells (table top centrifuge, max speed, 1 minute). The supernatant was discarded. 150  $\mu\text{l}$  of P1 buffer was added and the cell pellet resuspended by pipetting up and down. 150  $\mu\text{l}$  of P2 lysis buffer was added and tubes were inverted multiple times followed promptly by adding 150  $\mu\text{l}$  P3 neutralization buffer. Tubes were inverted several times again. After

spinning for 5 minutes on the table top centrifuge (max speed) the supernatant was added to a fresh eppendorf tube containing 900  $\mu$ l ethanol. The tubes were mixed briefly and spun again for 2 minutes. The supernatant was poured off and the DNA pellet washed with 75 % ethanol. Another last spin of 2 minutes was followed by aspirating off all remaining ethanol. The pellet was air dried on the bench top and resuspended in 20 EB buffer with 20  $\mu$ g RNase.

#### **4.21.2. Plasmid Maxi Purification**

In order to isolate and purify larger amounts of plasmid the Qiagen Plasmid Maxi Purification Kit was used. 3 ml LB medium containing appropriate antibiotics were inoculated with a single bacteria colony or a tiny amount of the glycerol stock and incubated for 8 hours, shaking at 37°C. In the afternoon 1 ml of the starter culture was expanded in 500ml LB containing antibiotics and incubated shaking at 37°C, overnight. The following morning the cells were harvested (spin at 6000g, 15 min, 4°C) and resuspended in 10 ml P1 buffer. The cells were lysed by adding 10 ml of P2 buffer and inverting the tube multiple times and incubation at RT for 5 min. 10 ml P3 buffer were added to neutralize the reaction and again the tube was inverted multiple times to mix the solution. The tube was then incubated on ice for 20 min and the precipitates removed by centrifugation (20.000g, 30 min, 4°C). The supernatant was removed immediately and loaded onto a funnel lined with filter paper to remove remnants of precipitates. A Quiagen-tip 500 was equilibrated with 10 ml QBT buffer. The flow through containing the DNA plasmid was applied to the column and allowed to enter the resin by gravity flow. The tip was washed twice with 30 ml QC buffer each time and the DNA eluted with 15ml QF buffer in a polycarbonate tube. Dna was precipitated by adding 10.5 ml isopropanol and collected at the bottom of the tube by spinning (15.000g, 30 min, 4°C). The supernatant was discarded, the pellet washed carefully with 75% ethanol and the the tube centrifuged again (15.000g, 10 min, 4°C). The supernatant was discarded again and the pellet allowed to air dry. The DNA pellet was dissolved in a suitable volume of water (200-500  $\mu$ l). The concentration and purity were determined by spectrophotometry and a sample was run on an agarose gel.

#### **4.22. Agarose Gel Electrophoresis**

Agarose gel electrophoresis is an easy way to separate DNA fragments by their size. DNA is negatively charged at neutral pH due to its phosphate backbone and will migrate towards the positive pole (anode) when an electric potential is placed. The relationship between charge and size of the DNA is constant, i.e. linear doublestranded DNA fragments show a linear correlation between the decadic logarithms of the fragment lengths and the relative distance it traveled in the gel. 0.8-1 % agarose gels with 0.5 µg/ml ethidium bromide were run at 100V in TAE buffer. DNA fragments were visualized under UV light.

#### **4.23. Expression and Purification of GST-Fusion-proteins**

Small Scale: In order to express and purify recombinant GST-Fusion-Proteins and test whether the recombinant protein is water soluble, GST-Fusion-Proteins were expressed on a small scale. XL-10-Gold cells or origami cells were transformed with pGEX4T1-vHnf1<sub>245-438</sub> and pGEX4T1-vHnf1<sub>704-881</sub>.

5 ml of LB medium with 50 µg/ml Ampicillin (LB-Amp) were inoculated with transformed XL-10-Gold or origami cells and grown overnight at 37°C. The culture was diluted 1:20 with fresh LB-Amp and incubated at 37°C until OD<sub>600</sub> reached 0.6. Protein expression was induced by adding IPTG to a final concentration of 0.5 mM to half of the culture. Hourly samples of induced and uninduced samples were collected and the cells were incubated to 3 hours in total. The cells were collected (spin the cells at 8000 rpm, 4°C) and resuspended in 20 µl sample buffer (2x). All samples were either boiled for 5 min for whole lysate sample or purified with glutathione beads and followed by SDS-PAGE.

The bacterial pellet (after 3 hours of protein expression) was resuspended in 500 µl buffer A containing 2 mg lysozyme, 0.5 µl benzonase and PMSF (to 2 mM). The solution was inverted several times and incubated at room temperature (RT) for 15 minutes on a slow shaker. 500 µl lysis buffer were added, followed by another incubation (5 min., RT) and centrifugation step (10.000 rpm, 20 min.). To precipitate the proteins the supernatant was mixed with 25 µl glutathione beads which were prewashed with TG buffer and incubated with slow agitation for 10 min at RT. After washing with TG buffer

three times using a small syringe the sample was mixed with equal volume of SB buffer (2x), boiled and spun briefly and analyzed with SDS-PAGE.

Large scale: The chosen recombinant proteins which were water soluble and were expressed at sufficient levels were expressed on a large scale to send out for antibody production as well as affinity purification later on.

## **4.24. Peptide Antibody**

### **4.24.1. Generation of the Peptide**

Two highly antigenic regions of vHnf1 were used to generate the *vHnf1* antibody.

Primer:

Primer for vHnf1<sub>245-439</sub>: EcoRIF-245 and XhoIR439

Primer for vHnf1<sub>704-881</sub>: EcoRI704 and XhoIR881

A cDNA clone of PCS2-vHnf1 was used as template. The fragments were amplified with a standard PCR reaction. The amplicons were cut, purified and subcloned into pGEX-4T1 vectors. The peptides were generated and purified with methods described before.

1 mg of each antigen vHnf1<sub>245-439</sub> and vHnf1<sub>704-881</sub> respectively were mixed and send to Sigma Genosys for antibody production where two rabbits were immunized and 6 bleeds were sent back. Bleeds were tested on wildtype embryos for specific, nuclear, signal in the intermediate mesoderm.

### **4.24.2. Storage of Serum**

Serum was aliquoted and stored at -80°C. To the working antibody solution glycerol was added to a final concentration of 50 % and the tube stored at -20°C.

### **4.24.3. Test of Antibody**

24 hours old zebrafish (24hpf) were fixed in either Dent's fixative (overnight) or formalin fixative (2hrs at RT or overnight at 4 °C) and washed with PBT buffer three times. Zebrafish were permealized with acetone (-20°C, 7min) and washed with PBT three times for 10 min each. Afterward unspecific sites were blocked (10% Horse serum, fetal bovine serum or normal goat serum in PBT, 30 min, RT) and incubated with diluted

antisera from each rabbit (1:1000, in blocking solution, RT, 3 hours). After incubation was done the fish were washed with PBT five times for 20 minutes each.

The secondary antibody coupled to a fluorophore was diluted 1:200 in blocking solution and incubated 2 hours at room temperature followed by washing with PBT buffer (five times for 20 minutes each).

#### **4.25. DEAE Affi-Gel Blue Gel purification**

DEAE Affi-Gel Blue gel is a bifunctional affinity/ionexchange chromatography matrix. Part of it functions as an ionic, hydrophobic, or sterically active binding site for proteins with dinucleotide folds, such as albumin. The other part contains a diethylaminoethyl functional group which functions as an anion exchanger and will bind proteins with isoelectric points higher than the pH of the mobile phase. Chromatography on DEAE Affi-Gel Blue gel was used as an initial step towards purifying the serum when the whole serum did not allow a satisfying signal/noise ratio in immunohistological stainings.

##### **4.25.1. Preparing Blue Gel Column**

5ml of blue gel were poured onto a 50 ml column and washed with 5 volumes of prewash buffer. Since the blue gel has an excess of dye the wash will elute residual dye which might be eluted in serum protein fractions. Then the blue gel was washed with 7 volumes of water followed by 2 volumes of 1.4 M NaCl. The column was equilibrated with 3 volumes of PBS.

##### **4.25.2. Purifying Serum on Blue Gel**

1ml of the first bleed as well as 1ml of the sixth bleed of the rabbit (ID number 778) were applied onto the blue gel column and eluted with 2 volumes of PBS. The effluents were collected to test via immunohistochemistry and further purify.

##### **4.25.3. Ammonium Sulfate Precipitation**

Saturated ammonium sulfate solution was added to the blue gel effluent to a saturation of 45% and incubated rotating at 4°C for one hour. Afterwards the solution was split into

two tubes and collected by centrifugation (4000 rpm, 10min, 4°C). The supernatant was discarded and the pellet containing the antibody resuspended carefully in 2 ml PBS.

#### **4.25.4. Dialysis**

Dialysis is a simple process in which small solutes diffuse from a solution with high concentration to a low concentration solution across a semipermeable membrane until equilibrium is reached. Smaller solutes and fluid pass through the membrane while retaining larger molecules. A dialysis chamber was chosen depending on sample volume as well as molecular weight. The protein sample which was to be was loaded into a dialysis prewettet dialysis chamber using a 5 ml syringe and 20G11/2 needle. After the sample was loaded the syringe was used to remove all the air out of the dialysis chamber. A styrofoam floating device was added to the dialysis chamber and it was dialysed in 2 l of PBS with a magnetic stirrer overnight at 4°C. The next morning air was added into the chamber to facilitate complete removal of the sample with a syringe.

#### **4.26. Bugbuster**

To isolate proteins on a small scale a bugbuster kit was used. The extraction was performed as follows: 3 ml were inoculated and incubated overnight at 37°C, the overnight culture was diluted 1:20 in fresh medium and grown for 1 hour. The solution was divided in two tubes, one was activated with IPTG, the other was not and they were incubated for another 2 hours at 37°C, shaking. Cells were spun down at 4000 rpm for 20min., the supernatant was discarded and the remaining pellet was transferred into eppendorf tubes. Cells were incubated at -80 °C for 5 min, thawed at room temperature and mixed with 500 µl bug buster reagent, including 0.5 µl benzonase. The tube was incubated at room temperature on a rotating mixer for 20 minutes, spin on tabletop centrifuge at 4°C for 1 min, the supernatant was removed and spun again for 20 min at 4°C; the pellet was kept on ice. 25 µl of 50 % prewashed glutathione beads were added to the supernatant from the second spin and incubated at room temperature for 5 min. the supernatant was discarded. TG buffer was added, the beads resuspended gently and spun again for 1 min, the supernatant was discarded again.

25  $\mu$ l 2X SDS sample buffer was added and the sample boiled for 5 min. 50 $\mu$ l of 2x SDS sample buffer was added to the saved pellet, resuspended and boiled as well. Samples were spun briefly and 10  $\mu$ l loaded onto SDS gels.

For a large scale protein extraction the same protocol was used but modified for bigger volumes to accommodate the starting volume of 1 liter. 50 ml bugbuster were used for 1 liter bacterial solution.

#### **4.27. Protein Purification on Immobilized Glutathione**

Immobilized glutathione beads were used to purify peptides. The procedure was performed as follows:

The cell lysate was filtered through a funnel lined with filter paper. 1 ml of glutathione slurry was loaded onto a column, washed with 5 volumes TG buffer, the cell lysate was applied onto the column and the flow-through reapplied twice onto the column. The column was washed with 5 ml cold TG buffer 3 times. The column was closed, 500  $\mu$ l elution buffer added and incubated for 1 min. The eluate was collected. The elution procedure was repeated several times and the eluates collected in separate eppendorf tubes. The protein recovery was measured by OD<sub>280</sub> and using Ponceau S staining on a small droplet on a nitro cellulose membrane.

##### **4.27.1. Glutathione beads regeneration**

5 bed volumes of regeneration buffer 1 were added, followed by 5 volumes of water, then 5 volumes of regeneration buffer 2 were applied and finally 5 volumes of water again.

##### **4.27.2. Aqueous Coupling of Affi Gel**

Affi-Gel 10 and Affi-Gel 15 are activated immunoaffinity supports that react with primary amino groups of proteins. Ligands with free alkyl or aryl amino groups will couple spontaneously with Affi-Gel10 or Affi-Gel 15 supports and replace the N-hydroxysuccinimide group and form a stable amide bond.

In order to affinity purify vHnf1 whole serum Gst purified vHnf1 peptides were coupled with Affi-Gel 10 and Affi-Gel 15. 500  $\mu$ l Affi-Gel 10 and 500  $\mu$ l Affi-Gel 15 were mixed in an eppendorf tube and washed 3 times with cold deionized water to remove isopropanol. Gst-purified vhnf1 antigen vHnf1<sub>245-438</sub> and vHnf1<sub>704-881</sub> were added to the affi-Gel mix and coupled at 4°C (4 hrs while slowly rotating). Afterwards 150  $\mu$ l of 1 M Ethanolamine HCl (pH 8) was added to block any active ester sides. The gel cake was transferred to a column and washed with cold deionized water.

#### **4.27.3. Purifying Serum on Affi Column**

The column which contained the bound antigen to beads was washed with 10 bed volumes of 10 mM Tris (pH7.5), then washed with 10 bed volumes of 100 mM glycine (pH 2.5), washed with 10 bed volumes of 10 mM Tris (pH 8.8). The column was calibrated with 10 mM Tris (pH 7.5) to the pH 7.5.

The blue gel purified serum was passed through the column three times. The column was washed with 20 bed volumes 10 mM Tris (pH 7.5), then with 20 bed volumes 500 mM NaCl, 10 mM Tris (pH 7.5). The elution was done using 10 bed volumes of 100 mM glycine (pH 2.5) and the eluate collected in a tube containing 1 bed volume of 1 M Tris (pH 8.0). The column was washed with 10 mM Tris (pH 8.8) until the pH reached 8.8. The second elution step was performed using 10 bed volumes of 100 mM triethylamine (pH 11.5), the eluate was collected in a tube containing 1 bed volume of 1 M Tris (pH 8.0). The antibody fractions were pooled and dialyzed against PBS overnight at 4°C.

#### **4.28. TUNEL Assay**

The TUNEL kit allows detection of apoptotic cells by a method called terminal deoxynucleotidyl transferase dUTP nick end labeling (TUNEL). In order to label apoptotic cells in embryos, embryos were fixed with formalin at the desired developmental stage, treated with acetone and with 0.1 % triton x-100 solution for 15 minutes. Embryos older than 1 dpf were treated with proteinase K. Standard immunohistochemistry with a vHnf1 antibody was performed as preciously described. Afterwards 45  $\mu$ l of TUNEL label and 5  $\mu$ l of TUNEL enzyme were mixed and embryos were incubated at 37°C for 1 hour. Embryos were then washed with PBT, flat mounted and analyzed under a fluorescent microscope. For analysis of apoptosis in tissue



sections, cryosections were rehydrated in PBT for 10 minutes at room temperature, blocked for 10 minutes at room temperature (PBT, 10% HS) and incubated in a mixture of 45  $\mu$ l of TUNEL label and 5  $\mu$ l of TUNEL enzyme for 1 hour at room temperature in a humid chamber. Afterwards, the sections were washed with PBT three times for 20 minutes each and mounted with vectashield.

#### **4.29. BrdU Proliferation Assay**

Embryos at the desired age were manually dechorionated and placed into a glass dish containing ice cold 10 mM BrdU (5-bromo-2-deoxyuridine) solution in embryo medium. The dish was kept on ice during a 20 minute incubation time. BrdU was washed out with embryo medium multiple times and embryos were incubated at standard temperature (28.5°C) in fresh embryo medium for one hour. Embryos were then fixed in formalin as described before. Using 2N HCl solution embryos were permeabilized for 1 hour at room temperature and then washed with PBT. Standard immunohistochemistry followed using an anti-BrdU antibody and vHnf1 antibody.

#### **4.30. SDS PAGE**

##### **4.30.1. Embryo tissue preparation**

Embryos were processed the following way before running the proteins on a SDS-PAGE: 30 embryos were manually deyolked in a petri dish in ice cold embryo medium. Embryos were transferred to an eppendorf tube and the supernatant removed. 50  $\mu$ l 2X SDS sample buffer was added and the tissue homogenized on ice using a microfuge pestle until a homogenate was obtained. Afterwards 1  $\mu$ l fresh DTT and 1  $\mu$ l fresh  $\beta$ -mercaptoethanol were added and the sample boiled for 5 min. The eppendorf was spun briefly and 10  $\mu$ l were loaded onto an SDS PAGE.

##### 10% Resolving gel (15 ml total):

For 2 mini gels:

<b>Reagent</b>	<b>Volume</b>
40 % Bis/acrylamide	3.75 ml

1.5 M Tris, pH 8.8	3.75 ml
20 % SDS	75 $\mu$ l
ddH <sub>2</sub> O	7.4 ml
10 % APS	50 $\mu$ l
TEMED	10 $\mu$ l

The first 4 ingredients were mixed first, APS and TEMED were added last and the gel poured immediately. Isopropanol was layered on top of the gel. After the gel had hardened, isopropanol was washed out with water, water remnant were cleaned up filter paper.

#### Stacking gel:

<b>Reagent</b>	<b>Volume</b>
40 % Bis/acrylamide	490 $\mu$ l
0.5 M Tris pH 6.8	1.25 ml
20 % SDS	25 $\mu$ l
ddH <sub>2</sub> O	3.2 ml
10 % APS	25 $\mu$ l
TEMED	5 $\mu$ l

#### **4.30.2. Coomassie Staining**

The SDS-Gel was fixed for 15 minutes in SDS-Fixative (500 ml Methanol, 700 ml acetic acid, water ad 10 L) on a shaker at RT. The fixative was replaced with Coomassie Blue staining solution and incubated shaking overnight at RT. The next morning the SDS-Gels were destained in destaining solution until the background weakened and washed in water three times for 5 min each time. Afterwards the gel was dried using a Gel-Dry Kit.

#### **4.30.3. Gel Drying**

After SDS-gels were stained and destained with Coomassie blue, gels were washed three times for two minutes each in deionized water on a rotary shaker at room temperature. The water was replaced with 35 ml fresh Gel-Dry drying solution,

equilibrated for 15 minutes and trimmed. Two sheets of cellophane were equilibrated with Gel-Dry drying solution (20 seconds) and the SDS-gel carefully sandwiched between the cellophane sheets using the Dry-Ease drying frame. All air bubbles were gently pushed out and wrinkles smoothed out. The drying frame was lifted, excess drying solution shaken off and the gel dried upright over night at room temperature.

#### **4.31. Western Blot**

After the SDS-PAGE was completed, the stacking gel was removed from the resolving gel, the resolving gel trimmed and equilibrated briefly in transfer buffer along with a 0.2  $\mu\text{m}$  nitrocellulose membrane, the sponges and filter paper. The transfer sandwich was assembled while all parts were submerged in buffer. The transfer tank was filled with transfer buffer and a stir bar and the whole tank embedded in an ice bucket with ice. The transfer was performed overnight in the cold room at 15 V or for 2 hours at 350 mA. Afterwards the membrane was removed and the orientations marked and the efficiency of transfer checked with Ponceau S, then destained in water and stored airtight at 4°C until ready for immunoblotting.

The immunoblot was performed as follows: the membrane was blocked using 5 % fat-free milk powder, 1 hour at RT with gentle rocking, the membrane was rinsed in TBST, the primary antibody was incubated for 1 hour at RT, diluted in TBST. Then the membrane was washed in TBST and incubated in secondary HRP-antibody for 1 hour at RT, diluted in TBST (1:4000). The membrane was washed again and processed with the ECL western blot detection kit (Amersham). 2ml of solution A and 50  $\mu\text{l}$  of solution B were mixed and the membrane incubated with the ECL mixture for 2 minutes at RT. Afterwards, the membrane was drained from excess ECL solution, placed onto film and developed.

#### **4.32. Live imaging of cilia beating**

Scorpion and wildtype embryos were incubated in 75  $\mu\text{M}$  phenylthiourea (PTU) starting at day 1 to prevent pigment formation. The image analysis was performed at 3 dpf and 5 dpf. Embryos were immobilized and the heart beat was stopped using 50 mM 2,3-

Butanedione monoxime (BDM) and 0.02 % Tricaine in 4 % methyl cellulose. The embryos were positioned in a mold and placed oblique, slightly dorsally, to prevent interference of the yolk sac. The anterior and medial region were imaged taking 200 frames /second for 1 second intervals. The movie was then analyzed by slowing down the beat frequency to 10 frames/second.

### **4.33. Yeast two hybrid assay**

Scorpion was subcloned into the pGBKT7 bait vector from matchmaker 3 system (Clontech, Mountain View, CA). The pGBKT7-sco was transformed into *S. cerevisiae* strain AH109 and *S. cerevisiae* strain mAV103 respectively. Transformants were selected on yeast drop out media plates lacking tryptophan. A positive colony was grown up and transformed with two different cDNA libraries: a 1 month old whole zebrafish cDNA library and a human, embryonic kidney cDNA library. Colonies were selected on drop out media lacking adenine, histidine, leucine and tryptophan (for AH109 cells) and lacking uracil, histidine, leucine and tryptophan and adenine (for mAV103 cells) and grown at 30°C for one week. X-gal filter assays were performed to determine lacZ activation.

#### **4.33.1. Yeast Transformation**

The small scale transformation was performed as follows:

1 ml of YPDA or SD-Trp medium was inoculated with colonies 2–3 mm in diameter, vortexed vigorously and the culture expanded into 50ml YPDA or SD-Trp. The cells were incubated at 30°C overnight, shaking at 200 rpm until the stationary phase was reached ( $OD_{600} > 1.5$ ). The culture was diluted 1:10 to reach an OD of  $OD_{600}$  up to 0.2–0.3. Then the culture was grown for 3 hours and the OD was measured. Cells were collected by spinning at 1,000 x g for 5 min at RT, the supernatant was discarded, the pellet was suspended in TE. The cells were spun again at 1000 g at room temperature and the pellet resuspended in Lithium acetate in TE. 350 ng of library cDNA was added along with 200 µg of salmon sperm carrier DNA. 100 ml of yeast competent cells were added to the mixture and mixed by vortexing, then 600 µl PEG/LiAc solution were added, mixed

and incubated at 30°C for 1 hour. Then 70 µl of DMSO were added, the cells gently mixed and heat shocked for 15 min in a 42°C water bath. Cells were cooled down on ice for 1–2 min, spin down again and the supernatant removed. The cell pellet was resuspended in TE buffer and different dilution series plated to calculate the transformation efficiency.

#### 4.33.2. Test of Transformation Efficiency

100 µl of the transformation were plated onto SD agar plates that will select for the desired transformants. Different dilutions, such as 100 µl of a 1:1000, 1:100, and 1:10 dilutions were plated on 100-mm SD agar plates.

Plates were incubated upside-down for several days at 30°C until colonies appeared. To calculate the cotransformation efficiency, the colonies (cfu) growing on the dilution plate from that has 30–300 cfu were counted and the efficiency calculated as follows:

$$\frac{\text{cfu} \times \text{total suspension vol. } (\mu\text{l})}{\text{Vol. plated } (\mu\text{l}) \times \text{dilution factor} \times \text{amount DNA used } (\mu\text{g})} = \text{cfu}/\mu\text{g DNA}$$

#### 4.33.3. X-Gal Filter Assay

All colonies from the read out plate as well as positive and negative controls were transferred to a nitrocellulose membrane and placed onto a piece of floating aluminum foil in a liquid nitrogen bath to gently freeze the colonies and avoid cracking of the membrane. Afterwards it was placed on top of a filter paper that was soaked with X-Gal containing buffer Z. The petridish was sealed with parafilm to avoid aspiration of the buffer and incubated at 37°C. The strongest positive control developed a blue color reaction after 30 min, but mostly the colonies and weaker controls needed up to 8 hours to show a blue signal.

Interacting clones were identified by isolating the plasmid, sequencing it and using a BLAST sequence analysis tool.

#### **4.33.4. Yeast Zymo-prep II for isolation of plasmids**

In order to isolate plasmids from yeast, the Zymoprep II Kit (Zymoresearch) was used. Single colonies were picked from a fresh plate, resuspended in 200  $\mu$ l Solution 1 including 3  $\mu$ l Zymolase solution and incubated for 1 hour at 37°C. 200  $\mu$ l solution 2 were added and the tubes vortexed. After adding 400  $\mu$ l solution 3 and carefully mixing the tubes, the eppendorf tubes were centrifuged on a tabletop centrifuge at maximum speed for 3 minutes. The supernatant was transferred to a Zymo Spin I column and centrifuged again (30 seconds, max. speed, RT). The flow through was discarded and the column washed by adding 550  $\mu$ l washing buffer and centrifuging again (2 minutes, max. speed, RT). The flow through was discarded and the column placed into a fresh eppendorf tube. Plasmid DNA was eluted with 10  $\mu$ l water and a 30 second spin.

# **Project 1**

## **Characterization of the Embryonic Kidney Development in *Danio rerio***

## 5.1. INTRODUCTION

Much of our genetic knowledge about kidney development comes from studies in mice. These studies are usually limited to the development of the metanephric kidney but several genes essential for murine kidney development that show a distinctive expression patterns have been shown to play roles in other embryonic kidney forms, including the pronephros and mesonephros.

The zebrafish pronephros is generated from an undifferentiated mesenchymal clump of cells that undergoes mesenchymal to epithelial transition (MET) to form the pronephros. The pronephros forms within the first two days of development and can be divided into three major subunits: the pronephric ducts, tubules and glomeruli. Transcription factors and signaling molecules share similar expression patterns in zebrafish and kidneys of higher vertebrates. Furthermore, areas of the intermediate mesoderm fated to become the glomerulus, tubule or duct can be defined as sequential anterior-to-posterior subdomains of the intermediate mesoderm that roughly correspond to the expression domains of *wt1*, *sim1*, *pax2* and *vhnf1* (Fig. 3).

### 5.1.1. *Wilm's tumor suppressor (WT1)*

Wilm's tumor suppressor gene (WT1) is one example and was initially isolated as the gene mutated in pediatric nephroblastoma (Call *et al.*, 1990; Gessler *et al.*, 1990). It is expressed during embryogenesis in the urogenital system in humans and mice which strongly correlates with its role during nephrogenesis (Pritchard-Jones., 1990; Armstrong *et al.*, 1993). WT1 gene encodes a zinc finger transcription factor, whose expression is regulated by Pax2, Pax8 (Dehbi *et al.*, 1996; Fraizer *et al.*, 1997 ; McConnell *et al.*, 1997) and by itself (Rupprecht *et al.*, 1998). Mice lacking WT1 fail to form kidneys and the urogenital system (Kreidberg *et al.*, 1993) due to a failure of the ureteric bud to grow out of the nephric bud.

### 5.1.2. *Pax2*

Another early marker for the kidney is Pax2 which is expressed in the urogenital system during development (Dressler *et al.*, 1990). Pax2 is a transcription factor containing a homeobox DNA-binding domain. Pax2 null mice fail to develop kidneys (Torres *et al.*, 1995). The nephric duct forms only partially and is degenerated later while the



mesonephric and metanephric mesenchyme fail to form an epithelium. The *noi* mutant (*no isthmus*) is mutated in a *pax2* homologue in zebrafish and fails to form tubules, leaving only the glomerular and duct region intact (Majumdar *et al.*, 2000). Similarly to WT1 mutations, mutations in the Pax2 gene have been found in humans. Patients with mutations in PAX2 develop renal-coloboma syndrome affecting the renal system and the optic fissure (Sanyanusin *et al.*, 1995).

### **5.1.3. *vHnf1***

Variant hepatic nuclear factor 1 (*vHnf1* also known as Hnf1 $\beta$ , LF-B3 and Tcf2) is a homeobox transcription factor that was also found to be expressed in the urogenital system. *vHnf1* is highly homologous to *Hnf1* (*Hnf1 $\alpha$* ). Both have overlapping but distinct expression patterns. Human patients with mutations in *vHnf1* were linked to MODY5 (maturity onset diabetes of the young, type 5) and glomerulocystic kidney disease (GCKD) (Horikawa *et al.*, 1995; Nishigori *et al.*, 1998; Lindner *et al.*, 1999; Bingham *et al.*, 2001). MODY5 patients are characterized by pancreatic beta-cell dysfunction and an early-onset renal disease. GCKD is a renal disease that predominantly affects the glomerulus which develops cystic dilations of Bowman's space and the anterior tubule. *vHnf1* appears to play an important role during embryogenesis and kidney development in particular. *vHnf1* has been shown to be important for the proper expression of genes involved in polycystic kidney disease (PKD), such as PKD2 (mutated in ADPKD) and Pkhd1 (mutated in ARPKD) and renal specific knock outs of *vHnf1* lead to a severe cystic phenotype at birth.

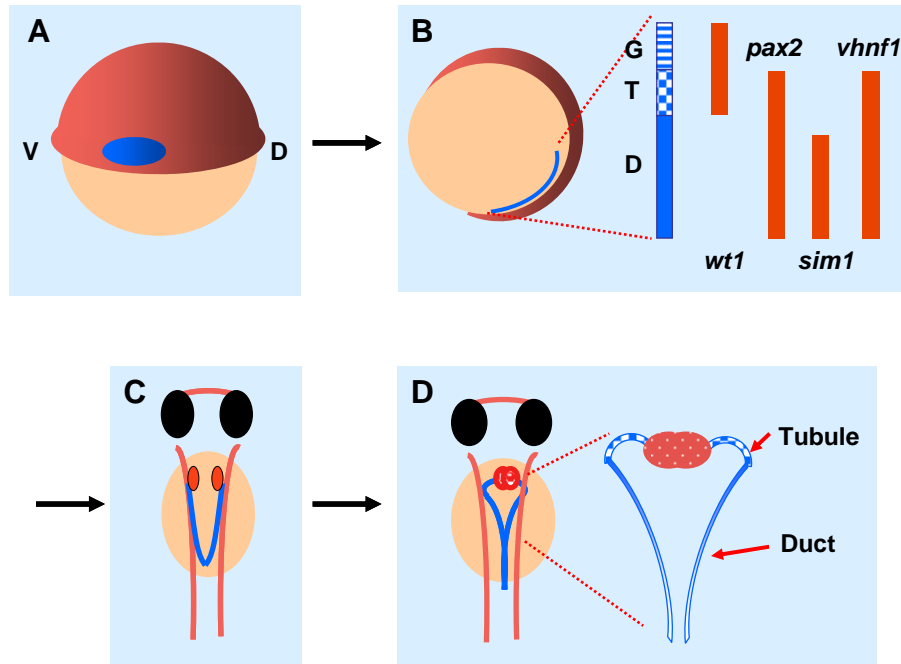


**Fig.3: Schematic development of the zebrafish kidney and expression pattern of kidney specific transcription factors.**

(A) At early gastrulation a undifferentiated clump of cells is localized between the dorsal and ventral part of the embryo. (B) during early somitogenesis the bilateral intermediate mesoderm expresses different transcription factors, such as wt1, pax2, sim1 and vHnf1. (C) At 24hpf, glomeruli begin to migrate towards the midline and fuse around 50hpf (D) resulting in a pair of nephrons with fused glomeruli at the midline which are connected to the pronephric duct via tubular segments. (Adapted and modified from Z. Sun).

#### 5.1.4. Mesenchymal-to-Epithelial Transition

As schematically depicted in Fig. 3, an undifferentiated clump of cells undergoes many changes to form the pronephros within 2 days. The intermediate mesoderm is a thin stretch of cells on both sides of the embryo that can be labeled with markers for different transcription factors, e.g. pax2 and vHnf1. Interestingly, the cells are fated to become a specific region of the future pronephros; the most anterior part of the intermediate mesoderm will give rise to the glomerulus, posterior structures give rise to the tubules and duct. At 24hpf, glomeruli begin to migrate towards the midline where they fuse. The pronephric ducts are connected via tubules with the glomeruli and are responsible to convey the filtrate to the cloaca.

### **5.1.5. Renal Epithelial Polarity**

Normal renal epithelial cells are highly differentiated and possess apical and basolateral membranes which show distinct lipid and protein compositions. In addition, they extend a hair like organelle called a cilium into the lumen from the apical membrane. Cysts in the kidney can form when normal tubulogenesis is impaired or when the cell loses its potential to maintain this highly differentiated state, which can be induced for example by ischemia (Calvet *et al.*, 1995). Additionally, hyperproliferation and unregulated apoptosis are known to be involved in renal cystic phenotypes. The formation of polarized epithelia requires specific cellular processes. The golgi apparatus and centrosomes are known to reposition themselves between the nucleus and the apical membrane. Thus centrosome localization is widely used as a read out for epithelial polarity. In our study we examined the centrosome orientation to determine if cells polarized correctly.

### **5.1.6. Mechanisms of Lumen Formation**

Many organs contain tubes and tubules that are used for fluid and cell transport and act as physiological barriers between different compartments. The formation of tubes can occur via very different mechanisms leading to a wide variety of tubules that differ in size and shape. Examples of tubular organs include the vascular system, the lungs, kidneys, pancreas, gut, mammary and salivary glands as well as the heart and central nervous system during early developmental stages. Several mechanisms for tube formation exist. An epithelial sheet might roll up and close, resulting in formation of a tube. This mechanism is used to generate much of the neural tube and primitive gut in higher vertebrates. An alternative mechanism is the creation of a lumen within a solid structure by vesicle fusions. The accumulation of fluid is thought to create the lumen. This process is called cavitation, canalization or lumenization and found in parts of the female reproductive tract (Crosby and Hill, 1962) and in exocrine glands, where solid epithelial buds form tubules of cells. Understanding the molecular and cellular events that underlie tubule formation and maintenance is very important as many human diseases, including arteriosclerosis and cystic kidney disease arise from defects in tubular architecture.

### 5.1.7. Planar Cell Polarity (PCP)

Planar cell polarity (PCP) describes a cell's or organ's polarity orthogonal to its apical-basolateral axis in a single plane. This phenomenon controls the actin-dependent planar organization of structures in a wide range of settings, including *Drosophila melanogaster* wing hairs (Adler *et al.*, 2004) and the lamellipodia of cells engaged in morphogenetic cell movements. A well studied example of planar organization is convergent extension (CE) during vertebrate gastrulation. During CE lateral groups of cells converge towards the midline and intercalate, resulting in a mediolateral narrowing and antero-posterior elongation of the embryo (Shih and Keller, 1992; Topczewski, 2001; Wallingford *et al.*, 2000; Fanto *et al.*, 2004; Karner *et al.*, 2006). The non canonical wnt signaling pathway has been shown to be an important mediator for CE and PCP thus it is sometimes called PCP signaling pathway. Wnt ligands bind to Frizzled (Fz) receptors and transduce beta-catenin independent signals through a multifunctional protein called dishevelled (dsh) (Sokol, 2000). Morphogenetic wnt proteins, such as Wnt1 and Wnt5, act primarily through the non canonical wnt pathway, which is similar to the PCP pathway found in *Drosophila melanogaster* (Heisenberg *et al.*, 2000; Tada and Smith, 2000; Djiane *et al.*, 2000; Wallingford *et al.*, 2000). In flies, a molecular readout of PCP is the localization of the proteins strabismus/van gogh (Stbm/ Vang), and prickle (Pk) on the proximal side of the cell and diego (Dgo), Fz and Dvl on the distal side. Another protein, flamingo/starry night (Fmi/Stan) is also required for PCP, but its localization is not polarized. The localization of these proteins in the zebrafish kidney has yet to be determined.

### 5.1.8. Cilia and Wnt Signaling

It has been shown that ciliary defects affect wnt signaling (Simons *et al.*, 2005; Corbit *et al.*, 2008; Jones *et al.*, 2008) and wnt signaling proteins affect cilia formation (Park *et al.*, 2006; Oishi *et al.*, 2006). It has been hypothesized that cilia might mediate a switch between canonical and non-canonical wnt signaling (Simons *et al.*, 2005). In the absence of wnt,  $\beta$ -catenin is degraded, due to phosphorylation by GSK-3- $\beta$  and binding to the destruction complex. The binding of the wnt ligand to its frizzled (Fz) receptor and Lrp coreceptor results in inactivation of the destruction complex. This in turn allows  $\beta$ -catenin to accumulate in the cytoplasm and translocate into the nucleus leading to transcription of wnt target genes in cooperation with Lef/Tcf co-factors. In the PCP signaling pathway Rho, Rac and Cdc42 GTPases act downstream of disheveled and

lead to rearrangement of the actin cytoskeleton and establish polarity. As mentioned before, PCP signaling regulates convergence extension movements (Jessen *et al.*, 2002; Tada *et al.*, 2000; Heisenberg *et al.*, 2000) in which cells from the lateral region migrate towards the midline and intercalate, leading to a lengthening of the tissue along the anterior-posterior axis (Keller *et al.*, 2002).

### **5.1.9. Cyst and PCP**

Recently a model was proposed in which the formation of cysts was linked to a misalignment of the mitotic angle in renal tubules (Germino *et al.*, 2005) and that PCP might regulate the alignment of the mitotic angle. Kidney development in mouse is accompanied by a high level of proliferation that leads to elongation of the tubule. The tubule diameter can be kept constant while the length increases when the mitotic angle is aligned perpendicular to the longitudinal axis of the duct thus giving rise to two daughter cells that lead to elongation of the duct but no increase in diameter. A subsequent study in PKD mouse models also showed that indeed the mitotic angle was randomized in cystic mutants compared to wildtype (Fischer *et al.*, 2006). This study did not necessarily prove that PCP signaling alone causes the cystic phenotype, but showed for the first time a link between aligned, polarized mitotic axes and cysts. Furthermore, disheveled (*dsh*) recently was shown to be implicated in correct positioning of basal bodies in ciliated epithelial cells (Park *et al.*, 2008). The role of PCP during kidney development is not fully understood therefore we used a PCP specific dominant negative construct in our studies to investigate its role in cystogenesis.

### Goals of Project 1

Most studies in the zebrafish pronephros have been performed during late somitogenesis due to a lack of early embryonic kidney specific markers or transgenic fish for the embryonic kidney development. However, *vHnf1 in situ* hybridization expression pattern identified *vHnf1* transcripts in the intermediate mesoderm in embryos as early as the 4 somite stage (Sun et al., 2001). Because it seemed like a promising marker, we developed an antibody against it to visualize cells of the intermediate mesoderm hoping this might open a new door to study the mechanisms of embryonic kidney development and thus provide insights into the pathogenesis of cystic kidney diseases.

### **Specific aims we sought to address in this project included:**

1. Can we generate an antibody specific for the embryonic kidney using vHnf1?
2. When do unpolarized mesenchymal cells become polarized?
3. When do polarized cells of the intermediate mesoderm form a tubular, lumenized structure?
4. Do apoptosis and proliferation play a major role in lumen formation?
5. Are cilia present during lumen formation?

## 5.2. RESULTS

### 5.2.1. Variant hepatic nuclear factor1 (*vHnf1*) antibody specifically labels the intermediate mesoderm

In order to form a pronephric duct, undifferentiated cells undergo polarizing events and reorganize to form a cylindrical tubule (Fig. 4). We sought to generate a kidney specific antibody that would allow us to study the morphogenesis and development during early embryogenesis. So far all kidney specific antibodies available were not able to detect the early embryonic pronephros. A previously generated antibody in the lab against Cadherin 17 (Cdh17) is an excellent marker to label renal cells specifically but is not expressed prior to the 18 somite stage. Thus, the analysis on a cellular level during early somitogenesis was restricted to histological analysis.

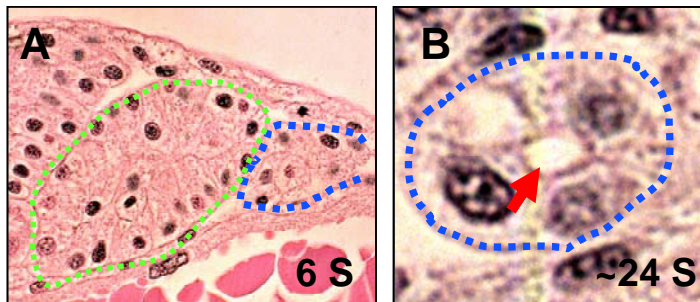


**Fig. 4: Cells rearrange and polarize to form pronephric duct.**

(A) 6 Somite stage embryo has a undifferentiated clump of cells between ventral and dorsal side of the embryo (blue) next to somites (green). (B) In 24hpf old embryos a lumen is visible in the center of the duct and cells are organized in a single layer around the duct.

A former study examining the role of *vHnf1* in zebrafish (Sun *et al.*, 2001) described the *in situ* expression pattern of *vhnf1* transcripts in the pronephric duct starting at the 4 somite stage (Fig. 5), as well as hindbrain and gut. The expression pattern of *vhnf1* seemed very promising to us and we decided to generate an antibody against this protein to label the embryonic kidney.

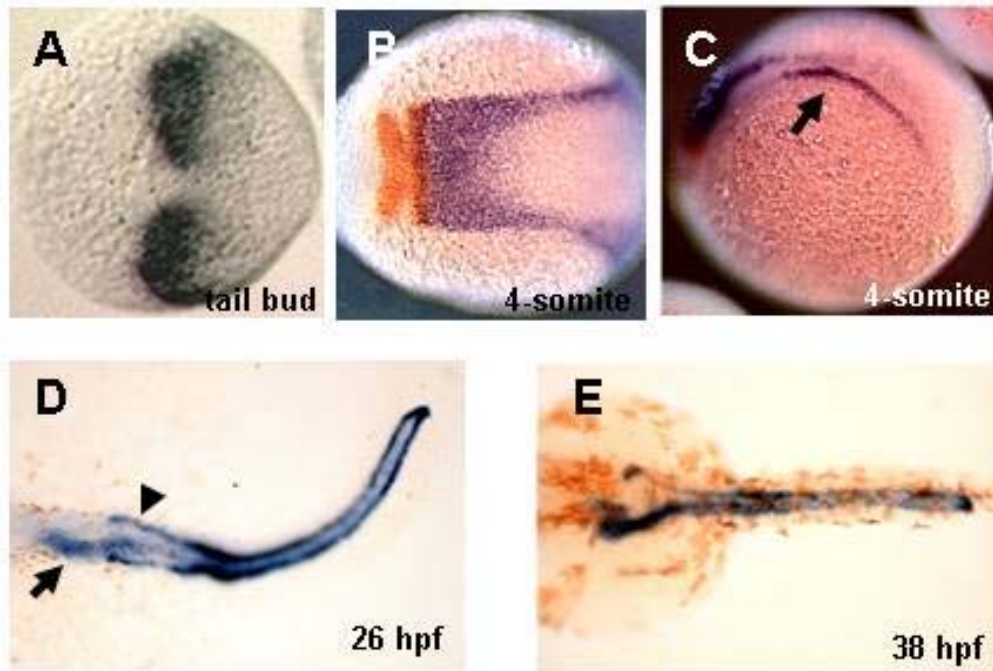


**Fig. 5: *vhnf1* expression during embryogenesis.**

(A-E) Whole-mount in situ hybridization shown in dorsal views, except for (D). Anterior is to the left. (B) *vhnf1* expression in tailbud-stage embryos. (C,D) *vhnf1* (blue) expression in 4-somite-stage embryos. Embryos were double stained with a *krox20* (red) probe. (D) is in a lateral view to show the intermediate mesoderm (arrow). (D-E) *vhnf1* expression in the gut (arrow), the pronephric tubules, and ducts (arrow head) in embryos at 26 hpf (hour post fertilization; E) and 38 hpf (F).

Images taken from Sun and Hopkins, 2001.

*vHnf1* (*Hnf1β*) is a transcription factor which has several conserved domains (Fig. 6 A). It has a POU and homeo domains to facilitate DNA binding, an amino-terminal dimerization domain and a carboxy-terminal transactivation domain. POU and homeo domains are very conserved and show a >90% homology to *Hnf1α*. The dimerization domain is 75% homologous and the activation domain is 47% homologous to *Hnf1α*.

Analyzing the predicted hydrophobicity and the level of antigenicity of the vHnf1 protein, we generated two peptides. Both peptides, amino acid 245-439 and 704-881 proved to be water soluble (Fig.6 B, highlighted in green). Peptides were generated in cell culture,



purified on immobilized glutathione beads, mixed (1:1 ratio) and send to Sigma Genosys for generation of polyclonal antibodies in rabbit.

After we received antibody sera from two different rabbits, we sought to determine whether it would be able to bind to the antigen in whole mount immuno staining of zebrafish embryos. Various conditions and titers were carried out on wildtype embryos and a very faint signal was detected in the nuclei of the presumptive pronephric duct. Blue gel purification of the antibody did not improve the signal to noise ratio significantly (not shown). However, affinity purification of blue gel purified serum resulted in a specific nuclear staining of the pronephric duct (Fig. 6 C). The signal could be observed along the entire length of the duct and was the strongest in the medial region.

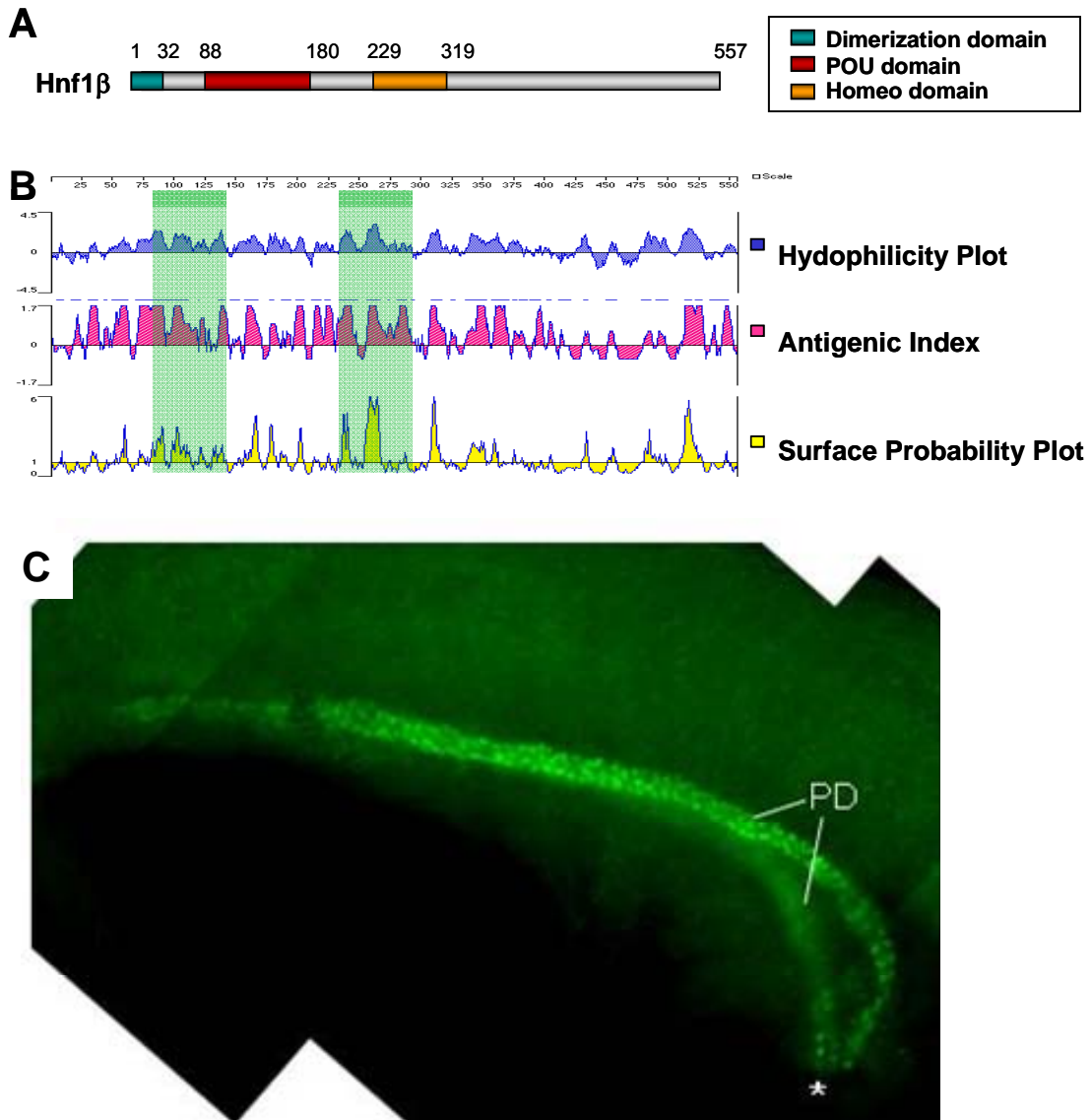


**Fig. 6: Domains of vHnf1 in zebrafish and choice of antigenic regions for antigenic peptides.**

Diagram of zebrafish vHnf1 protein domains. (A). vHnf1 (*Hnf1b*) is a transcription factor which has POU and homeo domains to facilitate DNA binding, a N-terminal dimerization domain and a C-terminal transactivation domain. POU and homeo domains are highly conserved and show a >90% homology to Hnf1a. The dimerization domain is 75% homologous and the activation domain is 47% homologous to Hnf1a. (B) Plot showing predicted hydrophilicity (blue), antigenic index (pink) and surface probability (yellow) of vHnf1 protein. The x-axis shows the amino acid positions of the protein. y-axis indicates the level of the analyzed properties. Positive y- values indicate a high level; negative y-values indicate a low level of the properties plotted.

(C) Whole mount fluorescent immunostaining performed with the antibody generated against vHnf1 peptides, on 18 somite stage wildtype embryo.

Anterior is to the left, ventral side is down. PD: pronephric duct. An asterisk marks the cloaca.

This is the first antibody that has been able to detect intermediate mesoderm in zebrafish specifically giving us the opportunity to address questions regarding the early events during pronephros development in zebrafish. Throughout this study *vhnf1* was used as a marker to visualize cells of the intermediate mesoderm and the pronephros.

### **5.2.2. Lumen formation starts at the 10-12 somite stage**

Lumen formation is an important feature of organogenesis. Cells can create luminal space via different mechanisms. The intestinal lumen in vertebrates is formed by an invagination process, where vesicles form small lumina that fuse to form the final lumen. The neural tube on the other hand is formed by cell migration (Lubarsky and Krasnow, 2003). The zebrafish gut is formed by invagination or hollowing. During that process, cells form cell-cell junctions and acquire apical-basolateral polarity *de novo* and form a small lumen. The lumen is expanded by adding more apical membrane to the existing one. An alternative mechanism describes lumen formation through polarity establishment of cells at the periphery of the cell cluster, possibly through interaction of the basement membrane. Cells in the center will undergo apoptosis and leave a luminal space behind (Coucovanis and Martin, 1995). The mammary salivary gland is one example that follows this process to form a tubule (Melnick and Jaskoll, 2000).

However, it is not known how a lumen in the zebrafish pronephros is created. To start answering the question, we first sought to analyze when the lumen forms in the zebrafish pronephros. For that matter, we performed a time course analysis and stained embryos at different developmental time points with phalloidin that stains for F-actin (Fig. 7). In 14-16 somites stage, embryos actin filaments were enriched at the center of the intermediate mesoderm along the longitudinal axis, indicating it was enriched at the apical membrane, which is characteristic for polarized epithelial cells (Fig.7F). In addition the gap between phalloidin signals of opposing cells let us think that lumen formation had occurred already. Analyzing younger embryos at the 10-12 stage embryos, we found that most cells did not show apical enrichment of F-actin yet. However, individual cells showed strong focal signals for phalloidin, which might represent cells that are undergoing polarization.

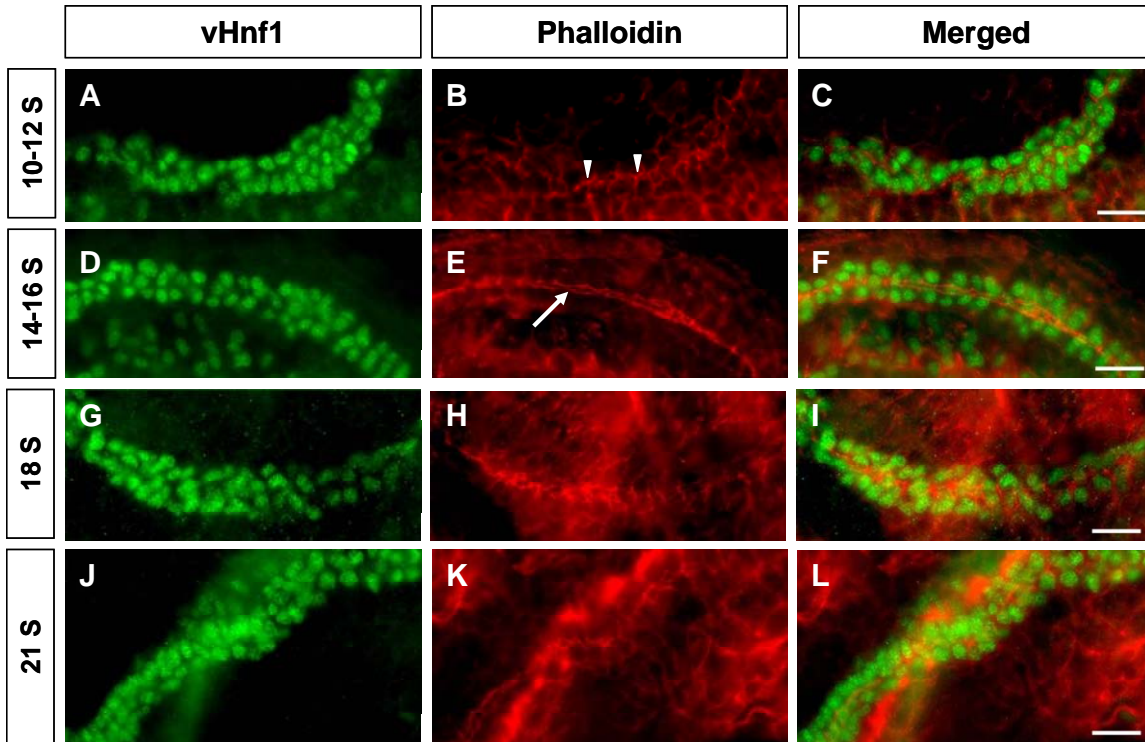


**Fig. 7: Analysis of lumen formation during embryonic kidney development.**

Whole mount fluorescent immunostaining with vHnf1 antibody and Rhodamine-Phalloidin in wildtype embryos. Phalloidin visualizes F-actin thus the apical membranes are labeled strongly. (A-C) At the 10-12 somite stage, focal enrichments for actin could be detected (arrowheads) which could represent formation of a local lumen. (D-F) At 14-16 somite stage a lumen was visible in the intermediate mesoderm (arrow) and spanned the entire duct. (G-I) 18 somite stage as well as 21 somite stage embryos (J-L) displayed a lumen in the entire length of their intermediate mesoderm.

Scale bars represent 10  $\mu\text{m}$ .

According to our data lumen formation appears to be occurring around the 10-12 somite stage in the zebrafish pronephros. Phalloidin staining might not be the ideal approach to answer the question due to the nature of a 3D tubule. It is difficult to determine whether a small cavity had formed yet or not. To further support our initial result, we performed histological cross sections at different stages (Fig. 9) and stained with hematoxylin and eosin. At 8 somites a mesenchymal clump of cells (outlined in blue) is located between the dorsal and ventral part of the embryo in close proximity to the somites (outlined in green). During development the cells undergo mesenchymal-to-epithelial transition and rearrange to form a tubular structure and the first contiguous lumen appears at the 14 somite stage.

### 5.2.3. Centrosome relocation in the intermediate mesoderm

Zebrafish kidneys consist of only two nephrons, one on each side of the embryo. Glomeruli are fused at the midline from which two tubules extend and connect to the pronephric duct which extend caudally and lead to the cloaca. During kidney development intermediate mesodermal cells give rise to the kidneys and have to undergo massive rearrangement and proliferation to form the final organ. During that process cells undergo mesenchymal to epithelial transition to finally result in a highly polarized epithelium. Epithelial cells have apical and baso-lateral membrane compartments which have distinct protein and lipid compositions. Additionally, polarized epithelial cells realign their centrosomes between nucleus and lumen similarly to cells that show oriented cell migration. It is not known how and when kidney cells acquire apical/ baso-lateral polarity. Since we observed that a pronephric lumen was established by the 14 somite stage, we were wondering when the cells might acquire apico-basolateral polarity. We used the localization of the centrosome as a marker for polarity and performed a time course analysis during kidney development.

Performing immunohistochemistry with antibodies against  $\gamma$ -tubulin (to label the centrosome/basal body) and *vHnf1* in 14 and 16 somite stage wildtype embryos (Fig.8 D-I), we observed all centrosomes localized in the central part of the intermediate mesoderm. This indicates to us that all centrosomes had already relocated towards the apical side of the cell. Examining 21 somite old embryos we saw, as expected that centrosomes were aligned at the middle part of the duct. We were interested in investigating when exactly that localization occurred and therefore went on to analyze younger embryos. At the 12 somite stage, we were able to detect some centrosomes at the apical side of the cell but also cells that clearly had their centrosome on the basal side (Fig.8 A-C). Since centrosome reorganization is a hallmark of epithelial polarity establishment, these results indicate that polarity establishment is an ongoing process at the 12 somite stage but completed by 14 somites.

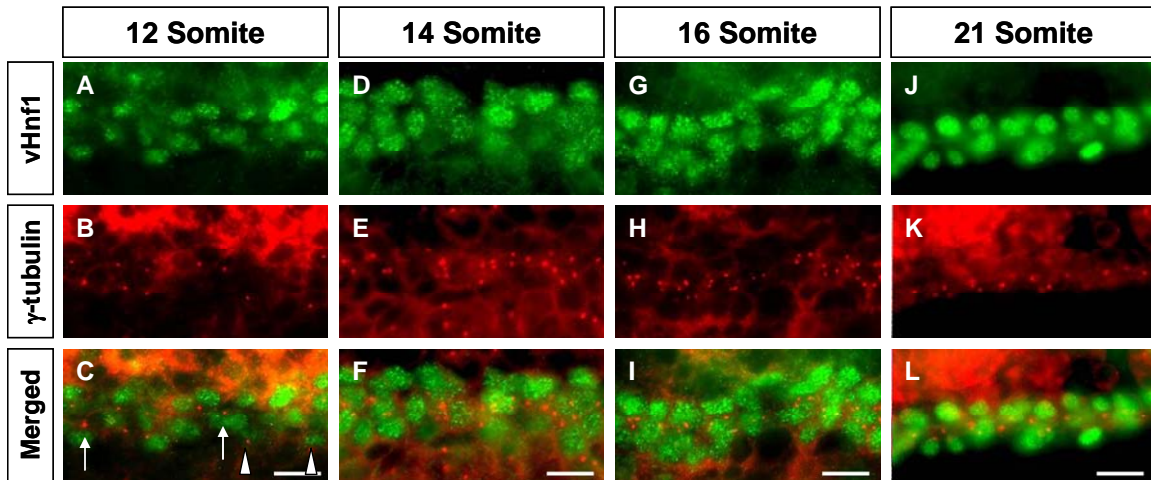


**Fig.8: Centrosome relocation during embryonic kidney development.**

Whole mount fluorescent immunostaining with antibodies for vHnf1 (A,D,G,J) and  $\gamma$ -tubulin (B,E,H,K) was performed on wildtype embryos at indicated developmental stages. (A-C) At 12 somite stage some cells showed a polarized centrosome, which was oriented between the nucleus and the putative apical side of the cell (arrows). These cells were interspersed with cells that had not reoriented their centrosomes yet (arrowheads). (D-F) At the 14 somite stage most cells of the intermediate mesoderm had reoriented their centrosomes towards the forming lumen which was evident in older embryos as well (G-L), in which the centrosomes of all cells were clearly oriented towards the center of the duct.

Scale bars represent 10  $\mu$ m.

#### 5.2.4. Cilia formation in the kidney duct

Cilia are hair like structures that extend out of the apical surface of the cell. They are thought to be the 'final touch' after the cell has exited the cell cycle and is fully polarized. Our results showed that polarity in the kidney duct started to be established around the 10-12 somite stage and was finished by the 14 somite stage. For a zebrafish embryo to develop from the 10 somite stage to the 14 somite stage a time window of 2 hours is all that is needed at standard temperature. During this narrow time window embryos are able to establish polarity and create a cavity in the intermediate mesoderm.

It is unknown which role cilia play during embryonic nephrogenesis. We sought to determine when cilia were being formed and if they might prelude or follow lumen formation and polarity establishment. We performed immunohistochemistry with antibodies against acetylated  $\alpha$ -tubulin, to detect the ciliary axoneme and *vHnf1* to highlight the intermediate mesoderm. Supporting our previous finding of lumen being present at the 14 somite stage, all embryos at 14 somite stage and older exhibited cilia in the luminal space of the pronephric duct (Fig. 9). Cilia appeared to increase in length with development and the luminal diameter seemed to decrease. Cilia in older embryos are spatially restricted and forced to bundle tightly and bend into the lumen. At the 8-10 somite stage cilia could be found on approximately half of the intermediate mesodermal cells. Cilia appeared very short and randomly distributed on the cell surface. Supporting the results of lumen formation and polarity establishment, the intermediate mesoderm at the 12 somite stage seemed to be undergoing polarization. Some cells appeared to be polarized, with a cilium extending into the center (potentially the lumen) of the duct while other cells in the same duct exhibited cilia on regions that were located outside of the future luminal space (Fig.9 D-F).

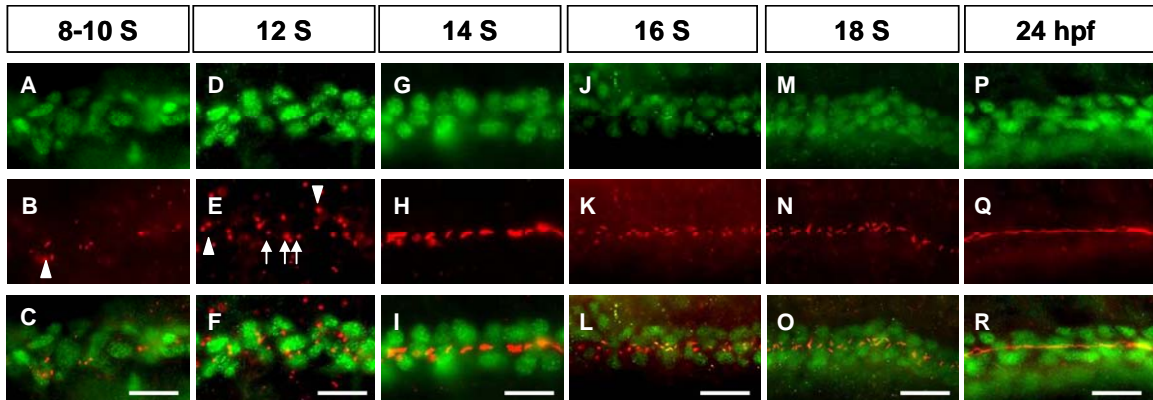


**Fig.9: Analysis of cilia formation during kidney development.**

Embryos were fixed at different developmental stages and stained with antibodies against vHnf1 (A,D,G,J,M,P) to visualize the intermediate mesoderm and acetylated  $\alpha$ -tubulin (B,F,H,K,N,Q) to label cilia respectively. Merged images are shown in (C,F,I,L,O,R). At 8-10 somite stage (A-C), cilia appear very short and some are clearly not orientated towards the center (arrowhead). At 12 somites stage (D-F), more cilia have formed but are still very short and therefore appear almost punctate. Cells that have a cilium orientate towards the center of the intermediate mesoderm (arrows) are dispersed between cells which display a randomly extending cilia (arrowhead). Older embryonic stages (G-R) show longer cilia which are all localized within the lumen of the duct.

Scale bars represent 10  $\mu$ m.



Taken all these data together, we think that lumen formation, polarity and ciliogenesis all occur almost simultaneously in a very narrow developmental window between the 10 and 12 somite stage (Fig. 10) and is finished at the 14 somite stage.

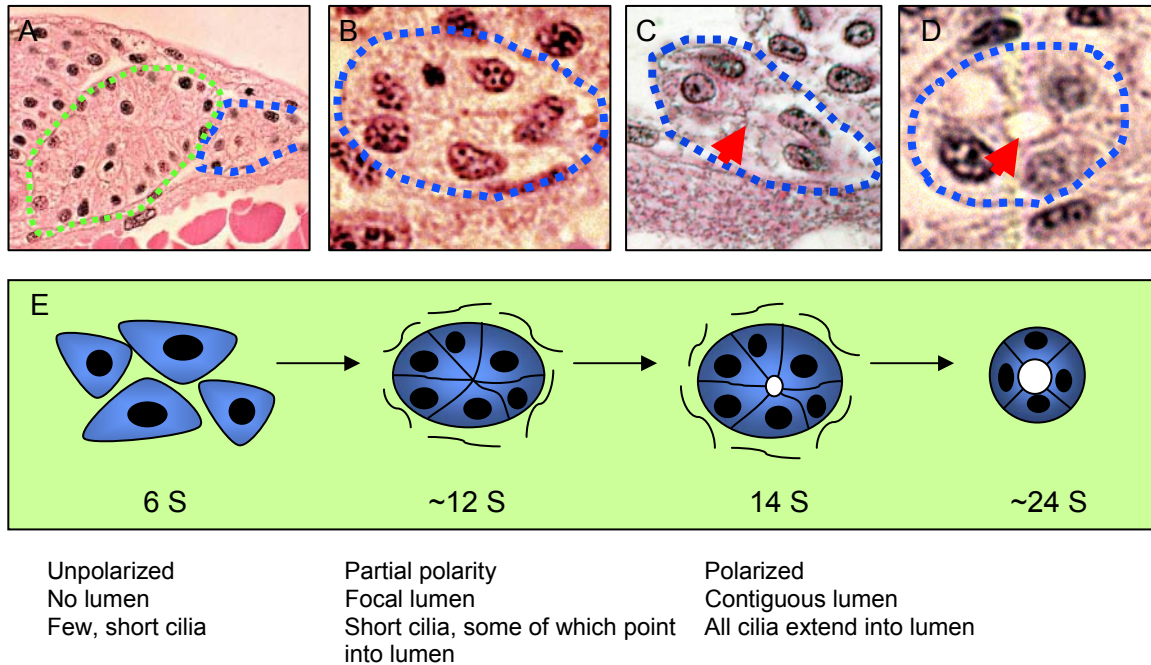


**Fig. 10: Maturation of the zebrafish pronephric duct.**

(A-D) Histological analysis of the intermediate mesoderm at 8 somite stage (A), 12 somite stage (B), 14 somite stage (C) and 24 somite stage (D). (A) Cells of the intermediate mesoderm (IM) first appear as a clustered clump of cells lateral to the somites (S). (B) Around the 12 somite stage the intermediate mesoderm appears structurally organized and displays a characteristic circular shape in cross sections. (C) At 14 somite stage a small lumen can be found in the middle of the intermediate mesoderm (arrow). (D) At the 24 somite stage the number of cells in the duct circumference has decreased.

(E) Schematic picture of the intermediate mesoderm development with list of key events that occur at each step.

### **5.2.5. The pronephric duct is narrowing and elongating during development**

We noticed during our analysis that the organization of the duct changed significantly during kidney development. Statistical analysis of the number of cells in the ductal diameter in whole mounted embryos of the medial ductal region was performed at 5 randomly chosen positions of the duct. Since the kidney duct is too small to be dissected and mounted as a single sheet the numbers we obtained are a reflection of the whole mounted kidney.

At the 14 somite stage the intermediate mesoderm had mostly 4 *vhnf1* positive nuclei ( $3.72 \pm 0.71$ ) in the ductal diameter. During the course of kidney development the duct was comprised of lesser cells and 2 dpf embryos had approximately 2 cells ( $1.78 \pm 0.46$ ) in the ductal diameter in the medial region (Fig.11). At the same time, the duct which was around 630  $\mu\text{m}$  long in 14 somite stage embryos, elongated significantly during the course of development and reached 1400  $\mu\text{m}$  at 2 dpf old embryos.

The narrowing could be explained in two ways. Firstly, cells could migrate and rearrange resulting in a narrower tissue or alternatively apoptosis in the duct could lead to fewer cells in the circumference of the duct. Since we did not detect TUNEL positive cells in the duct, we think that the narrowing is due to a migratory process of intermediate mesodermal cells that ultimately leads to a narrow and long pronephric duct.

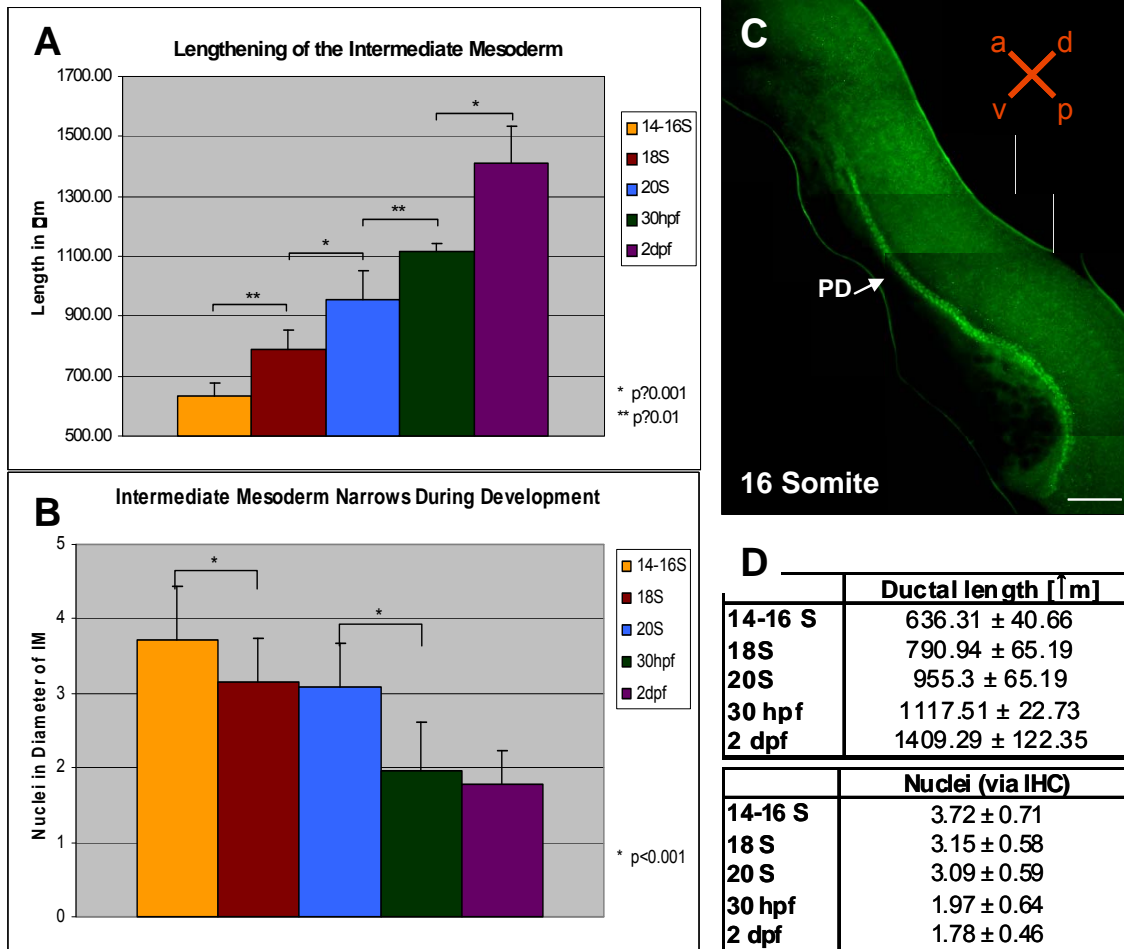


**Fig. 11: Cells undergo rearrangement during embryonic kidney development.**

Whole mount fluorescent immunostaining was performed on embryos at various developmental stages. Pictures were aligned to reconstruct the entire duct using Adobe illustrator (C). The length of the duct, labeled with vHnf1, was measured in Adobe Photoshop, 6.0, averaged and plotted on bar graphs (A,B). Scale Bar represents 100 $\mu\text{m}$ .

(A) During development of the intermediate mesoderm, the duct length showed a successive significant increase from 636  $\mu\text{m}$  at the 14-16 somite stage embryos to 1400  $\mu\text{m}$  in 2 dpf old embryos. (B) Lengthening of the duct was accompanied by a narrowing of the intermediate mesoderm. 5 regions within the medial region of the duct were randomly chosen in each embryo. A line was drawn at these 5 locations perpendicular to the longitudinal axis of the duct and the number of nuclei documented. During development, the number of nuclei that were counted with that method decreased from approximately 4 nuclei in 14-16 somite stage embryos to 2 nuclei in 2 dpf embryos. (D) Data displayed in Graph (A, B).

### **5.2.6. The Zebrafish pronephros shows a low rate of proliferation throughout development**

Elongation and narrowing of the duct could happen via two alternative mechanisms: (a) proliferation and apoptosis or (b) rearrangement of cells. Since we do not have a kidney specific promoter to follow cell migration or rearrangements using time lapse microscopy, we sought to test the first hypothesis using antibodies for phosphorylated Histone H3 (PH3) and TUNEL for apoptosis.

Histone H3 is specifically phosphorylated during mitosis and meiosis. Upon exit of mitosis a global dephosphorylation of histone H3 takes place. When we performed our analysis we noticed two things. First, PH3 positive cells undergoing mitosis were sometimes located in direct proximity to *vhnf1* positive cells but were mostly *vhnf1* negative. This might be due to the nature of histone H3 phosphorylation in the kidney duct. During the cell cycle, histones are phosphorylated starting in late interphase and dephosphorylation begins in anaphase and is completed prior to telophase. In contrast, with *vhnf1* being a transcription factor, upon break down of the nuclear envelope which happens around prometaphase, *vhnf1* cannot be detected anymore. Co-localization of *vhnf1* with histone H3 was very rare for that reasons. Fig.12 A-C shows an example of a PH3 positive cell that happened to be positive for *vhnf1* as well. Fig.12 G-I on the other hand shows an example of a PH3 positive cell that very likely is part of the intermediate mesoderm but in which *vhnf1* was degraded or diluted throughout the cell. For older embryos *Cdh17* was used as a ductal marker. Very rarely proliferating cells were found in the duct. This is not due to penetration problems of the antibody, since other parts of the embryo showed mitotic cells (Fig.12 D-F). A quantification of the result is shown in Fig.12 M. The overall mitotic rate during kidney development was very low with a drop in proliferation especially after 16 somite stage. Using a TUNEL assay we performed immunohistochemistry with *vhnf1*. Even though TUNEL positive cells were detected in other regions of the embryo, especially the somites, no apoptotic cells could be detected in the intermediate mesoderm.

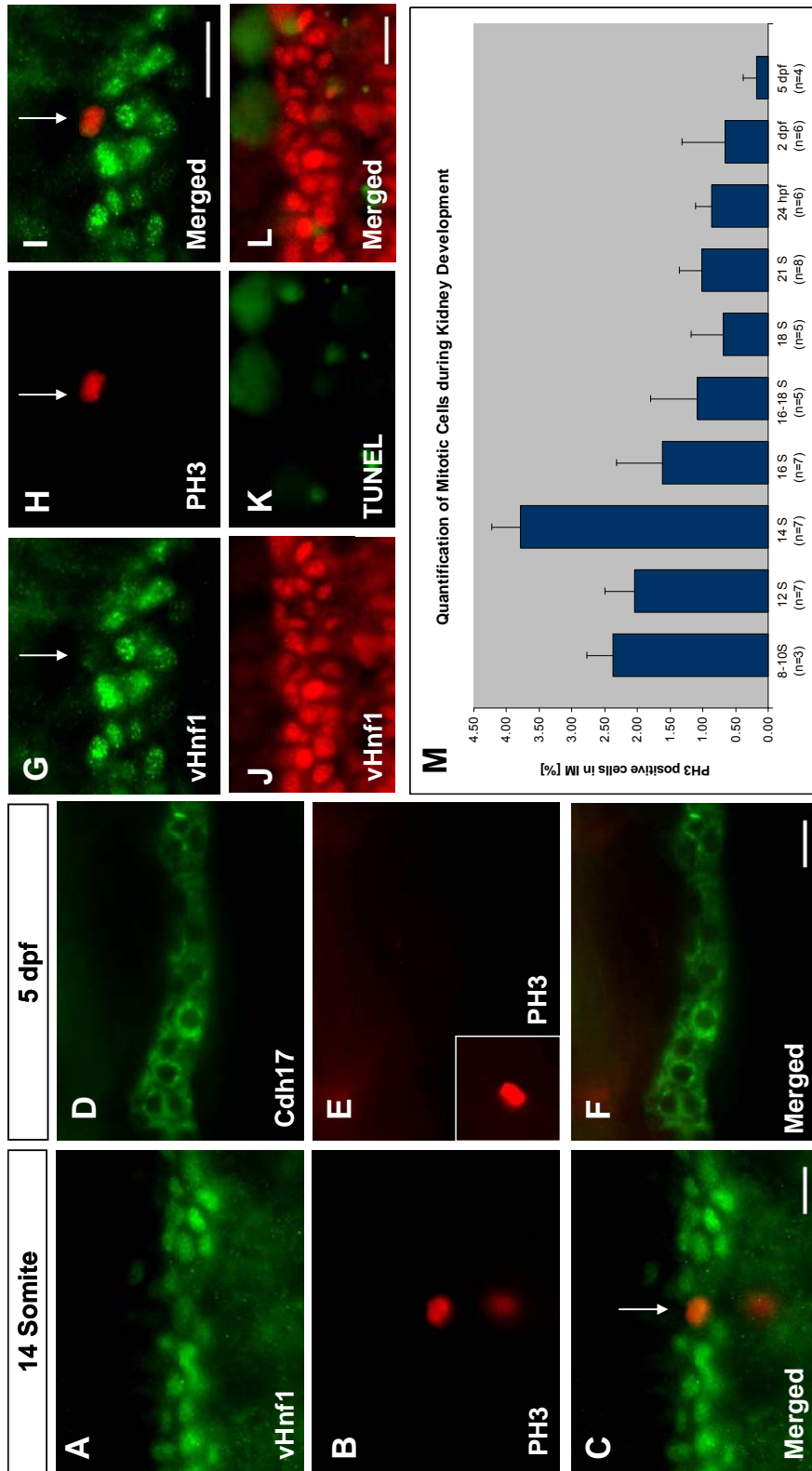


Fig. 12

**Previous page:**

**Fig 12: Analysis of proliferation during kidney development.**

Whole mount fluorescent immunostaining was performed using antibodies against vhnf1 and phosphorylated Histone H3 (A-C; G-I), Cdh17 and phosphorylated Histone H3 (D-F) or vhnf1 and TUNEL (J-L). Examples are shown for each staining.

(A-C) Whole mount fluorescent immunostaining for vhnf1 (A), phospho-Histone H3 (B) on a 14 somite stage wildtype embryo. The arrow indicates the double positive cell (C). (D-F) In 5 dpf old embryos Cdh17 (D) was used for labeling of the kidney duct. Double labeling with Phospho-Histone H3 (E) almost never showed colocalization. Insert in (E) shows a Phospho-Histone H3 positive cell of the same embryo but other region than pronephric duct. (G-I) vhnf1 signal is often significantly reduced or absent when a cell is positive for Phospho-Histone H3 (arrow in (H)) due to disassembling of the nuclear envelope during cell cycle. When Phospho-Histone H3 signal was in direct proximity of vhnf1 positive cells it was counted as positive. (J-L) To label apoptotic cells we utilized TUNEL. Shown is an example of a vhnf1 (J) and TUNEL (K) double staining of the intermediate mesoderm in a 16 somite stage embryo. Even though many apoptotic cells were observed in muscle cells throughout the body during development, almost none were present in the intermediate mesoderm. TUNEL positive cells were found sometimes in proximity to the duct, but did not colocalize with vhnf1. (M) Bar graph showing the quantification of mitotic cells during kidney development analyzed by fluorescent immunostaining with Phospho-histone H3 and vhnf1 or Cdh17 antibodies respectively. Plotted is the mean with standard deviation. n= number of experiments. During a typical experiment between 60 and 250 vhnf1- positive cells were counted.

Scale bars represent 10  $\mu\text{m}$ .

**Next page:**

**Fig. 13: Cells of the intermediate mesoderm undergo realignment during embryogenesis.**

Whole mount fluorescent immuno staining with antibodies against vhnf1 and Rhodamine-Phalloidin. (A-C) At the 10-12 somite stage, cells of the intermediate mesoderm appeared randomly organized and did not exhibit a particular orientation. (D-F) Embryos at 21 somite stage displayed various degrees of alignment of intermediate mesoderm cells along the longitudinal axis. The shown example shows a highly aligned region of the intermediate mesoderm. The cell number as well the orientation of the duct appears to be highly regulated.

Scale bars represent 10  $\mu\text{m}$ .

### 5.2.7. The intermediate mesoderm undergoes rearrangement during kidney development

While we were doing our analysis of the embryonic kidney, we made the interesting observation that the intermediate mesoderm appeared to realign itself along the longitudinal axis. In the 10-12 somite stage embryos, the intermediate mesoderm was non-uniform, and the number of cells in the ductal diameter was highly variable and the orientation of nuclei appeared random (Fig.13). In older embryos we found that the intermediate mesoderm showed a more regular pattern even though not the whole duct was aligned perfectly. A highly organized region of the duct is shown in Fig. 13. In addition, nuclei which are more oval shaped seemed to be aligned along the axis of the duct resulting in a highly organized pattern. This might be due to planar cell polarity which describes the polarity within a planar sheet of cells, orthogonal to the apico-basal axis.

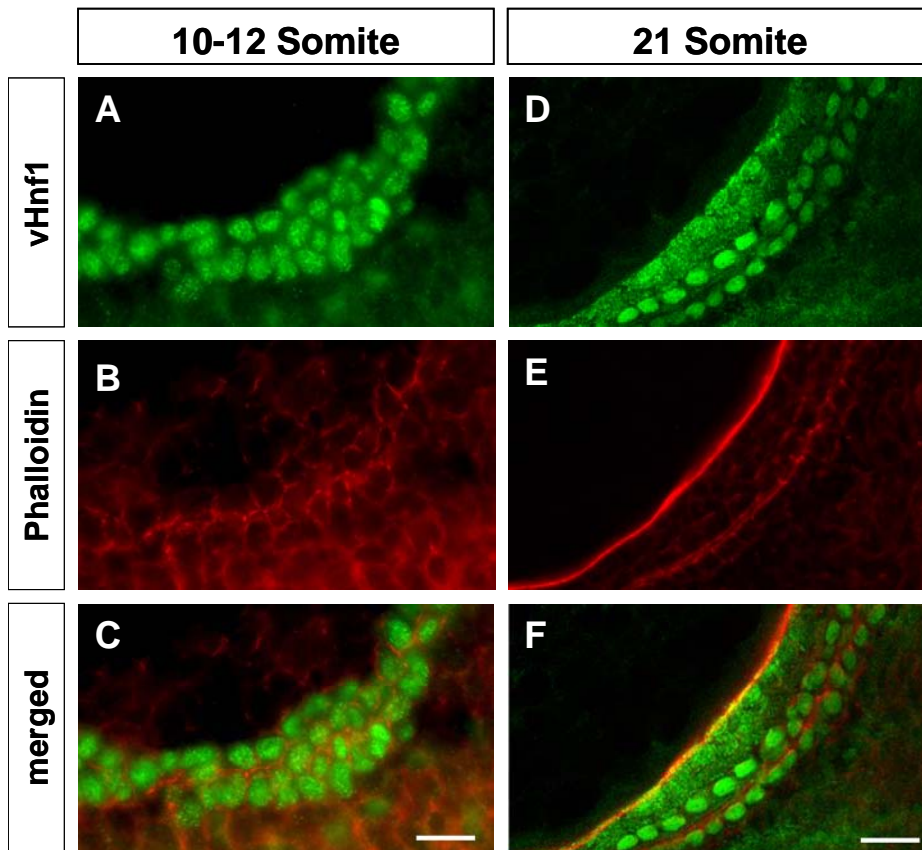


Fig. 13

### **5.2.8. Inhibition of the planar cell polarity pathway leads to duct dilation**

Observing the rearrangement as well as the thinning and elongation of the duct, we speculated that this organized cell movement and rearrangement might be due to planar cell polarity (PCP). PCP was originally identified in *drosophila melanogaster* and is essential for establishing the cellular polarity in the plane of the epithelium orthogonal to the apico-basolateral axis. In zebrafish, PCP is responsible for convergent extension (CE) movements, a morphogenetic process through which groups of cells converge towards the midline and intercalate. This leads to coordinated narrowing and elongation of the tissue. CE is not driven by cell division or cell shape changes, but rearrangements and movement of the cells.

To test whether PCP plays a role during kidney development and cyst formation, we focused on disheveled (*dsh*) a key player in this pathway. *Dsh* is best known as a component of Wnt–Frizzled signaling that regulates two pathways through distinct protein domains (Boutros and Mlodzik, 1999). The N-terminal DIX domain of *Dsh* is required to activate the canonical *Wnt* signaling pathway that regulates target gene transcription. *Dsh* DEP domain and the PDZ domain are essential for its function in the PCP pathway. The construct we used, *Dsh* DEP, lacks the DIX as well as the PDZ domains and acts as a dominant negative allele specific for the PCP pathway. *In vitro* transcribed *Dsh*-DEP mRNA was injected into zebrafish embryos at the 1-4 cell stage (Fig.14).



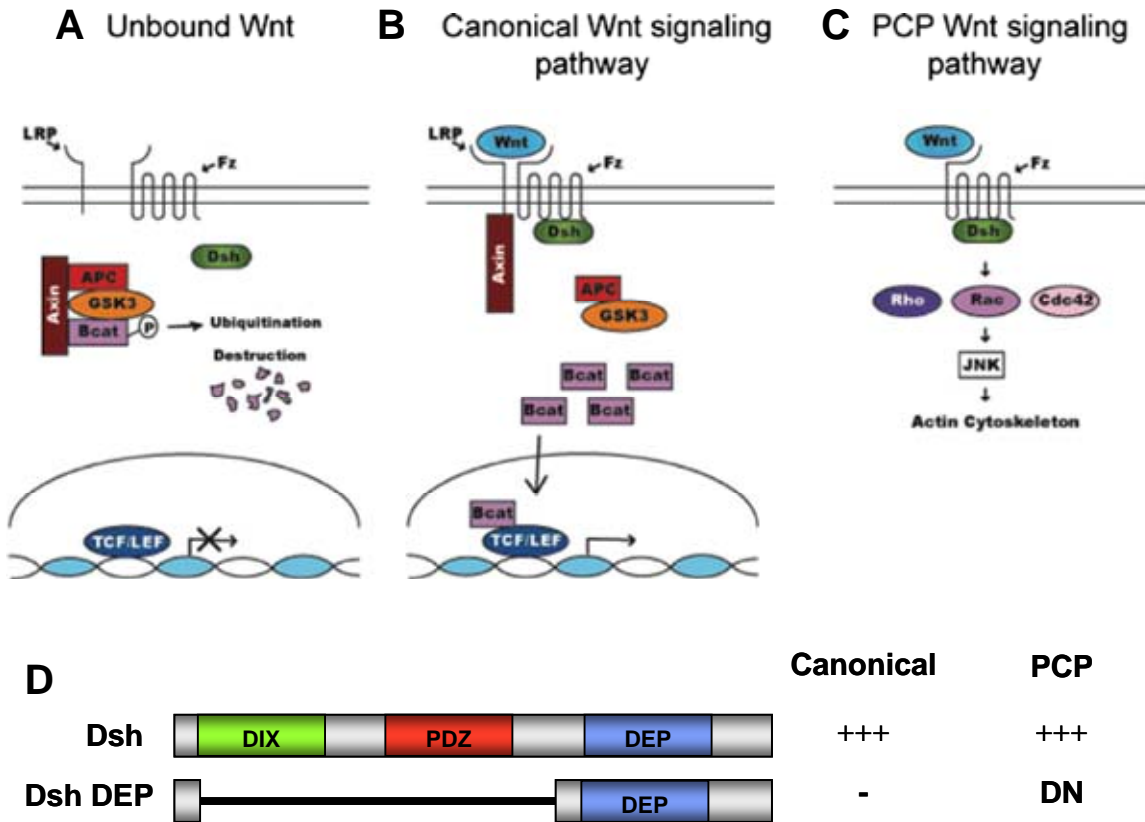


**Fig. 14: Canonical wnt signaling and PCP signaling pathway and diagram of Dsh-DEP construct.**

(A) In the absence of bound Wnt ligand,  $\beta$ -catenin is degraded, due to phosphorylation by GSK-3 beta and binding to the destruction complex. (B) In canonical signaling, binding of a Wnt to its Fz receptor and Lrp co-receptor results in inactivation of the destruction complex. This allows  $\beta$ -catenin to accumulate in the cytoplasm and translocate into the nucleus, where it activates transcription of Wnt target genes in cooperation with Lef/Tcf co-factors. (C) In the planar cell polarity (PCP) pathway, Rho, Rac and Cdc42 act downstream of Dsh and function to rearrange the actin cytoskeleton and establish cell polarity.

(D) Diagram of Dsh DEP, which lacks the DIX and PDZ domain. It acts as a dominant negative allele of dsh specifically for the PCP pathway.

Diagram (A-C) taken from Merkel *et al.*, 2007.

At 1 dpf after having injected *Dsh* DEP mRNA into zebrafish eggs, the characteristic phenotype associated with PCP defects, such as a shortened body axis and broader somites on approximately 60% of embryos is visible. We performed immunohistochemistry for acetylated  $\alpha$ -tubulin and *vHnf1* on injected embryos. Disrupting the PCP pathway during embryogenesis leads to a dramatic increase in the diameter of the ductal lumen visualized by upright cilia that are not forced to bend within a tight lumen anymore as well as staining with Phalloidin (Fig.15). Interestingly, duct dilation does not occur within the entire length of the duct, but is restricted to the medial portion of the duct. This might indicate that cystic duct dilations first happen in the medial regions, and performing a time course might help to answer that question.

Our results indicate that planar cell polarity might play a role in cystogenesis and duct dilation. However, disrupting PCP signaling in the whole embryo presents a big drawback of our approach. Possibly an overall shortening of the body could have led to passive duct dilation as a consequence of the shorter body. In some cases, embryos with a shorter body axis were detected with only one of the two nephrons showing a dilated phenotype, indicative for a kidney specific role of PCP. However, the optimal way to address that question would be to have a kidney specific PCP phenotype. Unfortunately no kidney promoter for the young zebrafish embryo is available at this time. An alternative way would be to introduce a heat shock inducible *Dsh* DEP construct into embryos and heat shocking and thereby activating them at a later time point which would not disrupt gastrulation movements and leave the body axis unaffected, but might show dilation in the kidney.

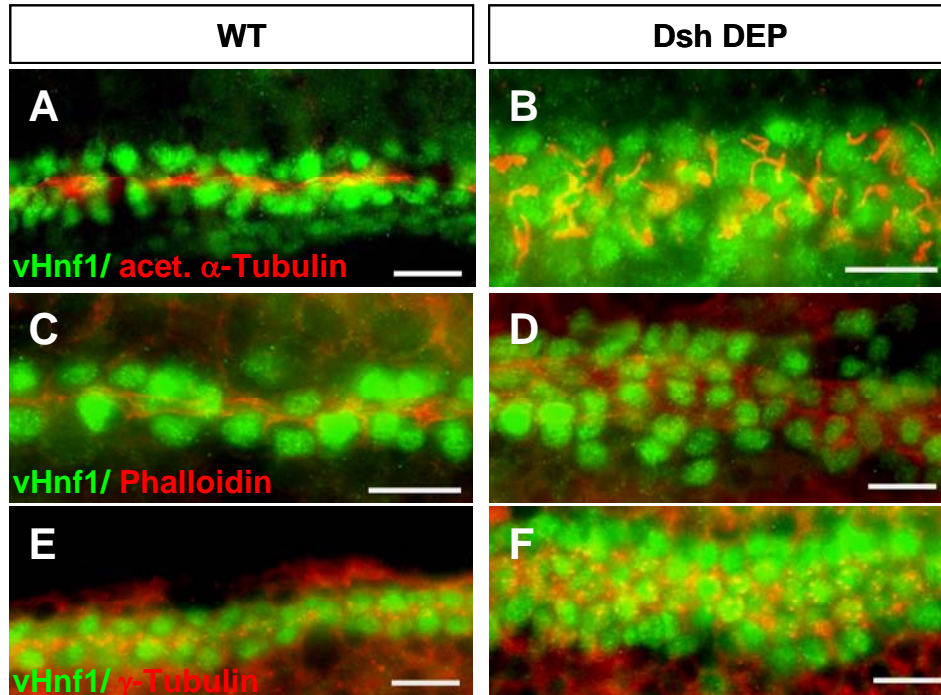


**Fig. 15: Disruption of PCP signaling pathway leads to duct dilation and increase in cell number in duct circumference.**

Whole mount fluorescent immunostaining was performed on 1dpf old embryos which were injected at 1-4 cell stage with Dsh DEP mRNA (B, D, F) to disrupt the PCP pathway. Age matched siblings were used as control (A, C, E)

(A-B) Fluorescent immunostaining for *vHnf1* and acetylated  $\alpha$ -tubulin which labels cilia. Cilia do not appear as a tightly bundled rope due to the enlargement of the duct (B). The uninjected wildtype control (A) exhibit bundled cilia of multiciliated cells that align tightly within the lumen.

(C-D) Fluorescent immunostaining for *vHnf1* and Phalloidin which labels the apical membrane. Disruption of PCP pathway did not inhibit the apico-basolateral polarity.

(E-F) Fluorescent immunostaining for *vHnf1* and  $\gamma$ -tubulin, which labels the basal bodies. The ductal lumen is dilated and more cells are in the ductal diameter compared to wildtype but the apico-basolateral polarity appears grossly intact.

Scale bars represent 10  $\mu$ m.

### **5.2.9. Disruption of PCP does not inhibit apico-basal polarity in the pronephric duct**

Disrupting the planar cell polarity by injection of *Dsh* DEP did not have an adverse effect on positioning of basal bodies (Fig. 15, E, F) and actin enrichment at the apical membrane (Fig. 15, C, D), indicating that formation of apico-basal polarity is intact and confirming that *Dsh* DEP acts specifically as a dominant negative allele for the PCP signaling pathway. Despite having more cells in the diameter compared to wildtype ducts, all basal bodies, visualized by immunohistochemistry with  $\gamma$ -tubulin antibody, localized to the center of the intermediate mesoderm. This is most obvious to see in the outmost cells of the duct which orientate their basal bodies towards the lumen.

## 5.3. DISCUSSION

Zebrafish is emerging as a powerful model organism to study development. Despite having a simplified pronephros, the expression pattern is very similar to mammalian kidneys and many genes that are involved in human cystic kidney diseases also cause a pronephric cystic phenotype in zebrafish when mutated.

To characterize the cellular events that transform the relatively unstructured intermediate mesodermal cell cluster into a highly organized tubule, an antibody against *vHnf1* was generated. This antibody labels the intermediate mesoderm specifically and allowed us to perform time course analysis during the embryonic development.

Our results show that lumen, cilia, and polarity formation, all occur around the 12 somite stage in wildtype zebrafish embryos and are completed by the 14 somite stage. The intermediate mesoderm rearranges to form a rosette-like structure which is apparent at the 10-12 somite stage. The lumen forms at the apical center of this rosette. The signal or cue for this cellular reorganization is not known but a similar process has been described in the Kupffer's vesicle (KV). The KV is a transient structure that is the zebrafish equivalent to the embryonic node in mouse, contains motile cilia that generate a leftward fluid flow which leads to a break in body symmetry and laterality in fish. Recently a study showed that during polarity formation of dorsal forerunner cells (KV precursor cells) into a rosette-like structure, polarity is not formed *de novo* but depends on 'cell seeds' that originate from the surface epithelium and serve as progenitors (Oteiza *et al.*, 2008). Lumen formation in the KV has striking similarities to the cavitation process in the pronephric duct. Both arise from undifferentiated cluster of cells that form rosette-like structures, create a cavity at the apical center and result in highly polarized epithelia that extend cilia into a fluid filled lumen. It might be possible that the intermediate mesoderm contains similar 'seed' cells that serve as progenitors and contain polarity information. Other cells of the intermediate mesoderm might then cluster subsequently around those 'seed' cells and form the rosette. It is purely hypothetical at this point since we do not have any transgenic fish to follow the migration, ingression and rearrangements of intermediate mesodermal cells. Using the *vHnf1* promoter driving a fluorescent marker such as GFP would be very powerful and allow us to study early mechanism of kidney development.

During pronephric duct development, we detected a relatively low level of proliferation, analyzed by immunostaining for phosphorylated histone H3 and almost no apoptotic cells, visualized with TUNEL. Cavitation can occur either via apoptosis in the center of a solid cell cluster leaving behind cells at the periphery that become polarized, or by forming a lumen *de novo*, a process that e.g. is used for formation of the gut lumen in zebrafish. Cells acquire apico-basolateral polarity *de novo* and form several small apical lumina that eventually fuse into a single big lumen (Bagnat *et al.*, 2007). The lack of apoptosis in the pronephric duct supports a mechanism similar to the one in the gut. We did not perform detailed analysis yet to determine whether such multiple small lumen exist during kidney formation. Due to the small size of the pronephric duct compared to gut (approximately 1/50), it might be very challenging to observe the tiny lumina that might coalesce to form a central lumen. Electron microscopy might be helpful to find a definitive answer.

While we performed the proliferation analysis it would have been very interesting to measure the mitotic angle as well. Recently the mitotic axis has been in the spot light regarding its role in tubule dilation and cyst formation. In one study ARPKD mouse models were used to analyze the mitotic angle in proliferating tubules. Interestingly in wildtype mice the majority of proliferating cells displayed a mitotic angle smaller than 20° (Fischer *et al.*, 2006) in regard to the longitudinal axis of the tubule. Proliferation with a small mitotic angle will result in two daughter cells that lead to a lengthening of the duct without increase in diameter. In contrast, ARPKD mice showed a randomized mitotic angle which might lead to an increase of the ductal diameter. It would have been very interesting to determine whether the duct in zebrafish shows the same phenomenon but our antibody for phosphorylated histone H3 (PH3) did not allow us to distinguish the two mitotic daughter cells. We used three individual clonal antibodies, including the one used in the aforementioned study. However, our signal was most of the time circular. In very rare events a mitotic angle could be seen but among all PH3 positive cells counted less than 5 showed a clear defined angle. This might be due to the nature of cell division in zebrafish versus mouse. In addition, zebrafish contains two kidney ducts only which show a low level of proliferation. Mice have a million tubules in each kidney which undergo extensive proliferation even after birth providing a higher probability of catching the cells at this specific time point.

PH3 provides a snap shot about the proliferative state at this particular moment of the embryo. On the other hand, BrdU (5-bromo-2-deoxyuridine) is permanently incorporated

into the DNA in S-phase during cell cycle and every daughter cell will inherit half of the amount in subsequent cell divisions. This can be utilized in experiments, where the rate of the cell cycle might be changed in the mutants but not the total number of proliferating cells. Using the PH3 staining method both, mutant and wildtype would appear the same, but using a BrdU shot would allow us to distinguish both populations after allowing them to develop further, allowing them to undergo several rounds of cell divisions. We performed extensive BrdU incorporation assays in order to support our results we obtained with PH3 as well as a basis for further studies with cystic kidney mutants we planned to analyze. Interestingly, BrdU incorporation appeared very inconsistent, ranging sometimes from 5% to 40% within the same experiment of sibling, age matched embryos. This might stem from inaccurate somite counting. But it might also arise from synchronous proliferation in the kidney as was shown to be the case in mouse tubules. Having millions of tubules next to each other is a big advantage when trying to analyze the mitotic angle. When newborn mouse tubules were stained with PCNA which is another proliferation marker, some tubules were almost entirely PCNA positive while others were entirely negative, indicating that a tubule autonomous mechanism governs synchronous proliferation along the tubule (Fischer *et al.*, 2006). Having only two ducts in zebrafish makes it more difficult to verify that indeed cells undergo a synchronized proliferation pattern. The best way to determine that would be to perform a time lapse video microscopy experiment using a kidney transgenic fish, unfortunately we do not have such animals at our disposal at this moment.

Disrupting PCP signaling in zebrafish did not lead to cyst formation but to dilation of the duct only. In contrast, overactivation of the canonical wnt pathway lead to duct dilation and cyst formation (data not shown), indicating that disruption of planar polarity alone is not sufficient to lead to cyst formation in zebrafish but disruption of both planar polarity as well as proliferation results in cyst formation. Unpublished data (Marco Pontoglio lab) indicate that in the mouse disruption of PCP might lead to cyst formation. However, in zebrafish with a very modest proliferation rate, the disruption of planar polarity alone is not sufficient. This might again be due to the different nature of kidney development in mouse versus zebrafish.

Our study is the first one to show a temporal analysis for key events such lumen formation, polarity establishment and cilia formation as well as the role of proliferation and planar polarity during embryonic kidney development in zebrafish. It might serve as

a frame work for future analysis of cystic kidney mutants and help understand the formation of duct dilation.



## **Project II**

### **Part 1**

#### **Characterization of the**

***scorpion*<sup>hi459</sup> Mutant**

**and *arl13b/ scorpion* Morphant**

## 6.1. INTRODUCTION

### 6.1.1. PKD and Joubert syndrome

Renal cystic kidney diseases can be caused by a variety of mutations and depending on the disease, cysts occur at different locations and at different time points during development, ranging from embryogenesis to adulthood. Autosomal dominant polycystic kidney disease (ADPKD) is among the most common monogenetic disorders in humans and the most prevalent form of renal diseases, occurring 1 in 400-1000 live births (Gabow, 1993; Grantham *et al.*, 2006; Wilson *et al.*, 2004; Yoder *et al.*, 2005). ADPKD is caused by mutations in the genes PKD1 or PKD2 and is characterized by the formation of fluid filled bilateral cyst in the kidney with extrarenal manifestations in the liver, pancreas and heart (Perrone, 1997).

ADPKD patients are typically diagnosed in adulthood and 50% of patients will progress to end stage renal failure (ESRF) by age 60 (Torres *et al.*, 2007). Cysts arise in all parts of the kidney with a majority of cysts forming in collecting ducts (Baert, 1978; Verani and Silva, 1988). By contrast, autosomal recessive polycystic kidney disease (ARPKD) is quite rare, occurring in 1 in 20,000 live births. ARPKD is characterized by bilateral renal cyst formation and congenital hepatic fibrosis. The renal pathology in ARPKD is restricted to the collecting duct with the more severe cases developing in utero (Zerres *et al.*, 1988) or in the neonatal period. The gene mutated in ARPKD is *PKHD1* (polycystic kidney and hepatic disease gene 1) and encodes for a protein named Fibrocystin/Polyductin. ARPKD causes infant mortality in up to 30% of cases (Onuchic *et al.*, 2002; Ward *et al.*, 2002). Approximately one third of patients that survive infancy progress to ESRF by the age of 10. ADPKD and ARPKD patients show a very distinct kidney phenotype. Whereas ADPKD cysts are focally derived and bud from all regions of the nephron, ARPKD results in fusiform dilatations of the collecting duct (Wilson, 2004). There are a number of other inherited forms of renal cystic disease, e.g. Nephronophthisis (NPHP) and Bardet-Biedl syndrome (BBS). NPHP is an autosomal recessive cystic kidney disease which is the most common cause of chronic renal failure in children (Hildebrandt and Zhou, 2007) and is characterized by formation of kidney cysts in the corticomedullary junction and tubulointerstitial fibrosis. Beside renal manifestations of the disease, NPHP also shows extra-renal defects in the eye (retinitis pigmentosa, retinal degeneration), brain (mental retardation, cerebellar malformations),

body axis (situs inversus), heart (cardiac ventricular septic defects) and liver (liver fibrosis). BBS results largely from mutations that affect the integrity of basal bodies and cilia. Patients present with many different defects including obesity, polydactyly, mental retardation, cystic kidneys and retinitis pigmentosa among others (Beales *et al.*, 1999). Proteins encoded by the genes mutated in NPHP and BBS have been shown to localize to the cilium or basal body, thus these diseases have been grouped together under the term ‘ciliopathies’ (Badano *et al.*, 2006). Another ciliopathic disease is Joubert syndrome (JS). JS is a rare, autosomal recessive disorder with an estimated prevalence of 1:100,000 that affects the cerebellum and brain stem which regulate motor control, balance and coordination. Joubert syndrome patients are characterized by the absence or underdevelopment of the cerebellar vermis and a malformed brain stem, which is called ‘molar tooth sign’ due to its shape when imaged by MRI (magnetic resonance imaging) (Fig. 16). The most common features of JS patients include ataxia (lack of muscle control), mental retardation, oculomotor apraxia (defects in motor nerves that result in movement problems of the eye), hypotonia (low muscle tone) and sleep apnea (pauses in breathing during sleep). In addition to the developmental defects seen in the classical form of JS, many patients show additional clinical features which have been associated with ciliary defects, such as cystic kidneys, retinal dystrophy, hepatic fibrosis, polydactyly among others and they are called Joubert syndrome and related disorders (JSRD).

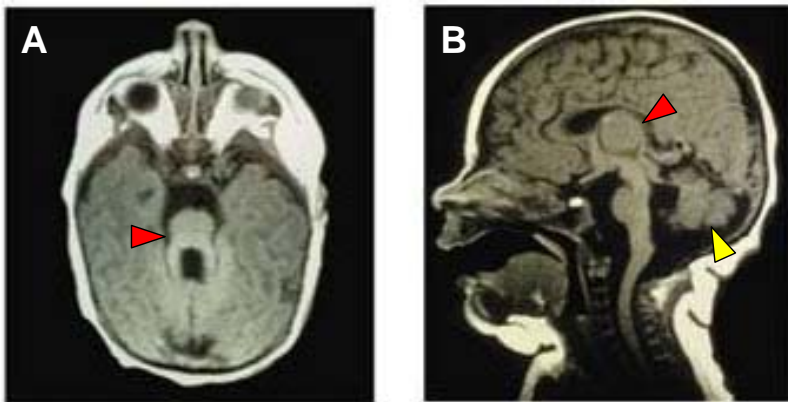


**Fig 16: Joubert Syndrome (JS) is diagnosed by the neurological finding of a “molar tooth sign” (MTS) on MRI.**

Axial (A) and mid-sagittal (B) MRI images from a JS patient are shown. (A) On axial sections the MTS is clearly visible, resulting from a malformed brain stem (red arrow head). (B) In mid-sagittal sections the underdeveloped cerebellum is visible (yellow arrow head) as well as the malformed brain stem (red arrow head).

Image taken from Arts *et al.*, 2007.

Thus far, mutations in seven genes *NPHP1* (Parisi *et al.*, 2004), *AHI1* (Eley *et al.*, 2008), *CEP290* (Kim *et al.*, 2008), *RPGRIP1L* (Arts *et al.*, 2007), *MKS3* (Baala *et al.*, 2007), *CC2D2A* (Gorden *et al.*, 2008) and *ARL13B* (Cantagrel *et al.*, 2008) have been identified in patients with JSRD and all of the gene products have been found to be essential for a functional cilium and/ or basal body. JSRD therefore belong to the expanding group of disorders resulting from ciliary dysfunction. Interestingly, in a recent study a direct link between human *ARL13B* and the classical form of JS was found in human patients (Cantagrel *et al.*, 2008). Even though the association between *ARL13B* and JS might be compelling on the first glance being consistent with the hypothesis that JS is a ciliopathy and caused by ciliary defects, it appears to be more complex. Patients that have been found to have underlying mutations in *ARL13B* present with the classical form of JS whereas patients with non classical forms of JS (JS and related disorders or JSRD) do not have mutations in *ARL13B* (Cantagrel *et al.*, 2008). Two models could account for the specificity of *ARL13B* in the classical form of JS. First, *ARL13B* could be functioning specifically in the cerebellum and brain stem, hence mutations in *ARL13B* would result in phenotypes affecting primarily the brain and mental development. The alternative model is, that mutations in *ARL13b* are rare and the identified alleles are not null but partial loss-of-function alleles. Different organs might have variable sensitivities to the level of *Arl13B*, thus reduced levels of *Arl13B* might lead to differential phenotypes in different organs. Here we provide a detailed analysis of the zebrafish mutant of *Arl13b* called *scorpion*<sup>hi459</sup> and its potential role in different organs during zebrafish development.

### 6.1.2. Cilia as mechanosensor

Many studies recently have focussed on the cilium since many proteins involved in ciliopathies have been found to localize to cilia. The ciliocentric model of PKD describes the cilia as a mechanosensory organelle (Fig. 2). Polycystin-1 and Polycystin-2 form a  $\text{Ca}^{2+}$ -channel complex on the ciliary membrane. Physical stress, such as bending of the cilium, triggers the channels to open and results in an elevation of cytoplasmic  $\text{Ca}^{2+}$  (Praetorius *et al.*, 2003; Praetorius and Spring, 2001). It is thought that this rise in calcium in turn triggers release of additional calcium from internal calcium stores which leads to upregulation of inversin and inhibition of the canonical Wnt signaling pathway, thus leading to antiproliferative signals (Simons *et al.*, 2005; Nauli *et al.*, 2003). It is possible that ciliary defects or absence of cilia could result in a failure to regulate growth

and proliferation and thereby leading to less differentiated and overproliferating tubular cells.

### 6.1.3. Polarity and secretion

Hyperproliferation, unregulated apoptosis, loss of apico-basolateral as well as planar cell polarity, excessive fluid secretion and dedifferentiation are hallmarks that accompany cyst formation. Na<sup>+</sup>/K<sup>+</sup>-ATPase is an ion pump that is responsible for pumping sodium and potassium ions across the membrane, thus creating an electrochemical gradient. Under normal conditions, Na<sup>+</sup>/K<sup>+</sup>-ATPase is expressed at the basolateral membrane. Some studies found ectopically targeted Na<sup>+</sup>/K<sup>+</sup>-ATPase in cystic epithelia to the apical membrane, which might lead to excessive fluid accumulation in the duct (Avner *et al.*, 1992; Drummond, 2003; Wildson *et al.*, 2000). Other studies could not reproduce that result and it is not clear whether Na<sup>+</sup>/K<sup>+</sup>-ATPase mislocalization and loss of polarity in general play major roles during cystogenesis.

### 6.1.4. Zebrafish pronephros

Zebrafish is a very attractive model to study kidney development as well as cyst formation at the cellular level. Each human kidney contains about 1 million tubules called nephrons which are the functional units of the kidney, responsible for the filtration and purification of the blood. Each nephron consists of a glomerulus that connects to the urine-collecting tubule. The glomerulus acts as a filter and to regulate the amount of water, salts, glucose and urea along other minerals in the body. Proteins and cells are kept in the blood stream whereas toxins, waste and fluid are allowed to pass through. The zebrafish pronephros is remarkably simplified in comparison, consisting of only two nephrons. Both are fused via their respective glomeruli at the midline and a tubular neck segment connects the duct to the glomerulus. The pronephros is the first kidney to form in all vertebrates, but is replaced by a more advanced form in mammals (Vize *et al.*, 1997). However, both the mammalian kidney and zebrafish pronephros are very similar regarding gene expression patterns and osmotic homeostasis (Drummond *et al.*, 1998).

Homologous to mammalian kidneys, the zebrafish glomerulus is the site of filtration. Liquid, salts and other small molecules are pushed in a nonselective manner into the Bowman's space. The tubules and ducts reabsorb salts and ions back into the body and the final filtrate is shunt out the body through the cloaca. Glomerular filtration is thought to start around 36-48 hpf (Drummond *et al.*, 1998). In contrast to land-living mammals, the zebrafish pronephros primarily designed for osmoregulation rather than excretion.

Zebrafish kidney epithelia can be single ciliated or multi ciliated (Liu *et al.*, 2007; Ma *et al.*, 2007). Cilia are mostly formed by a process called compartmentalized ciliogenesis (Avidor-Reiss *et al.*, 2004). The basal body is relocated to the anterior side of the cell just beneath the plasma membrane and assembly of the axoneme occurs by addition of new subunits to the growing ciliary tip (Johnson and Rosenbaum, 1992). This results in a membrane bound axoneme that projects out of the cell. The ciliary axoneme that extends from the basal body consists of nine microtubule doublets. Most motile cilia have an additional microtubule doublet in the center ((9+2) axoneme), while primary cilia lack the central pair ((9+0) axoneme). Zebrafish renal cilia have been shown to possess (9+2) cilia which are motile and beat in a coordinated manner which has been shown to be important for fluid flow through the pronephros (Kramer-Zucker *et al.*, 2005). In humans, fetal kidneys have been shown to transiently possess (9+2) cilia, but they are replaced by immotile (9+0) during embryonic development. Mature mammalian kidney epithelia possess immotile cilia with a (9+0) axonemal structure. Generally, cilia with a (9+2) axonemal structure have been shown to be motile whereas (9+0) axonemal cilia are immotile. An exception to this association between structure and motility are cilia that can be found on the embryonic node (nodal cilia), which possess a (9+0) axonemal structure but are motile and crucial for left-right determination.

### **6.1.5. *scorpion*<sup>hi459</sup> mutant**

It had been previously shown that the *scorpion*<sup>hi459</sup> mutant is characterized by a ventral body curvature and formation of kidney cysts at 2.5 dpf (Sun *et al.*, 2004). In addition, *scorpion*<sup>hi459</sup> mutants display a ciliary defect in the pronephros providing a link between cilia and renal cyst formation. Here we provide a spatial and temporal analysis of cyst formation in the zebrafish *arl13b* mutant, called *scorpion*<sup>hi459</sup> (*sco*). In order to understand whether differentiation, polarity formation or fluid secretion might be misregulated in *scorpion*<sup>hi459</sup> mutants, we followed the histological study with a cellular

analysis of cystic epithelial cells. Furthermore, in an effort to determine the role of *scorpion*<sup>hi459</sup> during early embryogenesis, we used morpholino oligos to knock down the expression of *arl13b/ scorpion* transcripts and found a novel role for Arl13b/ Scorpion in laterality formation during embryogenesis. This study might help to elucidate the role of Arl13b/ Scorpion in ciliogenesis as well as its role in cyst formation.

## 6.2. RESULTS

### 6.2.1. Phenotype of *scorpion*<sup>hi459</sup> mutants

The *scorpion*<sup>hi459</sup> mutant was originally identified in an insertional mutagenesis screen for recessive mutations that displayed cystic dilations in the pronephros (Sun *et al.*, 2004). Interestingly, most of the mutants that were found shared a very similar phenotype of kidney cysts and body axis curvature defects. The body curvature defect is not linked directly to development of kidney cysts, as some mutants develop cystic kidneys but have a straight body (*vhnf1* and *caudal*) and *vice versa* (Brand *et al.*, 1996). The body curvature phenotype was first recognizable around 26 hpf which is the earliest timepoint at which *scorpion*<sup>hi459</sup> mutants can be distinguished from their wildtype and heterozygous siblings. At 2.5 dpf a cystic dilation of the pronephros was visible under the light microscope just posterior to the otic vesicles, the ear structure in zebrafish (Fig.17, D). At 5 dpf the cystic dilation was significantly increased in size (Fig.17, H). Pericardiac edema was evident in *scorpion*<sup>hi459</sup> mutants between 2 dpf and 3 dpf and became progressively more severe during development of the embryo. General edema were also observed in most embryos and can be detected at 50 hpf. *scorpion*<sup>hi459</sup> mutants died around 6 dpf indicating that Arl13b/ Scorpion is crucial for early embryonic development.



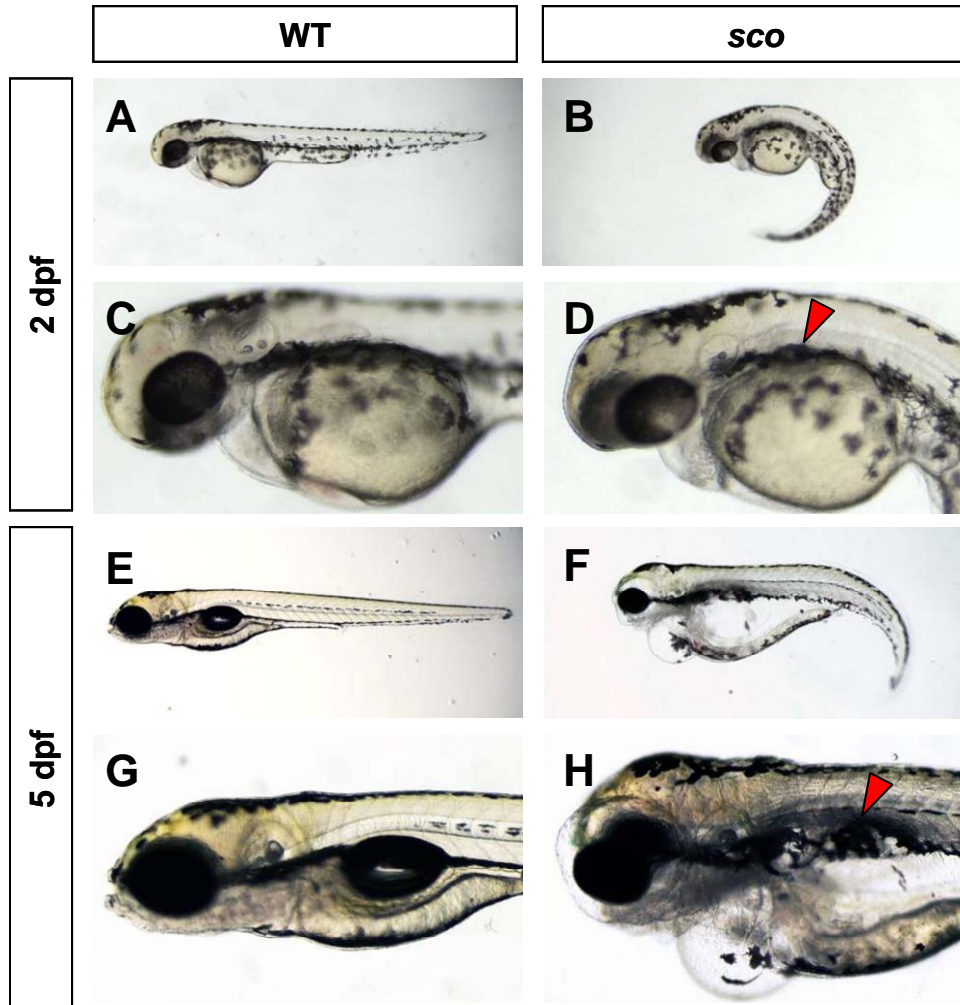


**Figure 17: *scorpion*<sup>hi459</sup> mutants develop kidney cysts**

(A-D) 2 dpf. (E-H) 5 dpf. At 2 dpf *scorpion*<sup>hi459</sup> mutants can be easily distinguished from siblings by their downward body curvature and kidney cysts. (C-D) Higher magnification images of (A-B) showing the cystic dilation in the anterior region of the pronephric duct. (F, H) At 5 dpf, the cystic dilations have increased in size and the fish presents pericardiac edema, which are not present in wildtype siblings (E, G). Kidney cysts are indicated by arrowheads and are positioned behind the otic vesicle and eye.

WT: wildtype, *sco*: *scorpion*<sup>hi459</sup>, dpf: days post fertilization

### 6.2.2. Cystic dilations first appear in medial tubules in *scorpion*<sup>hi459</sup> mutants

In order to study the temporal and spatial development of cystic dilations in the pronephric duct of the *scorpion*<sup>hi459</sup> mutants, a histological time course was performed.

To ensure comparison of similar regions in wildtype and mutant embryos, we used several landmarks of the zebrafish anatomy to help us define regions of the duct. The glomerulus is the filtration unit of the duct and is comprised of podocytes and fenestrated capillaries that are surrounded by an epithelium called Bowman's space. Throughout this study the anterior duct will refer to the most anterior part of the duct, just posterior after they connect to the tubules and where they start to extend laterally along the body, the gut is positioned on the left side of the embryo. The medial duct refers to the middle third of the duct. In the medial region the ducts are still located at the lateral side of the body and are far apart. The posterior duct refers to the last third of the duct, where the ducts are in close proximity to each other and the gut is positioned medially.

Pronephric cysts in *scorpion*<sup>hi459</sup> mutants were first observed under light microscopy in the glomerular/anterior region at 2.5 dpf (Fig. 17). In order to determine the spatial and temporal development of cyst formation we performed histological analysis on *scorpion*<sup>hi459</sup> mutants and their sibling controls. At early 2 dpf the pronephric duct in *scorpion*<sup>hi459</sup> and wildtype siblings were indistinguishable (data not shown). At late 2 dpf *scorpion*<sup>hi459</sup> mutants showed dilations in all regions of the duct. The severity of dilation that were observed differed from embryo to embryo but most showed dilation along the pronephric duct most prominently in the medial region. The glomerulus in *scorpion*<sup>hi459</sup> mutant embryos also showed dilations that progressed over time. The Bowman's capsule in *scorpion*<sup>hi459</sup> mutant embryos showed an increased volume of filtrate which probably led to a disorganization of the capillaries and associated podocytes. At 4 dpf the pronephric duct in *scorpion*<sup>hi459</sup> was grossly enlarged in every segment compared to age matched wildtype siblings (Fig. 18).

By performing this histological time course we found that cystic dilations in *scorpion*<sup>hi459</sup> mutants occur around 2 dpf and are often most severe in the medial region of the duct. Human PKD patients show the most prominent dilations in corresponding regions as well.

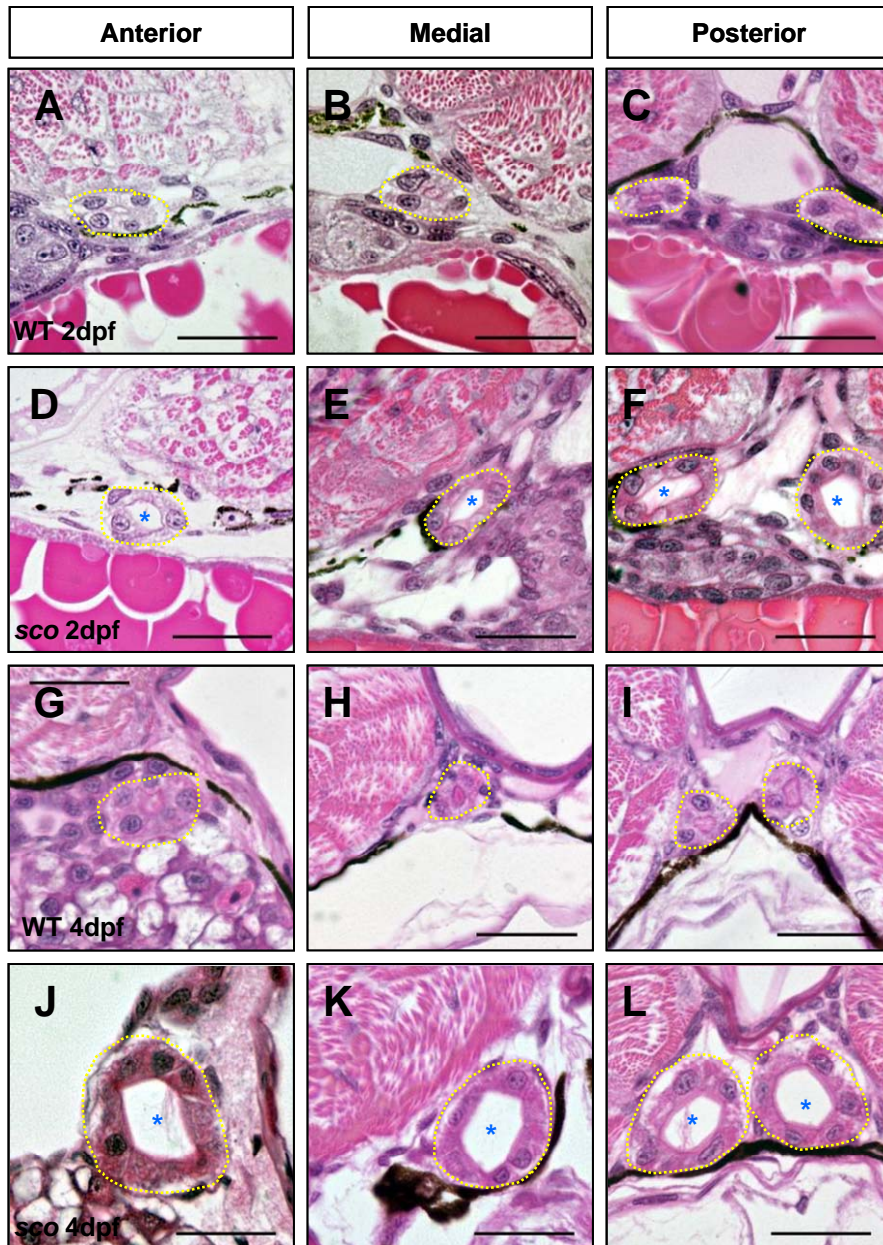


**Fig. 18: Temporal and spatial analysis of cyst formation in *scorpion*<sup>hi459</sup> mutants.** Wildtype and *scorpion*<sup>hi459</sup> cross sections are stained with Hematoxylin and Eosin at 2 dpf (A-F) and 4 dpf (G-L). All sections are 4  $\mu$ m thin JB-4 plastic sections. Wildtype kidney ducts at 2 dpf show a very homologous lumen size throughout various ductal regions (A-C). *scorpion*<sup>hi459</sup> mutants display enlarged kidney ducts in anterior (D), medial (E) and posterior (F) regions. (G-I) Wildtype ducts at 4 dpf. (J-L) *scorpion*<sup>hi459</sup> mutants at 4 dpf show a significantly enlarged duct in all regions and increased number of cells in the ductal circumference. Pronephric ducts are outlined in yellow dotted line. Asterix indicate enlarged lumen. Scale bars represent 20  $\mu$ m.

### 6.2.3. Proliferation in the duct is secondary to dilation

Proliferation and apoptosis are important cellular processes that must be strictly regulated in order to maintain correct tissue architecture. Many renal cystic diseases share features of increased cell proliferation, however it is not clear whether it is a result of the dilation or the underlying cause. Alternatively, the dilation of the pronephric duct observed in *scorpion*<sup>hi459</sup> mutants could also be due to an expansion of the cell surface. We sought to investigate the role of a potential increase in cell number by analyzing the cell numbers in the anterior, medial and posterior segment of the kidney duct. Serial sections of each segment were collected and stained with hematoxylin and eosin to distinguish the nuclei from the cytoplasm at 2 dpf and 4 dpf old embryos. Nuclei of the pronephric epithelium in 6 consecutive sections (4  $\mu$ m thin JB-4 plastic sections) of all regions were counted, averaged and plotted on a bar graph (Fig. 19; Table 1). Even though the duct is dilated along its entire length, only the medial region showed a significant increase in cell number indicating that proliferation might not be the leading cause for duct dilation. By 4 dpf, all segments of the pronephric duct displayed a significant increase in cell number in the ductal circumference compared to wildtype siblings (Table 1). The pronephric duct becomes very convoluted at the anterior region at around 4 dpf and counting nuclei becomes more and more difficult, thus the data for the anterior region at 4 dpf might be not exact.

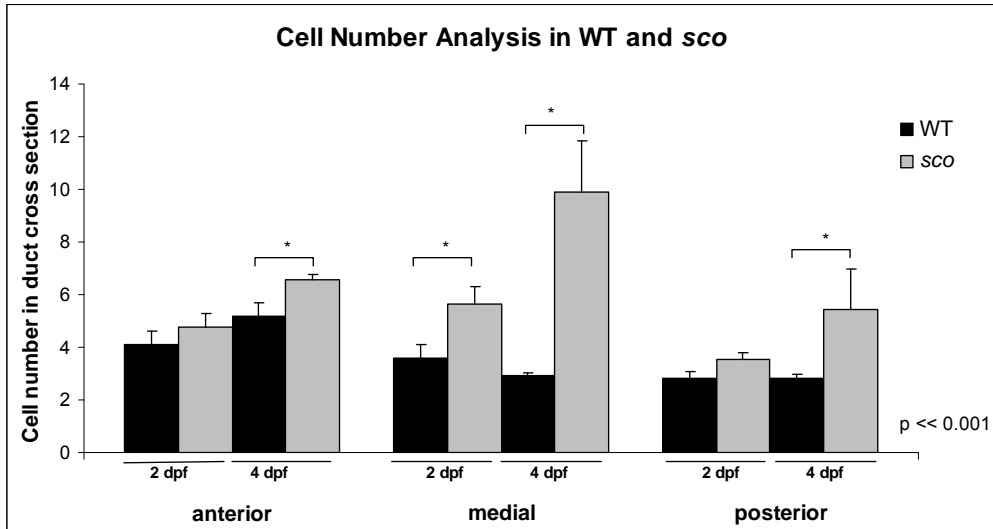


**Fig. 19: Average cell number surrounding the medial tubules in *scorpion*<sup>hi459</sup> mutants is increased at 2 dpf and 4 dpf.**

Bar graphs display the average cell number surrounding the anterior, medial and posterior tubule lumen at 2 dpf and 4 dpf in wildtype (black) and *scorpion*<sup>hi459</sup> mutants (grey). At 2 dpf there is not a significant increase in cell number surrounding the tubules between wildtype sibling and mutant populations in the anterior and posterior part of the duct. However, the medial pronephric duct of *scorpion*<sup>hi459</sup> mutant embryos shows a significant increase in cell numbers.

At 4 dpf a significant increase in the number of cells surrounding the pronephric duct lumen in *scorpion*<sup>hi459</sup> mutants in all segments is present.

In all graphs, the average with the error bars representing standard deviation is plotted.

2dpf	WT	n	sco	n	P value
anterior	4.11 ± 0.49	6	4.75 ± 0.53	4	4.4E-3
medial	3.6 ± 0.52	6	5.67 ± 0.66	6	3.4E-12
posterior	2.83 ± 0.82	6	3.56 ± 0.24	4	14.1E-3
4dpf	WT		sco		P value
anterior	5.17 ± 0.53	4	6.54 ± 0.25	4	11.9E-6
medial	2.94 ± 0.07	4	9.92 ± 1.94	5	1.4E-24
posterior	2.80 ± 0.18	4	6.00 ± 1.55	6	35.8E-15

**Table 1: Number of cells in the duct of wildtype and *scorpion*<sup>hi459</sup> mutant embryos at 2 dpf and 4 dpf.**

These data points are displayed in the bar graphs in figure 19 and represent the means followed by standard deviation. The mean was derived from the cell numbers of at least 6 consecutive sections in the anterior, medial and posterior region of the pronephric duct, respectively.

The sample size (n) refers to the number of tubules used for this statistical analysis. P value was obtained with Student-T-test calculated in Excel.

#### **6.2.4. *arl13b/scorpion* morphants phenocopy the *scorpion*<sup>hi459</sup> mutant phenotype**

Morpholino oligos are synthetic oligo nucleotides that can be used to knock down the message of a specific gene of interest in zebrafish embryos. We designed several *arl13b/scorpion* antisense morpholino oligos including translational start site blocking morpholinos. These start site morpholinos bind to 25 base pairs of the 5' UTR sequence upstream of the start site of the *arl13b/scorpion* gene. However, since morpholino oligos can have potential unspecific effects it is important to verify that any phenotype that is observed after injecting the morpholino is specific. To verify specificity, rescue experiments were performed by coinjecting full length *arl13b/scorpion* mRNA along with *arl13b/scorpion* morpholino.

As shown previously (Fig. 17) *scorpion*<sup>hi459</sup> mutants exhibit a downward body curvature defect and develop kidney cysts. A control morpholino that was designed not to target any gene in the zebrafish genome was used as control to verify that the morpholino injection itself did not cause a defect. 0.5 nl [1 mM] of either morpholino was injected into wildtype embryos at the 1-4 cell stage. At 2 dpf as well as 5 dpf control morphants, i.e. embryos injected with control morpholino, are indistinguishable from wildtype embryos. *arl13b/scorpion* morphants on the other hand display a ventrally curved body axis, a defect in the inflation of the swim bladder, pericardiac edema of varying degrees and formation of pronephric cysts which are first visible at 2 dpf (Fig. 20). This phenotype closely resembles the *sco*<sup>hi459</sup> mutant phenotype, which also develops a downward body curvature defect, pronephric cysts, pericardiac edema and fails to fully inflate the swim bladder. At 5 dpf, both mutant and morphant embryos exhibit an increased pronephric cysts (Fig. 20 H', I', red arrow heads) and a laterally curved body (which appears bent upward due to the angle of the image).



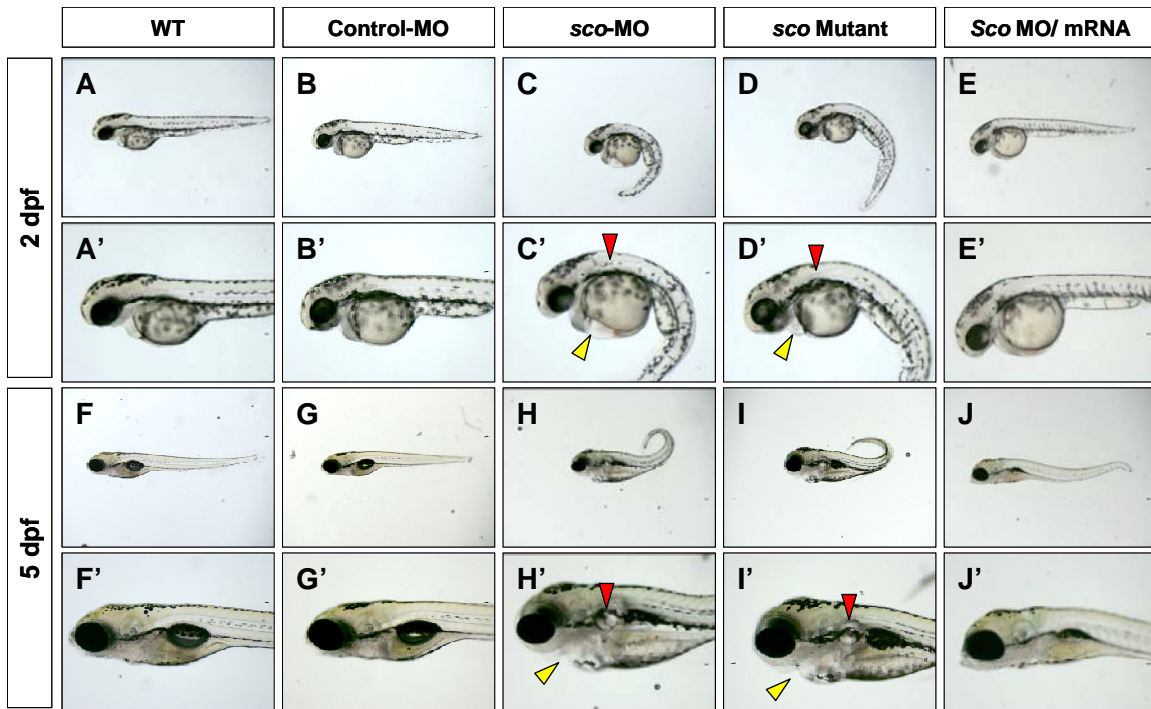


**Fig. 20: The *arl13b/scorpion* morphant phenocopies the *sco*<sup>hi459</sup> mutant phenotype.**

Lateral views of embryos at 2 dpf (A-E') and 5 dpf (F-J') are shown. Dashed images show a magnified view of the corresponding image.

Wildtype and control morphants are indistinguishable at 2 dpf (A, B) and 5 dpf (F, G). The mutant phenotype (D, I) is characterized by a ventrally curved body axis, a defective inflation of the swim bladder, formation of kidney cysts which are first visible at 2 dpf (red arrow head) and pericardiac edema (yellow arrow head) with variable degrees. Both, the size of kidney cysts as well as the severity of the edema increase during development (D, I) while the body curves laterally. *Ar13b/sco* morphants (C, H) phenocopy the mutant phenotype, exhibiting the same renal, body axis and pericardiac defects as *sco*<sup>hi459</sup> mutants at 2 dpf as well as 5 dpf. The morpholino can be rescued by coinjection of *arl13b/sco* mRNA, indicating that the morpholino induced phenotype is indeed specific to a knock down of the *arl13b/sco* message (E, J). Rescued embryos do not develop kidney cysts and show a straight or mildly curved body axis (J shows a mildly curved body).

*sco*: *arl13b/scorpion*, MO: morphant

Morpholinos were injected at the 1-4 cell stage.

### 6.2.5. The *arl13b/ scorpion* morpholino is specific

To verify that the observed phenotype we obtained with *arl13b/ sco* morpholino injections indeed was specific, we coinjected the morpholino with full length *arl13b/ scorpion* mRNA aiming to rescue the mutant phenotype thus proving specificity. At 2 dpf the rescued embryos appear straight and no pronephric cysts are visible (Fig. 20 E ). At 5 dpf most rescued embryos appear straight, with some embryos showing a mildly curved body (shown in Fig. 20 J). However, even mildly curved embryos do not form kidney cysts. The different kinetics of degradation of the morpholino as well as the mRNA might account for the mildly curved body axis defect we can observe at the later stages of the rescued embryos. Table 2 summarizes the rescue experiment, which was repeated three times.

	n	straight [%]	curved [%]	kidney cysts [%]
WT	146	100.00	0.00	0.00
control-MO	122	99.18	0.82	0.00
<i>sco</i> -MO	148	1.35	98.65	98.65
<i>sco</i> MO/ <i>sco</i> mRNA	139	90.65	9.35	2.88

**Table 2: *arl13b/ scorpion* morphants can be rescued by coinjection of *scorpion* mRNA.**

Summary of the rescue experiments are shown. Injection of *sco*-morpholino into wildtype embryos results in a curved body curvature in 98.65% of injected embryos with all of them developing kidney cysts. Coinjection of *sco*-morpholino with *in vitro* transcribed *arl13b/ sco* mRNA could almost completely rescue the mutant phenotype, with 90.65% of embryos being phenotypically wildtype.

All embryos were injected at the 1-4 cell stage into wildtype embryos. Embryos were scored for body curvature at 2 dpf and kidney cysts at 4 dpf.

### 6.2.6. Arl13b/ Scorpion is expressed in various ciliated tissues

Since *scorpion*<sup>hi459</sup> mutants develop kidney cysts, we sought to determine in which subcellular compartments Arl13b/ Scorpion would be localized to. Using an antibody raised against the C-terminus of the Arl13b/ Scorpion protein, we performed immunohistochemistry on wildtype embryos and detected what appeared to be a ciliary signal in the pronephric duct. We confirmed this finding with double labeling with an antibody for acetylated  $\alpha$ -tubulin, which labels the cilium. To our excitement, Arl13b/ Scorpion is exclusively localized to the cilium (Fig. 21).



It is known that most cell types in vertebrates are ciliated. Examining the expression pattern of Arl13b/ Scorpion in various tissues beside the kidney in zebrafish, we observed that it is localized to the cilium in the olfactory placode (nose), spinal cord canal, Kupffer's vesicle and lateral line organ (mechano-sensory organ that senses water movement) beside other regions, suggesting that Arl13b/ Scorpion might play a global role for ciliogenesis in a variety of ciliated organs.

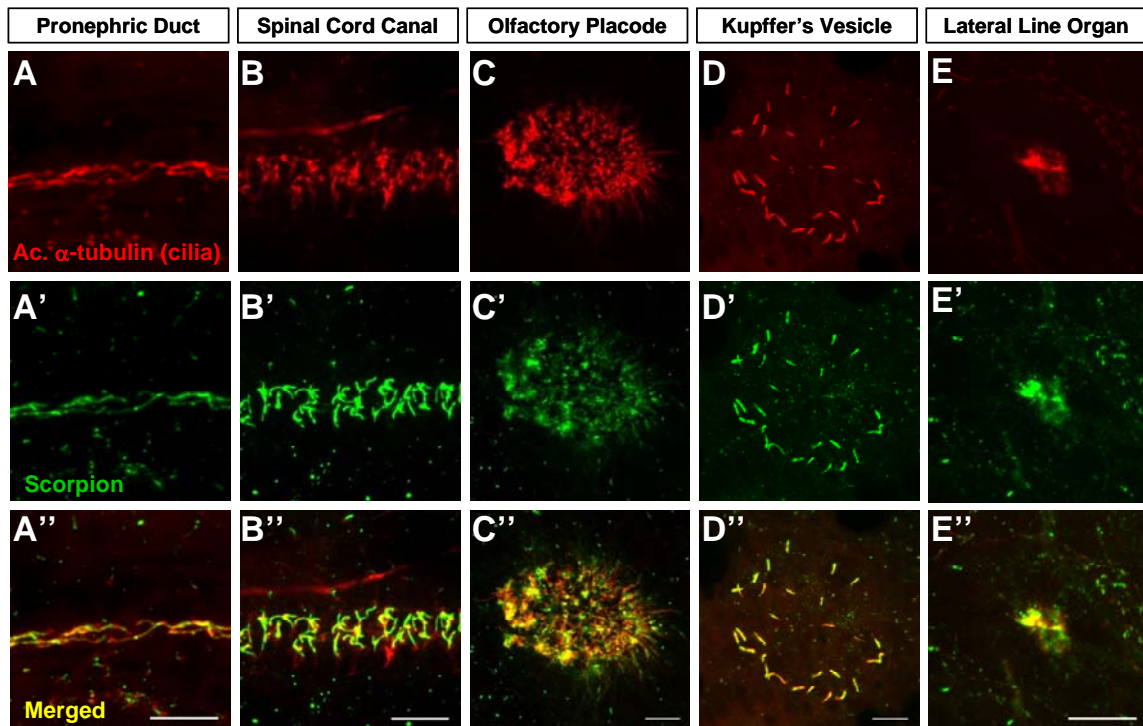


**Fig. 21: Arl13b /Scorpion is expressed on cilia in multiple ciliated tissues in zebrafish.**

Whole mount fluorescent immunostaining of Arl13b/ Scorpion (green) and acetylated  $\alpha$ -tubulin (red) shows colocalization indicating that Arl13b/ Scorpion is expressed on cilia. (A-A'') Pronephric duct, 2 dpf. (B-B'') Spinal cord canal, 2 dpf. (C-C'') Olfactory placode, 2 dpf. (D-D'') Kupffer's vesicle, 10 Somite stage. (E-E'') Lateral line organ, 2 dpf. Scale bars represent 10  $\mu$ m.

### 6.2.7. Otic vesicles in *arl13b/ scorpion* morphants and *sco*<sup>hi459</sup> mutants

Since *Arl13b/ Sco* is expressed on cilia in ciliated tissues, we sought to analyze the formation of otic vesicles in *arl13b/ sco* morphants and the *sco*<sup>hi459</sup> mutant embryo. The zebrafish ear serves auditory and vestibular functions and develops from the otic placode, a transient thickening of the ectoderm. The otic placode then hollows, hair cells are formed and otoliths attach firmly to kinocilia (Riley *et al.*, 2003). The number of otoliths is strictly regulated and a derivation from the regular two otoliths per otic vesicle can be used as a read out for underlying defects of the ear. In order to analyze whether *Arl13b/ Scorpion* might play a role in otolith formation, we analyzed wildtype embryos, *scorpion*<sup>hi459</sup> mutant embryos as well as *arl13b/ scorpion* morphant along with control morphant embryos. As expected, 2 dpf old wildtype embryos show two otoliths per otic vesicle (Fig. 22, A). However, *arl13b/ scorpion* morphants and mutants exhibit a variable number of otoliths, ranging from one otolith to three otoliths per otic vesicle, with the majority of embryos being able to maintain normal number of otoliths (Fig. 22, B-D). After performing statistical analysis the variability appears not to be statistically significant (see table 3) indicating that *Arl13b/ Scorpion* does not play an important role during otolith formation.

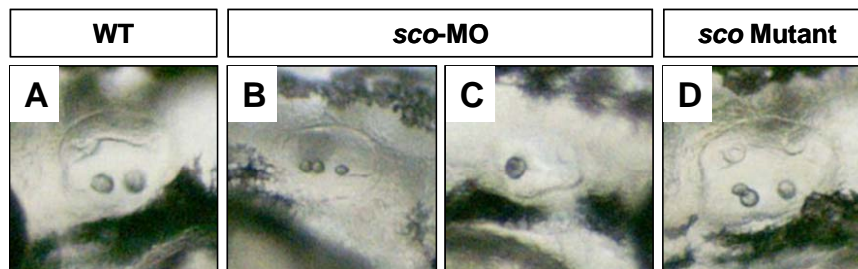


**Fig. 22: Number of otoliths in otic vesicles is not significantly altered in *sco*<sup>hi459</sup> mutants and *arl13b/sco* morphants respectively.**

Number of otolith formation was analyzed in WT (A), *arl13b/sco* morphants (B,C) and *sco*<sup>hi459</sup> mutants (D). Embryos injected with a control morpholino are indistinguishable from wildtype embryos. *arl13b/sco* morphants and *sco*<sup>hi459</sup> mutants exhibit a less strict regulation in the number and size of otolith formation, however it is not statistically significant (analyzed with T-Test).

All embryos were analyzed at 2 dpf.

	WT	Control-MO	Sco-MO	Sco mutant
Sum	2	1.97	1.9	2.1
stdev	0	0.2	0.6	0.5
T-test	/	0.286	0.564	0.394
n	35	33	36	39

**Table 3: Number of otoliths in otic vesicles is more variable in scorpion morphants and mutants, but not statistically significant.**

Morpholino injections were performed at the 1-4 cell stage in wildtype embryos. Embryos were analyzed at 2 dpf. WT: wildtype, sco: *arl13b/ scorpion*, MO: morphant, stdev: standard deviation, n: number of otic vesicles analyzed.

### 6.2.8. Small eye phenotype in severe *arl13b/ sco* morphant and *sco*<sup>hi459</sup> mutant embryos

Many ciliopathies are accompanied by defects of the eye, e.g. retinitis pigmentosa and coloboma. To analyze the eye size, the outer perimeter of the sclera ( $P_o$ ), which surrounds the eye and can be used as a tool to measure the degree of edema of the eye. Additionally, the eye size itself was measured ( $P_i$ ). At 2 dpf mutant, morphant and wildtype embryos are not distinguishable by their eye size and no difference in eye size is observed (data not shown). At 5 dpf, all morphant and mutant embryos develop an edemic phenotype with a subpopulation developing severe edema, which can be recognized as a big bubble-like enlargement of the pericardiac lumen (Fig. 23). These embryos will be referred to as SE (severely edemic) embryos in the following text. SE embryos, in *arl13b/ sco* morphants as well as *scorpion*<sup>hi459</sup> mutants, show a reduction in eye size by 20% -30% (see table 4). In contrast, mildly edemic embryos (ME) do not show a significant increase of the eye size but a significant increase of the outer circumference of the sclera only, indicating that indeed these embryos are edemic but do not exhibit a small eye phenotype yet.

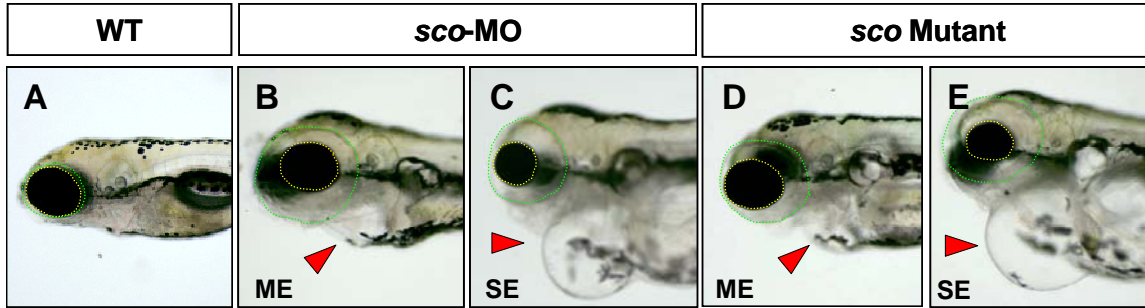


**Fig. 23: Severely edemic *sco*<sup>hi459</sup> mutant and *arl13b/sco* morphant embryos exhibit a smaller eye size.**

The perimeter of the sclera ( $P_o$ ) covering the eye in zebrafish as well as the circumference of the eye ( $P_i$ ) were measured using adobe photoshop and Image J. (A) In wildtype the sclera (outlined in green) is closely attached to the eye (outlined in yellow). (B-E) In *arl13b/sco* morphants (B, C) as well as *sco*<sup>hi459</sup> mutants (D, E), the sclera is enlarged due to an edemic phenotype which is recognizable by pericardiac edema (red arrowhead). The degree of the pericardiac edema is variable among morphant and mutant embryos and can range from mildly edemic (ME) to severely edemic (SE). Eye size in ME embryos is not significantly altered compared to wildtype. However, SE embryos exhibit a significantly smaller perimeter of the eye compared to wildtype embryos.

MO: morphant; *sco*: *arl13b/sco*; SE: severe edema; ME: mild edema  
All embryos are shown from lateral view at 5 dpf.

	WT	control-MO	<i>sco</i> -MO, ME	<i>sco</i> -MO, SE	<i>sco</i> -Mutant, ME	<i>sco</i> -Mutant, SE
Perimeter <sub>o</sub> [ $\mu$ m]	403.86 $\pm$ 14.41	419.03 $\pm$ 33.22	587.75 $\pm$ 46.22	618.01 $\pm$ 29.64	576.1 $\pm$ 39.72	620.77 $\pm$ 11.18
T-test		0.32	2.07E-06	6.29E-06	1.61E-06	1.34E-06
Perimeter <sub>i</sub> [ $\mu$ m]	400.74 $\pm$ 14.51	387.55 $\pm$ 26.40	376.24 $\pm$ 15.59	312.5 $\pm$ 14.04	377.39 $\pm$ 37.14	307.72 $\pm$ 1.56
T-test		1	0.22	7.10E-04	0.55	3.20E-04
Ratio ( $P_i/P_o$ )	0.96 $\pm$ 0.01	0.93 $\pm$ 0.02	0.64 $\pm$ 0.03	0.51 $\pm$ 0.05	0.65 $\pm$ 0.03	0.5 $\pm$ 0.01
T-Test [P-value]		0.01	2.94E-10	2.10E-07	1.44E-09	1.50E-09
n	12	16	12	4	12	4

**Table 4: Data of quantification of the small eye phenotype in severe edemic *arl13b/sco* morphants and *sco*<sup>hi459</sup> mutants.**

$P_o$ : outer perimeter, measuring the circumference of the sclera

$P_i$ : inner perimeter, measuring the circumference of the eye

MO: morphant

n: number of eyes analyzed

### **6.2.9. Arl13b/ Scorpion is necessary for maintenance of photoreceptor outer segments**

The eye exhibits a laminar pattern and during embryonic development, neurons of the zebrafish retina organize into three distinct nuclear layers (outer nuclear layer (ONL), inner nuclear layer (INL), ganglion cell layer (GCL)) which are separated by two plexiform layers, called inner (IPL) and outer plexiform layer (OPL) respectively. The outer nuclear layer, also called photoreceptor layer, contains rods and cones which are highly polarized cells and consist of an inner segment (IS) and an outer segment (OS). OS and IS are morphologically, functionally and biochemically distinct compartments that are connected only via a non motile cilium called connecting cilium. The outer segment is photosensitive, containing hundreds of discs with opsin and other proteins of the visual transduction cascade. The inner segment contains the protein biosynthesis machinery. The cell body ends in a synaptic terminal responsible for neurotransmission. The photosensitive OS membranes exhibit continuous turn-over with new disks being formed at the base and distal tips being shed and phagocytosed by the surrounding retinal pigment epithelium (RPE). Since the OS lacks the machinery for protein biosynthesis, it depends on the IS making protein and delivering them to the OS via the connecting cilium. The connecting cilium plays important roles in delivery and turnover of enzymes and substrates of the visual transduction cascade and membranes of the OS, thus plays a crucial role for the organization and function of photoreceptor cells.

The small eye phenotype that was observed in severely edemic mutant and morphants could hypothetically be due to either a delayed eye growth with all layers being present, or it might be due to a degraded or malformed layer. To distinguish these two possibilities, a histological analysis was performed using JB-4 microtome sections of the wildtype and mutant embryo eye that were stained with hematoxylin and eosin.

Fig. 24 shows a part of the retina of a wildtype (Fig.24 A) and *scorpion*<sup>hi459</sup> mutant embryo (Fig. 24 B) at 5 dpf. In wildtype embryos at this stage, elongated rods and shorter cones of the photoreceptor layer are visible in the ONL. Photoreceptor outer segments (OS) are clearly visible as lightly stained processes located between the dark stained nuclei of the ONL and the black retinal pigment epithelium (RPE) which apical processes surround the OS of retinal photoreceptors. In contrast, in *scorpion*<sup>hi459</sup> mutant

embryos, several defects of the outer retina are visible: the most obvious defect is the lack of photoreceptor outer segments. To ensure this was not an artefact due to slightly different angles of cutting the eye, serial sections for the entire eye were analyzed and the analysis repeated in multiple embryos. This confirmed that it is not an artefact but that mutant embryos indeed have photoreceptor layer defects. In addition, the ONL that in wildtype appears densely packed and shows elongated cells, shows acellular gaps (Fig. 24 B, yellow arrow) and pyknotic nuclei (Fig. 24 B, red arrow heads) instead, indicative of apoptotic events. Furthermore, the OPL and horizontal layer that appears as a highly oriented and organized single layer of cells between the ONL and INL, appears disorganized and interrupted in the mutant embryo. Lastly, the RPE appears to be thinner in mutant embryos and due to the lack of the OS does not intersperse with the photoreceptors.

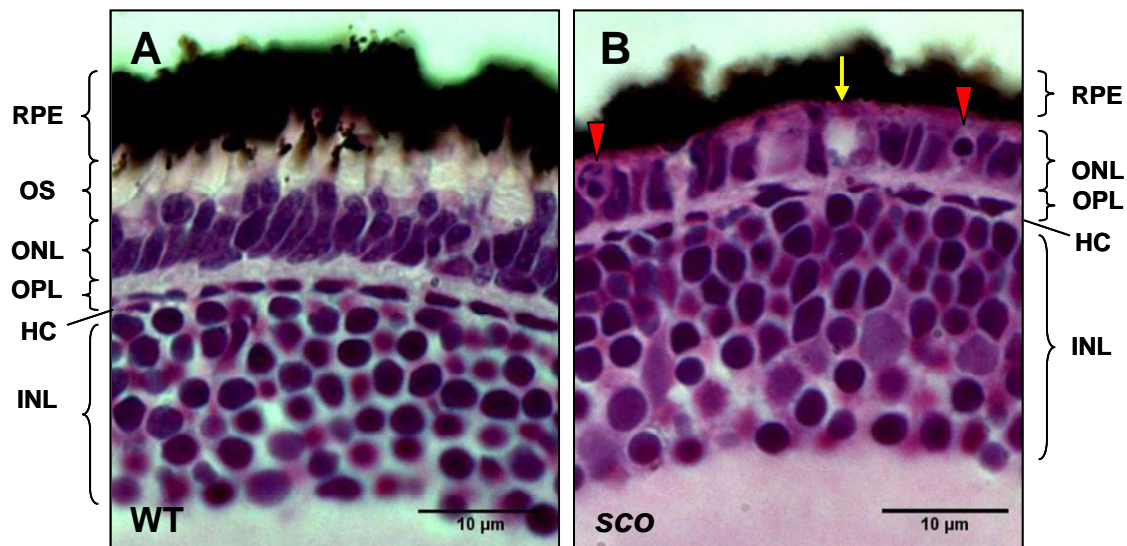


**Fig. 24: Arl13b/ Sco is necessary for maintenance of photoreceptor outer segments.**

The OS of retinal photoreceptors can be seen as lightly stained processes in wildtype (A) which interdigitate with processes of the RPE. *sco*<sup>hi459</sup> mutant photoreceptors lack the OS and show acellular gaps in the ONL (yellow arrow) and pyknotic nuclei (red arrow heads).

RPE: retinal pigment epithelium; OS: outer segment; ONL: outer nuclear layer; OPL: outer plexiform layer; INL inner nuclear layer

Sections are JB-4 microtome sections, cut at 4 μm and stained with hematoxylin and eosin.

Scale bars represent 10 μm.

### **6.2.10. *sco*<sup>hi459</sup> mutant embryos exhibit excessive apoptosis in retinal photoreceptor layer and outer segment atrophy**

Since the mutant retinal photoreceptors lack OS when analyzed with histological sections and the ONL exhibited acellular gaps and pyknotic nuclei, we sought to further investigate whether excessive cell death might play a role in the degeneration of the OS in *sco*<sup>hi459</sup> mutant embryos. Sagittal cryosections of the wildtype and mutant embryo eye were stained with a nuclear stain (DAPI) to visualize the laminar structure of the retina. Sections were co-stained with TUNEL (Fig. 25 A, D), labeling apoptotic cells. In wildtype embryos hardly any apoptotic cells are present at this developmental stage. However, *sco*<sup>hi459</sup> mutant embryos exhibit multiple TUNEL positive cells specifically in the ONL, indicating that excessive cell death occurs in the retinal photoreceptor layer. This result was confirmed with serial sections and analysis of multiple embryos. Due to the lack of rod and cone specific antibodies, an antibody against acetylated alpha-tubulin and rhodamine-phalloidin was used. Acetylated alpha-tubulin stains long ciliary compartments adjacent to the ONL (Fig. 25, B, yellow bracket). In *sco*<sup>hi459</sup> mutant embryos the length of the staining is greatly reduced (Fig. 25, E). Similarly, rhodamine coupled phalloidine, labeling F-actin, is heavily staining the OS (Fig. 25, C) as well as axon tracts of horizontal cells, resulting in comparably long OS labeling in wildtype embryos. Mutant embryos exhibit shorter photoreceptor OS indicated by a shorter phalloidin staining (Fig. 25, F).

It will be very interesting in the future to utilize cell type specific antibodies, e.g. against rod and cone, to distinguish whether all cell types are equally disrupted or whether a specific cell type shows a more profound defect due to loss of Arl13b/ Sco.



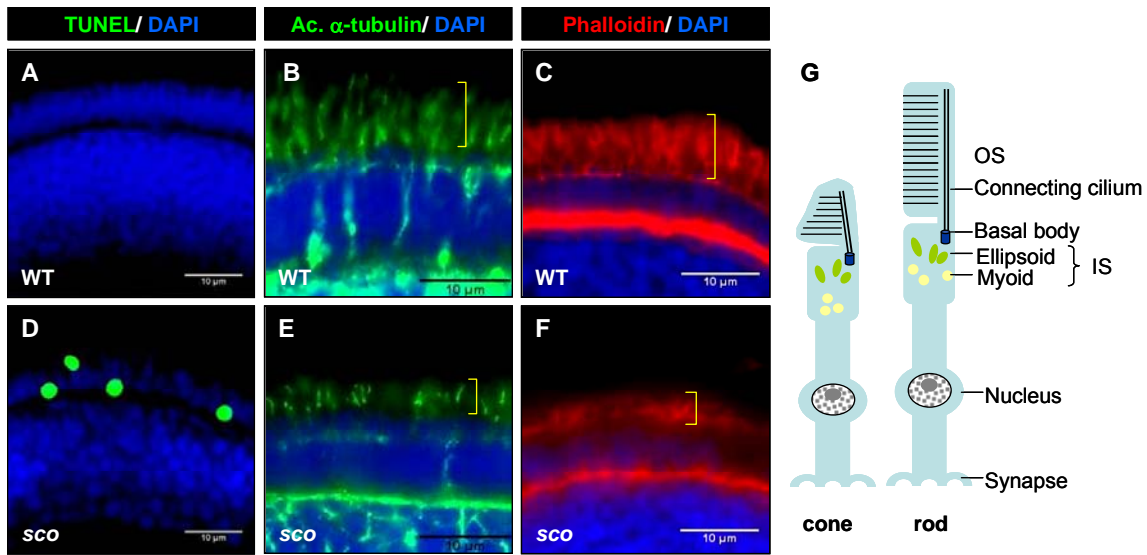


**Fig. 25: *sco*<sup>hi459</sup> mutant embryos show excessive apoptosis in the photoreceptor layer and have degenerated photoreceptor outer segments.**

Wildtype (A-C) and *sco*<sup>hi459</sup> mutant embryos (D-F) cryosections of the retina are shown. (A, D) TUNEL staining labels apoptotic cells. In wildtype apoptosis is hardly ever present in the photoreceptor layer (A) whereas in mutant embryos (D) excessive apoptosis can be observed in the ONL, the layer where photoreceptors reside. (B, E) Acetylated alpha-tubulin labels connecting cilia in photoreceptors. Mutant embryos show fewer and shorter connecting cilia (E) compared to wildtype siblings (B). Rhodamine coupled phalloidine labels F-actin and visualizes the OS of photoreceptors. In *sco*<sup>hi459</sup> mutant embryos, the OS is significantly reduced in length. (G) Schematic drawing of photoreceptor cones and rods, which contain connecting cilia that connect the OS to the remaining part of the cell.

All sections are 12 μm thick cryostat sections of 5 dpf old embryos.

Scale bars represent 10 μm.



### 6.2.11. Kupffer's vesicle in *scorpion*<sup>hi459</sup> mutants

Zebrafish possess a special ciliated organ called Kupffer's vesicle (KV). The KV is the functional equivalent to the mouse embryonic node (Brummet and Dumont, 1978; Essner *et al.*, 2002). Both structures are transient, fluid filled and ciliated organs that appear during gastrulation and are crucial for determining left/right asymmetry in the embryo (Bisgrove *et al.*, 2003; Hamada *et al.*, 2002). The mouse node and zebrafish KV have been shown to have motile cilia that beat in a counter clockwise orientation resulting in directional fluid flow towards the left side of the embryo (Nonaka *et al.*, 1998; Sulik *et al.*, 1994; Kramer-Zucker *et al.*, 2005). When the direction of this fluid flow was reversed resulted in *situs inversus*, where the body shows a mirrored body plan, whereas the absence of fluid flow resulted in a randomization of body laterality (Nonaka *et al.*, 2002). How exactly this directional fluid flow results in a break of the body symmetry is not clear yet. It might be possible that cilia-driven fluid flow results in a morphogen gradient or fluid flow itself is sufficient to signal possibly via sensory cilia at one side of the KV, resulting in calcium influx and left side specific gene expression.

As I showed previously, Arl13b/ Scorpion is expressed on cilia in the KV. Since the KV plays such an essential role for establishing left-right asymmetry, we sought to address whether *scorpion*<sup>hi459</sup> mutants would display a proper body laterality or not. A good laterality indicator is the position of asymmetrically localized organs such as the heart. In the zebrafish embryo the heart is the first organ to become positioned asymmetrically. During development, the heart progenitor cells converge from ventral and lateral regions of the embryo towards the embryonic axis and merge to form a linear heart. The heart then undergoes a complex looping morphogenesis process. At 24 hpf the heart jogs to the left side of the embryo and continues to further loop until 48 hpf, resulting in a two chambered heart with atrium and ventricle. In order to study laterality we performed in situ hybridization (ISH) for cardiac myosin light chain 2 (cmlc2), which is expressed in the cardiomyocytes in the atrium as well as ventricle (Chen *et al.*, 1997) and allows us to visualize heart looping of 1 dpf old embryos. In wildtype embryos we exclusively observed left sided hearts jogging (Fig. 26). The correct body laterality is called *situs solitus*. *scorpion*<sup>hi459</sup> mutants are not distinguishable from their wildtype siblings at this age yet. So we again turned to offspring of *scorpion*<sup>hi459</sup> heterozygous crosses expecting a mendelian ratio of 25% mutant embryos. If *scorpion*<sup>hi459</sup> mutants would have a laterality

phenotype we would expect 25% of the offspring to present a randomization in direction of heart jogging. However, all but one of the embryos showed *situs solitus*.

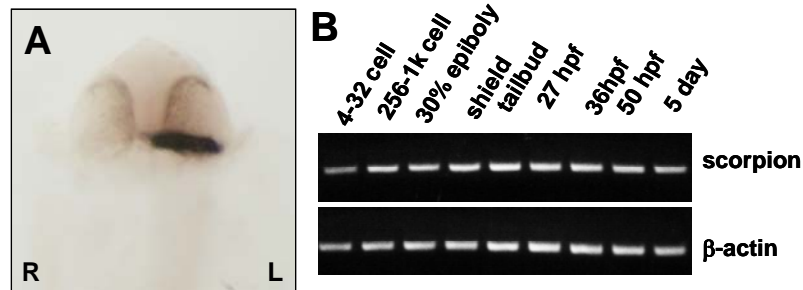


**Fig. 26: *scorpion*<sup>hi459</sup> mutants show *situs solitus* and exhibit maternal contribution.** (A) Ventral view of a wildtype embryo at 26 hpf subjected to in situ hybridization with a probe for *cmhc2*, visualizing the left-sided position of the heart. The entire clutch of *scorpion*<sup>hi459</sup> heterozygous crosses showed indistinguishable *cmhc2* expression patterns from wildtype embryos, indicating that *scorpion*<sup>hi459</sup> mutants exhibit a correct laterality. (B) Time course RT-PCR of *arl13b/scorpion* and actin as control. All transcripts detected up to 512 cell stage are due to deposition of maternal transcripts into the eggs. The first lane (4-32 cell stage) shows an amplified band indicating that *arl13b/scorpion* shows maternal contribution. (RT-PCR performed by Z. Sun).

Two explanations could account for the result. *Arl13b/Scorpion* does not play a role during early development and left/ right establishment. Alternatively, *Scorpion*'s effect is masked by maternal contribution. Maternal contribution describes the phenomenon of the mother animal depositing maternal transcripts into the eggs which support the earliest developmental steps of embryogenesis. Maternal to zygotic transition, i.e. the gradual transition from a maternally provided transcriptome to the start of zygotic transcription in the embryo, occurs around the 512-1000 cell stage in zebrafish (Westerfield, 2000). The maternal transcripts may mask the role of the mutant protein during early embryogenesis. A RT-PCR time course was performed (performed by Zhaoxia Sun) and a *arl13b/scorpion* transcript could be detected as early as the 4-32 cell stage, suggesting that *arl13b/scorpion* is indeed maternally deposited (Fig. 26, B).

In order to study the role of *Arl13b/Scorpion* during early development we used morpholino oligos to circumvent the issue of maternal deposition.

### 6.2.12. *arl13b/scorpion* morphants display left/ right axis randomization

After injecting 0.5 nl [1 mM] *arl13b/scorpion* morpholino oligo into wildtype embryos at the 1-4 cell stage, they were subjected to the same *in situ* hybridization protocol as performed before. Whereas wildtype embryos showed a strict left-sided jogging of the heart, only 58.14% of *arl13b/scorpion* morphants displayed a heart looping to the left. 17.92% of *arl13b/scorpion* morphants displayed hearts jogging to the right and 23.95% had a heart that remained in the middle (Fig. 27; Table 5).

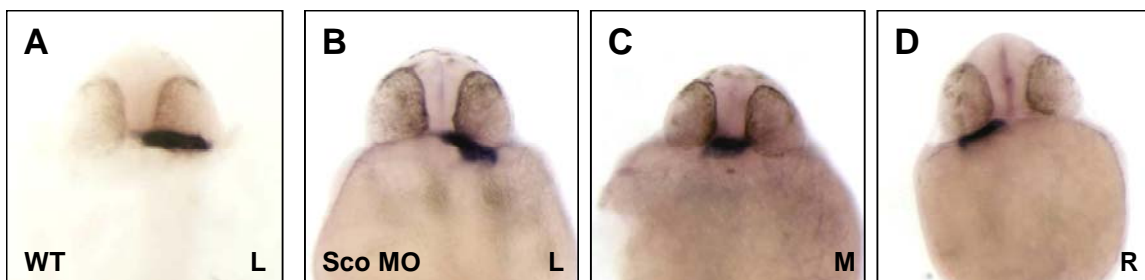


**Fig. 27: *arl13b/scorpion* morphants display randomized heart looping.**

Whole mount *in situ* hybridization was performed on 26 hpf old wildtype (A), offspring of *scorpion*<sup>hi459</sup> heterozygous crosses and *arl13b/scorpion* morphants (B-D) with *cardiac myosin light chain 2 (cmlc2)* probe, which labels the heart. Shown is the frontal view with the left side of the embryo pointing to the right. The yolk sac is in the bottom half of the image and eyes are visible as darkly pigmented regions.

All wildtype and more than 99% of the offspring of a *scorpion*<sup>hi459</sup> heterozygous cross displayed *situs solitus*, the heart looped to the left (A). (B-E) *arl13b/scorpion* morphants displayed randomized heart looping, in which the heart jogged to the left (58%), right (18%) or failed to jog sideways and stayed in the middle (24%).

	Left [%]	Middle [%]	Right [%]
<b>Wildtype</b> (n=76)	100	0	0
<b><i>sco</i><sup>+/-</sup> x <i>sco</i><sup>+/-</sup></b> (n=64)	99.22 ± 1.10	0.78 ± 1.10	0
<b><i>sco</i> MO</b> (n=152)	58.14 ± 4.29	23.95 ± 3.66	17.92 ± 0.63

**Table 5: Asymmetric heart positioning in *arl13b/scorpion* morphants.**

Wildtype embryos, offspring of *scorpion*<sup>hi459</sup> heterozygous crosses and *arl13b/scorpion* morphants were collected at 26 hpf and subjected to *in situ* hybridization with a probe for *cardiac myosin light chain 2 (cmlc2)*, allowing to visualize the direction of heart looping. Numbers (n) in parenthesis refer to the sample size.

### 6.2.13. The Kupffer's vesicle structure itself is formed in *scorpion*<sup>hi459</sup> mutant and morphants

Since *Arl13b/Scorpion* is expressed on the cilia in the KV and the KV has been linked repeatedly to the establishment of body laterality, it is tempting to speculate that *Arl13b/Scorpion* on the cilium is important for left/right establishment. However, it might be possible that the KV structure itself is affected, resulting in a laterality defect as a secondary effect which is the case in the *no tail* mutant. The *no tail* mutants which have a mutated T-box transcription factor *no tail*, fail to form a KV structure which results in a randomized left/ right body axis (Amack and Yost, 2004). Further support for the role of the KV in establishing left/ right asymmetry was shown by the selective suppression of dorsal forerunner cells, the progenitors of the KV, which resulted in inhibition of KV development specifically without leading to other developmental defects and ultimately resulting in randomization of left/right axis formation (Amack and Yost, 2004).

To rule out that a potential structural defect of the KV could account for the laterality defect in *arl13b/ sco* morphants, we examined the KV in wildtype, offspring of *scorpion*<sup>hi459</sup> heterozygous crosses, *arl13b/scorpion* morphants and control morphants. Examining the KV structure at the 8-10 somite stage by light microscopy revealed that in contrast to *no tail* mutants, embryos from either wildtype, offspring from *scorpion*<sup>hi459</sup> heterozygous crosses, control morphants and *arl13b/ scorpion* morphants were able to form the KV. Moreover, measurements of the KV size revealed no significant difference between wildtype, offspring from *scorpion*<sup>hi459</sup> heterozygous crosses, control morphants and *arl13b/ scorpion* morphants (Fig. 28, 30).

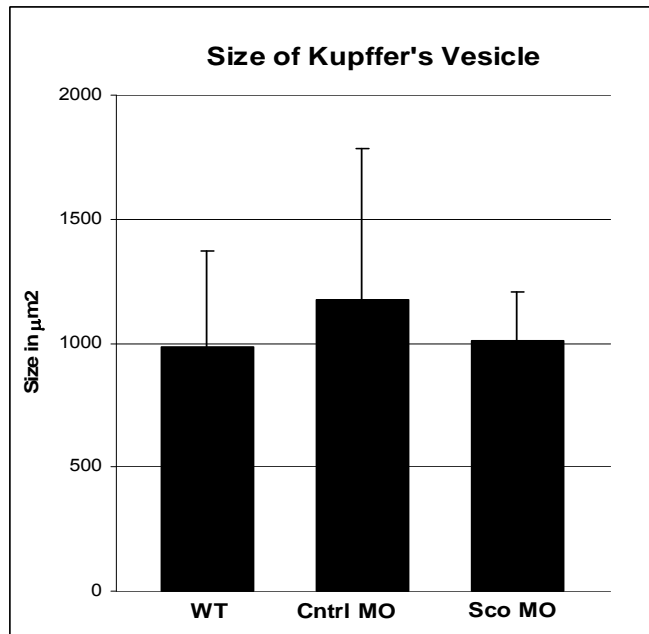


**Fig. 28: Quantification of the KV size.**

The size of the KV at the 10 somite stage was highly variable within each group but comparable among wildtype, control morphants, *scorpion*<sup>hi459</sup> mutants and *arl13b/scorpion* morphants.

The area of Kupffer's vesicle (KV) was measured using Adobe Photoshop 6.0.

	KV size [μm <sup>2</sup> ]	stdev	P value	n
<b>WT</b>	985.46	382.99		25
<b>cntrl MO</b>	1175.89	610.26	0.226	16
<b>sco MO</b>	1170.75	447.72	0.213	16

**Table 6: Data for analysis of the size of the Kupffer's vesicle in WT, control morphants and *arl13b/scorpion* morphants.**

Data points of Table 6 are displayed in the bar graphs in figure 28 and represent the means followed by standard deviation. The sample size (n) refers to the total number of embryos used for this statistical analysis. A Student's T-test was performed to determine the statistical significance.

### 6.2.14. Cilia formation in the KV is disrupted in *arl13b/ scorpion* morphants

Since *arl13b/ scorpion* morphants did not exhibit a defect in the KV structure itself, we sought to analyze the cilia within the KV. We performed immunohistochemistry using an antibody for acetylated  $\alpha$ -tubulin, which labels cilia and measured cilia length in the KV using Adobe Photoshop 6.0. As expected, all embryos of the *scorpion*<sup>hi459</sup> heterozygous cross showed similar lengths of KV cilia ( $3.64\mu\text{m} \pm 0.69 \mu\text{m}$ ) compared to wildtype embryos ( $3.01 \mu\text{m} \pm 0.325 \mu\text{m}$ ). However, to carefully analyze the role of Scorpion we again utilized morpholino oligo nucleotides. *arl13b/ scorpion* morphants were able to form cilia in the KV most of the time, however in some animals cilia in the KV area could not be detected at all. Furthermore, KV which contained cilia, had less they abundant and significantly shorter cilia with  $1.37 \mu\text{m} (\pm 0.272 \mu\text{m}, P < 0.001)$  compared to control morpholino injected wildtype embryos  $3.07 \mu\text{m} (\pm 0.319 \mu\text{m})$  (Fig.29, 30).

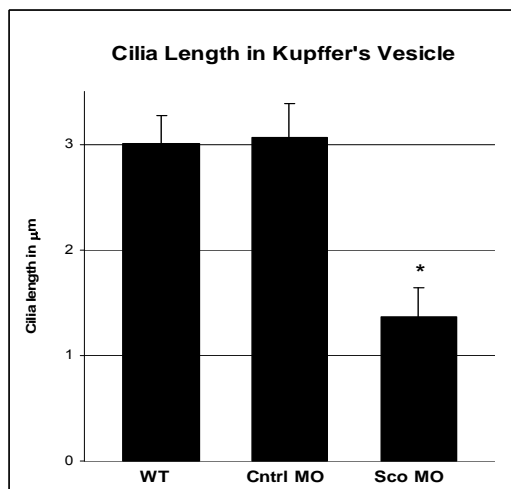


**Fig. 29: Quantification of cilia length in the KV.**

Cilia length was measured on embryos at the 10 somite stage on as many individual cilia as possible in each KV and averaged per embryo. The average with standard deviation is depicted on the graph.)

Cilia length in control morphants was not significantly different from wildtype but *arl13b/ scorpion* morphants showed a highly significant reduction in cilia length ( $P$ -value  $< 0.001$ ). Student's T-test was performed to analyze statistical significance.

	KV cilia length [ $\mu\text{m}$ ]	stdev	P value	n
WT	3.006	0.325		25
cntrl MO	3.069	0.319	0.986	16
sco MO	1.370 *	0.272	2.22E-19	16

**Table 7: Data for analysis of cilia length in the Kupffer's vesicle in WT, control morphants and sco morphants.**

Data points of Table 7 are displayed in the bar graphs in figure 29 and represent the means followed by standard deviation. The sample size (n) refers to the total number of embryos used for this statistical analysis. Asterisk (\*) indicates that the difference in cilia length between wildtype and control morphants and *arl13b/scorpion* morphant is statistically highly significant by Student's T-test ( $p$ -value  $< 0.001$ ).

This finding that the ciliary defect in *scorpion*<sup>hi459</sup> mutants results in a laterality phenotype is consistent with the laterality phenotype seen in PKD2 mutants in mouse models as well as zebrafish (Wu *et al.*, 1998; Wu *et al.*, 2000; McGrath *et al.*, 2003; Pennekamp *et al.*, 2002), which are able to form cilia in the KV and embryonic node respectively, but are not able to beat in a coordinated manner.

This supports the hypothesis that defective cilia, functional or structural, are indeed the cause for the defect in left/ right asymmetry.

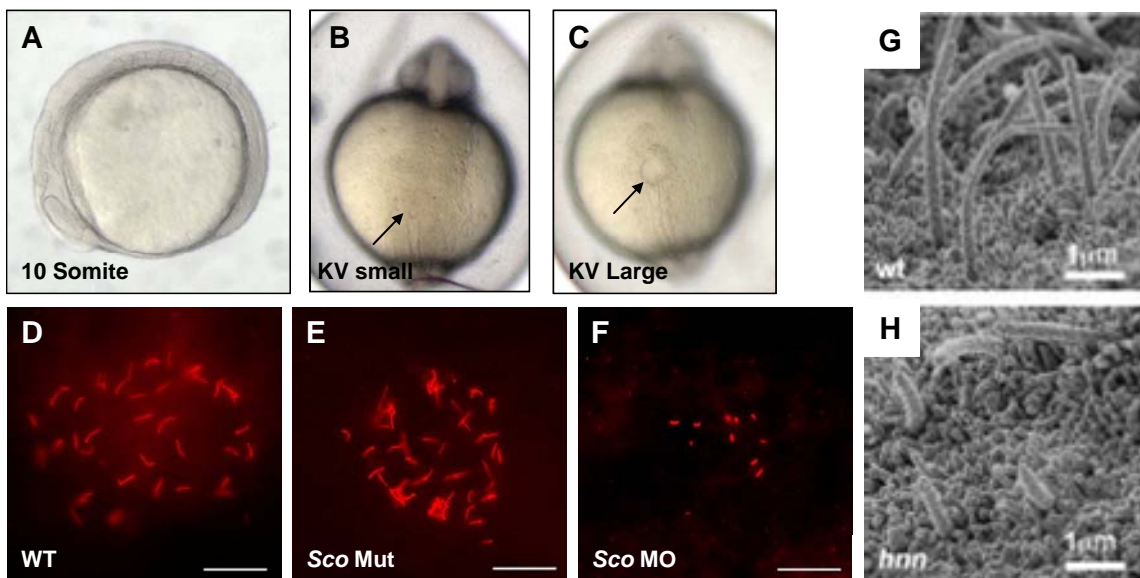


**Fig. 30: Arl13b/ Scorpion is required for cilia formation in Kupffer's vesicle.**

(A) Lateral view of wildtype embryo at the 10 somite stage. Kupffer's vesicle (KV) is a transient structure and was analyzed at this developmental stage. (B-C) Size of Kupffer's vesicle is highly variable. Wildtype examples of a small (B) and large (C) KV are shown and indicated by arrows. (D-F) Whole mount fluorescent immuno staining for acetylated  $\alpha$ -tubulin was performed on 10 somite stage embryos. Wildtype (D), control morphants and offspring from *scorpion*<sup>hi459</sup> heterozygous crosses (E) were indistinguishable regarding cilia length and abundance. *arl13b/scorpion* morphants displayed significantly shorter cilia and appeared to have less cilia in total (F).

(G-H) *Hennin*, the the Arl13b homologue in mouse has a similar ciliary phenotype in the embryonic node, the functional mouse equivalent of the KV (G-H Image taken from Caspary *et al.*, 2007), exhibiting shorter and less abundant cilia.

Scale bar in (D-F) represents 20  $\mu$ m.

### 6.2.15. *arl13b/scorpion* morphants display altered Nodal related signaling pathway

The Nodal signaling pathway (fig. 31) has been implicated in several processes from mesoderm induction, endoderm formation to neural patterning and anterior/ posterior specification as well as recent findings that it might play a role in the maintenance of undifferentiated embryonic stem (ES) cells. However, another role of the Nodal signaling pathway which is well established is its role in left/right patterning of the body axis. Nodal pathway ligands are highly conserved members of the TGF $\beta$  superfamily. In contrast to humans who only have one nodal ligand, zebrafish has multiple nodal-related ligands called *cyclops* (*cyc*), *squint* (*sqt*) and *southpaw* (*spaw*) which are expressed in the left lateral plate mesoderm (LPM) during early development but are exclusive from the right LPM (Schier *et al.*, 2003). This expression pattern is highly conserved among chordates and thought to determine 'left-sidedness' whereas absence or the ectopic expression of Nodal are thought to result in laterality defects.

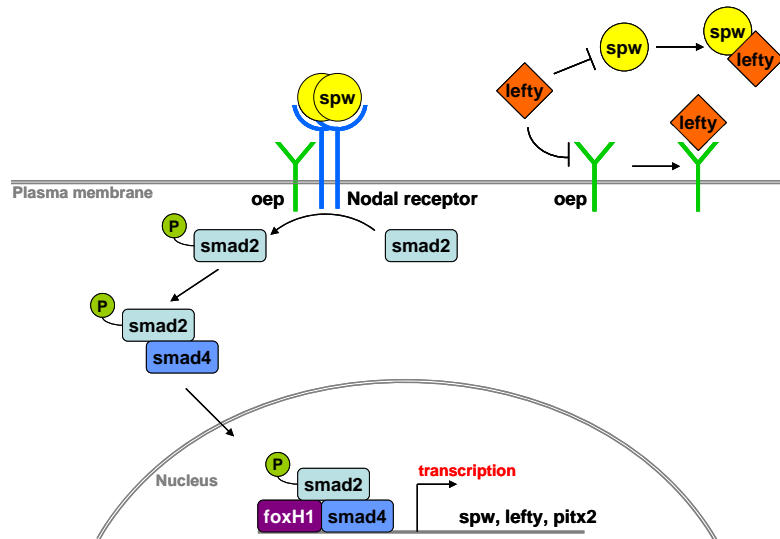


**Fig. 31: Model of Nodal related signaling pathway in zebrafish.**

The nodal ligand *southpaw* (*spaw*, in yellow) acts as a dimer by binding to two *spaw* receptors (blue) along with an essential co-receptor called *one-eyed-pinhead* (*oep*, in green). The receptor activation by binding of *spaw* leads to phosphorylation of SMAD2 which can associate with SMAD4 and translocate to the nucleus. In the nucleus the SMAD2/SMAD4 complex in turn can interact with the winged-helix transcription factor FoxH1 leading to transcriptional activation of nodal genes such as *spaw*, *lefty1/2* and *pitx2*. *Lefty1/2* is an inhibitor of Nodal signaling and can create a negative feed-back loop.



*spaw* is expressed around the KV and in the left side of the LPM. The left-sided expression of *spaw* represents the first break of body symmetry. The expression of *spaw* begins around 6-8 somite stage, progressively extending anteriorly until it reaches the anterior cardiac LPM around the 18-20 somite stage. We used this developmental stage to analyze the expression pattern of *spaw* in *arl13b/scorpion* morphants.

Since we knew from previous experiments that the control morphant did not exhibit any phenotype, we used uninjected wildtype siblings as control. *arl13b/scorpion* morphants and wildtype siblings were subjected to *in situ* hybridization for *spaw* at the 18-20 somite stage (17-19 hpf). The developmental stage was determined by counting somites and observing the elongation of the yolk extension since the time after fertilization alone is not accurate due to a delayed development process in morphants. In wildtype almost all embryos showed a left-sided expression pattern of *spaw* (Fig. 32; Table 8). The expression of *spaw* around the KV was not altered in *arl13b/scorpion* morphants, this is consistent with a previous study that showed that *spaw* expression around the KV is independent of *spaw* signaling not resulting in a downregulation of the expression even after morpholino injections. However, *spaw* expression in the LPM is specific and abolished in *spaw* morphants (Long *et al.*, 2003). The LPM in *arl13b/scorpion* morphants showed the correct expression pattern of *spaw* in only two thirds of embryos, whereas the remaining third of morphants showed ectopic expression for *spaw* either in the right LPM (7.14%), bilateral expression, i.e. in both right and left LPMs (7.14%) or no expression at all (21.43%) (Fig. 32; Table 8). Table 8 shows the distribution of a representative experiment.

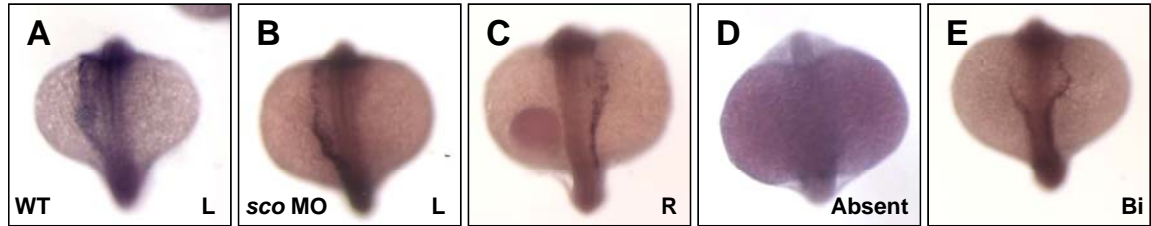


**Fig. 32: *arl13b/scorpion* morphants display altered *spaw* expression.**

Wildtype embryos and *arl13b/scorpion* morphants were subjected to *in situ* hybridization at the 18-20 somite stage. (A) Wildtype embryo with a correct *spaw* expression in the left lateral plate mesoderm (LPM). (B-E) Various *spaw* expression patterns in *arl13b/scorpion* morphants. (C) Ectopic expression of *spaw* in the right LPM. (D) Absent *spaw* expression. (E) Bilateral *spaw* expression on both sides of the LPM.

		left [%]	right [%]	bilateral [%]	absent [%]
<b>WT</b>	(n=133)	96.24	0.00	1.50	2.26
<b>sco MO</b>	(n=56)	64.29	7.14	7.14	21.43

**Table 8: *spaw* expression in *arl13b/scorpion* morphants.**

These data show a representative experiment of *spaw* expression in Wildtype and *arl13b/scorpion* morphant embryos collected at the 18-20 somite stage. *spaw* expression was visualized by *in situ* hybridization.

The vast majority of wildtype embryos (96.24%) displays left sided *spaw* expression. *arl13b/scorpion* morphants lack this stringent left sided expression pattern but show ectopically expressed *spaw* in the right LPM (7.14%) or bilaterally (7.14%). In many cases (21.43%) the *spaw* expression was absent.

Numbers in parenthesis (n) refer to the sample size.

As I showed before, Scorpion is expressed on cilia in various tissues. Knockdown of *arl13b/scorpion* in the KV resulted in a ciliary defect which in turn lead to a laterality defect in the embryo. Since Scorpion is expressed in pronephric duct cilia among other organs and given the link between JS and cystic kidneys, we sought to focus our attention on the kidney phenotype of *scorpion*<sup>hi459</sup> mutants next.

### 6.2.16. *scorpion*<sup>hi459</sup> mutants lose single cilia but partially maintain cilia on multi-ciliated cells

The pronephric duct in zebrafish has two different cell types, principal cells and multi ciliated cells (MCC). Principal cells (single ciliated cells, SCC) possess a solitary cilium on the surface with a (9+2) axonemal structure. In contrast, MCCs extend tight bundles of cilia consisting of 15-20 cilia from their apical surface which are thought to move in an organized fashion and foster fluid flow in the kidney duct towards the cloaca. MCCs are located at the medial/ posterior part of the duct and are absent from the apical as well as very posterior part of the kidney.

Initial analysis of the *sco*<sup>hi459</sup> mutant pronephric duct found a ciliary defect in the pronephric duct region (Fig. 33) (Sun *et al.*, 2004).

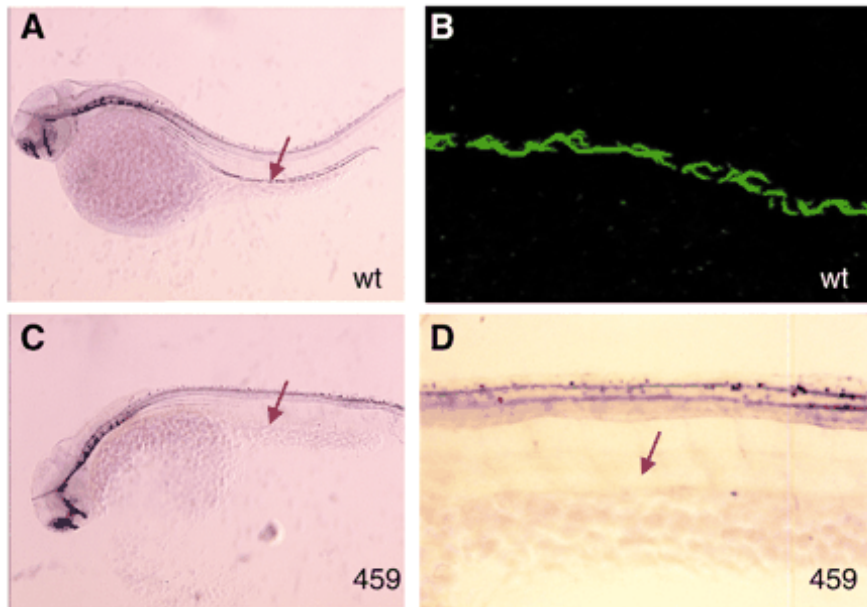


**Fig. 33. Ciliary defects in *scorpion*<sup>hi459</sup> mutants.**

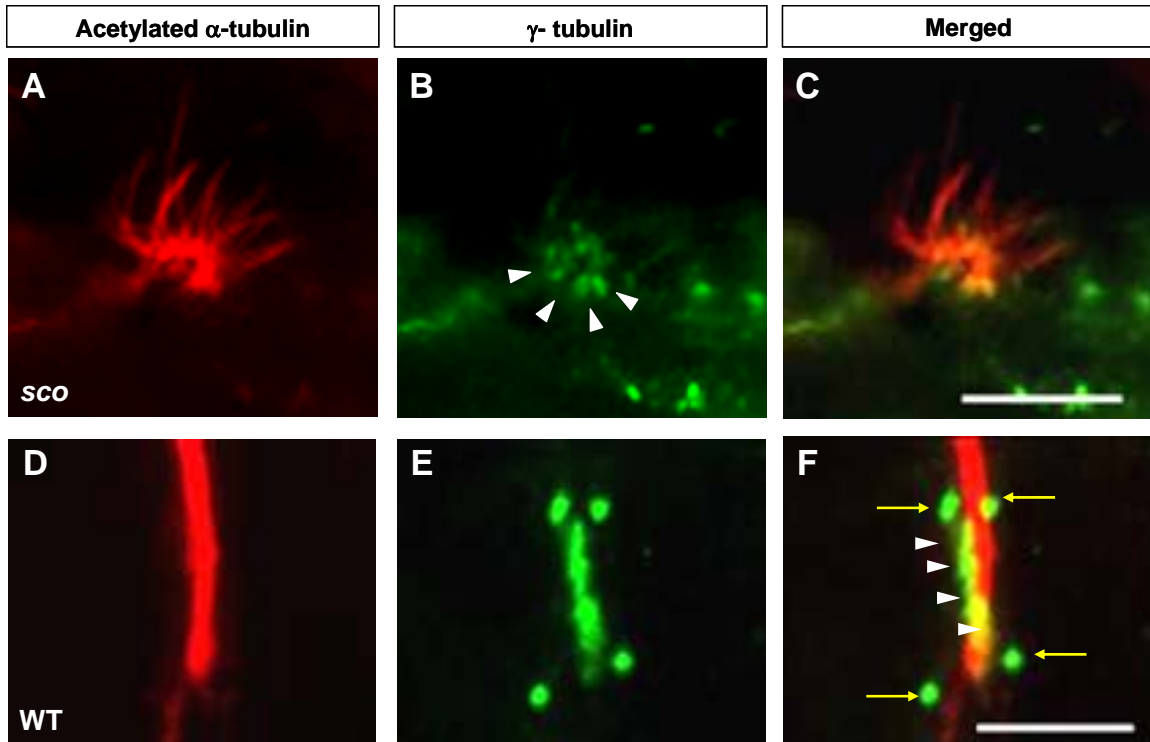
(A) The pronephric duct region (arrow) in a wild-type embryo at 50 hpf reacts strongly with an antibody against acetylated tubulin. (B) Confocal image shows cilia stained with this antibody in the pronephric duct of a wild-type embryo at 24 hpf. (C) Defect of the cilia in *scorpion*<sup>hi459</sup> at 50 hpf; (D) enlarged view of C. wt, wild type; 459, *scorpion*<sup>hi459</sup>.

Image taken from Sun *et al.*, 2004.

When we performed immuno histochemistry at a higher resolution allowing a more detailed analysis, we were surprised to detect tufts of cilia in *scorpion*<sup>hi459</sup> mutants (Fig. 34). Since the ductal lumen is enlarged it is possible to see distinct cilia within the tuft (Fig. 34) which is not feasible to do in wildtype, since bundles of cilia are very tightly squeezed into the lumen of the duct and individual cilia can hardly be distinguished from each other.

### **6.2.17. *scorpion*<sup>hi459</sup> mutants have disorganized basalbodies**

To study the organization of basal bodies in correlation to the cilia localization we performed sequential immunohistochemistry for  $\gamma$ -tubulin and acetylated  $\alpha$ -tubulin to visualize the basal bodies and cilia respectively. We observed that in wildtype embryos, MCCs display a row of basal bodies at the apical side (Fig. 34 D-F). Furthermore, the row of basal bodies seemed to 'wrap' themselves slightly around the duct with one basal body being staggered after the next one and so on. This phenomenon might be due to planar cell polarity within the single cell. In contrast, *scorpion*<sup>hi459</sup> mutants did not exhibit this highly regulated arrangement of basal bodies in MCCs but basal bodies were clustered together in an uncoordinated manner (Fig. 34 A-C). This is the first indication that basal bodies in multi ciliated cells might curve around the tubule in a highly organized fashion and that *scorpion*<sup>hi459</sup> mutants have lost this mechanism.



**Fig. 34: *scorpion*<sup>hi459</sup> mutants maintain cilia in MCC but lose intracellular PCP .**  
*scorpion*<sup>hi459</sup> mutants (A-C) and wildtype (D-F) embryos were stained at 2 dpf with antibodies for acetylated  $\alpha$ -tubulin and  $\gamma$ -tubulin to visualize the cilia and basal bodies, respectively. In wildtype embryos basalbodies (F, arrow heads) are not aligned linear but seem to ‘wrap’ themselves around the cilia bundle, indicating a ductal cell intrinsic PCP mechanism. *scorpion*<sup>hi459</sup> mutant embryos are able to form cilia on MCC but basal bodies are not aligned in oriented fashion but are clumped together (B), resulting in ciliary tufts.  
MCC: multi ciliated cell; *sco*: *scorpion*<sup>hi459</sup>; WT: wildtype  
Scale bars represent 5  $\mu$ m.

### 6.2.18. Kidney specific PCP is disrupted in *scorpion*<sup>hi459</sup> mutants

Beside this cell autonomous, intracellular planar cell polarity, a planar polarity among adjacent cells could be observed as well. In wildtype ducts, single ciliated cells (SCC) contain a single basal body at the apical side (Fig. 34, yellow arrow; Fig. 35 G-J). Similarly to the phenomenon of basal bodies of MCCs 'wrapping' the ductal lumen, single ciliated cells align their basal bodies in a manner that results in a spiral going around the duct. This results in a 'zig-zag' pattern across the duct (Fig.35 D-F, J).

Zebrafish renal cilia are motile and responsible for fluid movement through the tubule. Furthermore, recent studies have shown that cilia do not extend perpendicular out of the apical membrane as was thought initially but in a slight angle tilted towards the posterior end. Taken together, a constellation of single and multiciliated cells aligning in such a spiral like manner along the tubule might represent the most efficient arrangement for propelling fluid towards the cloaca.

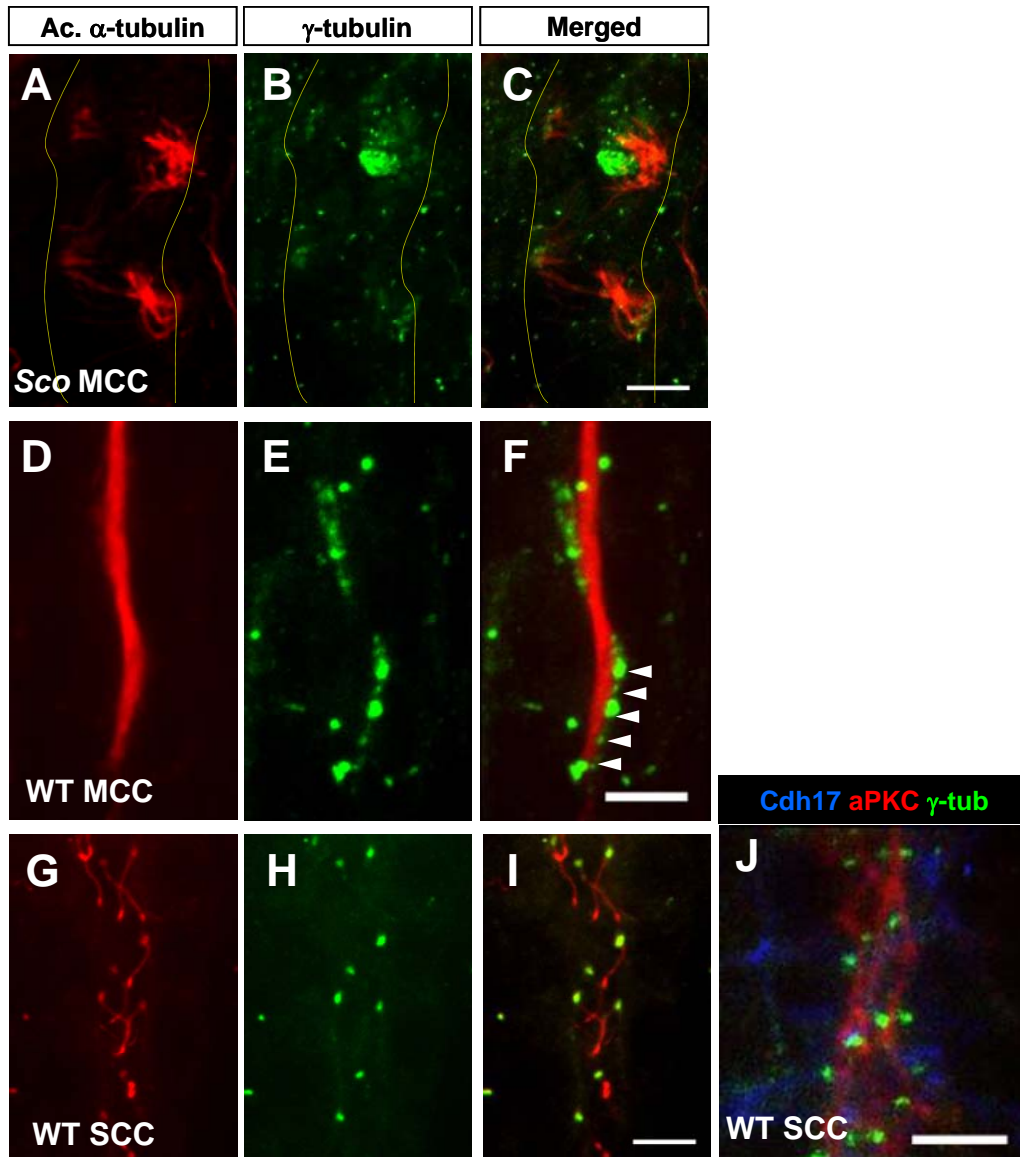


**Fig. 35: Organ specific planar cell polarity in the kidney duct is disrupted in *scorpion*<sup>hi459</sup> mutants.**

(A-I) Whole mount fluorescent immuno staining with acetylated α-tubulin (red) and γ-tubulin (green) of 2 dpf old embryos to visualize the cilia and basal bodies, respectively in WT and *scorpion*<sup>hi459</sup> embryos. (J) Whole mount fluorescent immuno staining with antibodies specific for Cdh17, atypical PKC and γ-tubulin at 2 dpf old WT embryos.

Basal bodies (arrowhead) of adjacent multiciliated cells (MCC) in wildtype are visible as almost contiguous signal along the cilia (D-F). They align not in a strict linear fashion on the longitudinal axis within the cell but seem to 'wrap' themselves around the duct, both on an intracellular as well as tissue level. In *scorpion*<sup>hi459</sup> mutants the oriented basal body alignment is lost and cilia appear as tufts (A-C). Single ciliated cells (G-J) display a planar cell polarity as well within the kidney, showing the basal bodies aligning in a coiled manner around the duct.

MCC: Multi ciliated cell; SCC: single ciliated cell; WT: wildtype; *sco*: *scorpion*<sup>hi459</sup>

Scale bars represent 5 μm.

### 6.2.19 Axonemal ultrastructure of pronephric duct cilia in *sco*<sup>hi459</sup> mutant embryos

Even though it was striking to see that *scorpion*<sup>hi45</sup> mutant embryos were able to maintain multi ciliated cells in the pronephric duct, it is not clear whether they possess a normal ultrastructure and motility. The Arl13b mouse mutant, *hennin*, has a axonemal ultrastructural defect in which the microtubule B-loop fails to attach to the A-loop (Caspary *et al.*, 2007). In order to analyze the ciliary ultrastructure of *scorpion*<sup>hi459</sup> we performed TEM on *scorpion*<sup>hi459</sup> and wildtype siblings at 4 dpf (Fig. 38). Wildtype pronephric duct cilia display a (9+2) axonemal structure with nine microtubule doublets surrounding a central pair of single microtubules as has been reported previously (Kramer-Zucker *et al.*, 2005). *scorpion*<sup>hi459</sup> mutant cilia of the pronephric duct interestingly have an intact (9+2) microtubule ultrastructure (Fig. 35 B, D). In addition, dynein arms are recognizable on some microtubule doublets and no B-loop closure defect or other major structural defect of the axoneme is present.



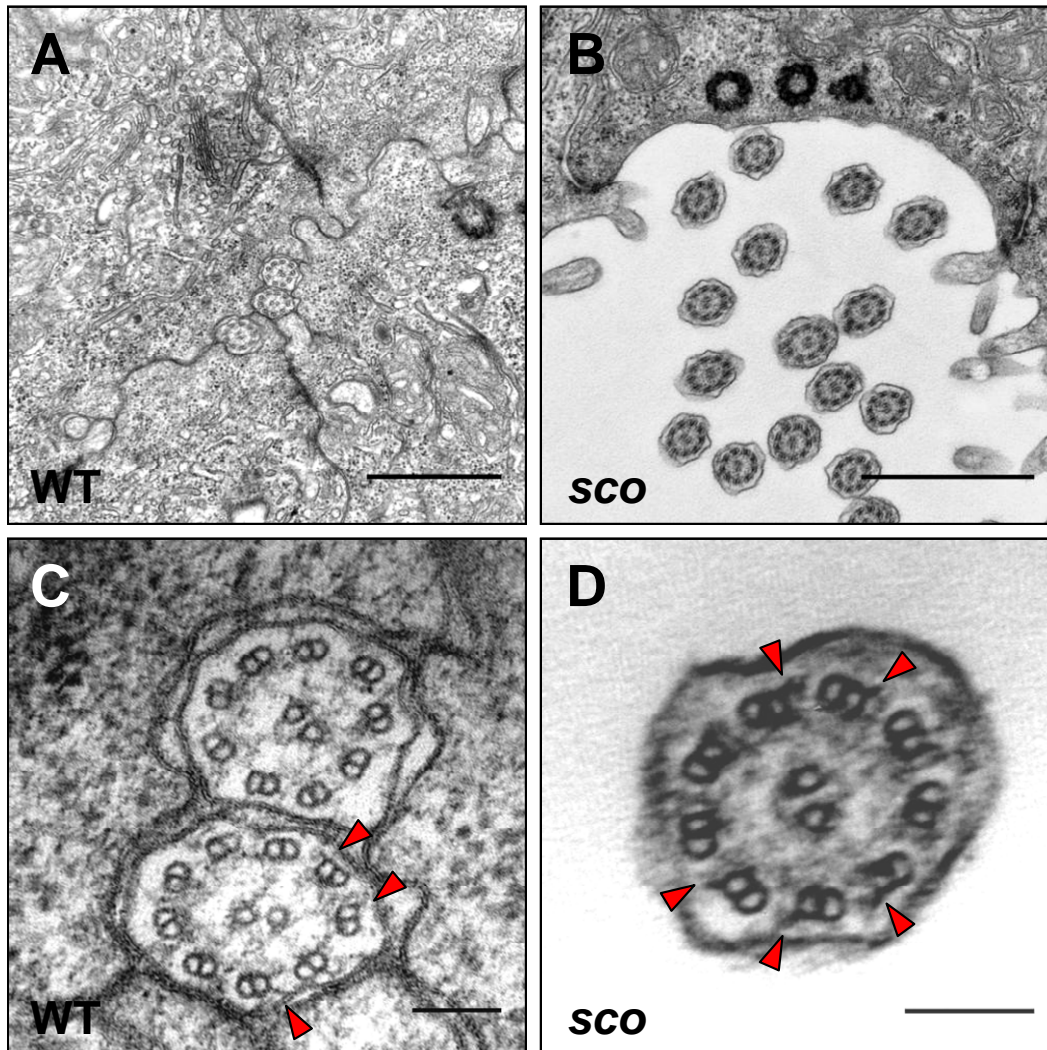


**Fig. 36: The axoneme of remaining cilia in *sco*<sup>hi459</sup> mutants have an intact (9+2) ultrastructure.**

Cilia of the pronephric duct in wildtype (A) show a (9+2) ultra structure, with nine microtubule doublets that surround a pair of single microtubules in the center. A higher magnification is shown in (C) which allows visualizing dynein arms (red arrowhead) of the microtubules. Since not all microtubules are in the same plane, not all dynein arms are visible in one section. In *sco*<sup>hi459</sup> mutant embryos, the duct is enlarged and multiple cilia are visible which appear to have an intact (9+2) ultra structure with closed microtubule doublets and present dynein arms (D, red arrow heads).

TEM was performed on wildtype (A,C) and *sco*<sup>hi459</sup> mutant embryos (B, D) at 4 dpf.

Scale bars represent 1  $\mu\text{m}$  (A, B) and 100 nm (C, D) respectively.

### 6.2.20. Cilia motility is defective in *scorpion*<sup>hi459</sup> mutants

Mutations that affect cilia formation or motility in the kidney have been repeatedly linked to cystic kidney phenotypes. In order to determine whether *scorpion*<sup>hi459</sup> mutant cilia are still motile, we used live video microscopy of *scorpion*<sup>hi459</sup> and wildtype siblings at 3 dpf of the anterior region as well as region at the level of the yolk extension. At 3 dpf, bundled cilia in the medial region of the kidney duct move in a highly coordinated manner. Electron microscopy cross sections of those cilia have been shown to possess a (9+2) axonemal structure (Kramer-Zucker *et al.*, 2005) and remaining cilia of *scorpion*<sup>hi459</sup> mutants show a (9+2) axonemal structure as well (Fig. 36). In order to ensure that ciliary motility was analyzed and not a passive movement due to the rhythmic beating of the heart, the heart beat was stopped using BDM (2,3-Butanedione monoxime). Embryos are still viable for an extended period of time and experiments were performed under 'no heart beat' conditions. The part of the kidney that lies at the level of the yolk sac was obstructed due to the position and size of the yolk sac. Under a 20x objective, 200 frames per second were recorded for one second increments and the beating frequency of a given cilia bundle was quantified. At 3 dpf old wildtype embryos we observed a beating frequency of  $43.2 \pm 9.1$  Hz which is in agreement with previous reports (Kramer-Zucker *et al.*, 2005; DiBella *et al.*, 2008). When we tried to measure the beating frequency in *scorpion*<sup>hi459</sup> mutants, we could not detect coordinated ciliary beating. This could be explained by several hypothetical scenarios: first, the cilia are non-motile and thus no ciliary beating could be detected. Second, it might be possible that cilia were beating but were too short or uncoordinated thus falling below the threshold of detection.

To increase the likelihood of detection, the same experiment was performed at 5 dpf, assuming that cilia might grow longer over time. At 5 dpf the beating frequency in wildtype embryos was  $46.75 \pm 3.91$  Hz, being slightly faster compared to 3 dpf old embryos. Surprisingly, at 5 dpf robust ciliary beating in the pronephric duct could be observed in *scorpion*<sup>hi459</sup> mutant embryos as well. *scorpion*<sup>hi459</sup> mutant embryos did not show an uniform beating frequency such as in wildtype embryos. Instead, 35% of cilia showed a normal ciliary beating pattern ( $43.43 \pm 4.79$  Hz) whereas 35% exhibited a slightly slower beating pattern ( $27.43 \pm 3.92$  Hz). The remaining 30% of cilia showed an extremely slow beating pattern ( $13.50 \pm 3.45$  Hz) (Fig. 37, Table 9).

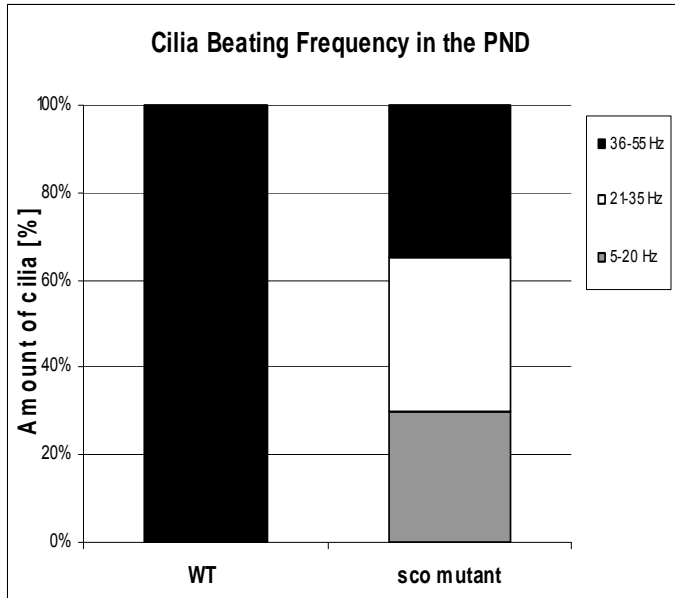


**Fig. 37: Pronephric cilia in *scorpion*<sup>hi459</sup> mutants remain motile but show aberrant beating kinetics.**

Wildtype and *scorpion*<sup>hi459</sup> mutant embryos were subjected to high speed video microscopy at 5 dpf to visualize the ciliary beating pattern in the pronephric duct. In wildtype embryos, pronephric duct cilia beat with a frequency of  $46.75 \pm 3.91$  Hz, whereas in *scorpion*<sup>hi459</sup> mutant embryos the cilia show a wide range in beating frequency with approximately one third of observed cilia beating normal ( $43.43 \pm 4.79$  Hz), one third beating significantly slower ( $27.43 \pm 3.92$ ) Hz in a medial range and another third beating very slow ( $13.50 \pm 3.45$  Hz).

	WT	sco Mutant		
	<i>fast</i> (36-55)	<i>slow</i> (5-20)	<i>medium</i> (21-35)	<i>fast</i> (36-55)
Frequency aver. [Hz]	46.75	13.50	27.43	43.43
stdev	3.91	3.45	3.92	4.79
T-test		1.66E-16	4.9E-12	0.08
portion [%]	100	30	35	35
n	12	12	14	14

**Table 9: Statistical analysis of data plotted in Figure 37.**

### **6.2.21. Cilia of multiciliated cells grow long in *sco*<sup>hi459</sup> mutant embryos**

Since ciliary beating could be detected at 5 dpf but not at 3 dpf, we sought to compare the lengths of cilia at 5 dpf with the ones previously observed at 3 dpf (Fig. 34, 35). Since the antibody against acetylated alpha-tubulin also stains axon tracts of motor neurons which are heavily acetylated, whole mount immunofluorescence and even mounting of embryos which are previously split along the midline unfortunately result in a poor quality image due to excessive signals of motor neuron axon tracts. To circumvent this problem, the entire glomerulus, tubules and pronephric ducts were microdissected manually from fixated tissue before processing it for immunofluorescence staining.

In this way, wildtype and *sco*<sup>hi459</sup> mutant embryos were stained with antibodies against Cadherin-17 (labeling the basolateral membrane of the pronephric duct) and acetylated alpha-tubulin (labeling cilia). In wildtype embryos, the lumen is very narrow and cilia are visible as tight bundles (Fig. 38 A). In *sco*<sup>hi459</sup> mutant embryos the duct is severely enlarged and multiciliated cells extend cilia into the lumen that fan out into tuft like structures (Fig. 38 B). Interestingly, *sco*<sup>hi459</sup> mutant cilia are significantly longer at this time point compared to 3 dpf (Fig. 34, 35, 38) and show greatly variable length. Single ciliated regions of the duct appear non-ciliated in mutant embryos or are severely stunted.

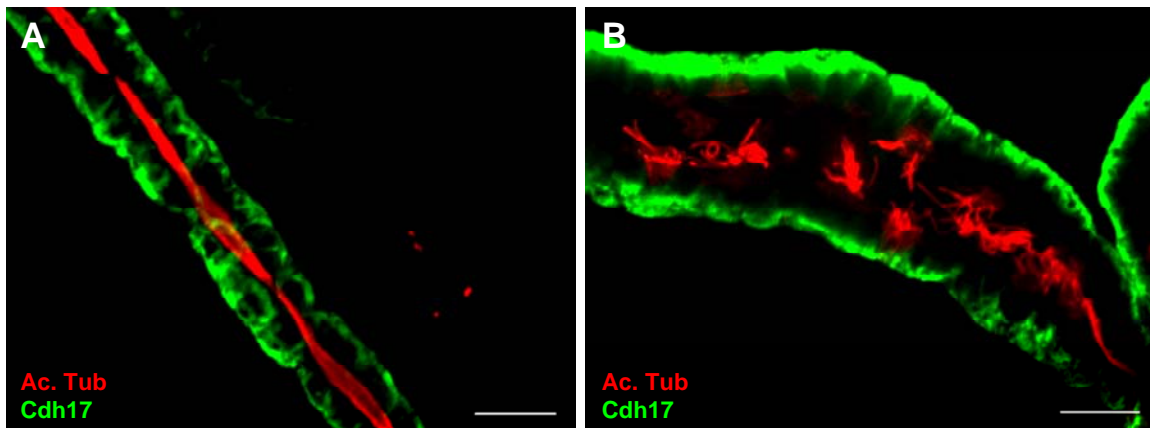


**Fig. 38: *sco*<sup>hi459</sup> mutant cilia grow long but appear disorganized.**

Pronephric ducts, tubules and glomeruli were manually microdissected out of 5 dpf old fixed embryos. Immunofluorescent antibody staining was performed using antibodies against Cadherin-17 and acetylated alpha-tubulin.

(A) In wildtype, the lumen is narrow and cilia are squeezed into a tight bundle. (B) *sco*<sup>hi459</sup> mutant embryos have enlarged pronephric duct lumen and cilia of multiciliated cells extend into the lumen in disorganized tufts.

Scale bars represent 20  $\mu$ m.

### 6.2.22. Arl13b/ Scorpion mislocalizes to apical membrane in *ift57*<sup>hi3417</sup> mutants

It is striking that Arl13b/ Scorpion displays an exclusive localization to cilia since most ciliary proteins are in addition found at other subcellular locations. One question we wanted to address was where Arl13b/ Scorpion would localize to in the absence of cilia using an IFT mutant embryo.

Flagellar assembly occurs at the distal tip of the cilium, which is far away from the cytoplasm, the site of protein synthesis. Intraflagellar transport (IFT) describes the bi-directional transport that is necessary to move flagellar precursors along microtubules from their assembly site to the tip of the flagellum. Since cilia undergo constant turnover, IFT is not only required for cilia formation but for maintenance of cilia as well. IFT particles shuttle non membrane bound cargo along the doublet microtubules of the flagellar axoneme. Anterograde transport from the base of the cilium to its tip is powered by the motor protein Kinesin-II. The retrograde transport back to the base of the cilium is provided by another motor protein called cytoplasmic Dynein-2. Studies in

*Chlamydomonas*, mouse and zebrafish showed that defective IFT particles or IFT motor proteins inhibit normal ciliary assembly. IFT particles can be divided into two multiprotein complexes, IFT complex A and complex B. Studies in *chlamydomonas* showed that complexes A and B play physiologically distinct functions. The current model suggests that complex B proteins are generally required for entry of IFT proteins into the ciliary axoneme via kinesin 2 driven anterograde IFT, whereas complex A proteins facilitate the removal/recycling of IFT proteins from cilia via IFT-dynein-driven retrograde IFT (Pedersen *et al.*, 2005; Blacque *et al.*, 2004; Ou *et al.*, 2007). IFT57 is part of complex B and required for efficient IFT transport thus maintaining normal cilia.

We used *ift57*<sup>hi3417</sup> mutants which are mutated in the gene coding for IFT57 (Gervais *et al.*, 2002; Majumder *et al.*, 2006; Banerjee *et al.*, 2006) as our model to address that question. In zebrafish *ift57*<sup>hi3417</sup> mutants, renal cilia are initially build and a substantial number of cilia can be detected at 1-2 dpf. However, from 3 dpf onwards the density of cilia is significantly reduced due to a degeneration of cilia. Immunohistochemistry was performed with antibodies against Arl13b/ Scorpion and Cdh17 (basolateral membrane marker) on cryosections of 4 dpf old *ift57*<sup>hi3417</sup> mutant and wildtype sibling embryos. In wildtype ducts (Fig.39 A-D) Arl13b/ Scorpion localized to a very narrow spot within the lumen of the duct. Since we observed on whole mount immunostainings that Arl13b/ Scorpion co-localized with a cilia marker (antibody for acetylated  $\alpha$ -tubulin) and we were not able to detect Arl13b/ Scorpion at the membrane on whole mount embryos, we can conclude that the expression of Arl13b/ Scorpion in cross sections indeed localizes to cilia. Interestingly, in *ift57*<sup>hi3417</sup> mutants Arl13b/ Scorpion mislocalized to the apical side of the cell (Fig.39 E-H). In regions where a cilium was still present, the majority of the Arl13b/ Scorpion protein was localized to the cilium (data not shown) next to a weaker staining at the apical side of the cell.

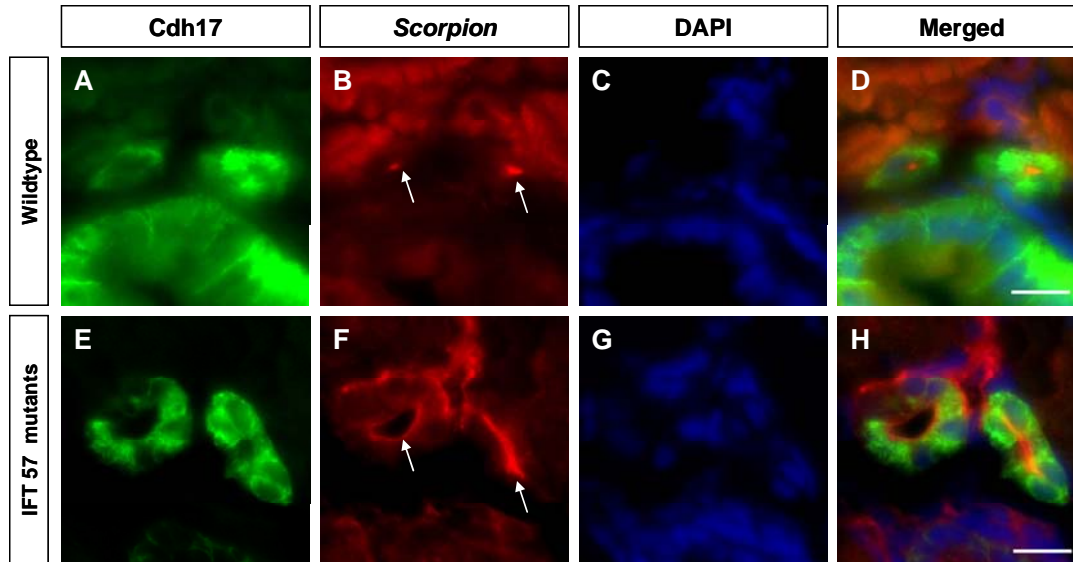


**Fig. 39: Scorpion localization in *ift57*<sup>hi3417</sup> mutants at 4 dpf.**

Fluorescent immunostaining on 14  $\mu$ m thin cryosections of 4 dpf old embryos. Cdh17 labels the basolateral membrane of the pronephric duct, DAPI labels the nuclei.

(A-D) On wildtype cross sections Scorpion localizes to cilia bundles within the duct (arrows). (E-H) *ift57*<sup>hi3417</sup> mutants at 4 dpf have degraded most of their pronephric duct cilia. Scorpion is enriched in an apical region of the duct (F). Scale bars represent 10  $\mu$ m.

To confirm that Arl13b/ Scorpion indeed localizes to the apical membrane and not sub-membranous organelles such as ER, we carried out double labeling with fluorescently labeled WGA (wheat germ agglutinin) and an antibody for Arl13b/ Scorpion. WGA is a carbohydrate-binding protein that selectively recognizes sialic acid and N-acetylglucosaminyl sugar residues which are predominantly found on the plasma membrane. In wildtype, we detected Arl13b/ Scorpion localization in a tight spot within the lumen and the signal was surrounded by WGA positive membrane (Fig.40, A-D). The Arl13b/ Scorpion signal within the WGA positive signal represents ciliary staining supporting our results from previous whole mount fluorescent antibody stainings. In contrast, in *ift57*<sup>hi3417</sup> mutants Arl13b/ Scorpion mislocalized to the same region as WGA, indicating that Arl13b/ Scorpion indeed is mistargeted to the apical membrane in the absence of cilia. Interestingly, we found that WGA and Arl13b/ Scorpion signals were inversely correlated; regions of strong WGA signals exhibited weaker Arl13b/ Scorpion signals and *vice versa*.



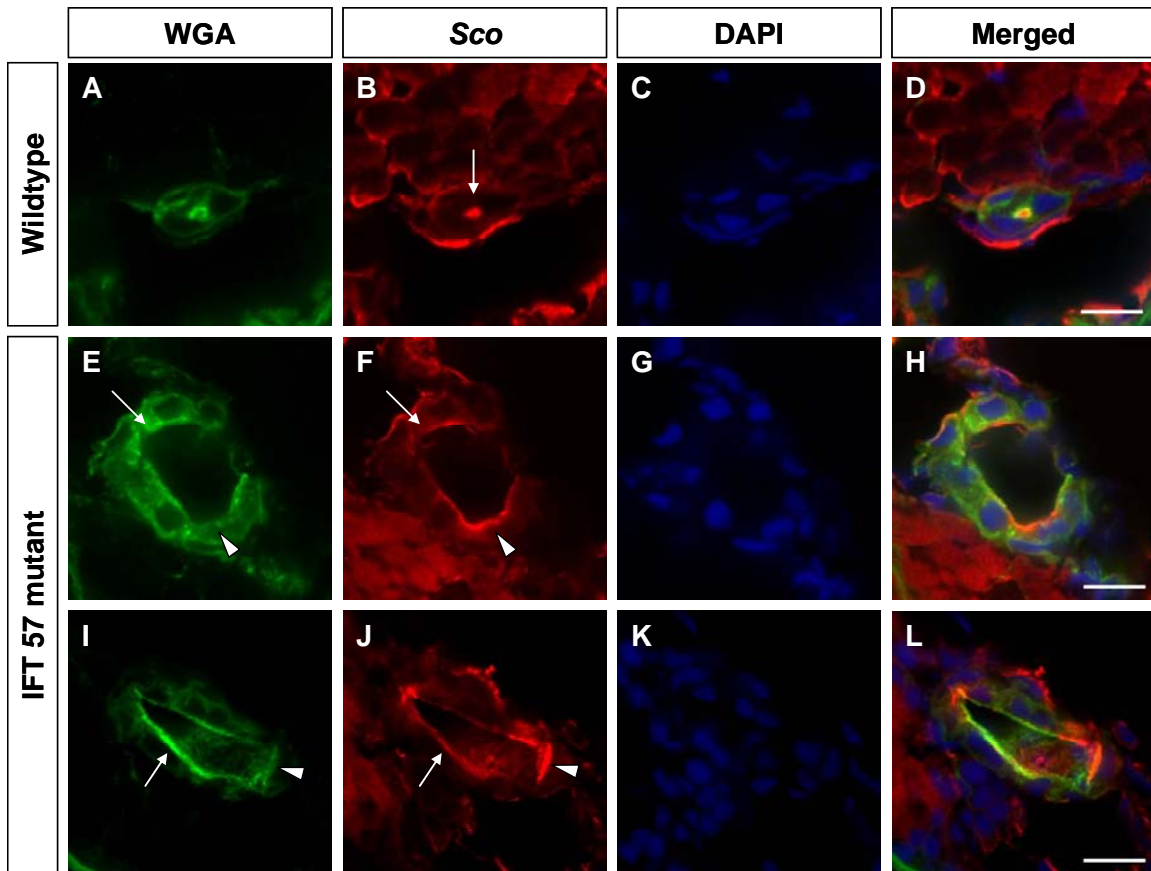


**Fig. 40: In *ift57*<sup>hi3417</sup> mutants Arl13b/ Scorpion is mistargeted to apical membrane and inversely correlates with WGA expression.**

Fluorescent immuno staining on 14  $\mu\text{m}$  thin cryostat cross sections of *ift57*<sup>hi3417</sup> mutants and sibling controls at 4 dpf.

(A-D) In wildtype embryos the Arl13b/ Scorpion signal is surrounded by WGA signal. WGA labels the apical membrane and Arl13b/ Scorpion localizes to the cilia. (E-L) In *ift57*<sup>hi3417</sup> mutants strong ectopic Arl13b/ Scorpion signal on the membrane was accompanied by the absence of WGA (arrowheads). Furthermore, membrane regions of strong WGA labeling showed a lower expression of Arl13b/ Scorpion (arrows).

Scale bars represent 10  $\mu\text{m}$ .



### 6.2.23. The pronephric duct in *scorpion*<sup>hi459</sup> mutants grossly maintains apical/basolateral polarity

Kidney cyst are fluid filled cavities in the nephron that are lined by an epithelium. The epithelium is highly polarized and expresses distinct membrane proteins, transporter and adhesion molecules on the apical and basolateral membrane respectively. During the course of PKD cystic cells were shown to dedifferentiate and/or change fluid secretion. Renal cells that change from being absorptive to being secretory are thought to be a leading cause of cystic fluid accumulation. (Grantham *et al.*, 2006). The Sodium/Potassium ATPase (Na<sup>+</sup>/K<sup>+</sup>-ATPase). Na<sup>+</sup>/K<sup>+</sup>-ATPase is an ion pump localized at the basolateral membrane and is a regulator of fluid secretion. It is absent from the apical side of the epithelium and localizes exclusively to the basolateral membrane of the duct epithelium.

Studies have shown that Na<sup>+</sup>/K<sup>+</sup>-ATPase can be found mistargeted to the apical surface of cystic epithelia, where secretion of sodium into the lumen could result in fluid accumulation (Avner *et al.*, 1992; Drummond *et al.*, 1998; Wilson *et al.*, 2000). Controversially, other studies with both human as well as murine cystic tissues failed to show altered targeting of Na<sup>+</sup>/K<sup>+</sup>-ATPase (Brill *et al.*, 1996; Thomson *et al.*, 2003). We therefore sought to analyze whether *scorpion*<sup>hi459</sup> mutants would be able to traffick Na<sup>+</sup>/K<sup>+</sup>-ATPase in a correct manner and generally be able to maintain a normal polarized epithelium in the pronephric duct.

For that purpose we immuno stained cryostat cross sections of 5 dpf old *scorpion*<sup>hi459</sup> mutant embryos for Na<sup>+</sup>/K<sup>+</sup>-ATPase. In wildtype cross sections Na<sup>+</sup>/K<sup>+</sup>-ATPase was strictly localized to the basolateral membrane but in cystic epithelia of *scorpion*<sup>hi459</sup> mutants Na<sup>+</sup>/K<sup>+</sup>-ATPase appeared less restricted and more diffuse (Fig. 41 A-B). However, it could not be detected at the apical membrane.

The misorganization of Na<sup>+</sup>/K<sup>+</sup>-ATPase could be a result of loss or disruption of apico-basolateral polarity in the cystic epithelium. Epithelial cells are highly differentiated cells, having an apical and basolateral plasma membrane, which differ in their protein and lipid compositions. The function of the epithelium depends on the proper polarized organization of epithelial cells. To determine whether the apico-basolateral polarity in *scorpion*<sup>hi459</sup> mutants is perturbed, we performed immunohistochemistry on 5 dpf old *scorpion*<sup>hi459</sup> and sibling control embryos and stained for apical plasma membrane and basolateral membrane specific proteins. aPKC in wildtype embryos localizes to the

apical membrane of the duct while Cdh17 labels the basolateral membrane (Fig.41 C-D). The ductal lumen in wildtype embryos was very small and surrounded by very few cells. In *scorpion*<sup>hi459</sup> mutants aPKC localization appeared normal and was restricted to the apical membrane. This result was supported by staining with phalloidin which labels F-actin. Phalloidin localization to the apical membrane in wildtype was maintained in cystic epithelia of *scorpion*<sup>hi459</sup> mutant embryos (Fig.41 E-F). It was very striking in cross sections to observe the increase of the ductal diameter and lumen in *scorpion*<sup>hi459</sup> mutants, which were evidently surrounded by a higher number of cells compared to wildtype siblings as described (Fig.18, 19). Furthermore, we observed that even though apical trafficking appeared normal and the gross apico-basolateral polarity was maintained, the basolateral targeting of both basolateral markers, Cdh17 and Na<sup>+</sup>/ K<sup>+</sup>-ATPase seemed less organized. This suggests that Scorpion might play a role in regulating the protein trafficking of membrane proteins to the basolateral cell membrane. An alternative explanation might be that the cystic epithelium is less organized in general, show higher convolution and the basolateral membrane targeting phenotype is an unspecific secondary effect. Considering that Scorpion is an Arl GTPase, a potential role in vesicle trafficking and/ or cytoskeletal regulation is very likely. It will be very interesting to try to elucidate a potential role of Arl13b/Scorpion in specific basolateral membrane trafficking.

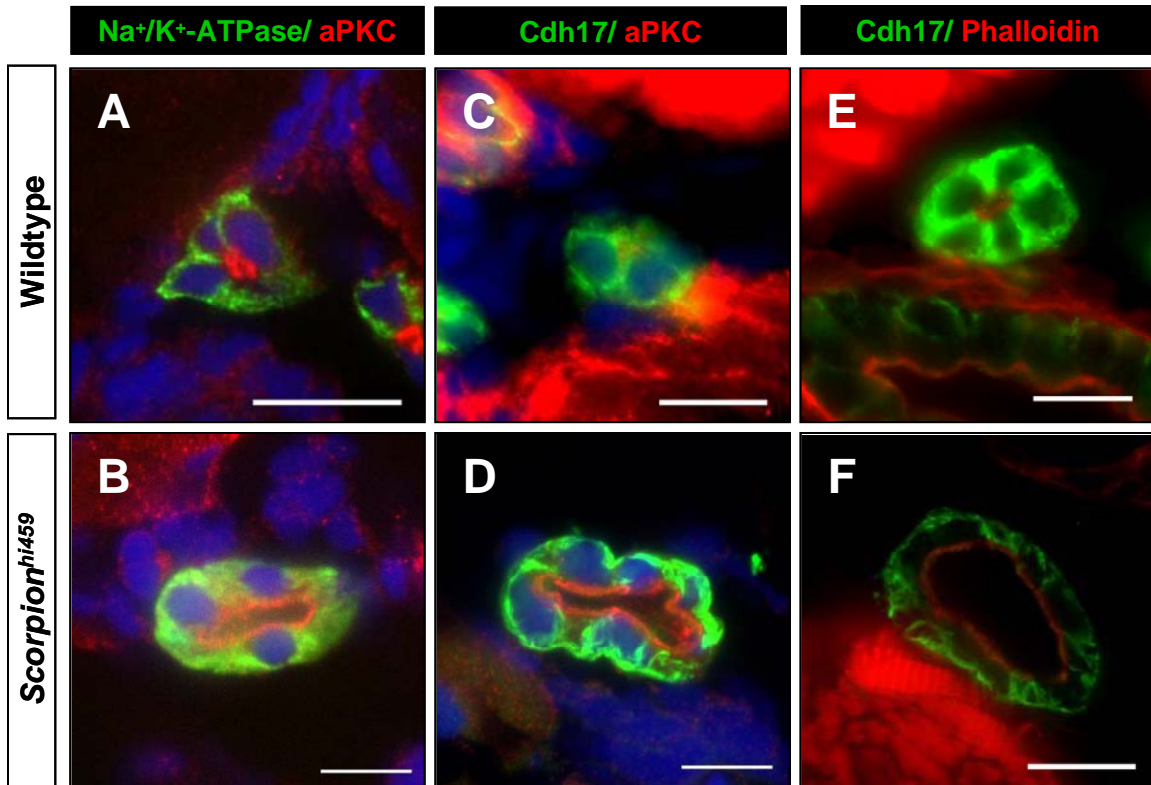


**Fig. 41: Apico-basolateral polarity in *scorpion*<sup>hi459</sup> mutants is grossly intact while basolateral membrane is not as organized.**

(A-B) Fluorescent immuno staining for Na<sup>+</sup>/ K<sup>+</sup>-ATPase, aPKC and DAPI. Na<sup>+</sup>/ K<sup>+</sup>-ATPase localizes to the basolateral membrane in 5 dpf old wildtype ducts (A) whereas *scorpion*<sup>hi459</sup> mutants at 5 dpf show a more diffuse staining of Na<sup>+</sup>/K<sup>+</sup>-ATPase (B). (C-D) Fluorescent immuno staining for Cdh17, aPKC and DAPI. Atypical PKC localizes to the apical membrane in wildtype and *scorpion*<sup>hi459</sup> mutants. (E-F) Fluorescent immuno staining for Cdh17 and Phalloidin. Apical Phalloidin staining is maintained in *scorpion*<sup>hi459</sup> mutants. Cdh17 staining (C-F) is less organized in *scorpion*<sup>hi459</sup> mutants compared to wildtype but remains localized to the basolateral surface.

All stainings are performed on 14 μm thin cross sections. (A-B) 5 dpf Dent's fixed embryos. (C-D) 4 dpf old Dent's fixed embryos. (E-F) Formalin fixed 5 dpf old embryos.

Scale bars represent 10 μm.

## 6.3. Discussion

Arl13b/ Scorpion has been linked recently to the classical form of the human disease Joubert syndrome (JS). JS patients show mostly developmental defects due to malformations in the brain. Joubert syndrome and related disorders (JSRD) is a term that describes disorders that have additional phenotypes in addition of the classical manifestations of JS, e.g. cystic kidneys, hepatic fibrosis or polydactyly, which are known to have a underlying ciliary defect. Since human patients with JS show a brain specific phenotype, it might be possible that Arl13B functions spatially restricted to the brain. Alternatively, mutations in ARL13B might be rare and result in partial loss-of-function allele, with complete null alleles and truncating alleles being hardly found possibly due to a embryonic lethal phenotype. This is supported by several animal models: the mouse *Arl13b* null mutant (*hennin*) is embryonic lethal and dies around E13.5-14.5 (Caspary *et al.*, 2007). Similarly, *arl13b/ scorpion* mutants in zebrafish die around 6 dpf and cannot be raised to adulthood, suggesting that Arl13b plays a critical role during early development and might provide one possible explanation for the low percentage of ARL13B mutations seen in human JSRD patients. Thus the brain specific phenotype observed in human patients might reflect a different threshold or sensitivity to the decreased level of ARL13B.

### 6.3.1. Arl13b/ Scorpion plays a global role in ciliated tissues

In our study we were able to show that Arl13b/ Scorpion is expressed in a wide range of ciliated tissues and that *scorpion*<sup>hi459</sup> mutants and morphants exhibit systemic ciliary defects with symptoms broader than in the classical form of JS and are not limited to the brain, indicating that Arl13b/ Scorpion plays a global role in ciliated tissues, such as eyes, kidneys and Kupffer's vesicles. Patients with JSRD have many other clinical abnormalities (such as polycystic kidneys and retinal degradation) beside defects in the brain stem and cerebellar malformations seen in the classical form of JS. The *sco*<sup>hi459</sup> zebrafish mutant recapitulates many defects which have been associated with JSRD thus making the zebrafish *scorpion*<sup>hi459</sup> mutant an excellent model for JS and JSRD.

### 6.3.2. Pathogenesis of duct dilation and cyst formation in *scorpion*<sup>hi459</sup> mutant embryos

Zebrafish has emerged as a very powerful model organism to study human disease. One reason is the possibility to perform detailed spatial and temporal analysis with ease. Due to multiple cellular defects observed in PKD and in other ciliopathies it has yet to be decided which cellular defect is the consequence and which one the cause of other defects. Duct dilation could possibly occur via two different mechanisms. First, cells lining the pronephric duct might stretch without an increase of cell numbers. Alternatively, an increase of the cell number in the duct might account for the duct dilation. In humans, increased proliferation of the cystic epithelia often is associated with PKD. To differentiate between those two hypothesis, we counted the cell numbers at 2 dpf and 4 dpf in all segments of the pronephric duct.

Based on our study, the data described here suggest that duct dilation preceded hyperproliferation in *scorpion*<sup>hi459</sup> mutants and the medial tubule of the pronephric duct was affected prior or more severely compared to the anterior and posterior region. As the disease progressed, all regions of the duct showed hyperproliferation and more cells in the ductal circumference as is reported in human patients. In addition, the glomerulus of *scorpion*<sup>hi459</sup> mutants did become dilated with varying severity as a secondary effect to the tubular dilation as reported in human renal cystic diseases as well as in mouse models for ADPKD (Bernstein, 1993; Tanner *et al.*, 2002).

Analyzing the *scorpion*<sup>hi459</sup> mutant at another slightly younger timepoint might be helpful to verify if ductal enlargement occurs first in the medial region without signs of hyperproliferation. A preliminary histological analysis of *scorpion*<sup>hi459</sup> mutant embryos around 20 hpf reveals neither a dilation nor a change in cell numbers surrounding the pronephric duct suggesting that dilation as well as an increase in the cell number around the medial region occur within the next 12 hours of embryonic development.

It will be very helpful to apply the proliferation assay that was established for wildtype on *scorpion*<sup>hi459</sup> mutants to verify the overproliferation phenotype as well as the rate of apoptosis in the future. Since hyperproliferation and misregulated apoptosis have been shown to be involved in PKD in humans in many studies (Simons and Walz, 2006) most of the therapeutic approaches for PKD try to target regulation of cell cycle (e.g. CDK inhibitor roscovitine, Ibraghimov-Beskrovnya, 2007) or proliferation (mTOR inhibitor

rapamycin, Shillingford *et al.*, 2006; Torres *et al.*, 2007). It might be interesting to determine whether any of those drugs might decrease the size, frequency or time of onset of cyst formation in the *scorpion*<sup>hi459</sup> mutant or whether it might play a different role in cyst formation and maintenance of epithelial integrity.

### 6.3.3. IFT and Arl13b/ Scorpion

Cilia are hair-like organelles that extend from the apical surface into the extracellular space, i.e. into the lumen in the pronephric duct. Cilia do not possess the machinery for protein biosynthesis and depend entirely on a process called IFT (intraflagellar transport) to transport axonemal and membrane components into the ciliary compartment. Using *ift57*<sup>hi3417</sup> mutants, we wanted to address where Arl13b/ Scorpion would traffic to in the absence of cilia. Even though *ift57*<sup>hi3417</sup> mutants do form cilia initially due to maternal contribution, they are degraded with progressing development. At 4 dpf most of the cilia are degraded. Performing our analysis at this time point, *ift57*<sup>hi3417</sup> mutant embryos exhibited mislocalized Arl13b/ Scorpion to the apical membrane of cystic epithelia which could be due to two possible mechanisms. Arl13b/ Scorpion trafficking could be dependant on IFT and disruption of IFT could lead to mistargeting of Arl13b/ Scorpion. Alternatively, Arl13b/ Scorpion trafficking could be independent of IFT. Trafficking to the cilium might be a multi-step process in which proteins are transported to the apical membrane first before being sorted to get trafficked to the cilium. The first step of getting transported to the apical membrane might be IFT-independent allowing Arl13b/ Scorpion to get transported to the apical membrane correctly. The cilium or parts of the cilium might act as an organizing and signaling center, directing protein trafficking through the transition zone into the ciliary compartment. In IFT57 mutant embryos, lack of cilia could possibly mean the lack of a crucial signal, thus proteins destined to traffick into the cilium might accumulate at the previous subcellular compartment such as the apical membrane. However, this is highly speculative and we do not observe Arl13b/ Scorpion at the membrane in wildtype embryos when analyzed via indirect fluorescent immunohistochemistry. This does not mean that this possibility is wrong, since an apical localization could be transient and only a small fraction of the endogenous protein might be localized there at any given point. Since the majority of the protein is found on the cilium, we might not be able to detect a weak, transient apical staining. Scorpion-GFP mRNA overexpression and further enhancement of the signal with a GFP specific

antibody might be one way to address that question. Another approach that we are currently following is immuno-gold electron microscopy, utilizing a newly generated Arl13b-GFP transgenic fish line and anti-GFP monoclonal antibodies since the Arl13b/Scorpion specific antibody was not feasible for this technique. The tissue of zebrafish embryos is very fragile thus generating high quality ultra-thin cryosections is very challenging but we have promising preliminary data and are optimizing the protocol to further gather information about the subcellular localization of Arl13b/ Sco in the pronephric duct and the cilium in particular.

#### **6.3.4. Apico-basolateral polarity**

Since Arl13b/ Scorpion was mislocalized and loss of apical-basolateral polarity has been reported in cystic epithelia, we sought to analyze the polarity in *scorpion*<sup>hi459</sup> mutants. Both basolateral markers we used, Cdh17 and Na<sup>+</sup>/K<sup>+</sup>-ATPase localized to the basolateral membrane in a less organized manner in *scorpion*<sup>hi459</sup> mutants, however, the gross polarity of the duct appeared normal. This could be explained either by a mistargeting of basolateral proteins to the membrane or by a structural defect of the convoluted duct. Zebrafish mutant embryos which have been previously reported to show defective basolateral trafficking of proteins specifically are *elipsa* and *fleer* (Omori *et al.*, 2008; Pathak *et al.*, 2007). Elipsa has been shown to provide a link between IFT particles and interestingly a small GTPase called Rab8 and to promote interaction with axonemal microtubules thus facilitating movement. Rab8 GTPase is thought to regulate basolateral membrane targeting and Rab8 depleted cells have a ciliary formation defect (Yoshimura *et al.*, 2008). Furthermore, *fleer* mutants exhibit mistargeting of basolateral membrane proteins as well (Drummond *et al.*, 1998). Studies on *fleer* showed that post-translational modifications such as polyglutamylation of tubulin are an underlying cause that can lead to defects in axonemal structure and cilia formation when not functioning properly. *fleer* exhibits a microtubule closure defect in the B-tubule of the ciliary axoneme. The same ultra structural defect was observed in the *hennin* mutant, a null allele of murine Arl13b. Since it is not feasible for us to measure the level of convolution at this point, we cannot rule out the possibility that the convolution is contributing to a less strict organized basolateral membrane. However, considering the similarities between *sco*<sup>hi459</sup> mutant embryos with the *elipsa* and *fleer* mutants, a perturbation of basolateral specific protein trafficking is a reasonable alternative explanation. When we

performed transmission electron microscopy in *scorpion*<sup>hi459</sup> and wildtype siblings at 4 dpf no obvious ultrastructural defect could be detected. Both wildtype and *scorpion*<sup>hi459</sup> mutant embryos presented a (9+2) microtubule arrangement with fully closed outer microtubules and present dynein arms. It is speculative, but Arl13b/ Scorpion might potentially regulate post-translational modifications via downstream targets that are necessary for cilia formation and/or targeting of proteins to the basolateral membrane. Thus loss of Arl13b/ Scorpion might result in mistargeting of proteins to the basolateral membrane as well as disruption of ciliogenesis and maintenance of cilia.

### 6.3.5. Ciliary tufts in *scorpion*<sup>hi459</sup> mutant embryos

Another striking similarity between *fleeer* and *scorpion*<sup>hi459</sup> mutants are the ciliary tufts in the pronephros that consists of cilia of varying lengths extending from multiciliated cells. It remains unclear why we are able to see longer cilia in multiciliated cells versus single ciliated, principal cells. One explanation could be provided by the motor protein kinesin. It has been suggested that different kinesins play distinct roles during ciliogenesis. In *C.elegans*, two kinesins, kinesin-2 and osmotic avoidance defective (OSM)-3 kinesin cooperate to drive two separate IFT pathways that are responsible for distinct cilia segments (Ou *et al.*, 2000). In addition, it was suggested that different kinesins might have different sensitivities or requirements for polyglutamylation. Supporting this hypothesis is the recent finding that mice that have a defective tubulin polyglutamylase show a reduction of neuronal tubulin polyglutamylation and a defective KIF1A cargo trafficking, whereas KIF3A and KIF5 transport is not affected (Ikegami *et al.*, 2007). This might be an explanation for the different sensitivity we see in pronephric duct cilia in *scorpion*<sup>hi459</sup> mutant embryos where multiciliated cells seem to be less affected compared to single cilia, that are absent or so short we were unable to detect them by immunofluorescence at 3 dpf as well as 5 dpf. It is possible that distinct kinesin motors function in multiciliated cells in the pronephros that are less sensitive to a changed tubulin polyglutamylation. However, this is an avenue we did not pursue yet but something that would be very interesting to do in the future.

Multiciliated cells contain multiple basal bodies which are replicated in the cytoplasm and targeted to the apical membrane by vesicular transport. The organized row of basal



bodies is responsible to align cilia which in turn beat in a coordinated fashion to move fluid through the tubule. Our study shows for the first time basal bodies become aligned in a linear fashion that appears to curve along the tubule, a process which might be governed by planar cell polarity (PCP). Furthermore, the neighboring multiciliated cells appeared to align in a manner that appeared to be contiguous with the previous one, resulting in a spiral of curved rows of basal bodies wrapping around the duct. Similarly, single ciliated cells appeared to orchestrate the position of the basal body with the neighboring cells as well, resulting in a spiral pattern of basal bodies. We speculate that PCP might govern the polarity of basal bodies cell autonomously as well as in the context of the whole tissue, leading to the most efficient configuration of cilia positions for efficient fluid movement. Our observation is only the beginning and it would be fascinating to analyze this phenomenon in detail. It will be very helpful to use a morpholino for a core PCP protein, such as Prickle1, to verify that it would result in a similar disruption of basal body alignment and confirm that our phenotype is specifically due to a defect in planar cell polarity. A similar phenomenon was recently reported in the organ of corti in mouse where IFT88 (polaris) is required for positioning polarized basal bodies which in turn play a crucial role for establishment of epithelial PCP and convergent extension of the cochlear duct (Jones *et al.*, 2007).

To determine whether the remaining cilia in the pronephric duct of *scorpion*<sup>hi459</sup> mutants are motile and could beat in a coordinated manner, we used video microscopy on 3 dpf and 5 dpf old embryos. We were not able to detect any ciliary beating movement in *scorpion*<sup>hi459</sup> mutant embryos at 3 dpf, whereas cilia in wildtype embryos showed coordinated beating with a frequency of  $43.2 \pm 9.1$  Hz. There are three possible explanations for it. First, technical issues, e.g. failing to find the correct region and/or focus for the multiciliated tufts in *scorpion*<sup>hi459</sup> mutants. However, considering that the entire medial/posterior region was analyzed and focused throughout the entire embryo, it is unlikely that the correct region and/or plane might have missed. Furthermore, anatomical landmarks such as the otic vesicle and yolk extension were used to find the right region and the striated muscle was used to aid in finding the right plane of focus.

Second, assuming that cilia tufts in *scorpion*<sup>hi459</sup> mutants might be able to move their cilia individually, it is very unlikely that all cilia originating from a ciliary tuft would be able

to bundle correctly in order to move in a coordinated manner. Uncoordinated ciliary movement of individual cilia in the kidney duct could be below our threshold to detect beating. Lastly, it is plausible that the remaining cilia in *scorpion*<sup>hi459</sup> mutants are not motile and therefore no movement could be detected by video microscopy. The experiment was repeated at a later time point at 5 dpf and interestingly, ciliary beating could be detected. The kinetics of the ciliary beating was altered and could be divided into three groups: 35% of analyzed cilia belonged to the fast group, with cilia beating with a frequency of  $43.43 \pm 4.79$  Hz which were comparable to wildtype cilia which have a frequency of  $46.75 \pm 3.91$  Hz. A second group of cilia (35% of cilia) was termed 'medium' and showed a frequency of  $27.43 \pm 3.92$  Hz ( $p < 0.001$ ). The last group were very slow beating cilia (30% of cilia) that were beating with a frequency of  $13.50 \pm 3.45$  Hz ( $p < 0.001$ ).

This could possibly mean that Arl13b/ Sco is not essential for cilia formation, growth and maintenance in cilia originating from multiciliated cells. Alternatively, since *scorpion*<sup>hi459</sup> mutant embryos are not true null mutants but closer resemble hypomorphic alleles due to maternal contribution, a very slow turnover of Arl13b/ Sco protein could potentially still be present at 5 dpf thus leading to cilia formation and growth. Cilia from single ciliated cells could not be detected via immunofluorescence, which might be indicative of a different role Arl13b/ Sco might play in single versus multiciliated cells. Single cilia are thought to be sensory organelles whereas ciliary bundles from multiciliated cells are responsible for fluid movement. Absent or a reduced intracellular concentrations of Arl13b/ Sco might be detrimental for the formation/ maintenance of a primary cilium but have a less severe effect on multiciliated cells, e.g. resulting in formation of cilia but exhibiting aberrant motility/ beating patterns.

### **6.3.6. Arl13b/ Sco and laterality formation**

Beside a functional role during ciliogenesis in the pronephric duct, we found a novel role for Arl13b/ Scorpion in the Kupffer's vesicle (KV) during embryogenesis. The KV is a transient structure and the functional zebrafish equivalent to the mouse node. It establishes left/right asymmetry in the embryo by breaking the symmetric body plan via cilia-dependant leftward fluid flow. Using *arl13b/scorpion* oligo morpholinos to knock down the transcript, we could detect randomization of the heart looping. This could have been caused by either a defect in KV formation itself or a functional or structural defect

of cilia within the KV. Our results confirmed our hypothesis that a ciliary defect in *arl13b/scorpion* morphants is the cause for the observed left/right asymmetry defect and the formation of the Kupffer's vesicle structure is not perturbed *per se*. *arl13b/scorpion* morphants have stunted and less abundant cilia in the KV. A recently published study on *hennin* (*Arl13b* null mouse) also showed a defect in left/right asymmetry (Caspary *et al.*, 2007) caused by stunted cilia in the embryonic node, supporting our finding that *Arl13b/Scorpion* plays an important role during embryogenesis and cilia formation.

One of the two genes mutated in ADPKD in humans is *PKD2*. *PKD2* encodes the protein polycystin-2, which localizes to cilia in the KV and embryonic node respectively and functions as a channel eliciting calcium signals specifically to the left side which is thought to be caused by bending of the ciliary axoneme in response to directional fluid flow across the nodal/ KV surface. Interestingly, *PKD2* mouse models that either introduced somatic mutations that resulted in a inactive *PKD2* allele (Wu *et al.*, 1998; Wu *et al.*, 2000) as well as *PKD2* null mice (Pennekamp *et al.*, 2002) showed situs inversus with randomized heart looping, position of pancreas, liver, lung and stomach (Pennekamp *et al.*, 2002; McGrath *et al.*, 2003). In addition, *PKD2* morphants in zebrafish show left/right asymmetry defects but do not exhibit structural defects of their cilia in Kupffer's vesicle (Bisgrove *et al.*, 2005).

Previous studies reported KV cilia to be  $3.3 \mu\text{m} \pm 1.1 \mu\text{m}$  in length and our measurements in wildtype were similar with an average length of  $3.01 \mu\text{m} \pm 0.325 \mu\text{m}$ . However, *arl13b/scorpion* morphants exhibited less abundant as well as shorter cilia in the KV with a ciliary length of  $1.37 \mu\text{m} \pm 0.272 \mu\text{m}$  on average. This defect is specific and not due to the injections of morpholino by itself, since control morpholino injections did not lead to any reduction in length ( $3.069 \mu\text{m} \pm 0.319 \mu\text{m}$ ) or abundance of cilia.

Taken together, the results of *PKD2* mutants and *arl13b/scorpion* morphants indicate that both, structural as well as functional defects that affect the cilium integrity in the Kupffer's vesicle lead to *situs inversus*.

The first gene known to be asymmetrically expressed is *nodal*. The zebrafish *nodal* genes are called *cyclops*, *squint* and *southpaw*. *arl13b/scorpion* morphant embryos display an altered left/right expression pattern of *spaw* and have a ciliary defect in the KV with stunted and less abundant cilia, making it nearly impossible for the remaining cilia to create a normal fluid flow. The current hypothesis states that cilia in the KV or

embryonic node beat in a coordinated manner that result in directed fluid flow which in turn is critical for the correct expression of nodal. How exactly fluid flow (or cilia motility) determines left-right patterning is not well understood.

In a wildtype embryo, *spaw* is expressed asymmetrically in the left lateral plate mesoderm (LPM) and the excluded from the right LPM. It is unknown whether the absence of *spaw* from the right LPM is a direct mechanism due to an asymmetric Nodal inhibition or an indirect mechanism resulting from the asymmetric concentration of a Nodal activator on the left side via nodal flow. Alternatively, it could be a combination of both pathways. In *ar13b/scorpion* morphant embryos, *spaw* expression is not restricted to the left LPM anymore, but can be found on either side of the embryo, on both sides or be absent. Bilateral *spaw* expression in the LPM indicates that in *ar13b/scorpion* morphants both the left and right side of the KV received an activation signal and/or no inhibition to prevent *spaw* expression. Accordingly, absent *spaw* expression indicates that the a nodal activation signal was not present on either side of the KV or was suppressed completely. Asymmetric expression in *ar13b/scorpion* morphant embryos, beeing restricted to either the left or right LPM, could be explained by a soluble morphogen randomly accumulating at one side of the KV independent of fluid flow. However, so far, the nature of a soluble morphogen that can initiate nodal activation or restriction in the KV is elusive.

Two models have been proposed for how fluid flow inf the KV or embryonic node could lead to establishment of left/right asymmetry. The first model is based on the presence of a soluble morphogen. Fluid flow in the embryonic node or KV respectively, could establish a gradient of this morphogen at the left side of the node/ KV, whereupon it interacts with its receptor and activates downstream targets and a cascade of asymmetric gene expression that eventually would result in left-sided nodal gene expression. Even though several secreted molecules, e.g. Nodal, Shh (Sonic hedgehog), GDF1 (growth and differentiation factor 1) and RA (retinoic acid) have been proposed in recent years to be possible candidates for the morphogen, results so far are not conclusive (Tanaka *et al.*, 2005). Fluid volume, flow rate, morphogen concentration and kinetics have to be highly regulated and coordinated in order to build and maintain a stable gradient of a soluble morphogen. Studies could show that artificial nodal flow could establish normal left/right asymmetry, independent of the volume or rate of fluid

flow. This suggests that the morphogen gradient based model alone does not recapitulate the process accurately.

The second model is based on sensory cilia in the node. Motile cilia are located in the center of the field whereas immotile cilia are concentrated on the periphery. Directional fluid flow caused by motile cilia could activate immotile, sensory cilia on the left side of the node, thereby triggering a signaling cascade that would result in left sided expression of nodal. However, immotile cilia have not been found in zebrafish KV yet and it remains to be seen whether this model is applicable in zebrafish.

It is quite likely that both models will play partial roles in left right asymmetry establishment. But how could fluid flow result in the asymmetric accumulation of a morphogen? The embryonic node in mouse and the KV in zebrafish are homologous structures, that were thought to bear a quite different morphology. The mouse embryonic node is a bowl-shaped structure which is covered with Reichert's membrane (Nonaka *et al.*, 1998) and contains a field of cells at the dorsal roof that are monociliated. The KV in zebrafish has been reported to be a spherical organ containing monociliated cells on the entire inner surface but a recent study found that in fact, the majority (80 %) of cilia are localized on the dorsal side of the KV, whereas the remaining cilia are ventrally localized (Kreiling *et al.*, 2007), thus making the node and KV more alike than previously thought.

Cilia at the mouse node were recently shown to be tilted toward the posterior axis (Nonaka *et al.*, 2005; Okada *et al.*, 2005) which would cause the rotating cilia close to the cell surface to result in a minor rightward flow and cilia further away from the cell surface to result in a strong fluid flow to the left (Shiratori and Hamada, 2006). The net flow in the embryonic node would result in a right-to-left flow along the surface of the node.

In zebrafish, if the entire surface of the KV would be evenly ciliated, the resulting fluid flow would cause a vortex within the KV making it impossible to form a left-sided morphogen gradient or to activate sensory cilia on one side specifically. Importantly, not only are cilia concentrated on the dorsal side of the KV but have been shown to be biased towards the anterior region of the KV (Kreiling *et al.*, 2007). This bias has been proposed to be responsible to cause an anterior-to-leftward net fluid flow which is further enabled by the fact that cilia are tilted towards the posterior in a 45° angle. The counter clockwise flow would be stronger in the anterior region due to the majority of cilia localized there, and weak in the posterior region. A study performing measurements of kinetics of fluid

flow in the KV supports this model, observing a faster left-sided flow from the anterior region of the KV ( $2.6 \pm 0.13$  seconds) and a slower right-sided flow ( $3.8 \pm 0.15$  seconds) in the posterior region (Kramer-Zucker *et al.*, 2005). This net left-sided flow could possibly result in stimulation of mechanosensory cilia on the left side of the KV and/or an accumulation of a morphogen on the left side. However, much is still unknown and more work remains to be done to determine and measure the net left-ward flow in zebrafish and its influence on expression of signaling factors and the asymmetric gene expression pattern.

### 6.3.7. *sco*<sup>hi459</sup> mutant embryos and the *Arl13b* null mutant *hennin*

Beside a defect in the KV cilia structure, *hennin* displays defects of the nervous system including exencephalie and neural tube closure defects (spina bifida), abnormal eyes and polydactyly (Caspary *et al.*, 2007). *scorpion*<sup>hi459</sup> mutants and *arl13b/scorpion* morphants do not exhibit a neural tube closure defect which could be due to different morphogenetic processes that are used to form the neural tube in mouse versus zebrafish. In mouse, neurulation occurs from an epithelial sheet that columnarizes and forms the so-called neural plate. The neural plate undergoes rolling and folding mechanisms to form the neural tube. A defect during this rolling mechanism would result in an open tube, called spina bifida. In zebrafish a different mechanism takes place. The epithelium columnarizes at first to form the neural plate but then forms a neural keel and subsequently a solid neural rod. The midline of the tube becomes distinct and forms a lumen starting from the ventral side. Therefore a defect during neurulation might not be as obvious as in spina bifida since at no point an open neural tube is present.

The study also found a sonic Hedgehog (Shh)-independent expansion of the domain of motor neuron progenitors in *hennin*. Full-length Gli3 acts as an activator but acts upon cleavage as a repressor. In *hennin*, the Gli3 repressor activity was normal but Gli activators were defective, suggesting that the ratio of activator to repressor is crucial and cilia are required to translate different levels of Shh ligands into different regulations of Gli transcription activators and repressors which implement Hh signals (Caspary *et al.*, 2007).

Cilia depend on IFT for their formation and maintenance (Scholey, 2003). IFT mutants were shown to fail to respond to Hh ligands (Houde *et al.*, 2006; Huangfu and Anderson, 2005; Liu *et al.*, 2005; May *et al.*, 2005). Furthermore, Hh responsive cells are ciliated and Hh signaling molecules have been found to localize to the cilium, e.g. smoothed is a transmembrane protein essential for Hh signaling and enriched in cilia of Hh responsive cells in mouse (Corbit *et al.*, 2005). In addition, Gli transcription factors are effectors of Hh signaling and overexpression studies showed Gli1, Gli2 and Gli3 localized to cilia (Haycraft *et al.*, 2005) and endogenous Gli3 and suppressor of fused (SuFu) have been found to localize to cilia as well (Dunaeva *et al.*, 2003; Haycraft *et al.*, 2005; Merchant *et al.*, 2004). However, in contrast to studies in mouse, *ift57*, *ift88* and *ift172* mutants in zebrafish have no effect on expression of Hh target genes in neural tube, forebrain, pectoral fins as well as somite formation or motor neuron patterning (personal communication with Brian Perkins, Texas A & M University). This suggests that IFT and cilia may be a recent adaptation to the Hh signaling pathway in higher vertebrates than teleost fish. Furthermore, zebrafish mutants that have a defective Hh pathway exhibit a myotome defect and have u-shaped somites which was never observed in *scorpion*<sup>hi459</sup> mutants and morphants respectively.

### **6.3.8. Arl13b/ Sco and retinal atrophy**

Many ciliopathies are associated with retinitis pigmentosa, a degenerative disease with affected patients slowly losing their eye sight. The photoreceptor outer segment (OS) is connected to the inner segment via a connecting cilium which is in fact a structural equivalent of the primary cilium of the renal duct and many proteins that localize to the basal body and cilium in the pronephros can also be found in the retinal photoreceptors. Furthermore, in analogy to IFT transport along the microtubules in kidney cilia, cargo (such as rhodopsin) is transported along microtubules from the inner segment (IS) of photoreceptors to the OS using a kinesin-2 containing motor complex and back into the IS via dynein-2 motor proteins.

*scorpion*<sup>hi459</sup> mutant embryos develop pericardiac edemic phenotypes starting at 2 dpf with varying degrees. Severe edema were accompanied by a small eye phenotype which was first discernible at late 5 dpf. Upon closer examination by hematoxylin and eosin staining as well as fluorescent immunostaining, the loss of the outer segment of the retinal photoreceptors was found. In addition, acellular gaps and pyknotic nuclei

could be observed and excessive TUNEL reactive cells were present in the photoreceptor layer exclusively. The remaining tissue of the *scorpion*<sup>hi459</sup> mutant embryo eye appeared normal and did not show elevated levels of apoptosis or loss of specific cell layers. Since Arl13b/Scm localizes to cilia in multiple tissues, it is highly likely that it would be expressed in the retinal connecting cilium as well. It is known that in IFT mutants, the defective IFT transport leads to accumulation of rhodopsin in the inner segment of the photoreceptor cells. Excessive rhodopsin in the cell body then triggers apoptosis (Nishimura *et al.*, 2004; Ross *et al.*, 2005). Fluorescent immunostaining labeling cilia in *scorpion*<sup>hi459</sup> embryos, revealed shorter and less abundant connecting cilia as well as short and/ or absent outer segments, being very analogue of the ciliary defect observed in the pronephric duct. It might be very interesting to further investigate cell specific roles Arl13b/ Sco might play in the retinal photoreceptors, e.g. rods versus cones, since the *scorpion*<sup>hi459</sup> mutant has distinct effects on cilia of single versus multi ciliated cells.

Taken together, we think that Arl13b/ Scorpion plays a general role in many ciliated tissues during ciliogenesis and maintenance. The *scorpion*<sup>hi459</sup> mutant fish recapitulates major phenotypes that have been associated with JS and JSRD such as polycystic kidneys and retinal dystrophy making it a attractive disease model to study the underlying genetic and biochemical mechanisms.

Furthermore, the role of Arl13b/ Sco does not appear be limited to embryogenesis but is fundamentally required for terminal differentiation and maintenance, based on unpublished data (personal communication with Zhaoxia Sun) showing that even after rescueing *scorpion*<sup>hi459</sup> mutants with arl13b/ *scorpion* mRNA injections, embryos cannot be raised to adulthood but die as juvenile fish. It will be very interesting to investigate how Arl13b/ Scorpion's function during embryogenesis differs from its role in epithelial maintenance and kidney development.



## **Project II**

### **Part 2**

# **Functional Analysis of Arl13b/ Scorpion During Embryonic Development in *Danio rerio***

## 7.1. INTRODUCTION

### 7.1.1. Arl13b and Joubert syndrome

A recent study found a link between mutations in *ARL13B* in humans and the classical form of Joubert syndrome (JS). JS is characterized by congenital cerebellar ataxia, hypotonia, oculomotor apraxia, and mental retardation. JS and related disorders (JSRD) have additional retinal, renal, polydactyly and hepatic phenotypes. Many of those phenotypes have been shown to be caused by genes that encode ciliary proteins. *ARL13B* (ADP ribosylation factor-like 13 B) belongs to the Ras superfamily of small GTPases. The small Arf GTP-binding proteins and the related Arl proteins have been shown to be involved in vesicle biogenesis, membrane targeting and trafficking (reviewed in Chavrier and Goud, 1999). Consistent with the idea that JS is a ciliopathy, mutations in *ARL13B* have been linked to defective cilia formation and kidney cysts in several model organisms.

### 7.1.2. *hennin* and *scorpion*<sup>hi459</sup>

*scorpion*<sup>hi459</sup> was identified in a retroviral insertional mutagenesis screen and the underlying mutation was cloned and identified as the gene *arl13b*. *scorpion*<sup>hi459</sup> mutants are characterized by a ventrally curved body and cyst formation in the kidney (Sun *et al.*, 2004) which are caused by a ciliary defect during kidney development (see previous chapter).

In mouse, *hennin* (*hnn*), was identified as a null allele of *Arl13b* (Caspary *et al.*, 2007). The study showed that *hnn* mutants exhibit ciliary defects in the embryonic node, the mouse homologue to Kupffer's vesicle in zebrafish, with shorter and less abundant cilia, similar to the ciliary phenotype observed in *arl13b/scorpion* morphants. Additionally, cilia in *hnn* mutants had a defective axonemal microtubuli structure with and phenotypes associated with a defective sonic hedgehog signaling pathway.

### 7.1.3. Intraflagellar transport

Arl13b/ Scorpion is highly enriched in the cilium and was not detectable by immunohistochemistry in other subcellular compartments. Since Arl13b/ Scorpion shows

a cilia-specific expression pattern, we sought to identify a potential ciliary localization signal or domains of the protein that would be necessary and sufficient for cilia targeting, analogous to the nuclear localization signal (NLS) which enables proteins to traffick into the nucleus.

Cilia are specialized cellular compartments that use IFT (intraflagellar transport) to build and maintain the cilium. IFT shuttles axonemal precursor proteins from the cytoplasm to the base of the cilium. Using a kinesin-2 motor for anterograde transport, axonemal precursor proteins are transported to the tip of the cilium where the addition of new subunits leads to cilia elongation at the tip (Johnson and Rosenbaum, 1992). The retrograde transport uses cytoplasmic dynein as a microtubule motor protein and transports turnover products as well as the kinesin motor back to the cytoplasm (Quin *et al.*, 2004). IFT was first discovered in the green algae *Chlamydomonas* (Kozminski *et al.*, 1993) but subsequently has been found on cilia in all higher organisms examined (Rosenbaum and Witman, 2002; Avidor-Reiss *et al.*, 2004; Scholey, 2003). Membrane proteins of the cilium are thought to be transported from the golgi complex in vesicles to the base of the cilium, where they are integrated by exocytosis (Rosenbaum and Whitman, 2002; Dwyer *et al.*, 1998; Dwyer *et al.*, 2001) and parts of the IFT proteins, e.g. IFT20 have been shown to be involved in the trafficking of ciliary proteins from the golgi to the cilium. Furthermore, KIF17, a mammalian kinesin-2 orthologue has been shown to play a role in ciliary targeting of olfactory cyclic nucleotide-gated (CNG) channels (Jenkins *et al.*, 2006). However the exact role of IFT in transporting proteins to the cilium as well as how proteins target the cilium independently of IFT is not yet fully understood.

#### **7.1.4. Ciliary localization signal**

Proteins that shuttle to the nucleus often display a specific amino acid sequence known as nuclear localization sequence (NLS) that is sufficient to shuttle the protein to the nucleus. However, a conserved cilia-localization signal has not been elucidated. So far, a number of post-translational modifications such as myristoylation and phosphorylation are known to play a role in ciliary trafficking. Myristoylation at an amino-terminal glycine appears to be important for ciliary trafficking, as was found in studies in *Trypanosoma*

*cruzi* and *Leishmania spp.* (Godsel *et al.*, 1999; Tull *et al.*, 2004). Furthermore, myristoylation seems to play a role during ciliary membrane targeting of a serine /threonine phosphatase in *C.elegans* (Ramulu and Nathans, 2001). Cystin, a ciliary protein as well as other numerous ciliary proteins have predicted amino-terminal myristoylation motifs (Hou *et al.*, 2002; Pazour *et al.*, 2005), suggesting that myristoylation might indeed be involved in ciliary targeting. Another recent study showed that phosphorylation might play a role in cilia targeting. Nephrocystin (NPHP1) localizes to the base of cilia dependent on its phosphorylation status (Schermer *et al.*, 2005), allowing and preventing trafficking to the cilium respectively. Beside post-translational modifications, a ciliary targeting motif in the protein sequence itself, as seen in NLS, might be involved in cilia targeting as well. Thus far, cilia localization sequences have been identified for a glucose transporter in *Leishmania spp.* and ciliary seven-transmembrane receptors in *C. elegans* (Dwyer *et al.*, 2001) and mammals (e.g. smoothed) (Corbit *et al.*, 2005). The cilia localization sequence in those seven-transmembrane receptors consisted of a hydrophobic and basic amino acid residue immediately carboxyterminal after the seventh transmembrane segment (Corbit *et al.*, 2005). Furthermore, in mammalian polycystin-2, the motif R<sub>6</sub>VxP was necessary and sufficient for trafficking to the cilium in MDCK or LLC-PK1 cell cultures (Geng *et al.*, 2006). However, this motif does not appear to be conserved among other ciliary proteins.

In contrast to other studies that used cell culture based systems to test cilia targeting, zebrafish allows us to perform cilia localization studies *in vivo*. We used deletion constructs of Arl13b/ Scorpion that were fused to GFP (green fluorescent protein) to determine whether a given domain would be necessary and/or sufficient for cilia targeting of the fusion protein.

### 7.1.5. Rescue experiments

It might be possible that Arl13b/ Scorpion has other functions independent from its putative role in trafficking and ciliogenesis. We performed rescue experiments on offspring of *scorpion*<sup>hi459</sup> heterozygous crosses. A mendelian ratio of 25% of those offspring is expected to be homozygous mutant for Arl13b/ Scorpion and the mutant

phenotype can be rescued by overexpression of *arl13b/scorpion* mRNA. However, a lack of this rescue ability would indicate a loss of functional Arl13b/ Scorpion. Performing rescue experiments with a series of deletion constructs in collaboration with Neil Duldulao (another student in the lab) allowed us to draw conclusions regarding the interplay between cilia localization, protein function and GTPase activity.

### **7.1.5. Yeast two hybrid**

Small GTPases participate in signal transduction depending on binding to effector molecules. The effectors for Arl13b/ Scorpion are not known and the data from an ongoing yeast two hybrid screen are also described in this chapter. The yeast two hybrid screen is a powerful tool to find novel protein interactors in a non biased approach.

This part of my thesis work will focus on the functional analysis of the Arl13b/ Scorpion protein to lay a foundation for the comprehensive understanding of it's function.

## 7.2. RESULTS

### 7.2.1. Arl13b/ Scorpion is highly conserved among species

The protein sequence of Arl13b/ Scorpion in zebrafish (NP\_775379) was compared to potential protein homologous in mouse, rat and human. The database search revealed arl13b is highly conserved among these species. Zebrafish Arl13b/ Scorpion shows close sequence similarities to all three species with rat (NP\_001100571) having 68.2% similarity, mouse (NP\_080853) sharing 67.7% similarity and humans (NP\_878899) sharing 66.2% homology with the zebrafish Arl13b/Scorpion protein sequence. The sequences are plotted against each other in figure 42 with homologous amino acids highlighted in dark. The first 194 N-terminal amino acids constitute a ras-like small GTPase domain which is highly conserved among all species. In addition, the C-terminal region proximal to the small GTPase domain appears highly conserved as well. These amino acids (195 until 241) form a coiled coil region, typically involved in protein-protein interactions.

7. FUNCTIONAL ANALYSIS OF THE *scorpion*<sup>hi459</sup> MUTANT IN *Danio rerio*

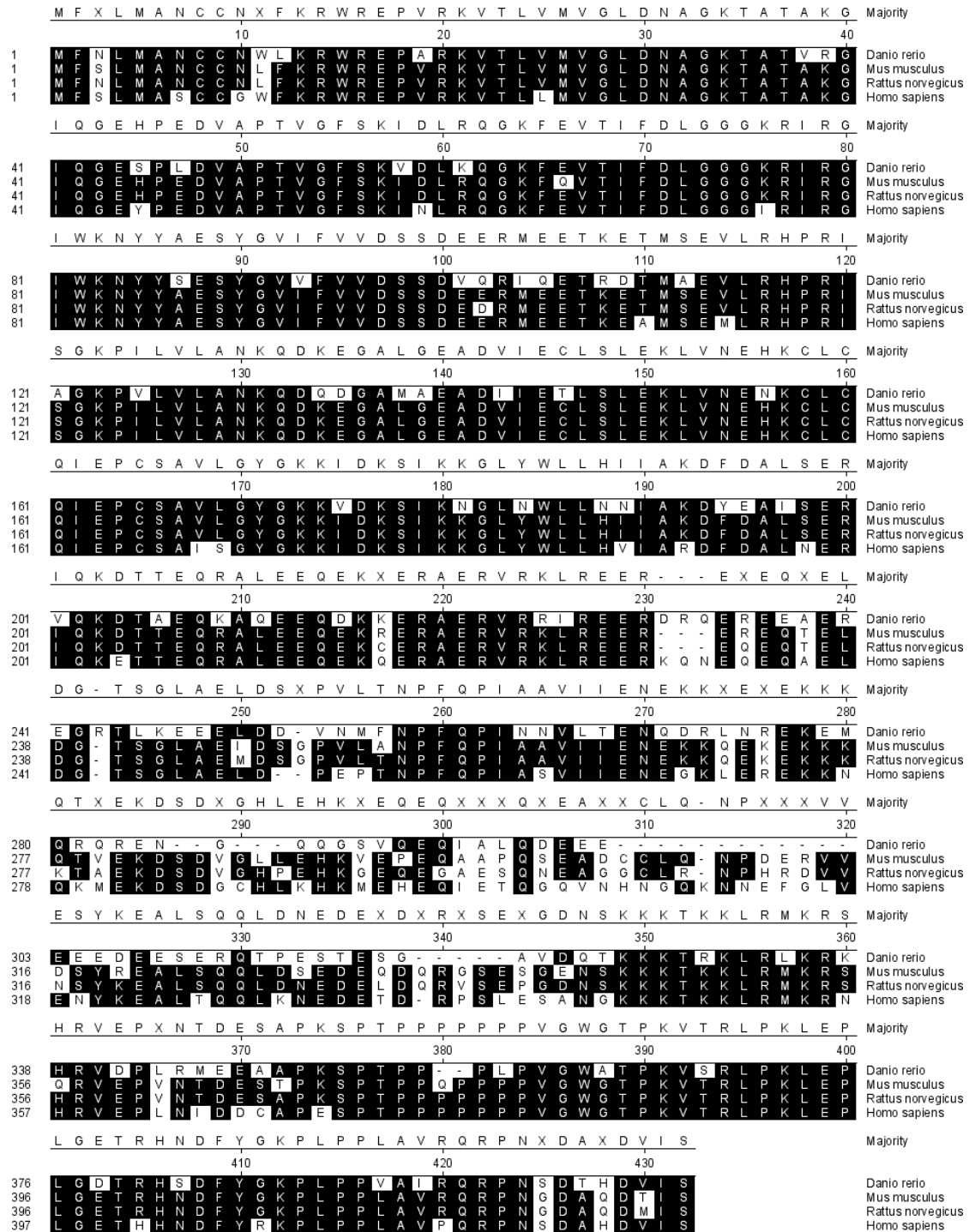


**Fig. 42: Arl13b/ Scorpion is conserved among different species.**

The protein sequence of Arl13b from Zebrafish, rat, mouse and humans is plotted against each other to compare homology (conserved amino acids are high lighted in black). Sequences were aligned using MegAlign.

### 7.2.2. Sco-eGFP localizes to cilia in the pronephric duct

Endogenous Arl13b/ Scorpion localized to the cilia in multiple tissues as shown in the previous chapter and has a very interesting and unique feature: it is almost exclusively localized to the cilium, whereas many other ciliary proteins can be found in other cellular compartments as well.

Polycystin-2 for example, localizes to the ciliary membrane but is also enriched in the ER and sarcoplasmic reticulum (Cai *et al.*, 1999; Qian *et al.*, 2003) and Polycystin-1 also localizes to the ciliary membrane but can be found at cell adhesion junctions (adherens junctions and desmosomes) and focal adhesions (Foggensteiner *et al.*, 2000; Wilson *et al.*, 1999; Peters *et al.*, 1999). IFT particles concentrate in the cilium and are responsible for the transport machinery within the cilium, but localize to the cytoplasm as well where they bind to vesicles and guide the trafficking towards the base of the cilia (Haycraft *et al.*, 2004; Qin *et al.*, 2004).

However, it is not known how Arl13b/ Scorpion gets trafficked to the cilium. In order to identify a domain within the protein that would be necessary and/or sufficient for trafficking the protein to cilia, we generated multiple deletion constructs which would allow us to dissect the role of each protein domain for its potential function as a ciliary targeting signal.

Unlike other small GTPases, Arl13b/ Scorpion consists of 407 amino acids, making it much bigger than other classical small GTPases. An amino-terminal GTPase domain is directly followed by a coiled coil motif, a domain that is known to enable protein-protein interaction. A glutamate rich region is located C-terminal to the coiled coil domain. The remaining C-terminus of Arl13b/ Scorpion is not conserved nor contains any known motifs.

In order to verify that overexpressed Arl13b/ Scorpion would localize to cilia and cause no phenotype, *in vitro* transcribed full length *arl13b/scorpion* mRNA (0.265 pg) was injected into wildtype embryos at the 1-4 cell stage. 6 hours post injection, GFP expression is visible throughout the entire embryo indicating that the protein is ubiquitously expressed. Embryos were fixed at around 30 hpf and fluorescent immuno staining was performed using an antibodies for acetylated  $\alpha$ -tubulin, visualizing cilia. At



that time, overexpressed Scorpion-eGFP is expressed in cilia of the pronephric duct similar to endogenous Arl13b/ Scorpion (Fig. 43). Importantly, the embryos appear phenotypically normal and do not show any body curvature defect or cystic phenotype.

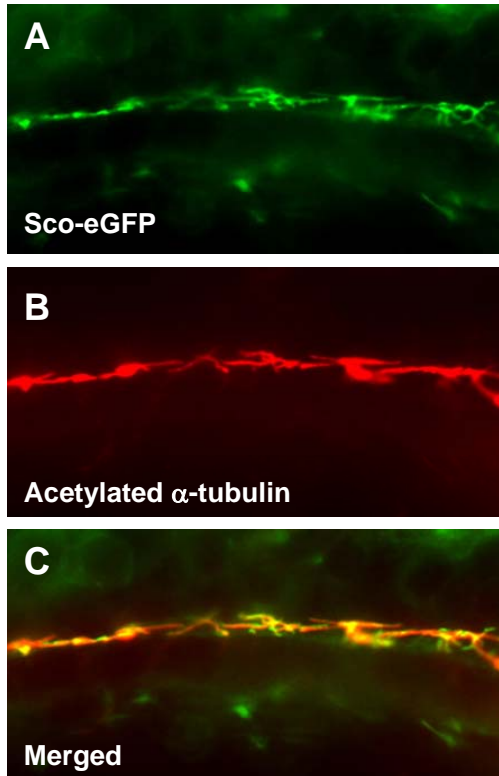


**Fig. 43: Overexpressed Scorpion-eGFP localizes to the pronephric duct cilia.**

(A-C) Wildtype embryos were injected with Scorpion-eGFP mRNA at the 1-4- cell stage and subjected to whole mount immuno staining with an antibody against acetylated  $\alpha$ -tubulin at 1 dpf. Sco-eGFP co-localizes with acetylated  $\alpha$ -tubulin, indicating it localizes to cilia of the pronephric duct.

### 7.2.3. The small GTPase domain of Arl13b/Scorpion is necessary but not sufficient for its cilia localization

Arl13b/ Scorpion contains a small GTPase domain at its N-terminus and belongs to the Ras superfamily of small GTPases. Small GTPases can bind guanosine triphosphate (GTP) and are active in their GTP bound form and inactive when bound to guanosine diphosphate (GDP). GDP can then be replaced by a free GTP, thus this mechanism allows the protein to be switched on and off. Generally, small GTPases are involved in a wide range of cellular processes, including cell differentiation, growth, cytoskeletal dynamics, movement and vesicular transport. The Arf subfamily has been associated with vesicular transport in particular. Arl13b/ Scorpion has a unique sequence which differs from other typical small GTPases. In addition to its N-terminal GTPase domain, it has a long C-terminal region that encodes a coiled-coil motif and has proline-rich as well as glutamate- rich regions and a putative ER-export signal.

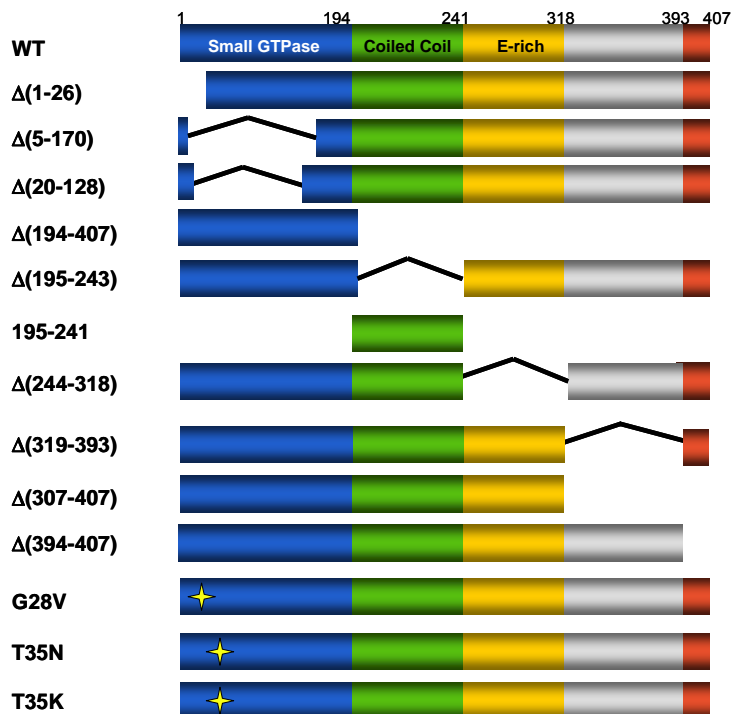
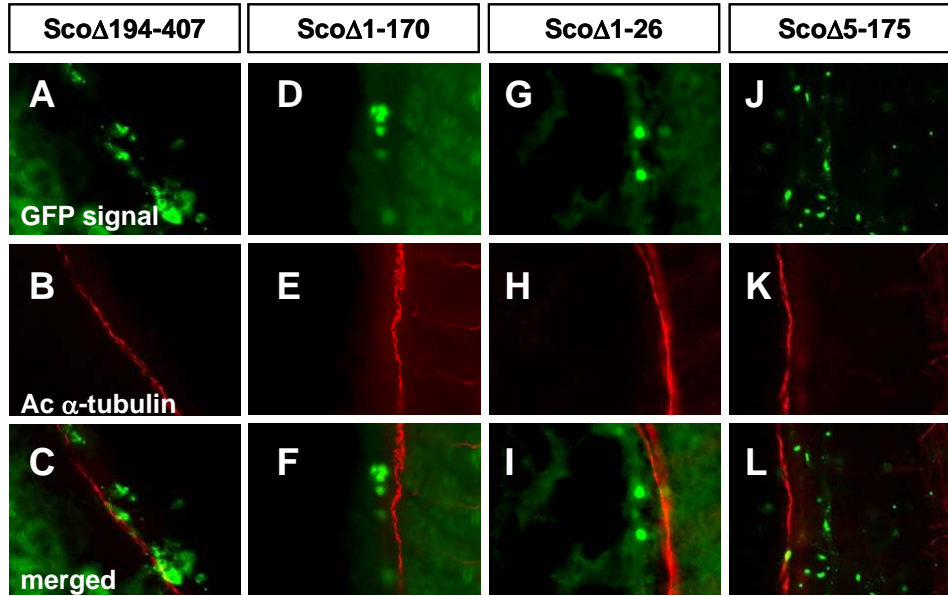


Table 10: Schematic of Arl13b/ Scorpion deletion constructs.

In order to examine the role of the small GTPase domain, we generated deletion constructs that would result in truncated forms of Arl13b/ Scorpion protein fused to eGFP (Table 10). Wanting to know which domains of the protein would be responsible for ciliary trafficking, ciliary fluorescent immuno staining was performed after injecting either of the generated deletion constructs.

Would the small GTPase domain by itself be sufficient to traffic Arl13b/ Scorpion to the cilium? As shown in figure 44, the construct which consisted of the small GTPase domain alone, Sco $\Delta$ (194-407), was not sufficient to traffic to the cilium but showed a cytoplasmic distribution. Deletion of amino acids 1-170 (Sco $\Delta$ (1-170)) which got rid of almost the entire GTPase domain but left the remaining part of the protein intact, resulted in a pattern of 3-7 GFP positive cells clustering at the ventral side of embryo; however, at this moment we do not know why this construct gets trafficked to these particular cells and what the nature of these cells are.

Since neither absence of the small GTPase domain nor the GTPase domain alone was sufficient to traffick to the cilium, smaller parts of the domain were successively deleted, resulting in constructs Sco $\Delta$ (1-26) and Sco $\Delta$ (5-175). Interestingly, all additional constructs failed to localize to the cilium showing that even small deletions in the small GTPase domain result in a loss of ciliary localization and display distinct cytoplasmic patterns. All embryos appeared phenotypically normal. These data suggest that the small Gtpase domain is essential for trafficking of Arl13b/ Sco to the cilium. .



**Fig. 44: The small GTPase domain is necessary but not sufficient for cilia targeting of Arl13b/Scorpion.**

Wildtype embryos were injected with indicated constructs at the 1-4 cell stage. Whole mount fluorescent immuno staining with acetylated  $\alpha$ -tubulin at 1 dpf old embryos is shown.

(A-C) Sco $\Delta$ (194-407) consists of the GTPase domain only whereas the remaining C-terminus of the protein was deleted. The constructs did not localize to the cilia.

(D-F) Deletion of almost the entire GTPase domain failed to localize to the cilium.

(G-L) Various deletions within the GTPase domain but an intact C-terminus disrupted ciliary localization of the Arl13b/ Scorpion protein.

#### **7.2.4. The coiled coil region of Arl13b/ Scorpion is necessary for cilia localization**

Arl13b/ Scorpion contains a predicted coiled coil motif from amino acid (195-241). Coiled coil domains facilitate protein-protein interactions and we sought to determine whether it might play a critical role for cilia targeting. We amplified all regions of *arl13b/scorpion* 5' as well as 3' of the coiled-coil domain and generated our final construct by a two piece PCR resulting in Sco $\Delta$ CC-eGFP (Fig. 45), which lacks the coiled-coil region only. On the other hand a construct that contained only the coiled-coil domain fused to GFP (Sco-CC-eGFP) was generated. After performing fluorescent immuno staining for cilia using the acetylated  $\alpha$ -tubulin antibody, we could not detect a ciliary localization signal from either constructs. Both failed to localize to the cilium but showed different subcellular localization patterns. Sco $\Delta$ CC was absent in the nucleus and was found in the cytoplasm throughout the embryo. Sco-CC on the other hand localized to a subset of cells at the ventral side of the embryo or to muscle cells, which we suspect to be unspecific targeting due to the common presence of coiled coil motifs.

#### **7.2.5. Part of the C-terminus is required for targeting Arl13b/ Scorpion to the cilium**

Since the coiled coil domain and GTPase domain by itself failed to traffick the Arl13b/ Scorpion fusion protein to the cilium, we wanted to examine whether both together, the small GTPase domain and coiled coil domain, would represent a minimal construct of Arl13b/ Scorpion that would allow the protein to traffick to the cilium.

Sco $\Delta$ (308-407) contains the GTPase domain as well as the coiled coil region. However, overexpression of Sco $\Delta$ (308-407) did not result in ciliary localization of Arl13b/ Scorpion fusion protein (Fig. 45). Interestingly, Sco $\Delta$ (308-407) displayed a membranous or cytoplasmic pattern. It might be interesting to analyze whether Sco $\Delta$ (308-407) indeed localizes to the membrane by using cross sections and double staining with membrane markers.

### 7.2.6. GTP binding activity is not necessary for cilia localization of Arl13b/ Scorpion

Within the GTPase domain a stretch of 8 amino acids with the sequence GLDxxGKT is known as P-loop and responsible for GTP binding. Mutations in the P-loop have been implicated in altered binding affinity for the nucleotide, thus changing the activity of the protein. A T31M missense mutation in human *Arl6* is known to cause Bardet-Biedl syndrome 3 (BBS3), a human pleiotropic disorder phenotypically characterized by kidney cysts, polydactyly and other abnormalities (Fan *et al.*, 2004, Chiang *et al.*, 2004). T30N mutation in *Arl2* in mouse has been shown to decrease the binding affinity for GTP hundred-fold resulting in a dominant negative allele. A G to V missense mutation in ras results in a dominant active allele and T35K mutation in zebrafish results in the *vicious* allele of Arl13b, developing kidney cysts and exhibiting a downward body curvature phenotype.

In order to determine whether the enzymatic activity of GTPase domain would have any effect on the localization of the protein, we introduced point mutations into the GTP binding loop of the GTPase domain in Arl13b/ Scorpion, which consists of amino acids (28-35).

We used three different GTP binding loop point mutations for our analysis. Sco G28V (presumptive dominant active allele), ScoT35K (*vicious*) and ScoT35N (presumptive dominant negative allele). As the other constructs before, all were fused to GFP at the C-terminus. Embryos were injected with *in vitro* transcribed mRNA (0.625 pg) at the 1-4 cell stage and analyzed at 1 dpf by immuno staining with the acetylated  $\alpha$ -tubulin antibody. In all three point mutation constructs, a distinct ciliary localization pattern was observed, indicating that the activity of the small GTPase domain did not determine the protein trafficking of Arl13b/ Scorpion (Fig. 45). All embryos appeared phenotypically normal.

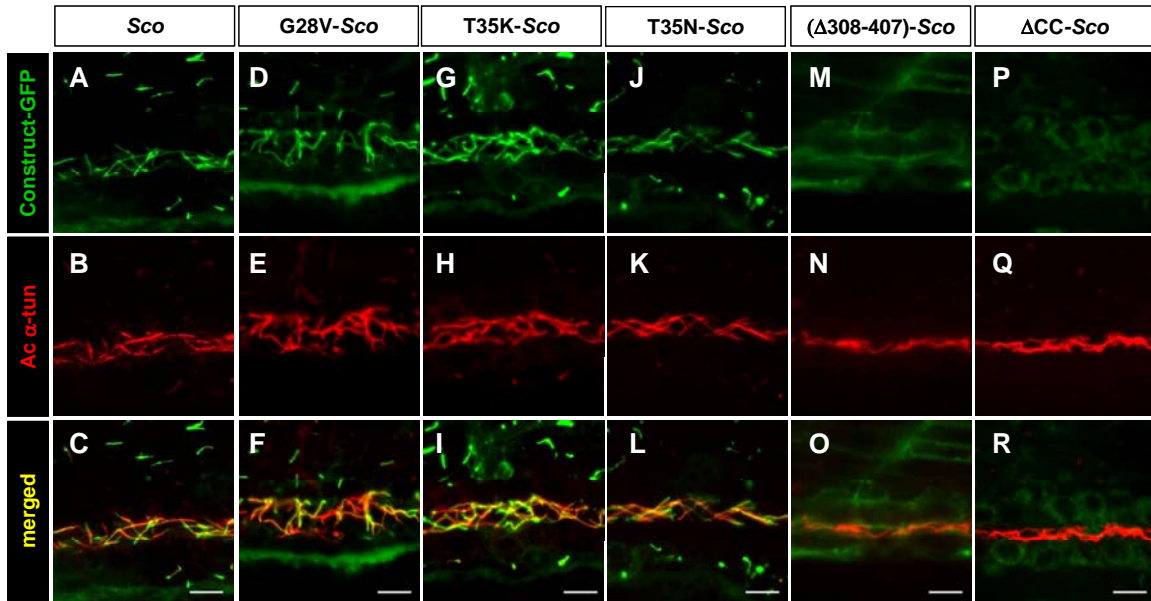


**Fig. 45: The enzymatic activity of the small GTPase domain does not influence cilia targeting whereas the coiled coil domain and C-terminus of Arl13b/ Scorpion are required for ciliary targeting.**

Whole mount fluorescent immuno staining with acetylated  $\alpha$ -tubulin on 1 dpf old embryos injected with indicated Scorpion constructs fused to GFP at the 1-4- cell stage.

(A-C) Full length Scorpion. (D-F) G28V is a presumptive dominant active allele of Arl13b/ Scorpion. (G-I) T35K is the causative mutation in the *vicious* mutant of Arl13b. (J-L) T35N is a presumptive dominant negative allele of Arl13b/ Scorpion. (M-O) Sco $\Delta$ (308-407) lacks part of the C-terminus. (P-R) Sco $\Delta$ CC lacks the coiled coil domain.

Scale bars represent 10  $\mu$ m.

### 7.2.7. Cilia localization of Arl13b/Scorpion is necessary for phenotype rescue

Overexpression of full length Arl13b/ Scorpion is able to rescue the *scorpion*<sup>hi459</sup> mutant phenotype as well as *arl13b/scorpion* morphants. A rescue was scored as a successful prevention of a downward body curvature defect and absence of pronephric cyst formation.

The function of Arl13b/ Scorpion is not known. But studying the other members of the Arl/Arf family might give a first hint. Members of the Arl/Arf family have been shown to be important for microtubule dynamics, lipid metabolism and vesicle trafficking although the exact function of these members are still elusive (Antoshechkin and Han, 2002; Hoyt *et al.*, 1990; Kahn *et al.*, 2006; Li *et al.*, 2004; Radcliffe *et al.*, 2000; Zhou *et al.*, 2006). Our cilia localization data suggests that Arl13b/ Scorpion does not have a single cilia targeting motif but requires the interplay between coiled coil motif, GTPase domain and part of the C-terminus. It is plausible to think that targeting of proteins to the cilia is a coordinated multi step process, in which each motif plays a role in a different part of trafficking to the cilium. We sought to investigate whether Arl13b/ Scorpion contains domains that might be necessary or sufficient for rescuing the mutant phenotype and whether those would directly correlate to its role in cilia localization.

The rescue analysis was performed in collaboration with another student in Zhaoxia Sun's laboratory, Neil Duldulao. We chose some of the same deletion constructs of *arl13b/scorpion* we used in the cilia localization study and injected them into offspring of *scorpion*<sup>hi459</sup> heterozygous crosses. Subsequently the body curvature phenotype was scored at 2 dpf and the presence of kidney cysts analyzed at 4-5 dpf. Since we crossed *scorpion*<sup>hi459</sup> heterozygous fish, a mendelian ratio of 25% of their offspring is expected to present a *scorpion*<sup>hi459</sup> mutant phenotype. A significant lower percentage than 25% in injected embryos would indicate rescue capability of the construct. For each experiment, uninjected siblings served as controls to determine the baseline of the *scorpion*<sup>hi459</sup> mutant phenotype. Table 11 summarizes the results from the rescue experiments.



### **7.2.8. The coiled-coil motif and GTPase domain are necessary for the rescue capabilities of Arl13b/ Scorpion**

Using the deletion constructs we used for the cilia localization study, we sought to answer the question whether the GTPase and coiled-coil domain respectively might be important for the function of Arl13b/ Scorpion using its rescue ability as a read out. Overexpression of full length Scorpion–eGFP rescued the body curvature and cystic kidney phenotype in almost all offspring of a *scorpion*<sup>hi459</sup> heterozygous cross with only 1% of offspring displaying a mutant phenotype compared to 23% of uninjected embryos. However, ScoΔ(1-26), ScoΔCC and ScoΔ(194-407) failed to rescue the mutant offspring indicating that the coiled coil domain being a protein-protein interaction domain as well as the the GTPase domain are essential for the function of Arl13b/ Scorpion during embryogenesis. ScoΔ(1-26) showed 27.6 % of mutant offspring, ScoΔ(194-407) showed 22.2 % mutant offspring and ScoΔCC had 23.8 % mutant offspring (Table 11).

### **7.2.9. Change of GTP binding activity of small GTPase domain inhibits its rescue ability**

During our cilia localization analysis all point mutations introduced in the P-loop of the GTPase domain resulted in a proper cilia localization of the fusion protein. Since point mutations in the nucleotide binding loop are known to be involved in changes of the activity state of the protein, we asked whether scoG28V , scoT25N and T35K would be still functional and able to rescue the mutant phenotype in offspring of a *scorpion*<sup>hi459</sup> heterozygous cross or if the change of enzymatic activity would lead to dysfunctional protein. Indeed, injection of the aforementioned constructs failed completely to rescue the *scorpion*<sup>hi459</sup> mutant phenotype in offspring: ScoG28V (25.1%), scoT35N (23.8%), scoT35K (24.0%). This indicated to us that the GTPase activity does play a functional role during embryogenesis but is dispensable for protein transport. We verified that the proteins were expressed by detecting fluorescence. The results are summarized in table 11. This again suggested a dual role for Arl13b/ Scorpion during pronephros development.

### 7.2.10. C-terminus of Arl13b/ Scorpion is not necessary for rescue ability

The region C-terminal to the coiled coil motif in Arl13b/ Scorpion is unique as it does not contain any conserved domains or known motifs. Nevertheless, a region enriched for glutamate and a putative ER export signal are localized in this region. We injected Sco $\Delta$ (308-407), Sco $\Delta$ (319-393) and Sco $\Delta$ (394-407) into offspring of a *scorpion*<sup>hi459</sup> heterozygous cross and examined the offspring as before. Interestingly, all these deletion constructs were able to rescue the *scorpion*<sup>hi459</sup> mutant phenotype with Sco $\Delta$ (308-407) resulting in 3.6 % mutants, Sco $\Delta$ (319-393) resulting in 2.9% mutants and no mutant phenotype detected in the Sco $\Delta$ (394-407) fish (table 11). This result was unexpected since Sco $\Delta$ (308-407) and Sco $\Delta$ (319-393) were not localized to the cilium in wildtype embryos thus were against our hypothesis that ciliary localization is required for rescue ability. To analyze this phenomenon further, a titration analysis was performed by Neil Duldulao. Progressively smaller amounts of either *arl13b/scorpion* full length mRNA or Sco $\Delta$ (308-407) mRNA were injected into offspring of a *scorpion*<sup>hi459</sup> heterozygous cross and the rescue ability scored. Interestingly, Neil found that 0.885 pg of full length Arl13b/ Scorpion were able to rescue the *scorpion*<sup>hi459</sup> mutant phenotype, whereas 88.5 pg of Sco $\Delta$ (308-407) were required to rescue the *scorpion*<sup>hi459</sup> mutant phenotype to the same extent, suggesting that full length Arl13b/ Scorpion has at least a 100-fold higher rescue activity compared to Sco $\Delta$ (308-407) and the previously observed rescue phenotype could possibly represent an overexpression artefact. To rule out that the Sco $\Delta$ (308-407) protein was degraded and therefore would result in a false negative result, Neil also performed a Western Blot at 1 dpf old embryos of embryos injected with either full length Arl13b/ Scorpion or Sco $\Delta$ (308-407) and both showed similar expression levels.

Allele	injected		*	uninjected	
	sco PH [%]	n		sco PH [%]	n
<b>Full length</b>	1.2	321	*	23.2	299
<b>GTPase</b>	22.2	221		22.3	386
<b>Δ(21-127)</b>	23.6	161		26.3	194
<b>G28V</b>	25.1	344		21.2	364
<b>T35N</b>	23.8	381		24.2	260
<b>T35K</b>	24.0	290		20.8	149
<b>ΔCC</b>	23.8	223		21.9	269
<b>Δ(244-318)</b>	2.3	261	*	24.1	286
<b>Δ(308-407)</b>	3.6	244	*	24.3	140
<b>Δ(394-407)</b>	0	76	*	23.2	112
<b>Δ(319-393)</b>	2.9	140	*	22.3	220

**Table 11: Summary of rescue experiments performed on offspring of *scorpion*<sup>hi459</sup> heterozygous crosses.**

The percentage of offspring embryos displaying a body curvature and cystic phenotype after injection of indicated *arl13b/scorpion* alleles is scored. Body curvature was scored at 2 dpf and cyst formation at 4-5 dpf.

The intact GTPase domain alone was not sufficient to rescue the mutant phenotype. However, changing of the GTP binding activity by introducing point mutations into the P-loop as well as deletion of the coiled coil motif lead to abolished rescue ability

Alleles marked with asterix show statistically significant rescue properties (p-value < 0.001) measured with  $\chi^2$  test.

n: number of embryos analyzed, sco PH: *scorpion*<sup>hi459</sup> mutant phenotype

This analysis was performed together with Neil Duldulao.

### 7.2.11. Identification of putative interacting partners for Arl13b/Scorpion

Since nothing is known about Arl13b/Scorpion's role and function during embryogenesis, we sought to perform a yeast-two hybrid assay in order to find interacting proteins that would allow us to elucidate its role and place it into a known pathway.

The yeast-two-hybrid assay is a powerful technique that is used to detect protein – protein interactions using the GAL4-transcriptional activator in yeast *Saccharomyces cerevisiae*. Most transcription factors consist of two physically discrete modular domains: one being a DNA-binding domain (DNA-BD) and the other one an activation domain (AD) (Fig. 46).



**Fig. 46: Schematic diagram of explaining the principle of the yeast two hybrid.**

The bait protein (Arl13b/ Sco) is fused to the GAL4-UAS DNA binding domain (DNA-BD). All cDNA of interest or a library are fused to the activation domain (AD). Only when DNA-BD and AD come into close proximity due to protein interaction transcription is activated and downstream reporter genes are transcribed.

The DNA-BD can bind to a specific promoter sequence and AD directs the RNA polymerase II complex to transcribe the downstream target genes. DNA-BD and AD act as independent modules. Neither of them can activate transcription on their own but they stay fully functional when fused to other proteins. These properties are utilized in the yeast-two-hybrid assay. The bait protein, in our case Arl13b/Scorpion, is expressed as a fusion protein to DNA-BD. A cDNA library is expressed as a fusion to the AD. Only when both, Arl13b/Scorpion and a protein interactor from the cDNA library come into close proximity, transcription of reporter genes will be activated. Yeast used in the assay are auxotroph for several amino acids and nucleotides, such as adenine, histidine, tryptophane and leucine. When they are grown on media that lacks those nutrients, the

yeast will fail to survive and die. The plasmids that contain Arl13b/ Scorpion also encode for tryptophan. The cDNA library plasmids encode for leucine, meaning that only yeast cells that have incorporated both, bait and prey during the transformation process, will survive on media lacking tryptophan and leucine (SD, -Leu, -Trp). Additionally, only yeast cells that contain bait and prey proteins which are interacting thus being in close proximity to each other will be able to successfully transcribe the downstream reporter genes (Ade, His) and allow growth on quadruple drop out media (SD, Leu, -Trp, -Ade, -His).

### **7.2.12. Transformation of both, embryonic human kidney cDNA library as well as adult zebrafish library, is highly efficient**

An outline of the yeast two hybrid assay is schematically depicted in Fig 46 and 47. The first step before starting the assay itself was to clone the *arl13b/scorpion* cDNA into the bait vector (pGBKT7) and to test whether this fusion construct (Sco-BD) would have any autoactivation characteristics. Some proteins are able to auto-activate the reporter genes, making them useless for screening purposes. Furthermore, histidine reporter genes have been reported to be 'leaky', being expressed even without proper activation. 3-AT is widely used to counteract the leakiness of the His reporter. In higher doses, 3-AT is toxic to cells and must be titrated for each construct. It was previously verified by another student in the lab that *arl13b/scorpion* was not able to autoactivate any of the reporter genes when fused to the DNA binding domain.

A highly efficient transformation of the library is important for the success of the whole screen. In order to optimize the transformation protocol, a small scale library transformation into the Sco-BD containing yeast was performed and plated in different titrations onto SD, -Leu, -Trp drop out media. This will allow the exact measurement of the transformation efficiency. The efficiency is measured in colony forming units (cfu) per  $\mu\text{g}$  of library cDNA used. A high transformation efficiency is crucial because screening through two individual libraries covering each more than 3-fold, with each library containing an estimated  $3.5 \times 10^6$  individual cDNAs would not be possible with a low transformation efficiency.

Previously in the lab the established transformation efficiency was in the order of 100 cfu/  $\mu\text{g}$  cDNA. This would make it almost impossible to perform a successful screen.

Trying to trouble shoot the protocol systematically, I was able to increase the efficiency significantly during the process. Finally, a transformation efficiency of  $5 \times 10^6 - 10^7$  cfu/ug cDNA could be obtained routinely.

After a successful transformation procedure was established, we repeated the same experiment on a large scale. The transformants were plated onto SD, -Leu, -Trp, -His drop out plates and grown for one week. Since we were putting strong positive selection onto the yeast transformants, we expected most of the colonies that formed to code for interacting proteins for Arl13b/ Scorpion. Afterwards, colonies were restreaked onto fresh onto SD, -Leu, -Trp, -His dropout plates. These colonies then were subjected to a X-Gal filter lift assay. One of the reporter genes was lacZ, a reporter gene that encoded for  $\beta$ -galactosidase.  $\beta$ -galactosidase produces a blue coloration through metabolism of X-gal (5-bromo-4-chloro-3-indoyl- $\beta$ -D-galactoside). Known interacting proteins of varying strength, e.g. DNA-BD-p53 in conjunction with AD-SV40 large T-antigen, DNA-BD-Fos with AD-Jun as well as DNA-BD-Rb with AD-E2F, were used as controls to verify the colorimetric reaction had taken place properly. Also, strong interacting proteins showed a color reaction within 30 minutes, whereas weak ones needed several hours to overnight. Following the filter lift assay, the prey plasmid was isolated using zymoprep, retransformed into *E.coli* since the yield from a yeast plasmid preparation is generally very low. The plasmid was isolated from *E.coli* and sequenced to identify the library protein. Lastly, Sco-BD together with our identified putative interacting partner-AD was co-transformed into empty yeast cells or alternatively, an empty BD plasmid was transformed along with the interacting AD-plasmid. Putting positive selection onto those transformants again, we expected only the first case to grow whereas the second group served as a negative control.

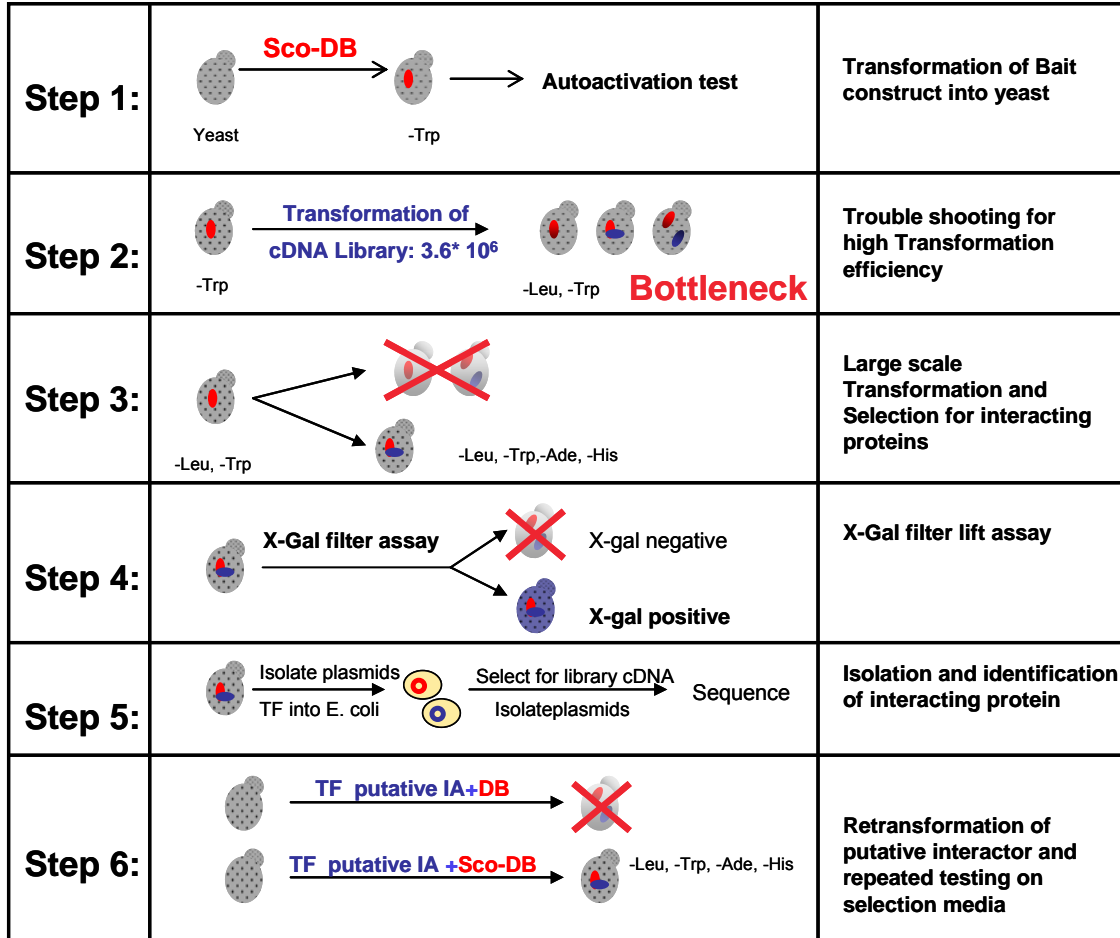


Fig. 47: Diagram of the yeast-two-hybrid assay from testing the bait construct to analyzing the positive clones.

### 7.2.13. Putative Arl13b/ Scorpion interacting proteins isolated from the human embryonic kidney library

Searching for an interacting partner for Arl13b/Scorpion we used two different cDNA libraries. One of them was a human embryonic kidney cDNA library (gestational week 21-30). The advantage using this library was that it was kidney specific and generated during embryogenesis. Putative interacting proteins included following proteins:

ID	Function
<b>Ubc9</b>	Sumoylation enzyme
<b>Emx1</b>	Transcription factor that is expressed early in the pronephric primordium
<b>HoxA7</b>	Transcription factor
<b>TCTP</b>	Translationally controlled tumor protein, activates Rheb, involved in mTOR pathway
<b>Phosphatase PP2</b>	Regulator of the wnt/-catenin signaling pathway, it localizes to centromeres and regulates mitotic spindle outgrowth
<b>Pax8</b>	Expressed in kidney and involved in metanephros differentiation and branching, homologous to Pax2 which is involved in ADPKD and nephronophthisis
<b>Nck2</b>	Adaptor molecule for SH2 that couples receptor tyrosine phosphorylation to downstream effector molecule

**Table 12: List of putative protein interactors of Arl13b/ Scorpion using the human embryonic kidney library.**

The yeast containing the potential interactors grew on selection plates (SD,-Leu, -Trp,-Ade, -His) and turned blue with the X-gal filter assay. Since this library is a kidney specific library, every putative interactor appeared to be plausible and interesting at the first glance, especially TCTP (translationally controlled tumor protein) and Pax8.

Translationally controlled tumor protein (TCTP) is a highly conserved protein upregulated in various tumor and an important player in the TOR (target of rapamycin, mTOR in mammals) signaling pathway.

mTOR coordinates cell metabolism, cell growth, cell-cycle progression and cell proliferation by sensing nutrients such as amino acids, and growth factors. Under normal circumstances, the PI3K/Akt pathway leads to phosphorylation and inactivation of the



TSC1/TSC2 complex which in turn leads to activation of mTOR via Rheb. Rheb is a ras related small GTPase and leads to activation of mTOR and subsequently activates S6K and inactivates eIF4E, resulting in cell proliferation.

Recently, defects in the mTOR pathway have been linked to cystic kidney diseases and studies with rapamycin support this hypothesis. Rapamycin is derived from the soil bacterium *Streptomyces hygroscopicus* and specifically inhibits TOR, resulting in reduced cell growth, reduced cell-cycle progression, and decreased cellular proliferation. Rapamycin treatment in patients decreased the severity of PKD and removed cysts and renal tumors in animal models as well as patients with TSC (tuberous sclerosis). Furthermore, the cytoplasmic tail of cleaved polycystin-1 was found to colocalize with mTOR. Taken together, a potential interaction of Arl13b/ Scorpion with TCTP seemed very promising.

Pax8 is a transcription factor expressed early during kidney development in the intermediate mesoderm and highly homologous to Pax2. Pax2 has been shown to be involved in ADPKD and Nephronophthisis providing an indirect link to a cystic kidney phenotype.

When we sought out confirm all putative protein interactors by retransformation into empty yeast cells, all constructs failed to prove to be real. Co-transformation of the putative interactors together with Sco-BD resulted in a strong regrowth, however, co-transformation with an empty BD-bait vector gave rise to colonies as well, indicating that putative interactors were able to auto-activate the reporter genes in the absence of Scorpion-BD, rendering them false positive. Since we had covered the library 2.7 fold, we decided to concentrate on the zebrafish cDNA library.

#### **7.2.14. Putative interacting proteins of Arl13b/Scorpion from adult zebrafish cDNA**

The second cDNA library we used for our screen was an adult zebrafish cDNA library which was generated from the entire embryo. Table 13 summarizes the preliminary data for the zebrafish screen. From initially 29 colonies, only the ones shown were able to regrow on selection plates (SD,-Leu,-Trp, -Ade, -His). However the ability to grow was not stable, which might indicate a weak interaction.

ID	Function
XP_684919.3	Intracellular region of protein with a galectin domain, which is implicated in cell migration, adhesion and spreading
NDP kinase	Kinase that was found exclusively in flagella of <i>Chlamydomonas</i> , unknown function
FGF receptor	Intracellular part of FGF receptor, signaling pathway
NM_001044319.1	Unknown protein; transcripts found in skin and kidney

**Table 13: List of putative interactors of the yeast two hybrid screen using the zebrafish adult cDNA library.**

XP\_684919.3 is a hypothetical protein that contains a Galactose binding lectin domain which has been implicated in cell migration, adhesion and spreading.

Nucleoside diphosphate kinases (NDP kinases) are responsible for the synthesis of nucleoside triphosphates (NTPs) via terminal phosphotransfer from a NTP such as GTP to any NDP. They are evolutionarily highly conserved and involved in numerous regulatory processes associated with proliferation, development, and differentiation. The NDP kinase has been reported to be expressed on the ciliary shaft in a punctate pattern in cell culture, *Chlamydomonas* and *Xenopus* kidney cells, suggesting that NDP kinases are a conserved and universal component of the cilium. Furthermore it has been suggested that NDP kinases are important for the maintenance and elongation of the cilium providing GTP essential for the ciliary microtubule turnover.

The fibroblast growth factor (FGF) signaling pathway has been known to mediate multiple processes during embryogenesis. Furthermore, bFGF was shown to be enriched in the urine of patients with ARPKD and overexpression resulted in cystogenesis in rodent kidneys. Recently, one study showed that FGF signaling regulates cilia length during embryogenesis, which might suggest that developmental defects and diseases associated with FGF signaling might be due in part to a loss of ciliary function.

The top three zebrafish results (Galectin containing protein, NDPkinase, FGF receptor) failed to metabolize X-Gal, indicating that they did not transcribe the LacZ reporter gene or did not do it at a sufficiently high rate, which would indicate a very weak interaction if

that. Since the last protein (NM\_001044319.1) represents an unknown protein with unknown function and no conserved domains, we initially did not proceed with further follow-up experiments. Interestingly though, the cDNA of that unknown protein was found to be expressed in skin and kidney and might be worth pursuing.

### 7.3. DISCUSSION

Cilia can be found on many different cell types and many different organisms, ranging from *Chlamydomonas* to humans. In recent years it has become more and more clear, that these once 'vestigial' organelles that were thought not to play any physiological role perform important roles in signal transduction and act as mechanosensory organelles (Nauli *et al.*, 2003). Cilia are involved in establishing proper left/right patterning, Ca<sup>2+</sup>-homeostasis and interpreting intercellular signals such as Hedgehog (Hh), Wnt and platelet-derived growth factor (PDGF) signaling pathways (Ross *et al.*, 2005; Schneider *et al.*, 2005; Eggenschwiler *et al.*, 2007; Tabin, 2006; Yoder, 2007; Corbit *et al.*, 2008). Mutations in genes encoding ciliary proteins and affecting cilia formation or function, have been implicated in multiple human diseases resulting in kidney cysts, retinal degeneration, polydactyly, obesity, left/right patterning defects, liver cysts and neural tube closure defects. Even though these diseases present different phenotypes and have mutations in different genes, they are grouped together as so called 'ciliopathies' to emphasize the common underlying ciliary defect. The pleiotropic nature reflects the diverse role cilia can play in mechanosensation and signal transduction. Since defects in cilia formation or function are the cause of many human diseases such as PKD, the understanding of the mechanisms involved in targeting proteins to the cilium as well as the transport of proteins localized in the cilium will provide important insights into the pathology of the diseases.

Joubert syndrome is a human 'ciliopathic' disease which affects mainly the nervous system. Recently *ARL13B* has been found to be mutated in patients with JS (Cantagrel *et al.*, 2008). The mutations in *Arl13b* in mouse, *hennin*, also develop multiple defects in the nervous system (Caspary *et al.*, 2007). *scorpion*<sup>hi459</sup> mutants are characterized by a body curvature defect and kidney cysts. The protein is localized to the cilium exclusively and so far the role and binding partners for Arl13b/ Scorpion are completely unknown.

Arl13b/ Scorpion belongs to the Ras superfamily of small GTPases, and its C-terminus shows a high homology to other members of the Arl family. Small GTPases contribute to numerous cellular and physiological processes with Arl family members being implicated specifically in vesicle trafficking and membrane targeting of proteins. The common

feature of small GTPases is the enzymatic activity to hydrolyze GTP to GDP and an inorganic phosphate (Takai *et al.*, 2001) and they oscillate between a GTP-bound and GDP-bound conformation. The GTP bound form is considered 'active' while the GDP bound form is 'inactive' (Stenmark, 2001). The so called P-loop within the GTPase domain is responsible for binding GTP and hydrolyzing it thus missense mutations in the P-loop result in aberrant activity of the GTPase, e.g. point mutations in the P-loop changing threonine to asparagine (T35N) abolishes GTP binding ability and rendering it inactive.

Epithelial cells are highly polarized and show a distinct apical and basolateral membrane that differs in lipid and protein composition. The polarized protein transport to the apical or basolateral membrane respectively has to be highly regulated. The transport of proteins is regulated at the trans-golgi network (TGN) and recycling endosomes via incorporation into vesicular intermediates. The polarized transport is mediated by microtubule and actin networks, the exocyst complex and Rab GTPases, which are localized to vesicular structures (Rodriguez-Boulant, 2005). A recent study in zebrafish provided the first link between the Rab GTPase Rab8 and a protein of the IFT machinery, IFT20. Rab8 can bind to Rabaptin5 which in turn binds to a protein called Elipsa. Furthermore Elipsa and IFT20 can interact, providing a bridge from Rab8 to IFT20 (Omori *et al.*, 2008). Interestingly, Elipsa localizes to the cilia in zebrafish embryos and *elipsa* mutants exhibit a downward body curvature defect and kidney cysts, making it very similar to the *scorpion*<sup>hi459</sup> mutant phenotype.

Rab8A localizes to cilia in cell culture. In addition, Rab8A, Rab17 and Rab23 are thought to play important roles for ciliogenesis in retinal pigmented epithelial cells (Moritz *et al.*, 2001; Nachury *et al.*, 2007; Yoshimura *et al.*, 2008). Guanosyl exchange factors (GEF) mediate the exchange from the GDP bound to the GTP bound state. Interestingly, Rabin8, which is the GEF for Rab8A, has been shown to interact with BBS4 (Bardet-Biedl Syndrome 4), which is localized to basal bodies and loss of Rabin8 lead to mistargeting of BBS4 (Nachury *et al.*, 2007).

Another study found Rab8A to be involved in trafficking basolateral cargo in polarized epithelia (Huber *et al.*, 1993; Ang *et al.*, 2003). Taken together, Rab8 seems to be involved in many processes that when disrupted result in similar phenotypes as seen in

*scorpion*<sup>hi459</sup> mutants. It will be very interesting to analyze a possible interaction between Rab8 and Arl13b/Scorpion in the future.

Arl GTPases belong to the Ras superfamily of G-proteins and have been shown to be involved in signal transduction events, secretion, endocytosis, vesicle trafficking and phagocytosis. Recently, two Arl GTPases (Arl6 and Arl13B), have been shown to be involved in human ciliopathies. *arl6* is mutated in BBS3, one of several genes known to be involved in Bardet-Biedl syndrome (Chiang *et al.*, 2004). Bardet-Biedl syndrome (BBS) is a genetically heterogeneous, pleiotropic disorder characterized by kidney cysts and multiple extra renal malformations including obesity, mental retardation and blindness (Mykityn and Sheffield, 2004). In mouse the null mutant of *Arl13b*, *hennin*, exhibited shorter cilia and abnormal hedgehog signaling (Caspary *et al.*, 2007). Mutations in *ARL13B* have been found in patients with the classical form of Joubert syndrome (Cantagrel *et al.*, 2008). However, it is not known how Arl proteins function to form or maintain cilia.

Arl13b/ Scorpion has an amino-terminal GTPase domain, followed by a coiled-coil region and a glutamate-rich region. The C-terminus of the protein is not conserved and only has a putative ER export signal. In the present study we sought to analyze the functional role of Arl13b/Scorpion. Post-translational modifications, such as myristoylation and phosphosphorylation, have been implicated in trafficking proteins to the cilium. In addition, at least in ciliary 7-transmembrane receptors, a hydrophobic and basic amino acid residue immediately carboxyterminal after the seventh transmembrane segment (Corbit *et al.*, 2005) was necessary for targeting the receptor to the cilium. Polycystin-2 (PC-2), one of the two genes that give rise to ADPKD when mutated, contains a R<sub>6</sub>VxP motif which was necessary and sufficient for targeting PC-2 to the cilium in cell culture (Geng *et al.*, 2006). The R<sub>6</sub>VxP ciliary targeting motif of PC-2 is not present in Arl13b/Scorpion. We utilized deletion constructs of Arl13b/ Scorpion which were fused at the C-terminus to eGFP to analyze whether we could identify a minimal motif that would be necessary and/or sufficient for cilia targeting. Furthermore, using full length Arl13b/ Scorpion with altered the GTPase activity of the protein by introducing point mutation into the P-loop in order to investigate whether the enzymatic activity plays an important role in cilia trafficking.

Our results showed that the GTPase domain, coiled coil domain and a C-terminal region are necessary but not sufficient for ciliary targeting. Another recent study in cell culture showed that the GTPase domain alone or the remaining C-terminus of Arl13b, respectively, failed to localize to the cilium by themselves (Hori *et al.*, 2008), supporting our results.

Many small GTPases form and act as homodimers or multimers (Zhang and Zheng, 1998; Daitoku *et al.*, 2001; Wittmann and Rudolph, 2004). Full length Arl13b/ Scorpion was shown to homodimerize via its GTPase domain *in vitro* and act as a dominant negative (DN) allele which caused a ciliogenesis defect when overexpressed (Hori *et al.*, 2008). It might be speculated, that the dominant negative (DN) effect is due to the GTPase domain sequestering the endogenous Arl13b/Scorpion protein and preventing it to shuttle and function properly. When we used our deletion construct which consisted of the GTPase domain only, we did not observe a DN phenotype. All injected embryos appeared phenotypically wildtyp and formed normal looking cilia. There are several possible explanations for this. The DN effect reported in cell culture is an artefact which does not recapitulates the events occurring *in vivo*. However, it is more likely that the reported DN effect is due to a high level of overexpression used in cell culture. In our *in vivo* experiments, we injected 0.625 pg of mRNA into the each embryo, which is a moderate amount. When a much higher amount was injected, we could observe signs of a possible DN phenotype, with embryos displaying a downward body axis and also shorter body axis. In those embryos preliminary results indicate that endogenous Arl13b/ Scorpion protein was mislocalized to the membrane and to clusters of the overexpressed construct, suggesting that indeed the truncated form of Arl13b/ Scorpion might be able to bind and sequester endogenous Arl13b/ Scorpion from its normal localization in the cilium which in turn could lead to a curved and shorter body phenotype. A shorter and wider body axis could also be observed with high concentrations of arl13b/ scorpion morpholino oligos for knocking down arl13b/ scorpion transcripts (data not shown). This further suggests that a total knockdown of Arl13b/ Scorpion during embryogenesis might indeed have an effect on the body axis length which is one of the phenotypes associated with the non canonical wnt (PCP) pathway. However, these results are only very preliminary and should be taken with caution since morpholinos are known to have unspecific off-target effects resulting in overall necrotic

and unhealthy embryos when used at high concentration. A controlled titration study using control morpholinos with the same concentration as well as a successful rescue of the additional phenotypes might allow clean and reliable answer of that question in the future.

As was shown in other model organisms, post translational modifications such as myristoylation and phosphorylation can act as a signal for shuttling the protein from the cytoplasm to the ciliary compartment. It is not known whether Arl13b/ Scorpion is subject to post translational modifications that enable the protein to traffick to the cilium. This is a not well studied area and would be interesting to pursue in the future. Furthermore, deletion of the coiled-coil region resulted in loss of cilia localization. This is not surprising since the coiled coil motif represents a protein-protein interaction interface. Arl13b/Scorpion might be required to act in a complex with other proteins or homodimer to be able to traffic to the cilium. Deletion of such a big region in the midst of the protein might lead to defective protein folding which often has detrimental effects on protein function. To analyze the functional properties of Arl13b/ Scorpion we used a rescue analysis which was performed together with with Neil Duldulao.

We analyzed the correlation between the cilia localization and the functional property, using the ability to rescue the mutant phenotype as a read out. Our results showed that the ability of Arl13b/ Scorpion to shuttle to the cilium was tightly linked to its capability to rescue the *scorpion*<sup>hi459</sup> mutant phenotype.

We showed that the activity of the GTPase domain did not influence the ciliary trafficking of Arl13b/Scorpion but that the presence of the small GTPase domain itself was sufficient. However, all point mutations in the GTPase domain result in either presumably dominant active or negative alleles, which fail to rescue the mutant phenotype. This is very exciting since it separates the trafficking of the protein from its functional properties. In *C. elegans*, a putative ortholog of Arl13b (Y37E3.5/ARL-13) has been shown to localize to cilia of sensory neurons (Blacque *et al.*, 2005) but lacks the G4 consensus motif required for binding GTP, indicating that the *C. elegans* form of Arl13b/ Scorpion might be a nucleotide free from that is still able to localize to the cilium. This supports our finding that a disrupted P-loop in *scorpion*<sup>hi459</sup> (resulting in a nucleotide free form or a GTP-locked form) does not disrupt targeting of Arl13b/Scorpion to the



cilium suggesting that the GTPase activity is not critically required for proper protein localization. Taken together, our data suggest that the enzymatic activity has to be highly regulated for the protein to be functional *in vivo* and rescue the *scorpion*<sup>hi459</sup> mutant phenotype but does not play a role during trafficking of Arl13b/ Sco.

It might be possible that Arl13b/ Scorpion has two distinct roles: targeting of proteins to specialized cellular compartments and acting as a potential signal transducer. Arl13b/ Scorpion, similarly to Rab8, might be responsible for targeting proteins to basolateral membrane based on our finding that basolateral proteins appear less organized in *scorpion*<sup>hi459</sup> mutant embryos, but apical proteins are properly targeted and confined to the apical membrane (shown in chapter 2). Interestingly, overexpression of either constructs does not result in an obvious phenotype, suggesting that the role of Arl13b/Scorpion might be permissive.

Another zebrafish mutant called *fleer* exhibits kidney cysts, randomized left-right asymmetry, hydrocephalus and ultrastructural defects in the axonemal microtubules (characterized by a B-tubule closure defect). The same microtubule closure defect was also reported in *hennin* mouse mutants and is thought to be caused by a defect in post-translational modification, e.g. polyglutamylation and polyglycosylation. Polyglutamylation and polyglycosylation of glutamate residues occur in an evolutionary conserved C-terminal motif in both  $\alpha$ - and  $\beta$ -tubulin (Gagnon *et al.*, 1996; Kann *et al.*, 2003; Vent *et al.*, 2005) and is thought to promote binding of microtubule-associated proteins to microtubules and to foster interaction with basic residues of the Kinesin motor. This will result in efficient microtubule based transport of Kinesin and Dynein-linked cargo (Okawa and Hirokawa, 2000; Thorn *et al.*, 2000; Westermann and Weber, 2003).

Arl13b/ Scorpion shows a region of high glutamate content in the C-terminal region with unknown function. Testing whether deletion of this region would have a detrimental effect on cilia localization and/or rescue, we found that *arl13b/ scorpion* alleles missing the glutamate rich region were still able to localize properly to the cilia and to rescue the mutant phenotype suggesting that this region does not play an important role for either trafficking or function and that polyglutamylation is not crucial in Arl13b/Scorpion or does not occur within that region.

The cilium has been emerged in recent years as an important signaling center. One of the first discoveries that presented cilia as a sensory organell was the finding that cilia lining the epithelium of renal tubules control kidney tissue homeostasis by acting as mechanosensors which monitor fluid flow and composition in the nephron (Praetorius *et al.*, 2001). Upon fluid flow cilia bend which caused an increase of intracellular levels of calcium, which in turn activated release of additional calcium stores from the ER. And inhibiting that sensory function by defects in either cilia formation or cilia function was shown to lead to PKD. Beside polycystin mediated signaling, other signaling pathways have been shown to involve the cilium, such as hedgehog (Hh), Wnt, FGF and Platelet-derived growth factor receptor alpha (PDGFR $\alpha$ ) which function during embryogenesis and in tissue homeostasis. It is possible that Arl13b/ Scorpion plays a role in one of those pathways and that the activity status of the protein plays an important role for its signaling properties. Interestingly, *hennin* shows a defective Hh signaling with spina bifida, polydactyly and laterality defects. Furthermore, IFT genes are essential for cilia formation as well as activation of Hh signaling pathway via Gli transcription factors in mouse. However, unpublished data from another laboratory indicate that disruption of IFT genes have no effect on expression of Hh target genes in the neural tube, forebrain, pectoral fin, somite formation or neuron patterning in zebrafish, indicating that the Hh possibly be a recent adaptation to the teleost lineage.

Our data support the model that Arl13b/Scorpion functions mainly through the cilium and further support JS and JSRD being ciliopathies. In order to study the pathway and interactions of Arl13b/Scorpion, it is important to identify protein interaction partners. We sought to find protein interaction partners using a yeast-two-hybrid screen in *Saccharomyces cerevisiae*. The yeast-two-hybrid screen utilizes the Gal4 transcription factor, which consists of two physically discrete modular domains: a DNA binding domain (BD) and a transcription activation domain (AD).

The BD domain was fused to Arl13b/Scorpion and the AD domain was cloned into a cDNA library. Only when both domains would be in close proximity to eachother they would be able to activate transcription of reporter genes, allowing the yeast cells to grow on minimal media and perform enzymatic colorimetric reactions. After performing the yeast-two-hybrid assay with two cDNA libraries, a human embryonic kidney library and an adult zebrafish cDNA library, we found several promising putative protein interactors.

Even though the yeast two hybrid assay is a powerful tool to find novel protein interactors it has a big downside being the rate of false positive or false negative results due to the nature of the experiment. A study estimated the rate of the false positive results to be as high as 50% (Deane *et al.*, 2002). There are many possible reasons for this high number: the assay investigates fusion-protein interactions which are overexpressed in yeast nuclei. Overexpression might lead to unspecific interactions. Also, proteins might be not folded correctly or lack/show post-translational modification in yeast. Furthermore, some interactions might be true in an overexpressed state in yeast, yet in the regular host organism the two proteins might never be expressed at the same time and/or in the same cell. Therefore results of the yeast two hybrid are not solid by itself and always requires further validation by other experiments. Our putative protein interactors from the human embryonic kidney cDNA library turned out to be false positive being able to bind to the DNA-BD without interacting with the Arl13b/ Scorpion protein thus auto-activating downstream reporter genes. Therefore we used another library from zebrafish, which was generated from adult (1 month old) whole fish. The advantage of this library is, that it was generated from the same organism as our protein of interest. But it also had a major disadvantage. The kidney develops during early embryogenesis and Arl13b/ Scorpion plays a crucial role during embryogenesis in laterality formation and kidney morphogenesis. It is possible that in the adult stage, Arl13b/ Scorpion has a different function than during embryogenesis. From 29 colonies that we identified in the first round, only the shown 4 colonies grew back when streaked onto selection plates. However, even those colonies eventually did not grow very well and all failed to activate the LacZ reporter gene. The fourth putative interactor NM\_001044319.1 is not verified yet but cDNA transcripts have been found on skin and kidney. More than 1kb of the putative interacting protein's cDNA was sequenced and it showed a high homology to pleckstrin-homology (PH) like family members. PH-domains have been found in cell signaling proteins such as serine/ threonine kinases, tyrosine kinases, endocytic GTPases as well as cytoskeletal associated molecules and lipid associated enzymes (Etournay *et al.*, 2005). Furthermore, members of PH-like family have been shown to localize to the golgi and to mediate post-golgi trafficking to the membrane (Krappa *et al.*, 1999). Interestingly, PH-like family members were shown to localize to the membrane in photoreceptor outer segments, which represent specialized forms of cilia as well as retinal ganglion cells and haircells in the ear (Xu *et al.*, 1999; Xu *et al.*, 2004). Another exciting link for a potential role of PH-like family members was provided by a study in rat

tracheal epithelial cells that were grown under conditions that stimulated cilia formation (Andrews *et al.*, 2000). When these cells were stimulated for ciliogenesis a pleckstrin homology domain protein was expressed along with a marker for ciliated cell differentiation (axonemal dynein heavy chain) but failed to co-express with a marker for mucous cell differentiation, indicating that it might play a specific role during cilia formation or cilia function (Andrews *et al.*, 2000). It will be very interesting to test, whether this putative interactor for Arl13b/ Scorpion might indeed be a real protein interactor, and if so what role they might play during embryogenesis and cilia formation and maintenance in particular.

Taken together, our results are indicative of multiple roles that Arl13b/ Scorpion might play during embryogenesis, e.g. targeting of proteins to the basolateral membrane, cilia formation and maintenance and possibly as a switch in signal transduction. It is of very high interest to find a protein interactor to integrate Arl13b/ Scorpion within a pathway and propose a model for its specific role for cilia formation/ maintenance and signaling. A yeast two hybrid approach may lead to the identification of a real protein interactor in the near future and allow a close examination of Arl13b/ Scorpion's role in the human pathological disease Joubert syndrome as well as Joubert Syndrome and related disorders.

## 8. Summary

Mammalian embryonic kidney development and the embryonic development of the zebrafish pronephros have many features in common. In general, undifferentiated, unpolarized mesenchymal cells condense tightly and subsequently polarize and undergo mesenchymal-to-epithelial transition. A lumen is formed, vascular invasion occurs and secretory functions are established. The zebrafish model is an ideal model organism to study kidney development due to the facts, that the embryo is transparent for the first days of life, it develops *ex utero* and can easily be manipulated. Furthermore, it contains only two nephrons whereas as single mammalian kidney contains approximately 1 million nephrons. Many human renal diseases lead to end stage renal failure and require patients to undergo dialysis or organ transplantation. Many genes that cause renal diseases have been discovered, however, how exactly the embryonic kidney develops in zebrafish is not clear yet.

The present study aimed to elucidate the earliest events during embryonic kidney formation in *Danio rerio*. We show for the first time that cells of the intermediate mesoderm acquire apico-basolateral polarity, undergo cavitation and exhibit oriented cilia concurrently around the 12 somite stage. At the 14 somite stage these processes are completed resulting in a contiguous lumen, fully polarized cells and lumen oriented cilia, showing that critical processes that allow the transformation from mesenchymal cells to highly polarized and organized epithelial cells occur within a time window of approximately 1-1.5 hours. Furthermore we were able to show that the intermediate undergoes extensive elongation during development while simultaneously containing fewer cells in the circumference of the pronephric duct. Our data strongly suggest that these processes are not due to apoptosis and proliferation but to a rearrangement of cells. The narrowing and thinning of the intermediate mesoderm might be governed by the planar cell polarity (PCP) signaling pathway. Disruption of the planar cell polarity pathway led to duct dilation but was not sufficient for cyst formation. In contrast, disruption of the canonical wnt pathway has been shown to be sufficient for duct dilation as well as cyst formation, indicating that especially in a setting with low levels of proliferation as is the case in the zebrafish pronephros, the disruption of the planar polarity is not sufficient to cause cyst formation but in conjunction with an increased rate in proliferation, as have been shown in rodent models, cyst formation occurs.

Furthermore, we found that basal bodies were aligned intracellularly as well as among multiple cells in a highly organized fashion that formed a spiral like pattern around the ductal lumen and might be regulated by the PCP pathway as well and might serve as a PCP read out for future studies.

During the second part of this study we showed that Arl13b/ Scorpion, a small GTPase, localizes to the cilium in various organs and plays a crucial role for ciliogenesis in the KV, retinal photoreceptor layer and the pronephric duct. Performing careful histological analysis in *scorpion*<sup>hi459</sup> mutant embryos, we could show that hyperproliferation and/ or defects in cell rearrangements occur as a consequence of dilation, and are not causative.

In addition, *scorpion*<sup>hi459</sup> mutant embryos extended cilia tufts from multiciliated cells but cilia were not visible on single ciliated cells suggesting that Arl13b/ Sco might play different roles in multiciliated versus principal cells. The remaining cilia showed a defective organization of their basal bodies, suggesting a potential PCP pathway defect. We could show that in contrast to the Arl13b null mutant in mouse, hennin, scohi459 mutant cilia possess cilia with an intact axonemal ultra structure of (9+2). Furthermore, at 5 dpf ciliary tufts in mutant embryos were motile with an aberrant beating pattern.

We identified a novel role for Arl13b/ Scorpion during embryogenesis. Arl13b/ Scorpion is required for ciliogenesis in the Kupffer's vesicle (KV) and *scorpion*<sup>hi459</sup> mutants exhibit stunted and fewer cilia in the KV, whereas the KV structure itself is indistinguishable from wildtype and control morphant embryos thus confirming the role for cilia of the KV for establishing left/right asymmetry in the embryo. As a consequence, *arl13b/ scorpion* morphants displayed a randomization of laterality. Our data suggest that Arl13b/ Scorpion acts upstream of the nodal signaling pathway, since *spaw* expression was disturbed and randomized in *arl13b/ scorpion* morphants as well.

The kidney epithelium is highly polarized and the basolateral and apical membrane compartments show distinct protein and lipid composition which is important for the proper function of the kidney. Analyzing the apical-basolateral polarity in *scorpion*<sup>hi459</sup> mutants we could find an intact apical membrane, however, the basolateral membrane was less organized suggesting that Arl13b/ Scorpion might have a role in trafficking

membrane proteins to the basolateral compartment specifically. A similar phenotype has been reported in mutants that affect the small GTPase Rab8.

In addition to the cystic renal phenotype, *scorpion*<sup>hi459</sup> mutant showed retinal dystrophy starting around 5 dpf which was characterized by excessive apoptosis in the photoreceptor layer and degradation of the photoreceptor outer segments. Both, the polycystic kidney phenotype as well as retinal dystrophy are defects associated with JSRD, further supporting *scorpion*<sup>hi459</sup> as a disease model to study Joubert syndrome and JSRD.

In IFT57 mutants that lack cilia Arl13b/ Scorpion mislocalized to the apical membrane and strong Arl13b/ Scorpion mislocalization was inversely correlated to WGA signals.

A deletion analysis of Arl13b/ Sco protein allowed us to study the roles of the truncation proteins in regards to cilia localization and the capability to rescue the mutant phenotype. The GTPase domain, coiled coil region and part of the C-terminus (C-terminal to amino acid 308) were necessary for proper ciliary targeting. We found a close correlation for cilia localization being necessary for the protein being able to rescue the mutant phenotype. In addition, despite the GTPase activity playing no role in trafficking the protein to the cilium, it was crucial for the rescue capability of the protein.

## 9. REFERENCES

Adler, P.N., Zhu, C. & Stone, D. (2004): Inturned localizes to the proximal side of wing cells under the instruction of upstream planar polarity proteins. *Curr. Biol.* 14:2046–2051.

Amack, J. D., and Yost, H. J. (2004): The T box transcription factor no tail in ciliated cells controls zebrafish left-right asymmetry. *Curr Biol.* 14:685-90.

Andrews, C. T. (1949): Kartagener's syndrome. *Br Med J* 2:1269.

Ang AL, Fölsch H, Koivisto UM, Pypaert M, Mellman I. (2003): The Rab8 GTPase selectively regulates AP-1B-dependent basolateral transport in polarized Madin-Darby canine kidney cells. *J Cell Biol.* 163(2):339-50.

Antoshechkin I, Han M. (2002): The *C. elegans* *evl-20* gene is a homolog of the small GTPase ARL2 and regulates cytoskeleton dynamics during cytokinesis and morphogenesis. *Dev Cell.* 2(5):579-91.

Armstrong JF, Pritchard-Jones K, Bickmore WA, Hastie ND, Bard JB. (1993): The expression of the Wilms' tumour gene, WT1, in the developing mammalian embryo. *Mech Dev.* 40(1-2):85-97.

Arts HH, Doherty D, van Beersum SE, Parisi MA, Letteboer SJ, Gorden NT, Peters TA, Märker T, Voesenek K, Kartono A, Ozyurek H, Farin FM, Kroes HY, Wolfrum U, Brunner HG, Cremers FP, Glass IA, Knoers NV, Roepman R (2007): Mutations in the gene encoding the basal body protein RPGRIP1L, a nephrocystin-4 interactor, cause Joubert syndrome. *Nat Genet.* 39:882–888.

Avidor-Reiss, T., Maer, A. M., Koundakjian, E., Polyanovsky, A., Keil, T., Subramaniam, S., and Zuker, C. S. (2004): Decoding cilia function: defining specialized genes required for compartmentalized cilia biogenesis. *Cell* 117:527- 39.

Avner ED, Sweeney WE Jr, Nelson WJ (1992): Abnormal sodium pump distribution during renal tubulogenesis in congenital murine polycystic kidney disease. *Proc. Natl. Acad. Sci. U. S. A.* 89:7447–7451.

Baala L, Romano S, Khaddour R, Saunier S, Smith UM, Audollent S, Ozilou C, Faivre L, Laurent N, Foliguet B, Munnich A, Lyonnet S, Salomon R, Encha-Razavi F, Gubler MC, Boddaert N, de



## 9. REFERENCES

---

Lonlay P, Johnson CA, Vekemans M, Antignac C, Attie-Bitach T (2007): The Meckel- Gruber syndrome gene, MKS3, is mutated in Joubert syndrome. *Am J Hum Genet* 80:186–194.

Badano, J.L., Mitsuma, N., Beales, P. L., and Katsanis, N. (2006): The ciliopathies: an emerging class of human genetic disorders. *Annu Rev Genomics Hum Genet* 7:125-48.

Baert, L. (1978): Hereditary polycystic kidney disease (adult form): a microdissection study of two cases at an early stage of the disease. *Kidney Int* 13:519-25.

Bagnat M, Cheung ID, Mostov KE, Stainier DY. (2007): Genetic control of single lumen formation in the zebrafish gut. *Nat Cell Biol.* 9(8):954-60.

Banerjee M, Majumder P, Bhattacharyya NP, Dattagupta JK, Sen U. (2006): Cloning, expression, purification, crystallization and preliminary crystallographic analysis of pseudo death-effector domain of HIPPI, a molecular partner of Huntingtin-interacting protein HIP-1. *Acta Crystallogr Sect F Struct Biol Cryst Commun.* 62(Pt 12):1247-50.

Barr, M.M. and Sternberg, P.W. (1999): A polycystic kidney-disease gene homologue required for male mating behaviour in *C. elegans*. *Nature* 401:386-389.

Bernstein J. (1993): Glomerulocystic kidney disease--nosological considerations. *Pediatr Nephrol* 7:464-70.

Bingham C, Bulman MP, Ellard S, Allen LI, Lipkin GW, Hoff WG, Woolf AS, Rizzoni G, Novelli G, Nicholls AJ, Hattersley AT. (2000): Mutations in the hepatocyte nuclear factor-1beta gene are associated with familial hypoplastic glomerulocystic kidney disease. *Am J Hum Genet.* 68(1):219-24.

Bisgrove, BW, Essner, JJ and Yost, HJ. (1999): Regulation of midline development by antagonism of lefty and nodal signaling. *Development* 126:3253-62.

Bisgrove, B. W., Essner, J. J., and Yost, H. J. (2000): Multiple pathways in the midline regulate concordant brain, heart and gut left-right asymmetry. *Development* 127:3567-79.

Bisgrove BW, Morelli SH, Yost HJ. (2003): Genetics of human laterality disorders: insights from vertebrate model systems. *Annu Rev Genomics Hum Genet* 4:1-32.

## 9. REFERENCES

---

Bisgrove, B. W., Snarr, B. S., Emrazian, A., and Yost, H. J. (2005): Polaris and Polycystin-2 in dorsal forerunner cells and Kupffer's vesicle are required for specification of the zebrafish left-right axis. *Dev Biol* 287:274-88.

Blacque, OE., Reardon MJ, Li C, McCarthy J, Mahjoub MR, Ansley SJ, Badano SJ, Mah AK, Beales PL, Davidson WS, Johnsen RC, Audeh M, Plasterk RH, Baillie DL, Katsanis N, Quarmby LM, Wicks SR & Leroux MR. (2004): Loss of *C. elegans* BBS-7 and BBS-8 protein function results in cilia defects and compromised intraflagellar transport. *Genes Dev* 18:1630-42.

Blacque OE, Perens EA, Boroevich KA, Inglis PN, Li C, Warner A, Khattra J, Holt RA, Ou G, Mah AK, McKay SJ, Huang P, Swoboda P, Jones SJM, Marra MA, Baillie DA, Moerman DG, Shaham S and Leroux MR. (2005): Functional genomics of the cilium, a sensory organelle. *Curr Biol*. 15(10):935-41.

Blacque OE, Leroux MR. (2006): Bardet-Biedl syndrome: an emerging pathomechanism of intracellular transport. *Cell Mol Life Sci*. 63(18):2145-61.

Boutros M, Mlodzik M. (1999): Dishevelled: at the crossroads of divergent intracellular signaling pathways. *Mech Dev*. 83(1-2):27-37.

Brill, S. R., Ross, K. E., Davidow, C. J., Ye, M., Grantham, J. J., and Caplan, M. J. (1996): Immunolocalization of ion transport proteins in human autosomal dominant polycystic kidney epithelial cells. *Proc Natl Acad Sci U S A* 93:10206- 11.

Brummett AR, Dumont JN. (1978): Kupffer's vesicle in *Fundulus heteroclitus*: a scanning and transmission electron microscope study. *Tissue Cell*. 10(1):11-22.

Burd, C.G., Strohlic, T.I., and Gangi Setty, S.R. (2004): Arflike GTPases: Not so Arf-like after all. *Trends Cell Biol*. 14:687–694.

Cai Y, Maeda Y, Cedzich A, Torres VE, Wu G, Hayashi T, Mochizuki T, Park JH, Witzgall R, Somlo S. (1999): Identification and characterization of polycystin-2, the PKD2 gene product. *J Biol Chem* 274:28557-28565.

Calvet JP. (1998): Molecular genetics of polycystic kidney disease. *J Nephrol*. 11(1):24-34.

Calvet, J.P. & Grantham, J.J. (2001): The genetics and physiology of polycystic kidney disease. *Semin. Nephrol*. 21:107–123.

Cantagrel V, Silhavy JL, Bielas SL, Swistun D, Marsh SE, Bertrand JY, Audollent S, Attié-Bitach, Holden KR, Dobyns WB, Traver D, Al-Gazali L, Ali BR, Lindner TH, Caspary T, Otto EA, Hildebrandt F, Glass IA, Logan CV, Johnson CA, Bennett C, Brancati F. (2008): The International Joubert Syndrome Related Disorders (JSRD) Study Group, Valente EM, Woods CG and Gleeson JG. Mutations in the cilia gene ARL13B lead to the classical form of Joubert syndrome. *Am J Hum Genet.* 83(2):170-9.

Caspary, T., Larkins, C. E., and Anderson, K. V. (2007): The graded response to Sonic Hedgehog depends on cilia architecture. *Dev Cell* 12:767-78.

Chauvet V, Tian X, Husson H, Grimm DH, Wang T, Hiesberger T, Igarashi P, Bennett AM, Ibraghimov-Beskrovnaya O, Somalo S, Caplan MJ. (2004): Mechanical stimuli induce cleavage and nuclear translocation of the polycystin-1 C terminus. *J Clin Invest* 114:1433–1443.

Chavrier and Goud. (1999): The role of ARF and Rab GTPases in membrane transport. *Curr Opin Cell Biol.* 11(4):466-75.

Chen Z, Huang W, Dahme T, Rottbauer W, Ackerman MJ, Xu X. (2008): Depletion of zebrafish essential and regulatory myosin light chains reduces cardiac function through distinct mechanisms. *Cardiovasc Res.* 79(1):97-108.

Chiang AP, Nishimura D, Searby C, Elbedour K, Carmi R, Ferguson AL, Secrist J, Braun T, Casavant T, Stone EM, Sheffield VC. (2004): Comparative genomic analysis identifies an ADP-ribosylation factor-like gene as the cause of Bardet- Biedl syndrome (BBS3). *Am. J. Hum. Genet.* 75:475–484.

Crosby and Hill. (1962): Embryology of the Mullerian duct system. Review of present-day theory. *Obstet Gynecol.* 20:507-15.

Corbit, K.C., Shyer, A.E., Dowdle, W.E., Gaulden, J., Singla, V. and Reiter, J.F. (2008): Kif3a constrains beta-catenin-dependent Wnt signalling through dual ciliary and non-ciliary mechanisms. *Nat. Cell Biol.*, 10:70-76.

Corbit KC, Aanstad P, Singla V, Norman AR, Stanier DYR, Reiter JF. (2005): Vertebrate smoothed functions at the primary cilium. *Nature* 437:1018–1021.

Coucouvanis E, Martin GR. (1995): Signals for death and survival: a two-step mechanism for cavitation in the vertebrate embryo. *Cell*. 83(2):279-87.

Daitoku H, Isida J, Fujiwara K, Nakajima T, Fukamizu A. (2001): Dimerization of small GTPase Rab5. *Int J Mol Med*. 8(4):397-404.

Deane, JA, Cole DG, Seeley S., Diener DR, Rosenbaum J (2001): Localization of intraflagellar transport protein IFT52 identifies basal body transitional fibers as the docking site for IFT particles. *Curr Biol* 11:1586-90.

Dibella LM, Park A, Sun Z.. (2008): Zebrafish Tsc1 Reveals Functional Interactions Between the Cilium and the TOR Pathway. *Hum Mol Genet*. (Nov 13, Epub ahead of print).

Djiane A, Riou J, Umbhauer M, Boucaut J, Shi D. (2000): Role of frizzled 7 in the regulation of convergent extension movements during gastrulation in *Xenopus laevis*. *Development*. 127(14):3091-100.

Drummond, IA., Majumdar, A., Hentschel, H., Elger, M., Solnica-Krezel, L., Schier, A. F., Neuhauss, S. C., Stemple, D. L., Zwartkruis, F., Rangini, Z., Driever, W., and Fishman, M. C. (1998): Early development of the zebrafish pronephros and analysis of mutations affecting pronephric function. *Development* 125:4655-67.

Drummond IA. (2004): Zebrafish kidney development. *Methods Cell Biol*. 76:501-30.

Dressler GR, Deutsch U, Chowdhury K, Nornes HO, Gruss P. (1990): Pax2, a new murine paired-box-containing gene and its expression in the developing excretory system. *Development*. 109(4):787-95.

Dunaeva M, Michelson P, Kogerman P, Toftgard R. (2003): Characterization of the physical interaction of Gli proteins with SUFU proteins. *J Biol Chem*. 278(7):5116-22.

Dwyer ND, Troemel ER, Sengupta P, Bargmann CI. (1998): Odorant receptor localization to olfactory cilia is mediated by ODR-4, a novel membrane-associated protein. *Cell*. 93:455-466.

Dwyer ND, Adler CE, Crump JG, L'Etoile N, Bargmann CI. (2001): Polarized dendritic transport and the AP-1 m1 clathrin adaptor UNC-101 localize odorant receptors to olfactory cilia. *Neuron* 31:277-287.

Eggenschwiler JT, Anderson KV. (2007): Cilia and developmental signaling. *Annu Rev Cell Dev Biol.* 23:345-73.

Essner, J. J., Amack, J. D., Nyholm, M. K., Harris, E. B., and Yost, H. J. (2005): Kupffer's vesicle is a ciliated organ of asymmetry in the zebrafish embryo that initiates left-right development of the brain, heart and gut. *Development* 132:1247-60

Fan Y, Esmail MA, Ansley SJ, Blacque OE, Boroevich K, Ross AJ, Moore SJ, Badano JL, May-Simera H, Compton DS, Green JS, Lewis RA, van Haelst MM, Parfrey PS, Baillie DL, Beales PL, Katsanis N, Davidson WS, Leroux MR. (2004): Mutations in a member of the Ras superfamily of small GTP-binding proteins causes Bardet-Biedl syndrome. *Nat. Genet.* 36:989–993.

Fanto M, McNeill H. (2004): Planar polarity from flies to vertebrates. *J Cell Sci.* 1;117(Pt 4):527-33.

Ferland RJ, Eyaid W, Collura RV, Tully LD, Hill RS, Al-Nouri D, Al-Rumayyan A, Topcu M, Gascon G, Bodell A, Shugart YY, Ruvolo M, Walsh CA. (2004): Abnormal cerebellar development and axonal decussation due to mutations in *AHI1* in Joubert syndrome. *Nat Genet* 36:1008–1013.

Fischer E, Legue E, Doyen A, Nato F, Nicolas JF, Torres V, Yaniv M, Pontoglio M. (2006): Defective planar cell polarity in polycystic kidney disease. *Nat Genet* 38(1):21-3.

Foggensteiner L, Bevan AP, Thomas R, Coleman N, Boulter C, Bradley J, Ibraghimov-Beskrovnya O, Klinger K, Sandford R. (2000): Cellular and subcellular distribution of polycystin-2, the protein product of the *PKD2* gene. *J Am Soc Nephrol* 11:814-827.

Fraizer GC, Shimamura R, Zhang X, Saunders GF. (1997): *PAX 8* regulates human *WT1* transcription through a novel DNA binding site. *J Biol Chem.* 272(49):30678-87.

Gabow PA. (1993): Autosomal dominant polycystic kidney disease. *N Engl J Med* 329: 332–342.

Gagnon C, White D, Cosson J, Huitorel P, Eddé B, Desbruyères E, Paturle-Lafanechère L, Multigner L, Job D, Cibert C. (1996): The polyglutamylated lateral chain of alpha-tubulin plays a key role in flagellar motility. *J Cell Sci.* 109( Pt 6):1545-53.

Geng L, Okuhara D, Yu Z, Tian X, Cai Y, Shibasaki S, Somlo S. (2006): Polycystin-2 traffics to cilia independently of polycystin-1 by using an N-terminal RVxP motif. *J Cell Sci.* 119:1383–1395.

Germino GG. (2005): Linking cilia to Wnts. *Nat Genet.* 37(5):455-7.

Germino GG, Weinstat-Saslow D, Himmelbauer H, Gillespie GA, Somlo S, Wirth B, Barton N, Harris KL, Frischauf AM, Reeders ST. (1992): The gene for autosomal dominant polycystic kidney disease lies in a 750-kb CpG-rich region. *Genomics* 13(1): 144-51.

Gervais FG, Singaraja R, Xanthoudakis S, Gutekunst CA, Leavitt BR, Metzler M, Hackam AS, Tam J, Vaillancourt JP, Houtzager V, Rasper DM, Roy S, Hayden MR, Nicholson DW. (2002): Recruitment and activation of caspase-8 by the Huntingtin-interacting protein Hip-1 and a novel partner Hippi. *Nat Cell Biol.* 4(2):95-105.

Gessler M, König A, Bruns GA. (1992): The genomic organization and expression of the WT1 gene. *Genomics* 12(4):807-13.

Godsel LM, Engman DM. (1999): Flagellar protein localization mediated by a calcium-myristoyl/palmitoyl switch mechanism. *EMBO J.* 18(8):2057-65.

Grantham JJ, Chapman AB, Torres VE. (2006): Volume progression in autosomal dominant polycystic kidney disease: The major factor determining clinical outcomes. *Clin J Am Soc Nephrol* 1: 148–157.

Griffin MD, Torres VE, Grande JP, Kumar R. (1997): Vascular expression of polycystin. *J Am Soc Nephrol* 8:616-626.

Guay-Woodford LM, Desmond RA. (2003): Autosomal recessive polycystic kidney disease: the clinical experience in North America. *Pediatrics* 111:1072–80.

Hamada, H. (2005): De novo formation of left-right asymmetry by posterior tilt of nodal cilia. *PLoS Biol* 3:e268.

Hateboer N, v Dijk MA, Bogdanova N, Coto E, Saggar-Malik AK, San Millan JL, Torra R, Breuning M, Ravine D. (1999): Comparison of phenotypes of polycystic kidney disease types 1 and 2. *Lancet* 353:103–7.

Haycraft, C. J., J. C. Schafer, Q. Zhang, P. D. Taulman & B. K. Yoder. (2003): Identification of CHE-13, a novel intraflagellar transport protein required for cilia formation. *Exp Cell Res* 284:251-63.

## 9. REFERENCES

---

- Haycraft CJ, Banizs B, Aydin-Son Y, Zhang Q, Mi. (2005): Gli2 and Gli3 localize to cilia and require the intraflagellar transport protein polaris for processing and function. *PLoS Genet.* 1(4):e53.
- Heisenberg, C.P., Tada, M., Rauch, G.J., Saude, L., Concha, M.L., Geisler, R., Stemple, D.L., Smith, J.C. and Wilson, S.W. (2000): Silberblick/Wnt11 mediates convergent extension movements during zebrafish gastrulation. *Nature* 405:76-81.
- Hildebrandt F. (2004): Juvenile nephronophthisis. *Pediatric Nephrology* (edited by Harmon WE, Baltimore, Williams & Wilkins) pp 665–673.
- Hildebrandt, F., and Zhou, W. (2007): Nephronophthisis-associated ciliopathies. *J Am Soc Nephrol* 18:1855-71.
- Hirokawa, N., Tanaka, Y., Okada, Y., and Takeda, S. (2006): Nodal flow and the generation of left-right asymmetry. *Cell* 125:33-45.
- Hirokawa, N. (1998): Randomization of left-right asymmetry due to loss of nodal cilia generating leftward flow of extraembryonic fluid in mice lacking KIF3B motor protein. *Cell* 95:829-37.
- Hori Y, Kobayashi T, Kikko Y, Kontani K, Katada T. (2008): Domain architecture of the atypical Arf-family GTPase Arl13b involved in cilia formation. *Biochem Biophys Res Commun.* 373(1):119-24.
- Houde C, Dickinson RJ, Houtzager VM, Cullum R, Montpetit R, Metzler M, Simpson EM, Roy S, Hayden MR, Hoodless PA, Nicholson DW. (2006): Hippo is essential for node cilia assembly and Sonic hedgehog signaling. *Dev Biol.* 300(2):523-33.
- Hoyt MA, Hyman AA, Bähler M. (1997): Motor proteins of the eukaryotic cytoskeleton. *Proc Natl Acad Sci U S A.* 94(24):12747-8.
- Huangfu D, Anderson KV. (2005): Cilia and Hedgehog responsiveness in the mouse. *Proc Natl Acad Sci U S A.* 102(32):11325-30.
- Huber LA, Dupree P, Dotti CG. (1995): A deficiency of the small GTPase rab8 inhibits membrane traffic in developing neurons. *Mol Cell Biol.* 15(2):918-24.

Hughes J, Ward CJ, Peral B, Aspinwall R, Clark K, San Millán JL, Gamble V, Harris PC.(1995): The polycystic kidney disease 1 (PKD1) gene encodes a novel protein with multiple cell recognition domains. *Nat. Genet.* 10:151–60.

Hou X, Mrug M, Yoder BK, Lefkowitz EJ, Kremmidiotis G, D'Eustachio P, Beier DR, Guay-Woodford LM. (2002): Cystin, a novel ciliaassociated protein, is disrupted in the cpk mouse model of polycystic kidney disease. *J Clin Invest.* 109:533–540.

Ibraghimov-Beskrovnya, O. (2007): Targeting dysregulated cell cycle and apoptosis for polycystic kidney disease therapy. *Cell Cycle* 6:776-9.

Ikegami K, Heier RL, Taruishi M, Takagi H, Mukai M, Shimma S, Taira S, Hatanaka K, Morone N, Yao I, Campbell PK, Yuasa S, Janke C, Macgregor GR, Setou M. (2007): Loss of alpha-tubulin polyglutamylation in ROSA22 mice is associated with abnormal targeting of KIF1A and modulated synaptic function. *Proc Natl Acad Sci U S A.* 104(9):3213-8.

International Polycystic Kidney Disease Consortium. (1995): Polycystic kidney disease: the complete structure of the PKD1 gene and its protein. *Cell* 81:289–98.

Iomini, C., V. Babaev-Khaimov, M. Sassaroli, G. Piperno. (2001): Protein particles in *Chlamydomonas* flagella undergo a transport cycle consisting of four phases. *J Cell Biol* 153:13-24.

Jenkins PM, Hurd TW, Zhang L, McEwen DP, Brown RL, Margolis B, Verhey KJ, Martens JR. (2006): Ciliary targeting of olfactory CNG channels requires the CNGB1b subunit and the kinesin-2 motor protein, KIF17. *Curr Biol.*16(12):1211-6.

Jessen, J.R., Topczewski, J., Bingham, S., Sepich, D.S., Marlow, F., Chandrasekhar, A. and Solnica-Krezel, L. (2002): Zebrafish trilobite identifies new roles for Strabismus in gastrulation and neuronal movements. *Nat. Cell Biol.* 4:610-615.

Johnson KA, Rosenbaum JL. (1992): Polarity of flagellar assembly in *Chlamydomonas*. *J Cell Biol.* 119:1605–1611.

Jones, C., Roper, V.C., Foucher, I., Qian, D., Banizs, B., Petit, C., Yoder, B.K., Chen, P. (2008): Ciliary proteins link basal body polarization to planar cell polarity regulation. *Nat. Genet.*, 40, 69-77.



## 9. REFERENCES

---

- Kahn RA, Volpicelli-Daley L, Bowzard B, Shrivastava-Ranjan P, Li Y, Zhou C, Cunningham L. (2005): Arf family GTPases: roles in membrane traffic and microtubule dynamics. *Biochem Soc Trans.* 33(Pt 6):1269-72.
- Karner C, Wharton KA Jr, Carroll TJ. (2006): Planar cell polarity and vertebrate organogenesis. *Semin Cell Dev Biol.* 17(2):194-203.
- Keller, R. 2002. Shaping the vertebrate body plan by polarized embryonic cell movements. *Science*, 298:1950-1954.
- Koulen P, Cai Y, Geng L, et al. (2002): Polycystin-2 is an intracellular calcium release channel. *Nat. Cell Biol.* 4:191-97.
- Kozminski KG, Diener DR, Rosenbaum JL. (1999): High level expression of nonacetylatable alpha-tubulin in *Chlamydomonas reinhardtii*. *Cell Motil Cytoskeleton.* 25(2):158-70.
- Kramer-Zucker, A. G., Olale, F., Haycraft, C. J., Yoder, B. K., Schier, A. F., and Drummond, I. A. (2005): Cilia-driven fluid flow in the zebrafish pronephros, 181 brain and Kupffer's vesicle is required for normal organogenesis. *Development* 132:1907-21.
- Kreidberg JA, Sariola H, Loring JM, Maeda M, Pelletier J, Housman D, Jaenisch R. (1993): WT-1 is required for early kidney development. *Cell.* 74(4):679-91.
- Lin F, Hiesberger T, Cordes K, Sinclair AM, Goldstein LS, Somlo S, Igarashi P. (2003): Kidney-specific inactivation of the KIF3A subunit of kinesin-II inhibits renal ciliogenesis and produces polycystic kidney disease. *Proc Natl Acad Sci U S A.* 100(9):5286-91.
- Liu, Y., Pathak, N., Kramer-Zucker, A., and Drummond, I. A. (2007): Notch signaling controls the differentiation of transporting epithelia and multiciliated cells in the zebrafish pronephros. *Development* 134:1111-22.
- Louie C.M. and Gleeson, J.G. (2005): Genetic basis of Joubert syndrome and related disorders of cerebellar development. *Hum. Mol. Genet.* 14 (Spec. No. 2) R235- 242.

## 9. REFERENCES

---

Low SH, Vasanth S, Larson CH, Mukherjee S, Sharma N, Kinter MT, Kane ME, Obara T, Weimbs T. (2006): Polycystin-1, STAT6, and P100 function in a pathway that transduces ciliary mechanosensation and is activated in polycystic kidney disease. *Dev Cell* 10:57–69.

Lubarsky B, Krasnow MA. (2003): Tube morphogenesis: making and shaping biological tubes. *Cell*. 10;112(1):19-28.

Ma, M., and Jiang, Y. J. (2007): Jagged2a-notch signaling mediates cell fate choice in the zebrafish pronephric duct. *PLoS Genet* 3:e18.

Magistroni R, He N, Wang K, Andrew R, Johnson A, Gabow P, Dicks E, Parfrey P, Torra R, San-Millan JL, Coto E, Van Dijk M, Breuning M, Peters D, Bogdanova N, Ligabue G, Albertazzi A, Hateboer N, Demetriou K, Pierides A, Deltas C, St George-Hyslop P, Ravine D, Pei Y. (2003): Genotype-renal function correlation in type 2 autosomal dominant polycystic kidney disease. *J. Am. Soc. Nephrol.* 14:1164–7428.

Majumdar A, Lun K, Brand M, Drummond IA. (2000): Zebrafish no isthmus reveals a role for pax2.1 in tubule differentiation and patterning events in the pronephric primordia. *Development*. 127(10):2089-98.

Marszalek JR, Ruiz-Lozano P, Roberts E, Chien KR, and Goldstein LS. (1999): Situs inversus and embryonic ciliary morphogenesis defects in mouse mutants lacking the KIF3A subunit of kinesin-II. *Proc Natl Acad Sci USA* 96:5043–5048.

McGrath, J., Somlo, S., Makova, S., Tian, X., and Brueckner, M. (2003). Two populations of node monocilia initiate left-right asymmetry in the mouse. *Cell* 114:61-73.

Merchant M, Vajdos FF, Ultsch M, Maun HR, Wendt U, Cannon J, Desmarais W, Lazarus RA, de Vos AM, de Sauvage FJ. (2004): Suppressor of fused regulates Gli activity through a dual binding mechanism. *Mol Cell Biol.* 24(19):8627-41.

Mitchell, B., Jacobs, R., Li, J., Chien, S. & Kintner, C. (2007): A positive feedback mechanism governs the polarity and motion of motile cilia. *Nature* 447:97–101.

Morgan D, Eley L, Sayer J, Strachan T, Yates LM, Craighead AS, Goodship JA. (2002): Expression analyses and interaction with the anaphase promoting complex protein Apc2 suggest

a role for inversin in primary cilia and involvement in the cell cycle. *Hum Mol Genet.* 11(26):3345-50.

Moritz OL, Tam BM, Hurd LL, Peränen J, Deretic D, Papermaster DS. (2001): Mutant rab8 Impairs docking and fusion of rhodopsin-bearing post-Golgi membranes and causes cell death of transgenic *Xenopus* rods. *Mol Biol Cell.* 12(8):2341-51.

Mykytyn, K., and Sheffield, V. C. (2004). Establishing a connection between cilia and Bardet-Biedl Syndrome. *Trends Mol Med* 10:106-9.

Nachury MV, Loktev AV, Zhang Q, Westlake CJ, Peränen J, Merdes A, Slusarski DC, Scheller RH, Bazan JF, Sheffield VC, Jackson PK. (2007): A core complex of BBS proteins cooperates with the GTPase Rab8 to promote ciliary membrane biogenesis. *Cell* 129(6):1201-13.

Nadasdy T, Laszik Z, Lajoie G, Blick KE, Wheeler DE, Silva FG. (1995): Proliferative activity of cyst epithelium in human renal cystic diseases. *J Am Soc Nephrol.* 5(7):1462-8

Nauli, S. M., Alenghat, F. J., Luo, Y., Williams, E., Vassilev, P., Li, X., Elia, A. E., Lu, W., Brown, E. M., Quinn, S. J., Ingber, D. E., and Zhou, J. (2003): Polycystins 1 and 2 mediate mechanosensation in the primary cilium of kidney cells. *Nat Genet* 33:129-37.

Nishigori H, Yamada S, Kohama T, Tomura H, Sho K, Horikawa Y, Bell GI, Takeuchi T, Takeda J. (1998): Frameshift mutation, A263fsinsGG, in the hepatocyte nuclear factor-1beta gene associated with diabetes and renal dysfunction. *Diabetes.* 47(8):1354-5.

Nishimura D. Y., Searby, C. C., Carmi, R., Elbedour, K., Van Maldergem, L., Fulton, A>B., Lam, B. L., Powell, B. R., Swiderski, R. E., Bugge, K.E. et al. (2001): Positional cloning of a novel gene on chromosome 16q causing Bardet-Biedl-syndrome (BBS2). *Hum. Mol. Genet.* 10, 865-874.

Nonaka, S., Tanaka, Y., Okada, Y., Takeda, S., Harada, A., Kanai, Y., Kido, M., and Hirokawa, N. (1998): Randomization of left-right asymmetry due to loss of nodal cilia generating leftward flow of extraembryonic fluid in mice lacking KIF3B motor protein. *Cell* 95:829-37.

Nonaka, S., Shiratori, H., Saijoh, Y., and Hamada, H. (2002): Determination of left-right patterning of the mouse embryo by artificial nodal flow. *Nature* 418:96-9.

## 9. REFERENCES

---

- Obara ME and Weimbs, T. (2006): Polycystin-1, STAT6, and P100 function in a pathway that transduces ciliary mechanosensation and is activated in polycystic kidney disease. *Dev Cell* 10:57-69.
- Obermüller N, Cai Y, Kränzlin B, Thomson RB, Gretz N, Kriz W, Somlo S, Witzgall R. (2002): Altered expression pattern of polycystin-2 in acute and chronic renal tubular diseases. *J Am Soc Nephrol.* 13(7):1855-64.
- Oishi, I., Kawakami, Y., Raya, A., Callo-Massot, C. and Izpisua Belmonte, J.C. (2006): Regulation of primary cilia formation and left-right patterning in zebrafish by a noncanonical Wnt signaling mediator, *duboraya*. *Nat. Genet.*, 38:1316-1322.
- Okada Y, Higuchi H, Hirokawa N. (2003): Processivity of the single-headed kinesin KIF1A through biased binding to tubulin. *Nature.*424(6948):574-7.
- Okada, Y., Takeda, S., Tanaka, Y., Belmonte, J. C., and Hirokawa, N. (2005): Mechanism of nodal flow: a conserved symmetry breaking event in left-right axis determination. *Cell* 121:633-44.
- Oteiza P, Köppen M, Concha ML, Heisenberg CP. (2008): Origin and shaping of the laterality organ in zebrafish. *Development.* 135(16):2807-13.
- Omori, Y., Malicki, J., (2006): *oko* meduzy and related crumbs genes are determinants of apical cell features in the vertebrate embryo. *Curr. Biol.* 16:945–957.
- Ou, G., M. Koga, O. E. Blacque, T. Murayama, Y. Ohshima, J. C. Schafer, C. Li, B. K. Yoder, M. R. Leroux, J. M. Scholey. (2007): Sensory Ciliogenesis in *Caenorhabditis elegans*: Assignment of IFT components into Distinct Modules Based on Transport and Phenotypic Profiles. *Mol Biol Cell.* 18(5):1554-69.
- Onuchic LF, Furu L, Nagasawa Y, Hou X, Eggermann T, Ren Z, Bergmann C, Senderek J, Esquivel E, Zeltner R, Rudnik-Schöneborn S, Mrug M, Sweeney W, Avner ED, Zerres K, Guay-Woodford LM, Somlo S, Germino GG (2002): PKHD1, the polycystic kidney and hepatic disease 1 gene, encodes a novel large protein containing multiple immunoglobulinlike plexin-transcription-factor domains and parallel beta-helix 1 repeats. *Am. J. Hum. Genet.* 70:1305–1317.
- Parisi MA, Bennett CL, Eckert ML, Dobyns WB, Gleeson JG, Shaw DW, McDonald R, Eddy A, Chance PF, Glass IA.. (2004): The NPHP1 gene deletion associated with juvenile

## 9. REFERENCES

---

nephronophthisis is present in a subset of individuals with Joubert syndrome. *Am J Hum Genet* 75:82–91.

Park, T.J., Haigo, S.L. and Wallingford, J.B. (2006): Ciliogenesis defects in embryos lacking inturned or fuzzy function are associated with failure of planar cell polarity and Hedgehog signaling. *Nat. Genet.* 38:303-311.

Park TJ, Mitchell BJ, Abitua PB, Kintner C, Wallingford JB. (2008): Dishevelled controls apical docking and planar polarization of basal bodies in ciliated epithelial cells. *Nat Genet.* 40(7):871-9.

Pathak, N., Obara, T., Mangos, S., Liu, Y., and Drummond, I. A. (2007): The zebrafish fleer gene encodes an essential regulator of cilia tubulin polyglutamylation. *Mol Biol Cell* 18:4353-64.

Pazour, G. J., Dickert, B. L., Vucica, Y., Seeley, E. S., Rosenbaum, J. L., Witman, G. B., and Cole, D. G. (2000): Chlamydomonas IFT88 and its mouse homologue, polycystic kidney disease gene tg737, are required for assembly of cilia and flagella. *J Cell Biol* 151:709-18.

Pazour GJ, San Agustin JT, Follit JA, Rosenbaum JL, Witman GB. (2002): Polycystin-2 localizes to kidney cilia and the ciliary level is elevated in orpk mice with polycystic kidney disease. *Curr Biol* 12:R378-380.

Pazour, GJ and Witman, G. B. (2003): The vertebrate primary cilium is a sensory organelle. *Curr Opin Cell Biol* 15:105-10.

Pazour GJ, Agrin N, Leszyk J, Witman GB. (2005): Proteomic analysis of a eukaryotic cilium. *J Cell Biol* 170:103–113.

Pedersen, L. B., M. S. Miller, S. Geimer, J. M. Leitch, J. L. Rosenbaum & D. G. Cole. (2005): Chlamydomonas IFT172 is encoded by FLA11, interacts with CrEB1, and regulates IFT at the flagellar tip. *Curr Biol* 15:262-6.

Pei Y, Watnick T, He N, Wang K, Liang Y, Parfrey P, Germino G, St George-Hyslop P. (1999): Somatic PKD2 mutations in individual kidney and liver cysts support a “two-hit” model of cystogenesis in type 2 autosomal dominant polycystic kidney disease. *J. Am. Soc. Nephrol.* 10:1524–29.

## 9. REFERENCES

---

Pennekamp, P., Karcher, C., Fischer, A., Schweickert, A., Skryabin, B., Horst, J., Blum, M., and Dworniczak, B. (2002): The ion channel polycystin-2 is required for leftright axis determination in mice. *Curr Biol* 12:938-43.

Perrone, R. D. (1997): Extrarenal manifestations of ADPKD. *Kidney Int* 51:202236.

Perrone RD, Grubman SA, Murray SL, Lee DW, Alper SL, Jefferson DM. (1997): Autosomal dominant polycystic kidney disease decreases anion exchanger activity. *Am J Physiol.* 272(5 Pt 1):C1748-56.

Peters DJ, van de Wal A, Spruit L, Saris JJ, Breuning MH, Bruijn JA, de Heer E.(1999): Cellular localization and tissue distribution of polycystin-1. *J Pathol* 188:439-446.

Praetorius, H.A., Spring, K.R., (2001): Bending the MDCK cell primary cilium increases intracellular calcium. *J. Membr. Biol.* 184:71–79.

Praetorius, H. A., Frokiaer, J., Nielsen, S., and Spring, K. R. (2003): Bending the primary cilium opens Ca<sup>2+</sup>-sensitive intermediate-conductance K<sup>+</sup> channels in MDCK cells. *J Membr Biol* 191:193-200.

Pritchard-Jones K, Hastie ND. (1990): Wilms' tumour as a paradigm for the relationship of cancer to development. *Cancer Surv.* 9(3):555-78.

Qian F, Watnick TJ, Onuchic LF, et al. (1996): The molecular basis of focal cyst formation in human autosomal dominant polycystic kidney disease type 1. *Cell* 87:979–87.

Qian Q, Hunter LW, Li M, Marin-Padilla M, Prakash YS, Somlo S, Harris PC, Torres VE, Sieck GC. (2003): Pkd2 haploinsufficiency alters intracellular calcium regulation in vascular smooth muscle cells. *Hum Mol Genet* 12:1875- 1880.

Qin, H., D. R. Diener, S. Geimer, D. G. Cole & J. L. Rosenbaum. (2004): Intraflagellar transport (IFT) cargo: IFT transports flagellar precursors to the tip and turnover products to the cell body. *J Cell Biol* 164:255-66.

Ramasubbu K, Gretz N, Bachmann S. (1998): Increased epithelial cell proliferation and abnormal extracellular matrix in rat polycystic kidney disease. *J. Am. Soc. Nephrol.* 9:937–945.

## 9. REFERENCES

---

Ramulu P, Nathans J. (2001): Cellular and subcellular localization, N-terminal acylation, and calcium binding of *Caenorhabditis elegans* protein with EF-hands. *J Biol Chem* 276:25127–25135.

Riley BB, Phillips BT (2003): Ringing in the new ear: resolution of cell interactions in otic development. *Dev. Biol.* 261:289–312.

Rodriguez-Boulan E, Kreitzer G, Müsch A. (2005): Organization of vesicular trafficking in epithelia. *Nat Rev Mol Cell Biol.* 6(3):233-47.

Rosenbaum JL, Witman GB. (2002): Intraflagellar transport. *Nat Rev Mol Cell Biol* 3:813–825.

Ross AJ, May-Simera H, Eichers ER, Kai M, Hill J, Jagger DJ, Leitch CC, Chapple JP, Munro PM, Fisher S, Tan PL, Phillips HM, Leroux MR, Henderson DJ, Murdoch JN, Copp AJ, Eliot MM, Lupski JR, Kemp DT, Dollfus H, Tada M, Katsanis N, Forge A, Beales PL. (2005): Disruption of Bardet-Biedl syndrome ciliary proteins perturbs planar cell polarity in vertebrates. *Nat Genet* 37(10):1135-40.

Rossetti S, Burton S, Strmecki L, Pond GR, San Millán JL, Zerres K, Barratt TM, Ozen S, Torres VE, Bergstralh EJ, Winearls CG, Harris PC. (2002): The position of the polycystic kidney disease 1 (PKD1) gene mutation correlates with the severity of renal disease. *J. Am. Soc. Nephrol.* 13:1230–37.

Rupprecht HD, Drummond IA, Madden SL, Rauscher FJ 3rd, Sukhatme VP. (1994): The Wilms' tumor suppressor gene WT1 is negatively autoregulated. *J Biol Chem.* 269(8):6198-206.

Sanyanusin P, Schimmenti LA, McNoe LA, Ward TA, Pierpont ME, Sullivan MJ, Dobyns WB, Eccles MR. (1995): Mutation of the PAX2 gene in a family with optic nerve colobomas, renal anomalies and vesicoureteral reflux. *Nat Genet.* 9(4):358-64.

Sato T, Mushiake S, Kato Y, Sato K, Sato M, Takeda N, Ozono K, Miki K, Kubo Y, Tsuji A, Harada R, Harada A. (2007): The Rab8 GTPase regulates apical protein localization in intestinal cells. *Nature.* 448(7151):366-9.

Sayer JA, Otto EA, O'Toole JF, Nurnberg G, Kennedy MA, Becker C, Hennies HC, Helou J, Attanasio M, Fausett BV, Utsch B, Khanna H, Liu Y, Drummond I, Kawakami I, Kusakabe T, Tsuda M, Ma L, Lee H, Larson RG, Allen SJ, Wilkinson CJ, Nigg EA, Shou C, Lillo C, Williams

DS, Hoppe B, Kemper MJ, Neuhaus T, Parisi MA, Glass IA, Petry M, Kispert A, Gloy J, Ganner A, Walz G, Zhu X, Goldman D, Nurnberg P, Swaroop A, Leroux MR, Hildebrandt F. (2006): The centrosomal protein nephrocystin-6 is mutated in Joubert syndrome and activates transcription factor ATF4. *Nat Genet* 38:674–681.

Schermer B, Höpker K, Omran H, Ghenoiu C, Fliegauf M, Fekete A, Horvath J, Köttgen M, Hackl M, Zschiedrich S, Huber TB, Kramer-Zucker A, Zentgraf H, Blaukat A, Walz G. (2005): Phosphorylation by casein kinase 2 induces PACS-1 binding of nephrocystin and targeting to cilia. *EMBO J* 24:4415–4424.

Schneider L, Clement CA, Teilmann SC, Pazour GJ, Hoffmann EK, Satir P, Christensen ST. (2005): PDGFR $\alpha$  signaling is regulated through the primary cilium in fibroblasts. *Curr Biol*. 15(20):1861-6.

Scholey JM. (2003): Intraflagellar transport. *Annu Rev Cell Dev Biol*. 19:423-43.

Schottenfeld, J., Sullivan-Brown, J., Burdine, RD. (2007): Zebrafish curly up encodes a Pkd2 ortholog that Restricts left-side-specific expression of southpaw. *Development* 134:1605–1615.

Shih J, Keller R. (1992): Cell motility driving mediolateral intercalation in explants of *Xenopus laevis*. *Development*. 116(4):901-14.

Shillingford, J. M., Murcia, N. S., Larson, C. H., Low, S. H., Hedgepeth, R., Brown, N., Flask, C. A., Novick, A. C., Goldfarb, D. A., Kramer-Zucker, A., Walz, G., Piontek, K. B., Germino, G. G., and Weimbs, T. (2006): The mTOR pathway is regulated by polycystin-1, and its inhibition reverses renal cystogenesis in polycystic kidney disease. *Proc Natl Acad Sci U S A* 103:5466-71.

Simons M, Gloy J, Ganner A, Bullerkotte A, Bashkurov M, Krönig C, Schermer B, Benzing T, Cabello OA, Jenny A, Mlodzik M, Polok B, Driever W, Obara T, Walz G. (2005): Inversin, the gene product mutated in nephronophthisis type II, functions as a molecular switch between Wnt signaling pathways. *Nat Genet*. 37(5):537-43.

Simons, M., Walz, G. (2006): Polycystic kidney disease: cell division without a clue? *Kidney Int*. 70:854–864.

Sokol SY. (1996): Analysis of Dishevelled signalling pathways during *Xenopus* development. *Curr Biol*. 6(11):1456-67.



Stayner, C. & Zhou, J. (2001): Polycystin channels and kidney disease. *Trends Pharmacol. Sci.* 22:543–546.

Stenmark H, Olkkonen VM. (2001): The Rab GTPase family. *Genome Biol.* 2(5):REVIEWS3007

Sullivan-Brown J, Schottenfeld J, Okabe N, Hostetter CL, Serluca FC, Thiberge SY, Burdine RD. (2008): Zebrafish mutations affecting cilia motility share similar cystic phenotypes and suggest a mechanism of cyst formation that differs from *pkd2* morphants. *Dev Biol.* 314(2):261-75.

Sun Z, Hopkins N. (2001): *vhnf1*, the MODY5 and familial GCKD-associated gene, regulates regional specification of the zebrafish gut, pronephros, and hindbrain. *vhnf1*, the MODY5 and familial GCKD-associated gene, regulates regional specification of the zebrafish gut, pronephros, and hindbrain. *Genes Dev.* 15(23):3217-29.

Sun, Z., Amsterdam, A., Pazour, G. J., Cole, D. G., Miller, M. S., and Hopkins, N. (2004): A genetic screen in zebrafish identifies cilia genes as a principal cause of cystic kidney. *Development* 131:4085-93.

Tabin, C. J., and Vogan, K. J. (2003): A two-cilia model for vertebrate left-right axis specification. *Genes Dev* 17:1-6.

Tada, M. and Smith, J.C. (2000): *Xwnt11* is a target of *Xenopus* Brachyury: regulation of gastrulation movements via Dishevelled, but not through the canonical Wnt pathway. *Development*, 127:2227-2238.

Tanner GA, Tielker MA, Connors BA, Phillips CL, Tanner JA, Evan AP. (2002): Atubular glomeruli in a rat model of polycystic kidney disease. *Kidney Int.* 62:1947–1957.

Taulman PD, Haycraft CJ, Balkovetz DF, Yoder BK. (2001): Polaris, a protein involved in left-right axis patterning, localizes to basal bodies and cilia. *Mol Biol Cell.* (3):589-99.

Thomson RB, Mentone S, Kim R, Earle K, Delpire E, Somlo S, Aronson PS. (2003): Histopathological analysis of renal cystic epithelia in the *Pkd2WS25*<sup>-/-</sup> mouse model of ADPKD. *Am. J. Physiol.: Renal Physiol.* 285:F870–F880.

## 9. REFERENCES

---

- Topczewski J, Sepich DS, Myers DC, Walker C, Amores A, Lele Z, Hammerschmidt M, Postlethwait J, Solnica-Krezel L. (2001): The zebrafish glypican knypek controls cell polarity during gastrulation movements of convergent extension. *Dev Cell*. 1(2):251-64.
- Torres VE, Mujwid DK, Wilson DM, Holley KH. (1994): Renal cystic disease and ammoniogenesis in Han:SPRD rats. *J Am Soc Nephrol*. 5(5):1193-200.
- Torres VE. (1995): Polycystic liver disease. *Contrib Nephrol*. 115:44-52.
- Torres, V.E. (1999): Extrarenal manifestations of autosomal dominant polycystic kidney disease. *Am. J. Kidney. Dis*. 34:xliv–xlviii.
- Torres VE, Harris PC, Pirson Y. (2007): Autosomal dominant polycystic kidney disease. *Lancet* 369:1287–301.
- Tsiokas, L., Kim, E., Arnould, T., Sukhatme, V. P., and Walz, G. (1997): Homo- and heterodimeric interactions between the gene products of PKD1 and PKD2. *Proc Natl Acad Sci U S A* 94:6965-70.
- Tull D, Vince JE, Callaghan JM, Naderer T, Spurck T, McFadden GI, Currie G, Ferguson K, Bacic A, McConville MJ. (2004): SMP-1, a member of a new family of small myristoylated proteins in kinetoplastid parasites, is targeted to the flagellum membrane in Leishmania. *Mol Biol Cell*. 15(11):4775-86.
- Verani, R.R., Silva, F.G. (1988): Histogenesis of the renal cysts in adult (autosomal dominant) polycystic kidney disease: a histochemical study. *Mod. Pathol*. 1:457–463.
- Vize PD, Seufert DW, Carroll TJ, Wallingford JB. (1997): Model systems for the study of kidney development: use of the pronephros in the analysis of organ induction and patterning. *Dev. Biol*. 188:189–204.
- Wallingford JB, Rowning BA, Vogeli KM, Rothbacher U, Fraser SE, Harland RM. (2000): Dishevelled controls cell polarity during *Xenopus* gastrulation. *Nature* 405(6782):81-5.
- Ward CJ, Turley H, Ong AC, Comley M, Biddolph S, Chetty R, Ratcliffe PJ, Gattner K, Harris PC. (1996): Polycystin, the polycystic kidney disease 1 protein, is expressed by epithelial cells in fetal, adult, and polycystic kidney. *Proc Natl Acad Sci U S A* 93(4): 1524-8.

## 9. REFERENCES

---

Ward CJ, Hogan MC, Rossetti S, Walker D, Sneddon T, Wang X, Kubly V, Cunningham JM, Bacallao R, Ishibashi M, Milliner DS, Torres VE, Harris PC. (2002): The gene mutated in autosomal recessive polycystic kidney disease encodes a large, receptor-like protein. *Nat. Genet.* 30:259–269.

Watnick TJ, Torres VE, Gandolph MA, Qian F, Onuchic LF, Klinger KW, Landes G, Germino GG. (1998): Somatic mutation in individual liver cysts supports a two-hit model of cystogenesis in autosomal dominant polycystic kidney disease. *Mol Cell* 2:247-251.

Wilson PD, Geng L, Li X, Burrow CR. (1999): The PKD1 gene product, “polycystin-1,” is a tyrosine-phosphorylated protein that colocalizes with alpha2beta1- integrin in focal clusters in adherent renal epithelia. *Lab Invest* 79:1311-1323.

Wilson, P. D., Devuyst, O., Li, X., Gatti, L., Falkenstein, D., Robinson, S., Fambrough, D., and Burrow, C. R. (2000): Apical plasma membrane mispolarization of NaKATPase in polycystic kidney disease epithelia is associated with aberrant expression of the beta2 isoform. *Am J Pathol* 156:253-68.

Wilson, P.D. (2004): Polycystic kidney disease. *N. Engl. J. Med.* 350:151–164.

Wingert, RA, Selleck R, Yu J. (2007): The cdx genes and retinoic acid control the positioning and segmentation of the zebrafish pronephros. *PLoS Genet.* 3:1922–1938.

Wittmann JG, Rudolph MG. (2004): Crystal structure of Rab9 complexed to GDP reveals a dimer with an active conformation of switch II. *FEBS Lett.* 568(1-3):23-9.

Wolfrum, U and Schmitt, A. (2000): Rhodopsin transport in the membranes of the connecting cilium of mammalian photoreceptor cells. *Cell Motil. Cytoskeleton* 46, 95-107.

Woychik, R. P. (2000): The Oak Ridge Polycystic Kidney (orpk) disease gene is required for left-right axis determination. *Development* 127:2347-55.

Wu G, D'Agati V, Cai Y, Markowitz G, Park JH, Reynolds DM, Maeda Y, Le TC, Hou H Jr, Kucherlapati R, Edelmann W, Somlo S. (1998): Somatic inactivation of Pkd2 results in polycystic kidney disease. *Cell.*93(2):177-88.

## 9. REFERENCES

---

Wu, G., Markowitz, GS, Li L., Agati VDD, Factor SM, Tiberl S, Tuchman J, Cai Y, Park JH, van Adelsberg J, Hou Jr H, Kucherlapati R, Edelmann W, Somlo S. (2000): Cardiac defects and renal failure in mice with targeted mutations in Pkd2. *Nat. Genet.* 24:75–78.

Wu, G. and S. Somlo (2000): Molecular genetics and mechanism of autosomal dominant polycystic kidney disease. *Mol Genet Metab* 69(1):1-15.

Yoder, B.K., Hou, X. and Guay-Woodford, L.M. (2002): The polycystic kidney disease proteins, polycystin-1, polycystin-2, polaris, and cystin, are co-localized in renal cilia. *J Am Soc Nephrol* 13:2508-2516.

Yoder BK. (2006): More than just the postal service: novel roles for IFT proteins in signal transduction. *Dev Cell.* 10(5):541-2

Yoder BK. (2007): Role of primary cilia in the pathogenesis of polycystic kidney disease. *J Am Soc Nephrol.* 18(5):1381-8

Yoshimura S, Haas AK, Barr FA. (2008): Analysis of Rab GTPase and GTPase-activating protein function at primary cilia. *Methods Enzymol.* 439:353-64.

Zerres K, Mücher G, Becker J, Steinkamm C, Rudnik-Schöneborn S, Heikkilä P, Rapola J, Salonen R, Germino GG, Onuchic L, Somlo S, Avner ED, Harman LA, Stockwin JM, Guay-Woodford LM. (1998): Prenatal diagnosis of autosomal recessive polycystic kidney disease (ARPKD): molecular genetics, clinical experience, and fetal morphology. *Am. J. Med. Genet.* 76:137–144.

Zhang B, Zheng Y. (1998): Negative regulation of Rho family GTPases Cdc42 and Rac2 by homodimer formation. *J Biol Chem* 273(40):25728-33.

Zhang Y, Gao X, Saucedo LJ, Ru B, Edgar BA, Pan D. (2003): Rhed is a direct target of the tuberous sclerosis tumour suppressor proteins. *Nat Cell Biol* 5:578–581.

Zhao Y, Haylor JL, Ong AC. (2002): Polycystin-2 expression is increased following experimental ischaemic renal injury. *Nephrol Dial Transplant.*(12):2138-44.

Zhao, C., Malicki, J. (2007): Genetic defects of pronephric cilia in zebrafish. *Mech. Dev.* 124:605–616.

Zhou C, Cunningham L, Marcus AI, Li Y, Kahn RA. (2006): Arl2 and Arl3 regulate different microtubule-dependent processes. *Mol Biol Cell*. 17(5):2476-87.

## ACKNOWLEDGEMENTS

I was very lucky to have been mentored not only by one but by two people and I owe them both a lot of gratitude. Prof. Bosch generously adopted me as his graduate student, served as a great thesis advisor and gave me intercontinental mentorship despite his own busy schedule. My second mentor was Zhaoxia, who was a steady source of support and inspiration along the entire journey of working toward this degree. I feel very lucky to have been part of her lab and that she gave me an exciting project, the freedom to pursue things that I was interested in and helped me to develop as a scientist.

The people I shared the lab with during the last three years influenced my everyday life hugely and I am happy that I had such great lab mates!

Linda, Ying, Nicole, Lu, Alice, Shialou, Neil and Jade - you all made my everyday life in the lab very pleasant and created a great environment to work in. Every single one has taught me something valuable- from tips and tricks in the lab, advice for teething infants and the art of balancing work and “ the other life”- but more than anything I am grateful for the wonderful attitude of everyone, staying positive and motivated and supportive towards each other!

I also want to thank SueAnn Mentone who allowed me to use her cryostat and microtome whenever I needed it and assisted with H/E staining. Also big thanks go to Christoph Rahner, who helped tremendously with electron microscopy. I want to thank also John Alvaro, without whom I could never have finished my work. He worked magic to grant me one extension after another to make it possible for me to stay in the lab and continue my work.

There are several special people, without whom the last three years would have been less enjoyable and at times difficult to bear. Let's start with Mari-Francis, who is one of the most adventurous and curious people I've ever met, a great scientist and was just always there to share laughter and tears, many a good bottle of wine and be supportive in every situation. I am so glad to call you my friend! Then there are Marie, Anna-Rita, Massi, Laura, Rushika, Romana and 'the protonpumps' subunits Zane and Roberto: Thanks so much for your wonderful friendships, the crazy concerts and all the good

times over the last years! And Guoneng, who has been a wonderful friend for the last several years and bravely/ crazily volunteered to teach me driving, thank you so much. I want to thank Eun-Joo and Henning, Eun-Jin, Swantje, Bruno, Min-Hee and Uchi for brightening up my days from the other side of the world. A big thank you also to Rachel for all her discussions on science and life and for sharing her experiences, cabernet and lemon crepes with me. Linda, you have been a wonderful friend since the first day I joined the lab. I want to thank you for all your kind words and everything you are showing me about taking risks and pursuing one's dream!

I want to thank also my parents, without whom this would not have been possible. Thank you so much for all your patience, your support and love throughout all those years. A very special thank you is reserved for my little monkey Yumi, who teaches me everyday about the wonders and what is most important in life. You just brought so much joy and love to us, I feel very blessed.

And of course, Markus, my best friend and rock of our little family, without your support all this would not have been possible.

## Curriculum Vitae

Name: Anna Sunjin Lee  
Anschrift: 40 Foster Street  
New Haven, CT 06511  
USA  
Geburtsdatum: 30.09.1978  
Geburtsort: Dinslaken  
Familienstand: Verheiratet  
Nationalität: Deutsch

## Ausbildung

1991-1998 Katholische Schule St. Marien  
6/1998 Abschluss: Allgemeine Hochschulreife  
10/1998 Beginn des Chemie Studiums an der Freien Universität/  
Technischen Universität Berlin; Schwerpunkt Biochemie  
4/2000 Beginn des Studiums der Biochemie/ Molekularbiologie  
an der Christian-Albrechts-Universität zu Kiel  
7/2003 Diplomhauptprüfung  
Hauptfach: Biochemie/ Molekularbiologie  
Nebenfächer: Neurochemie, Mikrobiologie, Immunologie  
7/2003-3/2004 Diplomarbeit am Max-Planck Institut für Neurobiologie in  
Martensried, Gruppe von Magdalena Götz  
4/2004 Abschluss: Diplom-Biochemikerin  
4/2004-9/2005 Forschungspraktika bei Prof. Pietro DeCamilli und Prof.  
Pasko Rakic, Yale Universität  
10/2005 Beginn der Promotionsarbeit  
Fachbetreuung durch Dr. Zhaoxia Sun, Abteilung fuer  
Genetik, Yale Universität  
Betreuung durch Prof. Bosch, Abteilung der Zoologie,  
Christian-Albrechts-Universität zu Kiel



## **Publications and Manuscripts**

Sunjin Lee\*, Neil Duldulao\*, Zhaoxia Sun

**Functional small GTPase domain and cilia localization are essential for in vivo functions of the Joubert syndrome protein Arl13b/ Scorpion**

Submitted to Development

\* equal contribution to this manuscript

Sunjin Lee and Zhaoxia Sun

**Characterization of the embryonic kidney development in *Danio rerio***

Manuscript in preparation.

Referent/in: .....

Ko-Referent/in: .....

Tag der mündlichen Prüfung.....

Zum Druck genehmigt: Kiel, den .....

Der Dekan